

**Non-invasive Assessment of Fruit Quality by
Near-Infrared Spectroscopy for Fruit
Grading in an In-line Setting.**

by

Colin Victor Greensill

A thesis submitted for the degree of

Doctor of Philosophy in Physics

to the

Central Queensland University

James Goldston Faculty of Engineering

and Physical Systems.

October, 2000.



ABSTRACT

Instrument criteria, in terms of wavelength range, wavelength resolution, signal to noise ratio, sensitivity and illumination/detector were defined for the use of near infrared (NIR) spectroscopy in the assessment of soluble solids content (SSC) in intact fruit in an in-line system. Techniques for predictive model generation and transfer of predictive models across a number of systems were assessed in terms of root mean squared error of prediction (RMSEP).

A comparative study of components making up an NIR spectroscopic system established that for the application of assessment of SSC in intact fruit, quartz halogen light sources could provide adequate low cost radiant energy and prisms could provide cheap, more efficient dispersion and higher throughput than flat diffraction gratings. Three wavelength dispersion elements (single equilateral prism, two prisms in series and a ruled diffraction grating) were separately assessed.

Calibration performance for sucrose in a water-cellulose matrix was significantly degraded by a signal to noise ratio (SNR) <5000:1, and when wavelength resolution was decreased beyond a FWHM of 16 nm (at 912 nm). Therefore either photodiode arrays or binned charge-coupled devices could be used as photodetecting elements if SNR is maintained above this level.

A body-transmittance optical path was preferred over reflectance optics to eliminate the 'noise' from specularly reflected light. However, physically contacting the fruit with an optical barrier to separate illuminated and detected

regions constrained process rates. Therefore, an illumination/detector configuration was designed to allow rapid, non-contact spectral measurements to be made. This configuration supported comparable calibration statistics for assessment of SSC of intact melons as a 'contact' configuration (e.g. root mean squared error of cross validation (RMSECV) of 0.74° and 0.65° Brix non-contact and contact, respectively).

Predictive models developed using partial least squares (PLS) regression were significantly more accurate than those developed using multiple linear regression, principal component regression or parallel regression. Wavelength selection techniques were examined. Predictive PLS models based on knowledge of spectrally important wavelengths (for SSC, 630 to 1040 nm) were superior to models based on other wavelength selection techniques. Assessment of data pre-treatment techniques showed that, in most cases, mean centred and autoscaled absorbance data provided the best results. Nine methods for transfer of calibration between instruments were compared against the performance of a simple model updating (MU) technique. While MU gave consistently better predictions on slave instruments, this approach requires maintenance of calibrations on every instrument. Of the established standardisation methods, direct standardisation of the wavelet coefficients was the most efficient.

These design criteria were used in the construction of a prototype fruit sorting system, with performance assessed over a period of two years. The hardware components of this system proved adequately robust to endure the rigours of a pack-house environment and the accuracy of the sorting achieved an RMSEP of

0.7° Brix (standard deviation and range of SSC in sample set, 1.5° and 8.5°, respectively).

Abstract.....	i
Table of Contents.....	iv
Table of Figures.....	ix
Table of Tables.....	xii
List of Abbreviations.....	xiv
List of Symbols.....	xvii
Acknowledgments.....	xxii
Declaration.....	xxiii

Contents

1. Introduction.....	1
2. Underpinning Technologies	6
2.1. Near Infrared Spectroscopy	6
2.1.1. Theory of Spectroscopy and NIR Spectroscopy	6
2.1.2. Theory of Scattering and Absorption.....	13
2.2. Hardware	19
2.2.1. Spectrometer Designs.	19
2.2.2. Light Source.....	27
2.2.3. Detectors:	29
2.3. Fruit Quality Components.....	36
2.3.1. Scattering and Absorption Centres	39
2.4. Chemometrics	40
2.4.1. Data Treatments	42
2.4.2. Multivariate Calibration	52

2.5. Standardisation of Instruments.....	64
2.5.1. Standardisation Techniques	65
2.5.2. Sample Selection for Standardisation	74
2.6. Conclusion	76
3. Literature Review/Case Studies.....	77
3.1. Introduction.....	77
3.2. Criteria Important to In-line Fruit Sorting System Design	77
3.2.1. Bandwidth	77
3.2.2. Resolution	79
3.2.3. Noise and Sensitivity	80
3.2.4. Light Detector Configuration.....	82
3.2.5. Other Factors.....	83
3.2.6. Summary	84
3.3. Spectrometer Case Studies.....	96
3.3.1. Filter Based Instruments	96
3.3.2. Gratings/Prisms Based Instruments	98
3.3.3. AOTF Based Instruments.....	99
3.3.4. LED Based instruments	100
3.3.5. Laser Based Instruments	101
3.3.6. Detectors	103
3.3.7. Optical Geometry	104
3.3.8. FT-NIR Based Instruments	106
3.4. Calibration Transfer	107
3.5. Conclusion	108
4. An Experimental Comparison of Simple NIR Spectrometers for Fruit Grading Applications.....	111

4.1. Introduction.....	111
4.2. Theory	114
4.2.1. Prism	114
4.2.2. Diffraction Grating.....	116
4.3. Experimental Method.....	117
4.3.1. Materials.....	117
4.3.2. Method	122
4.4. Results and Discussion.....	125
4.4.1. Comparison of Spectrometer Performance	125
4.4.2. Radiation Transmission by Limes.....	127
4.5. Conclusion	132
5. An Investigation into the Determination of the Maturity of Pawpaws (<i>Carica papaya</i>) from NIR Transmission Spectra	134
5.1. Introduction.....	134
5.2. Experimental Method.....	137
5.2.1. Spectrometer	137
5.2.2. Materials.....	140
5.3. Results and Discussion.....	141
5.3.1. (a) Characteristics of the Spectrometer	141
5.3.2. (b) Radiation Transmission by Pawpaw	142
5.4. Conclusion	151
6. Optimisation of Instrumentation Precision and Wavelength Resolution for the Performance of NIR Calibrations of Sucrose in a Water-Cellulose Matrix.....	153
6.1. Introduction.....	153
6.2. Experimental	156

6.2.1. Instrumentation	156
6.2.2. Determination of Coefficient of Variation.....	157
6.2.3. Determination of the Number of Layers of Filter Paper.....	158
6.2.4. Calibration of Sucrose Solutions on Filter Paper.....	159
6.3. Results and Discussion.....	160
6.3.1. Signal Coefficient of Variation.....	160
6.3.2. Number of Layers of Filter Paper.....	161
6.3.3. Calibration of Sucrose Solutions.....	164
6.4. Conclusion	166
7. A Remote Acceptance Probe and Illumination Configuration for Spectral Assessment of Internal Attributes of Intact Fruit.....	168
7.1. Introduction.....	168
7.2. Materials and Methods.....	173
7.2.1. Distribution of SSC within a rockmelon fruit.....	173
7.2.2. Optical design.....	176
7.2.3. Light penetration through rockmelon fruit.....	178
7.2.4. Comparison of optical configurations.....	179
7.3. Results and Discussion.....	184
7.3.1. Variation of Soluble Solids Content within Rockmelon Mesocarp.....	184
7.3.2. Light Scattering within Rockmelon Fruit	186
7.3.3. Design of illumination and detection system.....	190
7.3.4. Optimisation of optical geometry and sampling strategy with respect to calibration performance	195
7.4. Conclusion	203
8. Calibration Transfer between NIR Spectrometers in the NIR Assessment of Melon Soluble Solids Content.....	204

8.1. Introduction.....	204
8.1.1. Standardisation Techniques.	205
8.1.2. Sample Selection.....	209
8.1.3. Technique Selection.....	210
8.2. Experimental Method:.....	212
8.2.1. Data Sets.	212
8.2.2. Instrumentation	212
8.2.3. Spectral Data Treatment.....	213
8.3. Results.....	218
8.3.1. Comparison of Spectrometers.....	218
8.3.2. Comparison of Standardisation Techniques.	219
8.4. Conclusion:	227
9. Conclusion.....	229
10. References.....	236
11. Appendices.....	261
11.1. Appendix A	261
11.2. Appendix B	267
11.3. Appendix C	269
11.4. Appendix D	273

Table of Figures

Figure 2.1. Simple harmonic oscillator energy levels.....8

Figure 2.2. Anharmonic oscillator energy levels.9

Figure 2.3. Vibrational modes of a water molecule.11

Figure 2.4. Vibrational modes of a carbon dioxide molecule.12

Figure 2.5. Other vibrational modes.12

Figure 2.6. An illustration of the diffusing medium divided into parallel layers.....16

Figure 2.7. Representation of a blazed diffraction grating with defining angles.....21

Figure 2.8. Dispersion of white light through an equilateral prism.24

Figure 2.9. Transmission efficiency and refractive index of SF18 glass as a
function of wavelength in the visible and NIR region.25

Figure 2.10. Blackbody curve at 2900°C, typical silicon detector response and
diffraction grating efficiency curve.....29

Figure 4.1. Defining terms for an equilateral prism.....114

Figure 4.2. Defining terms for a diffraction grating.....115

Figure 4.3. Relationship between refractive index, optical transmission and
diffraction grating efficiency and wavelength.118

Figure 4.4. Representation of the optical geometries used for the single prism,
two prism and diffraction grating spectrometers.120

Figure 4.5. Representation of the NIR spectrometer.....121

Figure 4.6. Comparison of the relative resolution and bandwidth of the
diffraction grating, single prism and double prism spectrometers using a
HgAr discharge source.....123

Figure 4.7. Transmission spectra of limes at two stages of ripeness using the
diffraction grating spectrometer.....129

Figure 4.8. Transmission spectra of limes at two stages of ripeness using the dual prism spectrometer.	130
Figure 4.9. Transmission spectra of limes at two stages of ripeness using the single prism spectrometer.	130
Figure 5.1. Diagrammatical representation of the NIR spectrometer.	138
Figure 5.2. Spectrometer transmission results using a HgAr discharge source.	142
Figure 5.3. Typical averaged transmission spectra of pawpaw at an immature stage of maturity. Grade (i)	143
Figure 5.4. Typical averaged transmission spectra of pawpaw at the transition stage of maturity. Grade (ii)	144
Figure 5.5. Typical averaged transmission spectra of pawpaw at late mature green stage of maturity. Grade (iii).	145
Figure 5.6. Typical averaged transmission spectra of pawpaw at the colour break stage of maturity. Grade (iv).	146
Figure 5.7. Typical averaged transmission spectra of pawpaw at the four stages of maturity. Grades (i).(ii), (iii), and (iv).	147
Figure 6.1. Transmission of light through water soaked filter paper at ~ 800 nm....	161
Figure 7.1. Sampling positions in relation to fruit anatomy.	174
Figure 7.2. Schematic of illumination and detector probe configurations assessed for the non-contact assessment of fruit.	175
Figure 7.3. Soluble solids content of inner and outer mesocarp tissue of twelve equidistant slices of a fruit.	187
Figure 7.4. Soluble solids content of inner and outer mesocarp tissue of median slices.	188
Figure 7.5. Three dimensional representation of light penetration through a fruit. ..	189

Figure 8.1. White reference spectra representative of differences observed between MMS1 spectrometers.....	220
Figure 8.2. A plot of the means of data set A (absorbance units in the range 628 to 1042 nm) highlights differences existing between two typical spectrometers.....	221
Figure 8.3. PDS residual plotted against DWPDS residuals.....	222
Figure 9.1. Western Australian (a) rockmelon fruit and honeydew (b) sorted by the prototype system.	233

Table of Tables

Table 2.1. Position and assignment of absorption peaks in the spectral region 700 to 1100 nm.	13
Table 2.2. Comparison of Ruled and Holographic Gratings.....	23
Table 2.3. Bandwidth and normalised reciprocal NEP (D^*) of some semiconductor materials and photodetector devices.....	31
Table 2.4. Typical characteristics of PDA and CCD detectors.....	34
Table 2.5. Typical concentration of some macro-constituents of fruit.	38
Table 3.1. Wavelengths in the SW-NIR region associated with sucrose or SSC in fruit sample.	78
Table 3.2. List of patents relating to hardware for sorting of vegetables or fruit using NIR technology.	85
Table 3.3. List of publications relating to the determination of quality parameters in fruit, vegetables and fruit juice.	89
Table 4.1. Observed and calculated resolution of the three spectrometer configurations.....	125
Table 4.2. Summary of features observed in the transmission spectra of limes taken with the prism and diffraction grating spectrometer configurations.	131
Table 4.3. Intensity ratios as indicated of selected features according to lime maturity for the prism and diffraction grating based spectrometer configurations.....	131
Table 6.1. Effect of signal precision on calibration of sucrose solutions (0-20% w/v) on cellulose.	162

Table 6.2. Effect of wavelength resolution, reported for four emission lines of a HgAr calibration lamp, on calibration of sucrose solutions (0-20% w/v) on cellulose. signal level maintained by adjusting integration time.	163
Table 7.1. PLS calibration performance for spectra collected using the 'contact' and 'non-contact' (without lens) illumination/detector optical configuration, across eleven populations of differing cultivars and growing districts.....	196
Table 7.2. PLS calibration performance for spectra collected in stationary and moving (0.5 m s ⁻¹) modes of the 'non-contact' illumination/detector system (without lens) configuration, across two populations.	198
Table 7.3. Results of calibration of spectra collected in moving (0.5 m s ⁻¹) mode of operation of the 'in-line' illumination/detector system with and without a lens across one population.	199
Table 7.4. PLS calibration performance for spectra collected of one population of fruit, with three sampling procedures employed in the extraction of a juice sample for SSC determination.....	200
Table 8.1. Performance of calibration transfer process reported in terms of RMSEP for the prediction of melon SSC using spectra collected on a slave spectrometer and a calibration generated on spectra of the same fruit, collected on a master instrument.....	224
Table 8.2. Ranking on RMSEP values achieved by each standardisation techniques based on 1 = lowest value, 2 = second lowest value etc	225
Table 8.3. Significance testing of the results a comparison of the technique with the lowset RMSEP against five nearest neighbours using Fearn's criteria to determine upper and lower significance limits of the RMSEP value.	226
Table 9.1. Recommended Design Criteria for a Rockmelon Fruit Sorting System Employing Silicon-based NIR Spectroscopy.....	234

List of Abbreviations

The following abbreviations are used throughout this thesis.

ADC	Analogue to Digital Converter	InGaAs	Indium Gallium Arsenide
ANN	Artificial Neural Network	Int and Mod.	Interpolation and photometric modification
AOTF	Acousto-Optical Tunable Filter	IR	Infrared
CCD	Charge-Coupled Device	IUPAC	International Union of Pure Applied Chemistry
CLS	Classical Least Squares	LED	Light Emitting Diodes
CV	Coefficient of Variation	LDA	Linear Discriminant Analysis
D	Detectivity	LOO	Leave one out (cross validation)
DM	Dry Matter	LV	Latent Variable
DMS	Dry Matter Solubility	MD	Mahalanobis Distance
DS	Direct Standardisation	MLR	Multiple Linear Regression
DT	Detrend	MMS1	Monolithic Miniature Spectrometer 1
DWPDS	Double Window Piecewise Direct Standardisation	MPLS	Multiple Partial Least Squares
ED	Euclidean Distance	MSC	Multiple Scatter Correction
FIR	Finite Impulse Response	MU	Model Updating
FT	Fourier Transform	NEP	Noise Equivalent Power
FTIR	Fourier Transform Infrared	NIPALS	Non-Iterative Partial Least Squares
FTNIR	Fourier Transform Near Infrared	NIR	Near Infrared
FWHM	Full Width Half Maximum	NIRS	Near Infrared Spectroscopy
GA	Genetic algorithm		
ILS	Inverse Least Squares		

NMR	Nuclear Magnetic Resonance	SA	Simulated Annealing
NN	Neural Network	SBC	Slope and Bias Correction
OBD	Optimum Brain damage	SDR	Standard Deviation Residual
OBS	Optimum Brain Surgery	SEC	Standard Error of Calibration
OSC	Orthogonal Signal Correction	SECV	Standard Error of Cross Validation
PC	Principal Component	SEP	Standard Error of Prediction
PCA	Principal Component Analysis	SGT	Savitzky-Golay Transform
PCR	Principal Component Regression	Si	Silicon
PDA	Photodiode Array	SIMCA	Soft Independent Modelling of Class Analogy
PDS	Piecewise Direct Standardisation	SMLR	Stepwise MLR
PLS	Partial Least Squares	SNR	Signal to Noise Ratio
PMSC	Piecewise Multiplicative Scatter Correction	SNV	Standard Normal Variate
QDA	Quadratic Discriminant Analysis	SSC	Soluble Solids Content
QTH	Quartz Tungsten Halogen	StDev	Standard Deviation
RDA	Regularised Discriminant Analysis	SW-NIR	Short Wavelength Near Infrared
RF	Radio Frequency	TLC	Thin Layer Chromatography
RMSEC	Root Mean Square Error of Calibration	UV	Ultra Violet
RMSEC V	Root Mean Square Error of Cross Validation	VIS/NIR	Visible and Near-Infrared
RMSEP	Root Mean Square Error of Prediction	WT	Wavelet Transform
ROD	Relative Optical Density	SMLR	Stepwise MLR

SNR	Signal to Noise Ratio
SNV	Standard Normal Variate
SSC	Soluble Solids Content
StDev	Standard Deviation
SW-NIR	Short Wavelength Near Infrared
TLC	Thin Layer Chromatography
UV	Ultra Violet
VIS/NIR	Visible and Near- Infrared
WT	Wavelet Transform

List of Symbols

The following symbols, listed in approximate order of appearance in text, are used throughout the thesis.

λ	wavelength	E_{vib}	Molecular vibrational energy
λ'	first derivative of the wavelength	E_{rot}	Molecular rotational energy
λ''	second derivative of the wavelength	$E_{rot-vib}$	Molecular combinational energy
ν	vibrational frequency	I_{cm}	moment of inertia
k_f	classical force constant	Y	percentage concentration of analyte absorber
m	mass	B_i	regression coefficient of the i th variable
a	acceleration	R_j	Reflectance of the j th sample
μ	reduced mass	E	random error
E	energy	x	thickness of layer
r	interatomic distance	$F(R)$	remission function
h	Planks constant	R_∞	observed reflectance at infinity
\hbar	Planck's Constant ($\hbar = h/(2\pi)$)	K	absorption coefficient
B_o	intercept from regression	S	scatter coefficient
X	Bold Upper case- Matrix	ς	$= \frac{(S + K)}{K}$
x	Bold lower case – vector	ϑ	$= \sqrt{\varsigma^2 - 1}$
ω	classical vibrational frequency	S_j	Scattering fraction of j flux
ν	vibrational quantum number	K_j	absorption fraction of j flux
x_e	anharmonicity constant		
y_e	anharmonicity constant		
l	rotational quantum number		

i	light flux travelling in direction of illumination	N_p	number of arriving photons
j	light flux travelling in direction opposite to i	η	quantum efficiency
I_0	original intensity	E_p	photon irradiance
d	periodic distance of diffraction grating	A_d	pixel area
R	Reflectivity	T_i	integration time
$\varepsilon(\lambda)$	pathlength	\bar{N}_p	mean number of arriving photons
a	absorptivity	N_{Ph}	photon noise
c	analyte concentration	N_{PE}	photon - electron noise
R_g	reflectance of the supporting layer	J_d	dark current density
θ	angle in the x-y plane	q	electronic charge
ϕ	angle in the x-z plane	N_{DC}	dark current noise
$I(\beta)$	intensity of refracted waves	N_{RS}	reset noise
ε	angle of prism	k	Boltzmann's constant
g	prism base width	T	absolute temperature
$d\beta/d\lambda$	angular dispersion	N_{WR}	white-readout noise
$dn/d\lambda$	dispersion	C_o	load capacitance
$R(\theta, \beta)$	grating efficiency	Δf	amplifier bandwidth
α	incident light angle to grating normal	G	amplifier gain
β	reflected light angle to grating normal	Z_o	amplifier first stage output impedance
m	diffraction order	$P_n(x)$	approximating polynomial of $f(x)$
N	number of grooves	f_0	first data point
n	refractive index	f_1	central data point
		f_2	last data point
		$wind$	window width

$O(wind^2)$	error term	b	MSC correction coefficient
e	order of the derivative	\bar{S}_k	mean centred (ideal) spectrum
γ	degree of the polynomial	$^{msc}S_i$	multiplicative scatter corrected spectrum
s	number of points to be fitted by the polynomial	w	loading weights
τ	$(s-1)/2$	\mathbf{X}	independent variable matrix
\mathbf{x}	vector of observed values	\mathbf{Y}	dependent variable matrix
\mathbf{T}	matrix of transforming coefficients	c_i	eigenvector of $\mathbf{Z}\mathbf{Z}^T$
\mathbf{x}_i	i th element of the uncorrected spectrum	λ_i	eigenvalue
$\bar{\mathbf{X}}$	mean of the spectrum	t_i	score
\mathbf{x}_{iSNV}	i th element of the SNV transformed spectrum	p_i	loading
\mathbf{x}_{iDT}	i th element of the DT transformed spectrum	f	number of OSC factors
W	absorbance value	\mathbf{X}_o	OSC corrected X matrix
a	intercept	\mathbf{S}	matrix of pure component responses
b	polynomial constant	\mathbf{x}	independent variable vector
c	polynomial constant	\mathbf{X}^+	pseudo-inverse of X matrix
I	number of population members	\mathbf{C}	matrix of concentration variables
i	sample index	\mathbf{b}	regression vector
j	dependent variable index	\mathbf{y}	dependent variable vector
k	independent variable (e.g. wavelength) index	\mathbf{T}	matrix of independent variable scores
mS	spectrum to MSC corrected	\mathbf{P}	matrix of independent variable loadings
a	MSC correction coefficient		

W	matrix of independent variable weights	s_0	mean distance between all objects belonging to the class model
t	vector of independent variable scores	e_{ij}^2	squared residual of object i on the latent variable j
p	vector of independent variable loadings	F	standardisation parameters
w	vector of independent variable weights	\mathbf{X}_m	independent variable matrix of master instrument
U	matrix of dependent variable scores	\mathbf{X}_s	independent variable matrix of slave instrument
Q	matrix of dependent variable loadings	\mathbf{x}_m	independent variable vector of master instrument
u	vector of dependent variable scores	\mathbf{x}_s	independent variable vector of slave instrument
q	vector of dependent variable loadings	x_{STDi}	new absorbance value at the new wavelength
\mathbf{E}_i	matrix of independent variable residuals	$a(i)$	intercept
\mathbf{F}_i	matrix of dependent variable residuals	$b(i)$	regression coefficient
bi_j	bias	$\overline{\mathbf{R}}_1$	matrix of absorbance values for a subset of standardisation samples measured on the master instrument
Bias	bias matrix		
$cf_k(x)$	classification score		
\mathbf{C}^{-1}	covariance matrix	$\overline{\mathbf{R}}_2$	matrix of absorbance values for the same subset of standardisation samples measured on the slave instrument
K	class descriptor		
$\overline{\mathbf{X}}_k$	absorption matrix of centroid of class K		
p	number of dependent variables	$\mathbf{r}_{2,un}^T$	new response vector of an unknown samples from the slave instrument
n	number of samples	$\hat{\mathbf{r}}_{1,un}^T$	standardised $\mathbf{r}_{2,un}^T$ to appear as a master response vector
r	number of PCs		

${}^m\mathbf{C}$	master calibration matrix
${}^m\mathbf{T}$	standardisation matrix
$d(u)$	minimum Euclidean distance
s	index of selected spectra
u	index of unselected spectra
R	coefficient of correlation
R	reflectance
R_C	correlation coefficient of calibration
RF	radio frequency
R_V	correlation coefficient of validation
A_{IF}	fibre area
a_s	segment area
r_{ff}	distance fruit to fibre
r_p	distance separating two planes
θ_k	angle of planes of illumination
Φ	radiant flux
L	radiant intensity
RoF	radius of fruit
θ_b	half segment angle
F_K	Fearn variable K
F_L	Fearn variable L

Acknowledgments

The author wishes to express sincere appreciation to Associate Professor Peter Wolfs for his guidance and support during a tumultuous period of this work and to Associate Professor Kerry Walsh for his many hours of guidance and assistance and his meticulous attention to detail during manuscript preparation has been invaluable.

My research group colleagues, John Guthrie and Brett Wedding deserve special thanks for their good-hearted banter, support and constructive criticism on all, even non-project related, subjects. Gary Brown and Colour Vision Systems Pty. Ltd. are thanked for their indispensable work on the design and construction of some of the equipment used in this work.

The Australian Research Council of Australia, the Plant Sciences Group of Central Queensland University and Colour Vision Systems Pty. Ltd. funded the project which formed the basis for the work undertaken for this thesis and are thanked for their financial contribution. The work was carried out under the administration and supervision of the 'Plant Sciences Group', Faculty of Arts Health and Sciences and the Faculty of Engineering and Physical Systems both of whom are also sincerely thanked for their logistic and financial support.

Finally and in particular, I wish to thank my wife Sandra and children, Thomas and Kathryn for their support, encouragement and tolerance, without which this educational journey would not have been completed.

Declaration

I hereby declare that the main text in this thesis is an original work and no part has been used in the award of another degree.

Signature Redacted

Colin Victor Greensill

Chapter 1

1. Introduction

Near infrared (NIR) spectroscopic technology has the potential for non-invasive analysis of the internal attributes of fruit for such parameters as sweetness, dry matter, acidity and other consumer-important characteristics. Used in an in-line setting it has the capability to offer fruit and vegetables of guaranteed internal quality thereby adding value to the product. For the first time retailers will be able to offer consumers fruit and/or vegetables of a guaranteed quality. When financial resources are limited and the quality of natural product is uncertain a consumer will most often choose the less healthy but quality-assured confectionary. The long term benefits to the individual and the nation are obvious if the healthy choice is made.

In response to consumer demand for high quality product and consistency, major fruit and vegetable wholesalers and retailers are increasingly subjecting producers to more stringent on-farm quality assurance programs. The sheer volume of product passing through large packing sheds each season has necessitated the employment of advanced technologies to increase the throughput rates of current sorting for 'external' features such as shape, weight, density colour and blemishes. Other technologies can be applied for the non-invasive assessment of internal attributes. Invasive methods of inspection for the determination of soluble solids content (SSC) are widely used, however non-invasive techniques do not damage saleable fruit and are preferred. Non-invasive methods include the use of ultrasonics, nuclear magnetic resonance (NMR)

Introduction

imaging and NIR spectroscopy. NIR spectroscopy uses optical techniques and is adaptable to automated sorting systems. It is the focus of this thesis.

The NIR portion of the spectrum is rather ill-defined but, for the purposes of this work, it will be sufficient to consider the region 780 to 2500 nm¹. The NIR spectral region was, in the past, discarded as “too difficult to use” by traditional spectroscopists because of its heavily overlapping, broad spectral features². The advent of high-performance desktop computers has allowed the use of powerful chemometric algorithms to extract information from these difficult to interpret spectra and the generation of predictive models. The fundamental elements of an NIR spectrometer are the same as any classical spectrometer, comprising a light source, collimating and focusing optics, a wavelength dispersing element, and a light detector³. The sample under analysis can be positioned either before or after the dispersing element, with the mode of operation being classified as post-dispersive or pre-dispersive, respectively. Short wavelength near infrared (SW-NIR) technology (700 – 1050 nm) can use silicon-based detector designs found in many low cost miniature spectrometers which have commercially proliferated since the mid-1990s. These technologies have found application in non-invasive sorting of large items such as fruit because of its inherent requirement of long path lengths due to low absorptivity in this spectral region. Long pathlengths means that data can be collected from deeply penetrating light or measurements made through thick samples thus making whole-fruit SSC assessment possible.

Extensive databases of the spectral responses of various compounds now exist (see, for example, the reviews of Putzig *et al.*⁴, Workman⁵ and Workman⁶). NIR technology is used in an ever increasing number of applications and industries.

Introduction

For example, NIR spectroscopy is used to monitor oxygen levels in the blood stream non-invasively⁷. NIR spectroscopy is used extensively for process control and product authentication in the petrochemical and pharmaceutical industries. NIR spectroscopy is also applicable to the grading of fruit for internal attributes, for example, soluble solids content (SSC) or dry matter (DM) content in melon⁸, citrus⁹, pineapple¹⁰, apples¹¹ and peaches¹².

Mathematical data pretreatment of the spectral data and chemometric techniques are essential for the non-invasive, non-contact analysis of internal attributes (e.g. SSC) of fruit. These techniques provide an invaluable tool for the generation of reliable calibrations and allows the extraction of information related to issues such as the identification of noise sources. However, due to manufacturing tolerances of the many components of a spectrometric system, no two systems can be identical hence no two spectrometers will give identical spectra for the same sample. These differences are enough to cause directly transferred predictive models to fail. Commercial applications demand transferability of calibrations rather than costly individual calibration generation. In this application of grading fruit, the requirement is to transfer calibrations between packhouses. This necessitates the transference of calibrations generated on one system for use by another system using chemometric processes. This thesis makes an extensive study of the available techniques and after extended trials, proposes a new method with improved performance.

Two Japanese companies (e.g. Fantec and Mitsui Mining Corporation) market NIR in-line sorting machines for use in packing sheds using full or partial

Introduction

transmittance or reflectance modes of operation. However, due to their government subsidies and tariffs, their purchase price to an offshore client is prohibitive (> \$300K per lane).

Despite the commercial availability of a few small generic spectrometers, the initial aim of this project was to design a spectrometer optimised for the application of non-invasive sorting of fruit for SSC content in a packline setting. In late 1990s a large number of generic, high quality, economical post-dispersive spectrometers became commercially available. Economic considerations dictated a change of focus for this study to the assessment of the spectrometer designs in a number of areas which had been shown to be critical to the commercial success of NIR technology in this application.

After examining the underpinning technologies and recent case studies, the thesis focuses on several key areas, namely:

- Comparisons of optical characteristics of spectrometer designs based on two dispersive elements in terms of resolution, linearity of output and range;
- Investigation of the impact of the system signal to noise ratio (SNR) and resolution on the development of predictive models for this application;
- Design of the illumination/detector systems suitable for a non-contacting system to rapidly sort fruit. (SSC distribution and light penetration are studied to optimise this design and a proposed illumination/detector configuration);

Introduction

- Transferability of predictive models among a number of systems. Ten standardisation techniques are tested for efficacy with respect to the transfer of predictive models used in the assessment of SSC in rockmelons.

In all of these cases, the chapters consist of the author's publications in these areas. Finally, the conclusion reviews the success of the project and highlights possible future developments.

2. Underpinning Technologies

2.1. Near Infrared Spectroscopy

2.1.1. Theory of Spectroscopy and NIR Spectroscopy

In 1800, Sir William Herschel¹³ noted that when ‘white’ light was separated with a prism into component colours and made to fall on a thermometer, little temperature change occurred over the visible range. However, when the thermometer was moved to regions beyond the visible (red) position the temperature increased. It was obvious from his observation that energy existed in a previously unknown region, which he named “infrared” (IR)(ca. Latin, below).

The NIR region is defined by International Union of Pure Applied Chemistry (IUPAC) as the region 780 to 2500 nm. The region 700 to 1100 nm is often referred to as the ‘Herschel region’ after its discoverer¹.

When a sample is illuminated by a white light source some of its continuous energy spectrum is absorbed by organic molecules causing deficiencies at discrete wavelengths of a measured spectrum. These measured deficiencies provide the identifying ‘finger print’ of the constituent molecule. In the NIR region the observed absorption bands are either overtones or combinations of overtones of fundamental bands originating in the mid infrared region (2500 to 25000 nm), with a characteristically broad bandwidth (typically 30-40 nm FWHM)¹⁴. The NIR region is generally defined as the spectral region 780 to 2500 nm¹⁵, while short-wave NIR (SW-NIR) refers to the region 700 to 1100

nm. The regions encompassing both these, 700 to 2500 nm, contains absorption bands corresponding to overtones and combinations of fundamental C-H, O-H and N-H vibrations due mainly to the large anharmonicity of the vibrations attributed to the hydrogen atoms. These overtones and combination bands are much weaker (typically by a factor 100) than their counterparts in the IR region. This fact allows the use of far greater path lengths within samples and hence the use of minimal or no sample preparation prior to spectra acquisition; a significant advantage for in-line analyses.

A thorough introduction to the topic of NIR spectroscopy is given by Eisberg and Resnick¹⁶ and Serway *et al.*¹⁷. A brief review follows:

For an ideal diatomic harmonic oscillator rough calculation of the fundamental band wavelengths can be achieved using Hooke's law ($F = -k_f x$) (F is force, k_f is the force constant and x is the distance travelled) and Newton's law ($F = ma$) (F is force, m is the mass and a is acceleration) to derive the following classical equation for simple harmonic oscillation (Eqn. 2.1).

$$\nu = \frac{1}{2\pi} \sqrt{\frac{k_f}{\mu}} \quad \text{Eqn 2.1}$$

where ν is the vibrational frequency, k_f is the classical force constant and μ is the reduced mass of the two atoms. Around 1900 Planck showed, whilst studying black body radiation, that this type of model was only appropriate for ideal systems. The assumption of equi-partition of energy was invalid and at a quantum level the energy of a simple harmonic oscillator was discontinuous.

The discrete energy level steps can be described by the equation $\Delta E = h\nu$, where E is energy and h is Plancks constant. Solution of Schrödinger's wave equation provides the quantum equivalent to the classical equation for a simple harmonic oscillator (Eqn 2.2)

$$E=(v+0.5)h\nu \quad (v = 0, 1, 2, \dots) \quad \text{Eqn 2.2}$$

where v is the vibrational quantum number¹⁶ (Fig. 2.1).

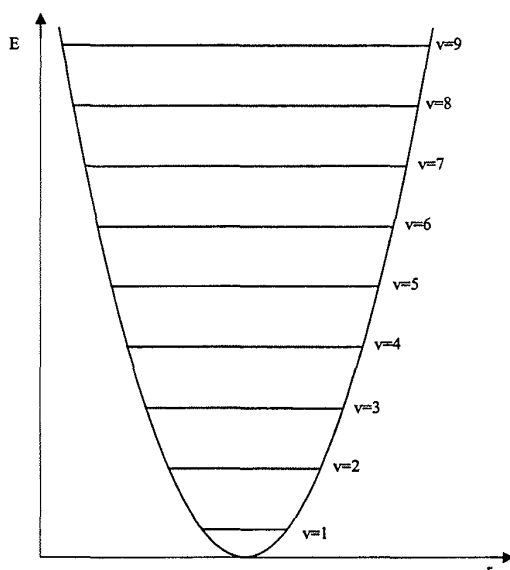


Figure 2.1. Simple harmonic oscillator energy levels. E is energy, r is interatomic distance and v is the vibrational quantum number.

In reality, however, molecules do not follow the laws of simple harmonic motion because other inter-nuclear forces also contribute to the energy distribution of the system. This interaction is best described by the equations for anharmonic oscillation

$$E_v = h\nu_o \left[\left(v + \frac{1}{2} \right) - x_e \left(v + \frac{1}{2} \right)^2 + y_e \left(v + \frac{1}{2} \right)^3 - \dots \right] \quad \text{Eqn 2.3}$$

where x_e and y_e are the anharmonicity constants. Usually the third term in this equation is small and so is neglected. The energy levels are not equally sized steps but the difference between the energy levels decreases as the v increases (Fig. 2.2). The selection rule now becomes $\Delta v = \pm 1, \pm 2, \pm 3, \dots$. Those quantum numbers greater than 1 are the transitions which create the overtones.

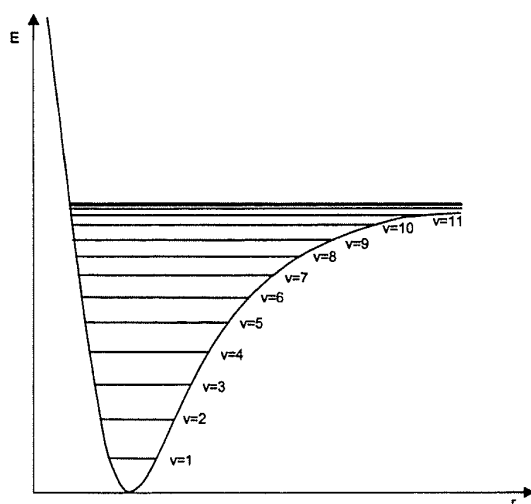


Figure 2.2. Anharmonic oscillator energy levels. E is energy, r is interatomic distance and v is the vibrational quantum number.

Electromagnetic energy absorbed by molecules in the infrared region is dependent on the presence of an electric dipole moment across the vibrating bond. That is molecular vibration must cause a change in the dipole moment of the molecule to be IR active. In the NIR region, it is principally energy interaction from triatomic molecules or AX_2 groups and AX_3 groups that is observed. This interaction takes the form of either stretching or bending vibrations of interatomic distance or angle, respectively, among the bonded atoms. A combination of both these vibrational and rotational interactions frequently occurs in nature. The centre of mass of the molecule must remain

stationary so only complementary movements of atoms are those allowed. There are approximately $(3n-6)$ degrees of vibrational freedom for poly-atomic molecules ($(3n-5)$ for linear molecules) where n is the number of atoms.

The equation defining energy levels for vibrational energy levels (E_{vib}) is

$$E_{\text{vib}} = \hbar\omega \left(v + \frac{1}{2} \right) \text{ where } v = 1, 2, \dots \quad \text{Eqn 2.4}$$

where v is the vibrational quantum number and ω is the classical frequency of vibration, ω related to the force constant k by $k = \mu\omega^2$ where μ is the reduced mass of the two atoms.

For rotational energy levels (E_{rot}):

$$E_{\text{rot}} = \frac{\hbar^2}{2I_{\text{cm}}} l \left(l + \frac{1}{2} \right) \text{ where } l = 1, 2, \dots \quad \text{Eqn 2.5}$$

where I_{cm} is the moment of inertia about the reduced mass and l is the rotational quantum number.

Finally, for energy levels of combinational bands ($E_{\text{rot-vib}}$) this relationship becomes

$$E_{\text{rot-vib}} = \frac{\hbar^2}{2I_{\text{cm}}} l \left(l + \frac{1}{2} \right) + \left(v + \frac{1}{2} \right) \hbar\omega \quad \text{Eqn 2.6}$$

$$= E_{\text{rot}} + E_{\text{vib}} \quad \text{Eqn 2.7}$$

For example, for a water molecule (H_2O) which has three atoms in a non-linear arrangement there are three vibrational modes as shown in Fig. 2.3.

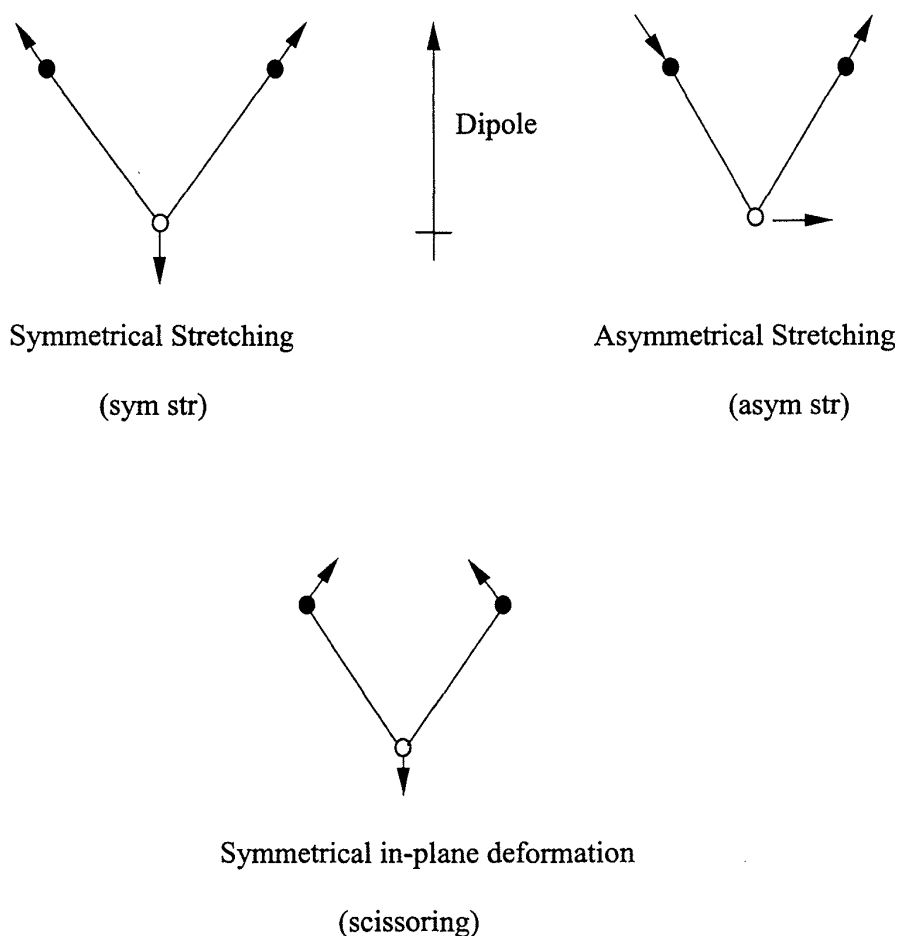


Figure 2.3. Vibrational modes of a water molecule.

For a linear molecule like carbon dioxide (CO_2) which also has three atoms there are four vibrational modes (+ and - designate in and out of page respectively)(Fig. 2.4).

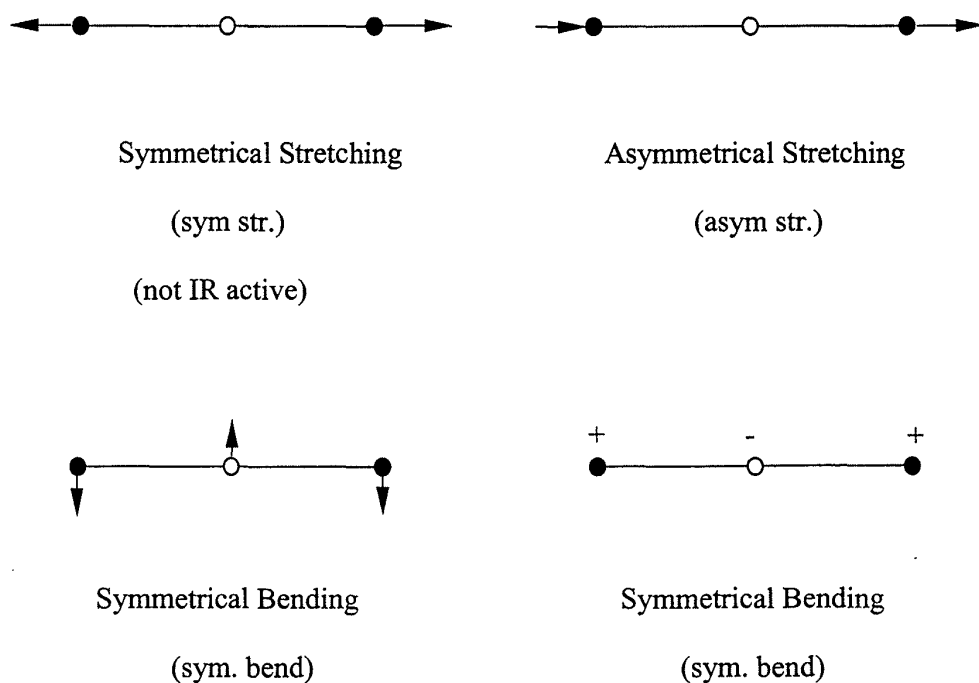


Figure 2.4. Vibrational modes of a carbon dioxide molecule.

Other vibrational modes existing but not observed in either water or carbon dioxide, are shown below (Fig. 2.5).

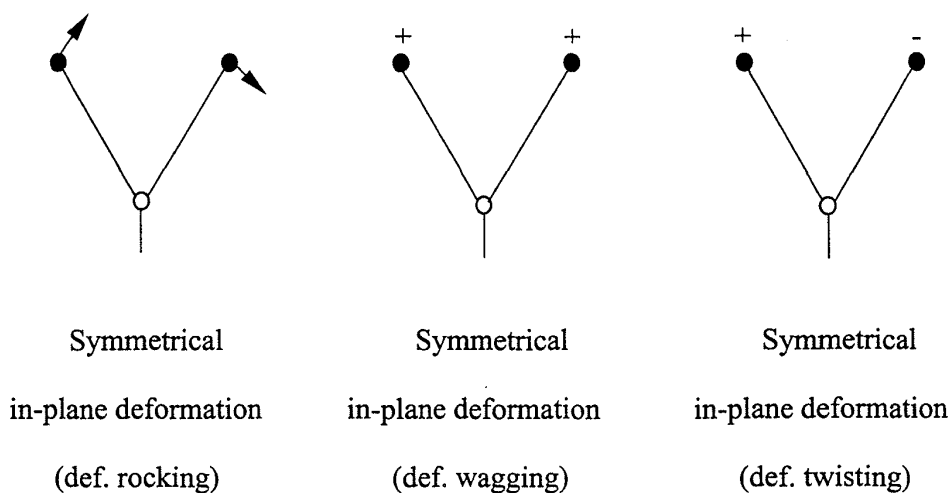


Figure 2.5. Other vibrational modes.

Table 2.1. Position and assignment of absorption peaks in the spectral region 700 to 1100 nm by Williams and Norris¹⁸).

Wavelength (nm)	Absorbing Species	Wavelength (nm)	Absorbing Species
834	H ₂ O	978	Sugar
838	Sugar	978	Cellulose
860	Cellulose	986	H ₂ O
888	Sugar	994	H ₂ O
905	Cellulose	1005	Sugar
913	Sugar	1010	H ₂ O
920	Cellulose	1030	H ₂ O
938	H ₂ O	1030	Starch
958	H ₂ O	1058	Cellulose
978	H ₂ O	1099	H ₂ O

NIR absorption spectra of fruit are characterised by features related to O-H and C-H bonds. These bonds are affected by other atoms present in the molecules therefore slightly modifying the observed vibrational mode frequencies. Both O-H and C-H bonds exhibit peaks at several wavelengths (Table 2.1). This causes severe overlapping and requires robust chemometric techniques to extract relevant information. For more specific band assignments see Appendix A.

2.1.2. Theory of Scattering and Absorption

Beer's Law describes the relationship between sample transmittance or reflectance absorption measurements and analyte concentration for a given pathlength. However, scattering effects due to particles of the sample matrix

often disrupt this relationship¹⁹. A commonly used multivariate regression equation used for instrument calibration is

$$Y = B_o + B_k(-\log R_j) + E \quad \text{Eqn 2.8}$$

where Y is percent concentration of absorber, B_o is intercept from regression, B_k is regression coefficient, k is index of wavelength used, R_j is its corresponding reflectance and E is random error. This is often shortened to (Eqn. 2.9)

$$Y = B_k(-\log R). \quad \text{Eqn 2.9}$$

NIR spectroscopic analyses can be based on diffuse reflectance or transmittance data. Diffuse reflectance is non directional radiation returning to the detector from a surface. Many physics textbooks describe diffuse reflectance in terms of surface roughness with reference to metallic materials. For non-metallic materials, some of the returned diffuse radiation originates at the rough surface and but some originates from within the sample²⁰. NIR reflectance spectroscopy tries to discard the surface component and use only that originating from within the sample for analyses.

A simple but widely adopted approach for describing the interaction of light with diffusing media has been formulated by Kubelka and Munk²¹. This theory has been widely used to relate the total diffuse reflection from a material to the scattering and absorption coefficients of the sample. In two-flux (Kubelka Munk) theory, radiation is assumed to be composed of two oppositely directed

radiation fluxes through a continuous medium. In this formulation the remission function, $F(R)$, for an ideal sample which is optically thick at the wavelength of choice and with a homogeneous distribution of absorbers and scatters throughout, is given by the Kubelka-Munk function, i.e.

$$F(R) = \frac{(1 - R_{\infty})^2}{2R_{\infty}} = \frac{K}{S} \quad \text{Eqn 2.10}$$

where R represents the observed diffuse reflectance from the surface of the sample and K and S represent absorption and scattering coefficients, respectively. $F(R)$ is proportional to the absorber concentration.

The derivation of this equation using an exponential solution makes the following assumptions:

1. The radiation flux (i and j) travels in two possible directions.
2. The sample is illuminated with monochromatic radiation of intensity I_0 .
3. The distribution of the scattered radiation is isotropic so that all regular (specular) reflection is ignored.
4. The interacting particles in the sample layer (defined as the region between $x = 0$ and $x = \text{sample depth}$) are randomly distributed.
5. The particles are very much smaller than the thickness of the sample layer.
6. The sample layer is subject only to diffuse irradiation.
7. Particles are much larger than the wavelength of irradiation (so that the scattering coefficient will be independent of wavelength - if only one wavelength is to be used then this requirement is not relevant).

8. The breadth of the macroscopic sample surface (in the yz plane) is great compared to the depth of the sample and the diameter of the beam of incident radiation (to discriminate against edge effects).

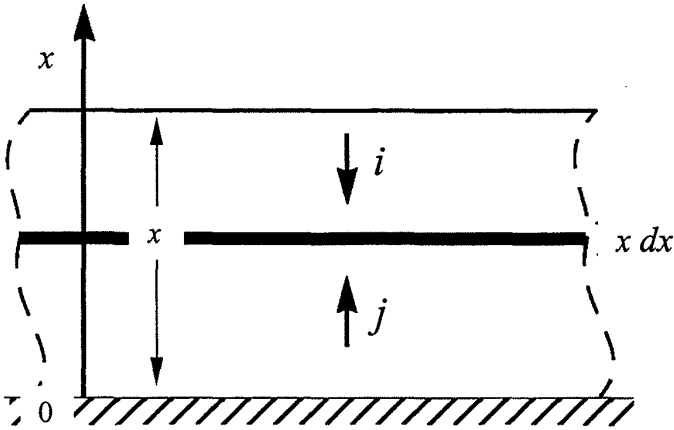


Figure 2.6. An illustration of the diffusing medium of a thickness (x) divided into parallel layers infinitely thin (dx). Fluxes travelling in opposite directions, descending and ascending, represented by arrows i and j .

Consider a layer of a thickness x (Fig. 2.6) of an infinite surface where boundaries are neglected and two fluxes i and j are travelling in opposite directions. Of the incident light flux, a fraction is absorbed (coefficient of absorption) and a fraction is scattered (coefficient of scattering). The model assumes that these coefficients do not vary in the layer studied. Balancing of the amount of flux transversing a infinitely thin layer (dx) to arrive at a position x leads to a system of linear differential equations for the coefficients. On transversing the infinite layer the flux j diminishes by Kj absorption and Sj scattering by an amount equal to an increase in Si , the fraction on the i flux scattered outside the thickness of the layer dx . This reasoning also applies to flux

i. After paying attention to the orientation of the axis x the following system results (Eqn 2.11).

$$\begin{cases} \frac{di}{dx} = (K + S)i - S j \\ \frac{dj}{dx} = S i - (K + S)j \end{cases} \quad \text{Eqn 2.11}$$

The mathematical solution to this system was presented in an article by Kubelka and Munk²¹. After simplification of the general solution other measurements than the coefficients of absorption and scattering become apparent. The final solution presents itself then in the condensed form (Eqn 2.12)

$$R = \frac{1 - R_g \cdot (\varsigma - \vartheta \cdot \coth(bSX))}{\varsigma - R_g + \vartheta \cdot \coth(bSX)} \quad \text{Eqn 2.12}$$

$$\text{with } \varsigma = \frac{(S + K)}{K} \text{ and } \vartheta = \sqrt{\varsigma^2 - 1}$$

where R_g is the reflectance of the supporting layer. It should be noted that R_∞ , the reflectance limit, is achieved when R_g tends toward infinity. Study of the equation shows that R_∞ depends on the interaction of K and S which leads to the relationship:

$$\frac{K}{S} = \frac{(1 - R_\infty)^2}{2R_\infty} \quad \text{Eqn 2.13}$$

The function $\frac{(1 - R_{\infty})^2}{2R_{\infty}}$ is known as the Kubelka-Munk function²². It can be seen that the measured reflectance is a function of the ratio of two constants, K and S and not their absolute values. Quantitative analyses can be achieved using the following equation.

$$\frac{K}{S} = \frac{\ln 10 \cdot a \cdot c \cdot \varepsilon(\lambda)}{S} \quad \text{Eqn 2.14}$$

where c is the analyte concentration, a is the absorptivity and $\varepsilon(\lambda)$ is the pathlength. This equation describes the logarithmic proportionality existing between K and the analyte concentration.

Although detailed investigations of the theory of diffuse reflectance spectrometry by many workers (e.g. Berntsson²³; Birth²⁴; Gerken²⁵; Maier²⁶; Reynolds²⁷; Tsai²⁸; Tsuchikawa²⁹) have been carried out since the turn of the century, only rarely are the treatments resulting from these studies useful in practice. A simple log (base 10) conversion of reflectance values is effective for many powdered samples being analysed by near infrared reflectance spectroscopy.

2.2. Hardware

2.2.1. Spectrometer Designs.

2.2.1.1. Fourier Transform (FT)

Fourier Transform Infrared (FTIR) spectroscopy has been well described (see Chen³⁰; Holland³¹; Iwata³²; Lin³³; Mattu³⁴; Noda³⁵; Petty³⁶; Reshadat³⁷) and only a brief review will be presented here. The theoretical basis of Fourier transform spectroscopy is that one light beam is split into two equal rays and their relative optical paths are changed. The resultant output of the recombination of the rays is then observed. For interference to occur a phase difference must exist between the two rays. A phase difference can be caused by lengthening the optical path distance, or by changing the refractive index and thereby slowing the velocity of the ray over the same distance³⁸. Large laboratory based instruments have achieved wavelength resolutions³ of < 0.00001 nm although for general use in the NIR region, > 2 nm resolution has been shown to be sufficient for use in the pharmaceutical industry³⁹ and is anticipated to be similar for other applications. All-fibre-optic Fourier transform spectrometers have been developed which use the dependency of refractive index on temperature to alter the optical path sufficiently that an interferogram, and hence the relevant data, can be acquired⁴⁰. Unfortunately this type of instrument has a relatively slow scan rate due to the time required for temperature changes. A piezo-electrically adjusted Fabry-Perot interferometer (Etalon) has also been developed which has relatively rapid scan rate, allowing an interferogram to be scanned at 6 μ s intervals⁴¹. Another Michelson type interferometric system which uses two prisms separated by a mechanical drive mechanism to adjust the

optical path distance has also been tested⁴². Optical path difference has also been manipulated by precisely stretching the optical fibre in an instrument⁴³. Fourier transform spectroscopy can extract valuable information from all wavelengths simultaneously although some systems use monochromatic light input. There are several input systems currently in use, not the least of which is an acousto-optical tunable filter (AOTF) which has the capability of selecting a particular wavelength of interest or scanning the entire range available if required. AOTFs have very high scan rates, currently of the order of a few μs and a high resolution (a few tenths of a nanometer)⁴⁴, although throughput is poor (typically $\sim 49\%$). AOTFs are discussed in more detail below.

2.2.1.2. Diffraction Gratings

Reflective diffraction gratings are frequently used in conventional spectrometers. The reflective surface of the grating is finely ruled (sometimes as often as 2400 lines per millimetre) with a specially shaped instrument to create a blaze angle to optimise the efficiency of the grating in the wavelength range of interest³. When a light beam is incident on a blazed diffraction grating, a significant portion of the available energy can be concentrated in the desired diffractive order instead of being specularly reflected as would otherwise be the case. The efficiency of a diffraction grating is in most cases less than 80% at the optimised wavelength and efficiency drops off rapidly away from this wavelength. The effective bandwidth of a diffraction grating is strictly limited by the choice of blaze angle and line frequency and is inversely proportional to the resolution capability. The theoretical resolution limit of a diffraction grating is dependent on the total number of diffracting lines.

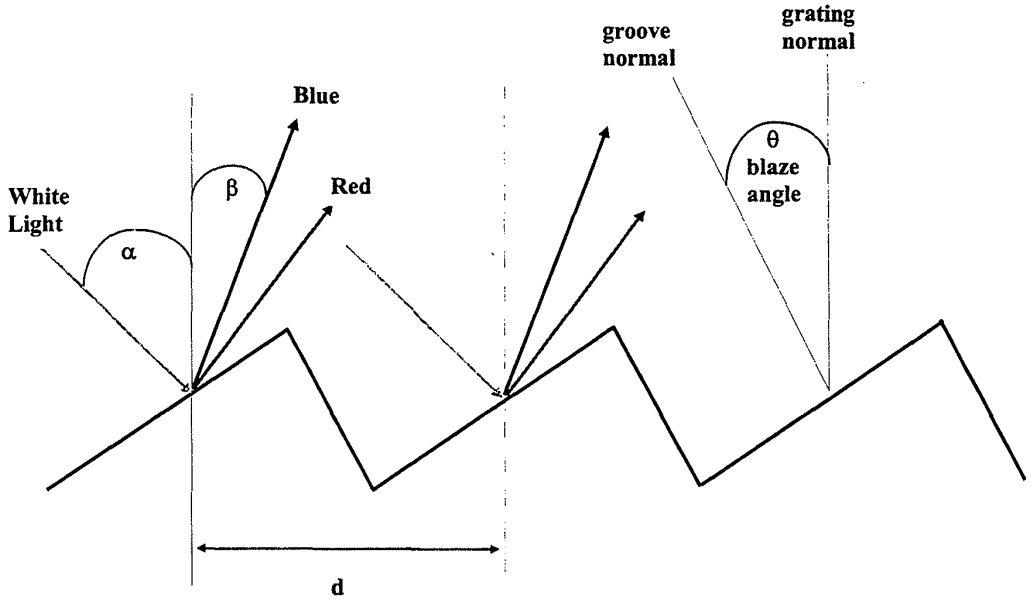


Figure 2.7. Diagrammatical representation of a blazed diffraction grating with defining angles.

For a typical grating 25 mm wide and 1200 lines per mm a resolution of approximately 3×10^{-2} nm is achievable. For a diffraction grating illuminated by a collimated beam of light of wavelength λ , incident at an angle α to the grating normal and reflected at an angle β on the opposite side of the normal (see Fig. 2.7), the grating equation is given by

$$d(\sin \alpha - \sin \beta) = m\lambda \quad \text{Eqn 2.15}$$

where m is the order of diffraction and d is the periodic distance of the grating.

If the grating has N lines, the intensity of diffracted waves, $I(\beta)$, is given by

$$I(\beta) = R(\theta, \beta) I_0 \frac{\sin^2(N\pi d \sin \beta / \lambda)}{\sin^2(\pi d \sin \beta / \lambda)} \quad \text{Eqn 2.16}$$

where I_0 is the incident light intensity and $R(\theta, \beta)$ defines the grating efficiency.

There are two main types of gratings: the classical ruled grating (described above) and the concave holographic grating. The holographic grating was developed to overcome imperfections inherent in mechanically ruled gratings by the creation of grooves on a photosensitive material using the interference pattern of two intersecting lasers. It is a hybrid device which both disperses and focuses ; the result of which is a compromise in which neither is performed as well as would be with individual components. However, use of this technology has enabled the production of gratings with a ‘flat-field’ output suitable for use with flat semiconductor photo-detectors. They are also capable of close to uniform efficiencies over a much broader band width than the classical ruled grating. Use of this type of grating has the added benefit of reducing of the number of components required for a spectrometer design. A comparison of each type of grating is given in the Table 2.2.

Gratings suffer from a phenomenon called ‘overlapping orders’, that is, where longer wavelengths from one order overlap shorter wavelengths of the next highest order. This necessitates the use of order sorting filters to restrict the effective bandwidth of the instrument. Since prismatic wavelength dispersion is not a result of wavefront interference patterns, prisms do not suffer this phenomenon.

Table 2.2. Comparison of Ruled and Holographic Gratings (adapted from Hayat⁴⁵)

Property	Classically Ruled Gratings	Holographic Gratings
Efficiency	60-99% (at blaze)	At maximum 35-99%. Efficiency curve can be made flatter than ruled gratings to cover wider spectral domain. In blazed holographic gratings, efficiency curve is identical to ruled gratings.
Ghosts	Approximately 10^{-5} of line	No ghosts
Scattered light	At best 10^{-5} to 10^{-6} at 5 Å of laser line in the visible	10^{-6} to 10^{-8} at 5 Å of laser line in the visible
Size	Generally limited to 200 mm x 200 mm for groove spacings of more than 600 g/mm	Up to 430 mm diameter in all groove spacings. Much larger size, up to 1 m is possible
Groove density	Maximum of 3600 g/mm; in general, stray light increases drastically with groove density	Up to 6000 g/mm. Stray light dose not increase with groove density
Aberration correction	Not possible	Possible

2.2.1.3. Prisms

Although grating spectrographs achieve higher resolving powers, they are generally more wasteful of light because they produce many orders of diffracted rays. Alternatively, a typical prism has a theoretical resolution limit of

approximately 0.3 nm (50 mm base, $dn/d\lambda = 4.7 \times 10^{-5}$, at 750 nm) and can be usefully employed when high resolution is not a significant factor. Rays of light corresponding to each wavelength component emerge mutually parallel after refraction by the prism and are viewed by a telescope focused for infinity³. When an incident beam (from an entrance slit) is focused through a prism, the emerging spectrum will focus in two dimensions in a manner similar to the exit beam focusing in the diffraction grating case. This will vertically intensify the available energy but reduce the resolution because the slit image can suffer slight aberrational blurring.

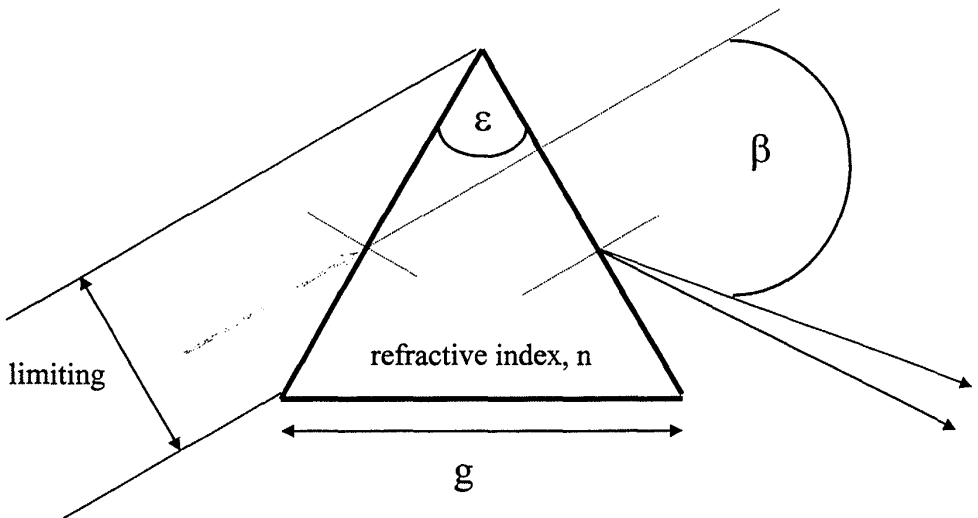


Figure 2.8. Dispersion of white light through an equilateral prism.

When passing through a prism, light is deflected by an angle β according to its incident and exit angles, the angle of the prism, ϵ , and the refractive index, n , of the prism material (Fig. 2.8). If the incident and exit angles are equal, the light travels parallel to the base of the prism and β defines the angle of minimum deviation. Under this condition, the angular dispersion, $d\beta/d\lambda$, is independent of

the prism dimensions and is a function of the prism angle and the dispersion, $dn/d\lambda$, through

$$\frac{d\beta}{d\lambda} = \frac{2 \sin(\varepsilon/2)}{\sqrt{1 - n^2 \sin^2(\varepsilon/2)}} \frac{dn}{d\lambda} \tag{Eqn 2.17}$$

The resolving power, $\lambda/\Delta\lambda$ is given by

$$\frac{\lambda}{\Delta\lambda} = g \frac{dn}{d\lambda} \tag{Eqn 2.18}$$

where g is the base width of the prism.

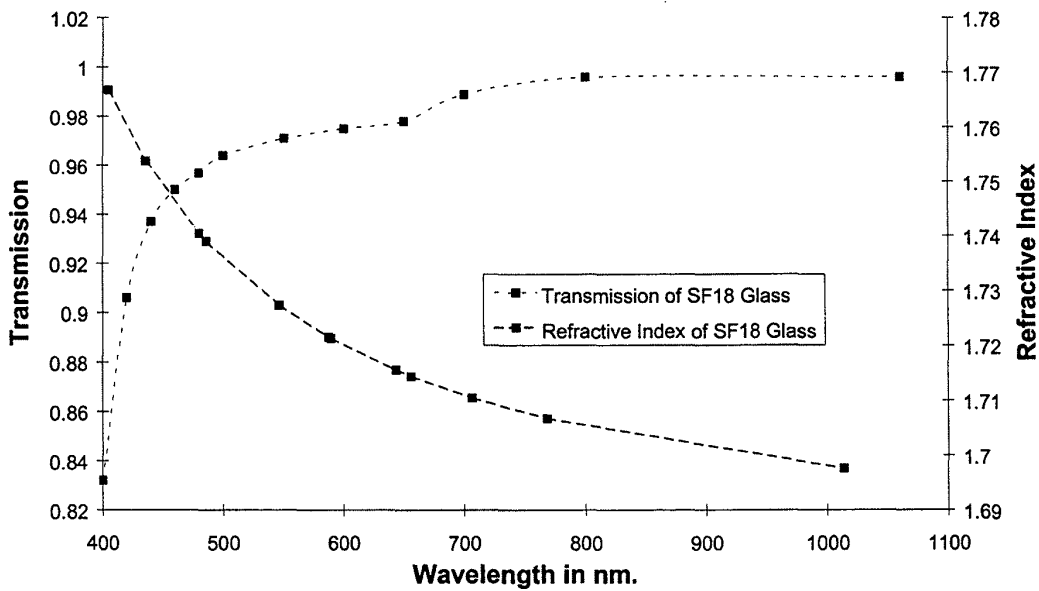


Figure 2.9. Transmission efficiency and refractive index of SF18 glass (10 mm thickness) as a function of wavelength in the visible (VIS) and NIR region.

Dispersion of a prism can be described by the wavelength-dependent difference in the refractive index for the prismatic material. For SF18 glass, a plot of refractive index versus wavelength is given in Figure 2.9 from data derived from

characteristics of the glass (Sumita Optical Glass, Inc., Urawa, Saitama, Japan).

A quadratic curve of the form

$$n(\lambda) = 1.6824828 - 5.0414119 / \lambda + 10422.619 / \lambda^2 \quad (\lambda \text{ in nm}) \quad \text{Eqn 2.19}$$

describes this relationship. The dispersion equation follows a trivial differentiation function yielding a weakly varying, linear function of wavelength in the NIR region.

2.2.1.4. Acousto-Optical Tunable Filter (AOTF)

An ATOF is an all-solid-state, electronic dispersive device which is based on the interaction of light and ultrasound⁴⁴. When an electric radio frequency (RF) signal is applied to a piezoelectric layer, attached to an anisotropic crystal, (typically paratellurite (TeO_2)), a diffracting grating is created⁴⁶. The acoustical wave produced in the crystal together with the spatial parameters of the crystal create a standing wave which defines the parameters of the diffraction grating. The Bragg equation (Eqn 2.20) describes the relationship between the wavelength and to the acoustic frequency which is dependent on the RF signal. Their aperture is typically $\sim 4 \times 4$ mm. It is this standing wave which acts as a diffraction grating to the incident light and so separates the incident light into a non-deviating polychromatic beam and two diverted oppositely polarised monochromatic beams of the wavelength which interacts with the spacing of the standing wave.

$$m\lambda = 2d\sin\theta \quad \text{Eqn 2.20}$$

where d is the period of the standing wave in the crystal, m is the order of diffraction and θ is the incident angle of the input radiation.

When polychromatic, collimated light is incident on the AOTF it is split into two, orthogonally polarised beams fulfilling the requirements of the Bragg equation and another beam of the remainder of the light. AOTFs have an extremely fast response time ($\sim 2\mu\text{s}$), high diffraction efficiency (typically $> 90\%$), high resolution (0.08 nm at 253.4 nm) and a wide tuning range (> 253 to 2500 nm)⁴⁷. The most significant disadvantages of AOTF are its low throughput of light (typically $< 4\%$, (Brimrose Corporation of America, 2000) and high sensitivity to temperature variation.

2.2.2. Light Source

Tungsten when heated to 2900 K (the normal operating temperature for quartz tungsten halogen (QTH) bulbs) has a peak emission at approximately 1000 nm, which coincides closely with the peak efficiency of a silicon (Si) based detector at approximately 950 nm^{3, 48} (Fig. 2.10). The life of a QTH lamp is dependent on its operating temperature, as is the spectral distribution of the output. Output is generally specified by QTH bulb manufacturers to be within 2% until failure, if operated at recommended voltage. To maximise the efficiency of a tungsten bulb, in terms of power and heat dissipation, as much as possible of the available radiant energy needs to be collected and focused to a convenient location. Parabolic reflectors are commonly employed with the filament positioned at the parabola focal point to generate a collimated beam of light (see for example, a

design reported by Musselman⁴⁹ which uses two parabolic reflectors). The finite extent of the filament (typically 4 mm) limits the effectiveness of collimation.

The Nernst glower is an alternative light source which is used in IR spectroscopy. This source has an electrode constructed from refractory material which is resistively heated to emit radiation from the visible to IR region (0.5 ~30 μm), although the visible/near infrared content is very low. Continuous and pulsed arc lamps are another source of radiant energy. Both are discharge sources but the pulsed arc generally has higher output in the ultra-violet (UV) region than the continuous arc. Optical designs can be more efficient using this type of source because they have a very small source region (electrode gap, typically < 1 mm), making focussing more precise. Their spectral output is weighted towards the shorter wavelengths (<500 nm) because of the extremely high operating temperatures compared to that of QTH lamps (typically > 5500°C and 2900°C, respectively). However, the output in the NIR region is comparable to the output of QTH lamps of the same power rating. Their elevated operating temperature makes them difficult to use in terms of heat management and their inherent arc noise and additional driver electronic noise can contribute additional noise to the system unless care is taken to avoid it. Because the cost of using a discharge source is very much higher than a QTH system and can have difficulties (electronic noise and heat) attached to it, a QTH is generally preferred, except in applications requiring high intensity visible light.

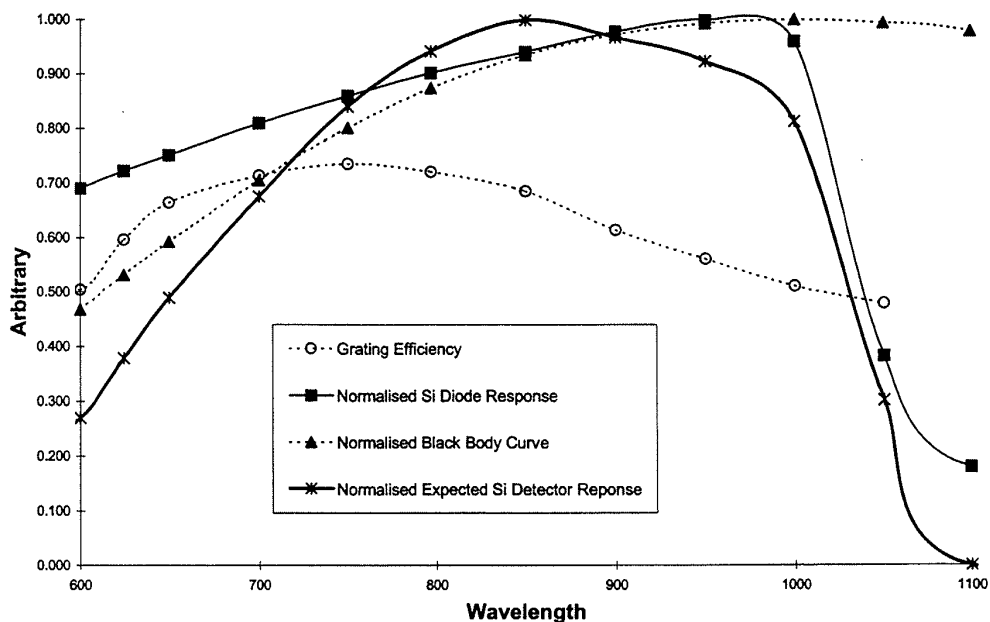


Figure 2.10. Blackbody curve at 2900°C, typical silicon detector response and diffraction grating efficiency curve (flat, ruled, gold coated, blazed for 750 nm, 1200 grooves per mm (Edmunds Scientific Co)). Normalised detector response is based on the convolution of grating, light out and detector response.

2.2.3. Detectors:

Low cost spectrometric designs employ silicon based detectors, as either linear photodiode arrays (PDA)(e.g. Zeiss MMS1, Carl Zeiss, Jena, Germany) or linear charge-coupled devices (CCD)(Ocean Optics S1000, Dunedin, Florida,USA.). Generally PDAs have a deep-well electron storage capacity ~ 100 times higher than that of CCDs which gives the PDA devices a competitive edge in terms of signal to noise ratio at high signal levels. Signal to noise of CCDs can be enhanced using a variety of techniques described below. CCDs have a higher (~ 100 to 1000 times) sensitivity than PDAs, although the sensitivity of PDAs can be enhanced by increasing the pixel size.

Area CCD arrays can be useful if spectral imaging is required. In such cases the area of the CCD can be optically segmented to provide spectral information from spatially separated sample areas. Area array CCDs have been used in designs described by Bellon *et al.*¹² and Martinsen and Schaare⁵⁰ and has been incorporated in some products from Oriel (Oriel MS127i and FICS, Stratford, CT, USA.).

Choice of semiconductor material used in the construction of a spectrometer is dependent on the spectral region under investigation, signal to noise ratio desired, sensitivity and desired cost. Sensitivity or detectivity (D) is often parameterised in terms of noise equivalent power (NEP). NEP is defined as the amount of signal required to generate a signal equal to the root-mean-square (*rms*) noise output from the detector; D is the reciprocal of NEP. D* (normalised D) compensates for differing detecting areas and operational frequencies. D* and spectral bandwidth for some commonly used semiconductor materials are listed below (Table 2.3).

Noise on photo-detection systems originates from two main sources, photon and electronic. The detection of light is a discrete process because the creation of photo-electrons results from the absorption of the photon. The detected signal is a function of the statistics of the quantum nature of the arriving light and thus has a Poisson distribution. Variation on this signal will have a root squared relationship to the mean number of arriving photons^{48, 51} (Eqn. 2.21).

$$\begin{aligned} \text{Photon Noise}(N_{Ph}) &= \sqrt{(2 \cdot \eta \cdot E_p \cdot A_d \cdot T_i)} \\ &= \sqrt{\overline{N}_p} \end{aligned}$$

Eqn 2.21

where η = quantum efficiency, E_p = photon irradiance, A_d = pixel area, T_i = integration time and \overline{N}_p = mean number of arriving photons. N_{Ph} noise is given in electrons.

Table 2.3. Bandwidth and normalised reciprocal NEP (D*) of some semiconductor materials and photodetector devices.

Semi-conductor Material	Wavelength	D* (cm Hz ^{0.5} W ⁻¹)
	Range (nm)	
Silicon (Si) PDA	300-1100	2x10 ⁹
Silicon (Si) CCD	300-1100	4x10 ¹²
Indium-Gallium-Arsenide (InGaAs)	800-2000	1x10 ¹²
Lead-Sulphide (PbS)	800-3800	4x10 ¹¹
Mercury-Cadmium-Zinc-Telluride (HgCdZnTe)	2000-12000	3x10 ⁷

Electronic noise on semiconductor photodetectors like a silicon photodiode array (PDA) or charge-coupled devices (CCDs) comes from a number of sources. For example, readout noise and white noise arising from the driver/amplifier electronics, the shot noise of the biasing of the photodetector (dark current shot noise), and the shot noise due to the photo-current may be present. Whenever there is a flow of electrons shot noise can be expected. It is a statistically based noise due to the arrival rate of electrons and thus has a Poisson distribution and a variation in signal (in electrons) with a square root proportionality (Eqn. 2.22). Dark current shot noise sets the limit of detectability of the signal. If the photon-

current is below the dark current shot noise level it will not be distinguished from it.

$$\text{Dark Current Noise } (N_{DC}) = \sqrt{\frac{(J_d \cdot T_i \cdot A_d)}{q}} \quad \text{Eqn 2.22}$$

where J_d = dark current generation density and q is electronic charge. The photo-electron shot noise (N_{PE}) has the same equation. N_{DC} noise is calculated in electrons.

The readout cycle creates its own noise in the form of reset and white noise which are defined (in terms of electrons) by

$$\text{Reset Noise } (N_{RS}) = \sqrt{\frac{(k \cdot T \cdot C_o)}{q^2}} \quad \text{Eqn 2.23}$$

and

$$\text{White Readout Noise } (N_{WR}) = \sqrt{\left(\frac{8 \cdot C_o^2 \cdot \Delta f \cdot Z_o \cdot k \cdot T}{3 \cdot q^2 \cdot G} \right)} \quad \text{Eqn 2.24}$$

respectively, where k = Boltzmann's constant, C_o = load capacitance, Δf = amplifier bandwidth, G = amplifier voltage gain, Z_o = amplifier first stage output impedance, T = absolute temperature and q = electronic charge.

The total *rms* noise for a system is calculated by the following equation:

$$\text{Total Noise } (N_T) = \sqrt{(N_{DC}^2 + N_{WR}^2 + N_{PE}^2 + N_{RS}^2)} \quad \text{Eqn 2.25}$$

When the detector is blacked out and a measurement made, the resulting dark current contains all the noises except the photon noise due to the light signal and the photo-electron shot noise. Because photo-electron noise is equated to the square root of the photo-electron signal, if the average signal is 3600 counts the N_{PE} due to the signal will be ~ 17 counts (assuming a typical CCD photo-electron to count conversion rate of 13 to 1 (Table 2.4)). If the typical dark current contribution is 1 count then the main source of noise in a non-dark measurement is shot noise due to the photo-current thus a larger signal will have a larger N_{PE} value but a higher SNR ratio. PDAs have a deep well structure allowing them to accumulate much more signal than a single pixel of a CCD (typically 100 times greater), although binning and/or accumulation of a number of readout cycles can compensate. Specifications for PDAs and CCDs given in Table 2.4 originate from Oriel Corporation's⁵² product information and can be used to develop estimates for typical SNRs for both PDAs and CCDs. For a typical CCD (ignoring N_{WR}) operating near saturation (using data from the Table 2.4):

Dark current = 13 e and at saturation = 2.5×10^5 e, therefore

$$\text{SNR} = \frac{250000}{\sqrt{(250000 + 13^2)}} \approx 500 : 1 \quad \text{Eqn 2.26}$$

and for a typical PDA photodiode array (ignoring N_{WR}) operating near saturation (using data from the Table 2.4):

Table 2.4. Typical characteristics of some detectors used in commercial spectrometers (Oriol Corp.⁵²). (Electronically summing groups of pixels is called binning.)

	PDA	CCD (256 binned)
Energy	at 600nm = $3.3107e^{-19}$ J	at 650nm = $3.056e^{-19}$ J
Pixel Size in μm	25 x 2500	27x27
Detection Limit	$3.3e^{-12}$ J cm^{-2}	$3.8e^{-15}$ J cm^{-2}
	$2.063e^{-15}$ J/pixel	$7.092e^{-18}$ J/binned pixels
	3800 electrons	13 electrons
Dark Current	$0.1e^{-12}$ A	$0.1e^{-15}$ A
	<2 counts	1 count
Saturation Exposure	$107e^{-9}$ J cm^{-2}	$250e^{-12}$ J cm^{-2}
	$6.688e^{-11}$ J/pixel	$4.666e^{-13}$ J/binned pixel
	125×10^6 e	250×10^3 e
		810×10^3 e (binned)
S/N	10000:1	900:1 (binned)
Electrons per count	1800 e	13 e

dark current = 3800e and the signal = 125×10^6 e , therefore

$$\text{SNR} = \frac{125000000}{\sqrt{(125000000 + 3800^2)}} = 10586 : 1.$$

Eqn 2.27

SNR of CCDs can be enhanced by binning across pixels, although this strategy is implemented at the expense of resolution. SNR should be improved by a square root proportionality to the number of pixels binned, however, in some cases, the physical storage capacity of readout buffers reduces the actual improvement (evidenced below). Since the dimensions of CCDs are frequently many times smaller than PDAs (~ 90 times in the given example) SNR can reach easily

acceptable levels. For example, a typical CCD might have a 1024 x 256 matrix of pixels, each 27 x 27 μm , so binning all 256 pixels vertically will give a theoretical SNR increase of 16 times and a new SNR estimate (using the above data) of 8000:1. The discrepancy between the calculated value and that presented in Table 2.4 (SNR = 900:1) is due to the manufacturers specified binned saturated exposure being ~ 9 times less than a simple summation of the individual pixels. With alternative readout processes the actual improvement in SNR may be enhanced.

The readout time for CCDs and PDAs can be very short, $< 4 \mu\text{s}$ per pixel, dependent on the clock speed of the analogue to digital converter (ADC) used. The pixel reset function for most CCDs occurs as part of and during the readout cycle time unlike most PDAs which, frequently require a separate reset time. Therefore CCDs can potentially acquire data at a faster rate since dead-time is reduced (a useful facility when assessing rapidly moving fruit). PDAs offer higher signal precision (or SNR) than CCDs (unless binning or multiple reads are used) but CCDs offer higher sensitivity. Since CCDs generally have smaller pixel dimensions than the PDAs, the wavelength resolution available in CCDs is generally higher than PDAs for a given instrument size. When data acquisition rate is the major consideration, response times and responsivity of the CCDs make them superior to PDAs in low signal level conditions. Also, enhanced quantum efficiency, low read out noise, wide dynamic range and the flexible timing characteristics of CCDs make them prime candidates for low-light applications⁵³.

The final detector response will represent a convolution of light source output, diffraction grating efficiency, glass transmittance and detector response. Interaction is inevitable between detector, light source and diffraction grating and thus these characteristics must be considered in the design process.

2.3. Fruit Quality Components

Angiosperm fruit consists of 'fertile', ie. seed bearing, leaves (sporophylls) fused to enclose and so protect the seed (creating a carpel). Several megasporophylls can be fused, parietally or centrally, to create a multi-chambered structure. In fleshy fruit (berry and hesperidium) the fruit remains fleshy at maturity. According to fruit type, different tissue growth is accentuated to form the edible component. For example, rockmelon fruit consists of the outer exocarp (skin), the outer mesocarp (the non-edible flesh just below the skin), the inner mesocarp (the inner edible flesh close to the seed cavity) and a thin layer of endocarp. In citrus the exocarp and mesocarp form the skin, with oil glands, and cells in the endocarp produce extensions (juice sacs) within the seed cavity.

Taste is a subjective measurement reflecting a primary (sweet, sour, bitter) sensation overlain by an olfactory sensation (esters) and texture of the sample (e.g. crispness)⁵⁴. Since NIR spectroscopy is a secondary correlative measurement technique its accuracy depends on the accuracy of the primary measurement method. The use of subjective analyses presents difficulties in accuracy but this type of assessment is still possible. For example, visible and

near-infrared (VIS/NIR) spectroscopy was used by Kawamura *et al.*⁵⁵ to generate calibration models (MLR) for rice taste evaluation of 61 short-grained rice samples. They found that the developed calibrations were not adequate to justify replacing sensory tests with the calibration model for evaluating rice taste however the results indicated that VIS/NIR technology could be used in classifying rice samples into broad qualitative groups, such as poor taste, better taste and best taste.

Fruit eating quality is generally linked to soluble solids content (SSC) or sugar (sucrose) content, with organic acid content (or sugar/acid ratio) playing an important role in some fruit types (e.g. citrus, pineapple). NIR spectroscopy was first applied to the measurement of SSC in melons by Dull *et al.*⁵⁶, operating in a reflectance mode. A standard error of prediction (SEP) of 1.6% for sliced fruit and 2.2% for intact fruit was reported. Subsequent reports of the use of NIR spectroscopy to assess the SSC of intact melon fruit show a progressive decrease in the SEP, from 2.2%⁵⁷ and 1.9%⁵⁸ to 0.4%⁵⁹. This improvement reflects change in the instrumentation used, in the optical geometry (light-sample-detector alignment) employed, and the use of improved chemometric techniques. NIRS technology is now in commercial use in Japan (e.g. Fantec, Mitsui), with a reported SEP of 0.5%.

Fresh fruit samples have high water content (typically 70% w/w)⁶⁰. The quality of spectral data is degraded by the presence of water due mainly to the effects of shifts and broadening of spectral peaks, even those not associated with OH groups. Temperature variation further exacerbates this situation by causing peak

shifts frequently linearly related to increasing values⁶¹. The SW-NIR region has an advantage in this respect in that water peaks are localised to two main regions (centred on ~ 760 and 970 nm) leaving the remainder of this region available for analysis.

NIR fingerprints of macro-constituents are commonly due to either O-H or C-H bonds (e.g. water, carbohydrates - sugar alcohols, sucrose, fructose and glucose). Warrington and Weston⁶² listed (see Table 2.5) some macro-constituents of fruit most of which have been shown to be quantifiable using NIR spectroscopy.

Table 2.5. Typical concentration (% by dry weight) of some macro-constituents of fruit.

Component	% by dry weight
Water	80-88
Carbohydrate	12-18
Organic Acids	1.0-2.5
Protein	0.11-1.2
Lipid	0.07-0.9
Minerals	0.45-0.74

Absorption in the NIR spectral region is extremely weak, therefore the identification of macro-constituents is the most common use of this technology. However, Aldridge⁶³ detailed the use of an automated system for at-line analysis of sulphur residues in pork products by thin layer chromatography which had detection limit of 80 pg for sulphurmethaxine spotted on a plate. Also, using NIR spectroscopy and a partial least-squares algorithm, very good calibration

statistics were obtained by Schulz *et al.*⁶⁴ for the prediction of gallic acid (concentration range = 0.01-0.2%), caffeine (0.3-5%), and theobromine (0.02-0.4%) with standard deviation/standard error of cross-validation (StDev/SECV) ratios ranging from 2.00 to 6.27. These substances have been identified as those contributing to varying taste attributes of tea. Dry matter content of the tea leaves was also analysed very precisely ($R^2 = 0.94$; StDev/SECV = 4.12) and it was possible to discriminate tea leaves of different age by principal component analysis.

Texture also contributes to taste perception. Lammertyn⁶⁵, in a study to determine the potential of VIS/NIR spectroscopy as a non-destructive measurement technique for measuring quality characteristics of Jonagold apples developed good predictive models (typically $R =$ of 0.93) for the prediction of pH, soluble solids content and stiffness factor although other texture parameters such as the elastic modulus of the flesh did not correlate as well. The proposed model for the stiffness factor and for the elastic modulus had SEPs of 2.49 and 0.26 respectively and an R of 0.90 and 0.75 respectively. Texture (crispness) probably reflects the turgor of cells, that is , the balance of solutes inside and outside the cell, thereby making NIR spectrometric assessment difficult.

2.3.1. Scattering and Absorption Centres

Osborne *et al.*⁶⁶ have discussed the physical principles of NIR reflection and transmission measurements relevant to the fruit processing industry in detail therefore only a brief overview will be given here. In the transmission mode of operation (illumination/detector angle $\sim 0^\circ$), light emerging from the fruit will be

Underpinning Technologies

an isotropically scattered beam. It will contain more information, with respect to the composition of the specimen than reflectance mode but will be weak due to attenuation by greater distances of travel within the fruit⁶⁷. A more powerful light source will alleviate the problem of low signal intensity but may introduce other problems, e.g. high heat loads.

When the illumination/detector angle is increased the detected signal may also contain specularly reflected light (reflectance mode). Data acquired using reflectance mode originates from a shallow sample region close to the fruit surface. Predictive models generated from data acquired using reflectance mode therefore utilise a form of double correlation. This correlation is established between spectral data from a shallow sample region and the analyte value (for the attribute of interest) which is generally determined from tissue from greater depths. For this reason many workers in this field prefer to use transmittance mode as new detector technologies make acquisition of the inherently weaker signals possible^{68, 69}. Use of full transmittance optics will, however, not be appropriate for fruit having a large, optically dense central seed (e.g. mango).

2.4. Chemometrics

Chemometrics is frequently defined as the application of mathematical, statistical, graphical or symbolic methods to maximise the chemical information which can be extracted from data⁷⁰. Chemometrics started in its present form around the early 1970s due largely to the efforts of Karl Norris. The use of the

term *chemometrics* first appeared around 1971⁷¹ to describe the growing use of mathematical, statistical and other logic-based methods in the field of chemistry and in particular analytical chemistry.

Multivariate analysis, as used by chemometricians, is any statistical, mathematical or graphical approach which considers multiple variables (dependent and independent) simultaneously. This description is slightly different from the statisticians' definition of multivariate analysis, which requires that multiple dependent variables be considered simultaneously in the analysis. It has been suggested that chemometricians should refer to what they do as multivariable analysis as this would eliminate confusion. This recommendation for the chemometric definition of multivariate analysis will be used for this work.

One of the primary goals of chemometrics is to reduce the number of dimensions needed to accurately describe the characteristics of the data set. This can be achieved by a variety of methods, e.g. selecting an important subset of the original variables, or creating a set of new variables which are more efficient than the original variables in describing the data. Two possible methods for the creation of new variables are projection and mapping. Projection is the more common technique and involves using weighted linear combinations of the original variables to define a new, smaller set of variables (latent variables or principal components) which contain nearly as much information as the original variables. The most frequently used projection technique is the principal components technique.

2.4.1. Data Treatments

The financial and temporal costs of the acquisition of good data is generally high, therefore extraction of the maximum amount of information is desirable. Chemometrics can achieve this in several ways, for example, data pretreatment techniques can assist by distinguishing overlapping spectral features using methods such as mean centring, differentiation, least squares peak and curve resolution and Fourier spectral deconvolution. Some data pretreatment techniques accomplish signal processing, e.g. increase the signal to noise ratio (SNR) by distinguishing between signal and noise, extracting the latter. Use of appropriate data pretreatment techniques can assist in obtaining reliable robust solutions to prediction problems. Some commonly used methods are discussed below.

2.4.1.1. Mean centring of spectra

As a first step in data pretreatment, data are frequently mean centred by subtraction of the mean absorbance spectrum (\bar{S}) of the calibration data set (S), (Eqn. 2.28). This step ensures that all results are interpretable in terms of variation about the mean spectrum. The mean spectrum is calculated as:

$$\bar{S}_k = \frac{1}{I} \sum_{i=1}^I S_{i,k} \quad \text{Eqn 2.28}$$

Subtraction of the mean spectrum will remove common, non-informative artefacts from the spectra highlighting features resulting from differences in analyte concentration.

2.4.1.2. Smoothing

Vibrational/rotational absorption peaks in the NIR spectral region are relatively broad (typically 40 nm). It is therefore not surprising that spectral resolution better than 10 nm (FWHM) has been demonstrated not to be necessary for good predictive model generation⁷². Smoothing within this bandwidth limit can greatly reduce the high frequency noise components in the spectra. A number of smoothing techniques are available, for example boxcar, Fourier, wavelet and Savitsky- Golay smoothing.

Boxcar smoothing is the simplest technique. It copes very well with data with broadband features like those inherent in NIR spectra. In this method the signal is convoluted with a box-like function. Thus, to find a value of a smoothed spectrum at some point, i , an average of all points between $(i-w)$ and $(i+w)$ is taken, where w is a box half width. It is the computationally least expensive method but will reduce resolution.

When data is smoothed using the Fourier transform, it is firstly transformed to the frequency domain where undesirable frequencies are removed (zeroed). These data are then inverse-Fourier transformed to the original time domain, returning to a signal like the original one but with the high-frequency components removed. In order to minimise adverse effects (Gibbs phenomenon, ringing) caused by abrupt cutoffs, apodisation should be used. That is, the observed signal is convolved with the Fourier transformed apodisation function; simply, the amplitudes of the frequencies close to the cut-off value are attenuated to smaller values. This method has a high computational cost but copes very

well with high frequency noise (dependent on correct choice of cutoff frequency).

Wavelet smoothing is a method derived from the principles of Fourier smoothing. Instead of performing a frequency analysis of the data, a scale analysis is used. A sinusoidal based transformation is perfectly localised in frequency but not in wavelength, whereas a wavelet transformation is localised in both wavelength and frequency. Wavelet transformation maps a single dimension wavelength signal into a joint, two dimensional wavelength-scale plane. Data can be easily smoothed by thresholding the ‘detail’ components at the desired level before signal reconstruction is performed. The resultant signal is the original signal without the high-frequency components and without degrading spectral information, if appropriate parameters are chosen. This method has a high computational cost.

The Savitsky-Golay algorithm is based on the application of least squares linear regression to fit a polynomial over a moving window centred on the point in the spectrum to be smoothed. The choice of polynomial order and/or window size may seriously degrade spectral information of the transformed spectrum so caution should be exercised when using this technique. A characteristic of this procedure is that noise is reduced approximately by the square root of the number of points used⁷³.

2.4.1.3. Differentiation

Differentiation is frequently used to enhance difficult-to-identify structures by removing sloping baselines and separating overlapping peaks. The goal of differentiation is to remove background and to increase spectral resolution⁷⁴. For example, Kawano *et al.*⁹ had success ($R = 0.97$, $SEP = 0.50$, peaches) using multiple linear regression (four wavelengths, 906, 878, 870 and 889 nm) and second derivative of the absorbance data to determine the SSC content of peaches. Two main methods used to derivatise a data sets are the numerical method and the Savitsky-Golay method.

For a first order derivative, simple numerical differentiating techniques calculate the difference in ordinand values over a predetermined window by subtracting lowest value from the highest and dividing by the window width. An example of a typical formula for a centred-difference differentiation is given in Eqn. 2.29⁷⁵.

$$P'_n(x_1) = \frac{f_2 - f_0}{2wind} + O(wind^2) \text{ (first derivative)} \quad \text{Eqn 2.29}$$

$$P''_n(x_1) = \frac{f_0 - 2f_1 + f_2}{wind^2} + O(wind^2) \text{ (second derivative)} \quad \text{Eqn 2.30}$$

$P_n(x)$ is the approximating polynomial of $f(x)$, f_0 is the first data point, f_1 the central point and f_2 the last data point in the selected window of width $wind$. The error term $O(wind^2)$ is dependent on the stepsize and, in application, often ignored.

Another technique which requires many more computations is the Savitsky-Golay method. The Savitsky-Golay algorithm is based on performing a least squares linear regression fit of a polynomial of degree γ over at least $\gamma+1$ data points in a moving window about each point in the spectrum which also smooths the data. The derivative is then calculated for fitted polynomial at each point. A modified algorithm for this calculation has been presented by Steinier *et al.*,⁷⁶ to calculate 1st through 9th derivatives. The calculation is performed with the abscissa data in low to high order. The e th derivative is given below (Eqn. 2.31) (note that the data set will be truncated by half the number of points in the window at each end of the spectrum).

$$\frac{d^e x}{dy^e} = (e!) \sum_{j=-\tau}^{+\tau} \mathbf{x}_i \mathbf{T}_{e+1,i-j} \quad \text{Eqn 2.31}$$

In matrix formulation this is achieved by

Let:

e = the order of the derivative

γ = the degree of the polynomial

s = the number of points to be fitted by the polynomial

$\tau = (s-1)/2$

\mathbf{x} = the vector of observed values

\mathbf{T} = the matrix of transforming coefficients

The largest single drawback with the use of differentiation is its inherent exaggeration of noise. Various smoothing functions are therefore often implemented prior and after differentiation. Differentiation using the Savitsky-

Golay method is accompanied by an inherent smoothing which reduces added differentiation noise to manageable levels. It should be noted that to apply Savitsky-Golay differentiation the step interval within a window must be fixed and uniform⁷³.

2.4.1.4. Standard Normal Variate and Detrending

Other signal improvement tools available are standard normal variate (SNV) and detrend (DT). These transformations mainly correct problems associated with sample size (pathlength) but also reduce the effects due to multi-collinearity and baseline shifting and curvature⁷⁷. SNV and DT, although often used together (either one first), can be used separately. SNV centres the spectra by dividing each data point by the mean of all data points in the spectrum and scales it to its own standard deviation, (Eqn. 2.32)

$$\mathbf{x}_{i(SNV)} = \frac{\mathbf{x}_i - \bar{\mathbf{x}}}{\sigma} \quad \text{Eqn 2.32}$$

where $\mathbf{x}_{i(SNV)}$ is the i th element of the transformed spectrum, \mathbf{x}_i is the i th element original spectrum, $\bar{\mathbf{x}}$ is the mean of the spectrum and σ is the standard deviation of absorbances at all wavelengths of the spectrum.

Detrending is applicable to spectra in which the correlation between concentration and the amplitudes of the wavelength variables is fairly linear. In practice, spectra are generally converted to absorbance ($\log(1/R)$) prior to implementation. Detrending transforms the spectra using a second order polynomial regression analysis of spectral responses (absorbance, dependent

variable) to wavelength (independent variable). Baseline curvature correction, for example, using this relationship are

$$\hat{x} = a + b \cdot W + c \cdot W^2 \quad \text{Eqn 2.33}$$

and

$$x_{i(DT)} = x_i - \hat{x} \quad \text{Eqn 2.34}$$

where \hat{x} is the estimated value of x_i calculated by Eqn 2.33. W is absorbance at a given wavelength, a , b and c are intercept and polynomial constants.

2.4.1.5. Multiplicative Scatter Correction

Absorbance spectra can be influenced by undesirable information originating from specular reflectance, particle size, path length and refractive index of the sample. Scattering is wavelength dependent and often results in a baseline offset or tilt to the spectrum. In highly scattering systems, a multiplicative effect can also occur, that is both offset and tilt. Multiplicative scatter correction (MSC) is a relatively simple spectra processing method that attempts to account for differences in measurement path lengths and scattering effects⁷⁸. The simplest implementation of MSC is based on the assumption that all samples have the same scatter coefficient at all wavelengths and uses a 'reference group of wavelengths (flat portion within or close to a spectrally significant region) to generate the MSC coefficients. This technique regresses a measured spectrum against an "ideal" reference spectrum, the mean centred spectrum (Eqn. 2.28). The measured spectra are then corrected using a slope value calculated from this regression for a 'reference group of wavelengths'.

The unknown multiplicative factor b and additive factor a are determined using :

$${}^mS_{iR} = b_i \bar{S}_R + a_i \quad \text{Eqn 2.35}$$

where R is the group of reference wavelengths.

and the corrected spectra is then given by:

$${}^{msc}S_{ik} = \frac{({}^mS_{ik} - a_i)}{b_i} \quad \text{Eqn 2.36}$$

where mS is the spectrum to be corrected and ${}^{msc}S$ is the corrected spectrum.

Isaksson and Kowalski⁷⁹ presented a slightly more complex variation of this technique (piecewise multiplicative scatter correction (PMSC)), in which the wavelength dependency of scattering was addressed by calculating a and b for each wavelength. This was achieved by regressing the absorbance value at each wavelength of a sample spectrum against a moving window of wavelengths, centred on the corresponding wavelength, of the ‘ideal’ spectrum. Vectors of correction coefficients (a and b) were then used to correct the new spectrum by the following equation (Eqn. 2.37):

$${}^{msc}S_{ik} = \frac{({}^mS_{ik} - a_i)}{b_i} \quad \text{Eqn 2.37}$$

The primary assumption of this technique is that the wavelength dependency of the scattered light is different to the analyte absorption. By correcting

multiplicative and/or additive scatter, differences between spectra due to these effects will be minimised whilst preserving analyte concentration information. Similar to SNV and DT, this technique is only applicable to spectra which have a fairly linear correlation to concentration, therefore these techniques are normally employed in conjunction with absorbance data.

2.4.1.6. Orthogonal Signal Correction

NIR spectra are often pre-processed in order to remove systematic noise. Some pre-processing techniques may also however, remove information from the spectra regarding the analyte. One technique which has been demonstrated to remove unwanted noise whilst maintaining analyte information is orthogonal signal correction (OSC). With OSC the \mathbf{X} -matrix (independent wavelength variable matrix) is corrected by subtraction of variation that is orthogonal to the \mathbf{Y} -matrix (dependent variable, analyte). Assuming the spectra have been mean centred, OSC can be achieved by the following⁸⁰:

In order to extract those \mathbf{X} (wavelengths variable) factors which include as much as possible variation in \mathbf{X} whilst remaining orthogonal to \mathbf{Y} (analyte), a vector of loading weights (w) is required. A suitable matrix formulation is $\max(w^T \mathbf{X}^T \mathbf{X} w)$ with the constraints $w^T \mathbf{X}^T \mathbf{Y} = 0$ and $w^T w = 1$.

A possible solution is that w is the first (largest) eigenvector of $\mathbf{M} \mathbf{X}^T \mathbf{X}$ where \mathbf{M} is

$$\mathbf{M} = \mathbf{I} - \mathbf{X}^T \mathbf{Y} (\mathbf{Y}^T \mathbf{X} \mathbf{X}^T \mathbf{Y})^{-1} \mathbf{Y}^T \mathbf{X} \quad \text{Eqn 2.38}$$

Because the matrix $\mathbf{MX}^T\mathbf{X}$ is not symmetric eigenvectors are more easily found directly by solving a symmetric $n \times m$ problem firstly. Let $\mathbf{Z} = \mathbf{XM}$. If c_i is an eigenvector of \mathbf{ZZ}^T and has an eigenvalue λ_i and unit length then

$$w_i = \lambda_i^{-1/2} \mathbf{MX}^T c_i \quad \text{Eqn 2.39}$$

is a normalised eigenvector of $\mathbf{MX}^T\mathbf{X}$ and has the same eigenvalue, λ_i .

The required score vectors are found by

$$t_i = \mathbf{X}w_i. \quad \text{Eqn 2.40}$$

and the vector of loadings is

$$p_i = \frac{\mathbf{X}^T t_i}{t_i^T t_i} \quad \text{Eqn 2.41}$$

$$= \frac{\mathbf{X}^T t_i}{\lambda_i} \quad \text{Eqn 2.42}$$

In the case when the number of X-variables exceeds the number of samples, strict orthogonality is obtained. Those factors orthogonal to \mathbf{Y} can be removed using

$$\mathbf{X}_o = \mathbf{X} - \sum_{i=1}^f t_i p_i^T \quad \text{Eqn 2.43}$$

(where f is the number of factors) giving an \mathbf{X}_o matrix which has the same covariance as \mathbf{Y} but not the unwanted noise.

2.4.1.7. Other Techniques

A number of other data preprocessing methods are in current use. For example, much work has been done with FTIR and analysing data available in interferograms directly⁸¹ and digital filters (to reduce noise and background) in conjunction with partial-least squares (PLS) regression have been used in the construction of acceptable multivariate calibration models⁸².

2.4.2. Multivariate Calibration

Spectroscopy is an indirect measurement technique; it relies on the ability to develop a calibration model that relates the spectral intensities at different wavelengths to the chemical composition of the product. The development of the calibration model is the crux of the use of this technology, and therefore use of appropriate methods is essential.

Chemometric analysis is subject to the normal constraints of any complex analysis technique, namely:

- The best chemometric methods must fail if the experimental data does not contain good information relating to the analyte concentration.
- It is possible to lose sight of the underlying techniques, and to inappropriately over-treat data.

Chemometric techniques are not magical, surefire methods to extract desired results from whatever data is available. They can only extract information from good data if it exists.

2.4.2.1. Classical Least Squares

The classical least squares (CLS) model^{83, 84} assumes that measurements are the weighted sum of linearly independent inputs. In spectroscopy, the CLS model assumes that measured spectra are the sum of spectra only from a combination of known pure component spectra weighted by the concentration of the analytes. Therefore, the model is:

$$\mathbf{x} = \mathbf{y} \mathbf{S} \quad \text{Eqn 2.44}$$

where \mathbf{x} is the measured response row vector (spectrum), \mathbf{S} is the matrix of pure component responses (pure analyte spectra) and \mathbf{y} is the row vector containing the weights, *i.e.* concentrations of the analytes. To generate a predictive model this equation needs to be manipulated to give the predicted analyte concentration from the vector of \mathbf{x} measurements. This is achieved by:

$$\mathbf{y} = \mathbf{x} \mathbf{S}^+ \quad \text{Eqn 2.45}$$

where \mathbf{S}^+ is the pseudo-inverse of \mathbf{S} , defined for CLS by:

$$\mathbf{S}^+ = \mathbf{S}^T (\mathbf{S} \mathbf{S}^T)^{-1} \quad \text{Eqn 2.46}$$

The main disadvantage of CLS is that all the pure responses \mathbf{S} (analyte concentrations) must either be known *a priori* or estimated from the data. This includes the responses of any minor constituents that may not be of interest themselves but may contribute to the measured signal. Given a vector of

concentrations \mathbf{c} and measured spectra \mathbf{x} , an estimate of the pure component spectra \mathbf{S}_{est} can be obtained from

$$\mathbf{S}_{\text{est}} = (\mathbf{c}^T \mathbf{c})^{-1} \mathbf{c}^T \mathbf{x} \quad \text{Eqn 2.47}$$

To obtain \mathbf{S}_{est} the concentration of all spectrally active species must be known and they must be linearly independent (otherwise $(\mathbf{c}^T \mathbf{c})^{-1}$ would not exist). Furthermore, the pure component responses must be linearly independent in order to obtain \mathbf{S}^+ . If they are not, $(\mathbf{S} \mathbf{S}^T)^{-1}$ is not defined. These assumptions can not be met for the approach of assessment of SSC in fruit.

2.4.2.2. Inverse Least Squares

It is possible to avoid the problem of having to know all constituent concentrations, that is, estimate \mathbf{S} , by using an inverse least squares (ILS) model^{83, 85}. ILS assumes that a regression vector \mathbf{b} can be used to determine a property of the system \mathbf{y} from the measured variables \mathbf{x} (a row vector, a spectrum). The ILS model is

$$\mathbf{y} = \mathbf{X} \mathbf{b} \quad \text{Eqn 2.48}$$

The regression vector \mathbf{b} must be determined using a matrix (\mathbf{X}) of \mathbf{x} measurements and the known values of the property of interest, \mathbf{y} . \mathbf{b} is estimated from

$$\mathbf{b} = \mathbf{X}^+ \mathbf{y} \quad \text{Eqn 2.49}$$

where \mathbf{X}^+ is the pseudo-inverse of \mathbf{X} . Of the many ways to determine a pseudo-inverse, the most obvious is MLR (also known as ordinary least squares). In this case, \mathbf{X}^+ is defined by

$$\mathbf{X}^+ = (\mathbf{X}^T \mathbf{X})^{-1} \mathbf{X}^T \quad \text{Eqn 2.50}$$

Collinearity of \mathbf{X} or when \mathbf{X} contains fewer samples than variables often causes this approach to fail. If the spectroscopic data is extremely ill-conditioned due to a high degree of correlation between absorbances at nearby wavelengths, which is often the case, MLR will not be successful⁸⁶. While the calibrations may fit the data, they are typically not useful for predicting the properties of new samples.

2.4.2.3. Principal Component Analysis (PCA)

Principal components analysis (PCA) is among the most versatile of all chemometric methods. It seeks to maximise the variance information present in a data set in as few new dimensions as is possible. Graphically, principal components analysis (PCA) twists the axes of the data to conform to new axes which contain a maximum amount of variance information. Mathematically, this is a simple linear algebra transformation for any number of dimensions. Principal components analysis helps to reduce the number of variables which need to be considered in an analysis, and often yields a new set of variables (principal components) which describes important, but unmeasurable properties of the system.

Principal components regression (PCR) is one way to deal with the problem of ill-conditioned matrices. Instead of regressing the system properties (e.g. concentrations) on the original measured variables (e.g. spectra), the properties are regressed on the principal component scores of the measured variables, (which are orthogonal and, therefore, well conditioned)⁸⁷. Thus, \mathbf{X}^+ is estimated as

$$\mathbf{X}^+ = \mathbf{P} (\mathbf{T}^T \mathbf{T})^{-1} \mathbf{T}^T \quad \text{Eqn 2.51}$$

where \mathbf{P} are loadings. Similarly to PCA, the number of principal components (PCs) to retain in the model must be determined; the purpose of the regression model is to predict the properties of interest for new samples. Therefore, the number of PCs that optimises the predictive ability of the model must be determined. This is typically done by cross-validation, a procedure where the available data is split between training and test sets. The prediction residual error on the test samples is determined as a function of the number of PCs retained in the regression model formed with the calibration data. The procedure is usually repeated several times, with each sample in the original data set being part of the test set at least once. The total prediction error over all the test sets as a function of the number of PCs is then used to determine the optimum number of PCs, i.e. the number of PCs which produces minimum prediction error. If all of the PCs are retained in the model, the result is identical to that for MLR (in the case of more samples than variables). Thus, it can be seen that the PCR model “converges” to the MLR model as PCs are added.

2.4.2.4. Partial Least Squares (PLS)

Partial Least Squares (PLS) regression⁸⁵ is related to both PCR and MLR and occupies a region between the two. PCR finds factors that capture the greatest amount of variance in the predictor variables, e.g. spectra. MLR searches for a single factor that best correlates predictor variables with predicted variables, e.g. concentrations of analyte. PLS attempts to maximise covariance by finding factors which capture both predictor variable variance and achieve predictor/predicted variable correlation. Of the many possible methods the most intuitive approach to calculate PLS model parameters is non-iterative partial least squares (NIPALS). NIPALS calculates scores **T**, loadings **P** and weights, **W**⁸⁵. Weights are required to maintain orthogonality of the scores. The NIPALS algorithm for PLS can also be applied when there is more than one predicted variable **Y**, and therefore scores **U** and loadings **Q** are also calculated for **Y**-block. A vector of “inner-relationship” coefficients (regression coefficients), **b**, which relate the **X**- and **Y**-block scores, must also be calculated. Using NIPALS, the scores (**t**), weights (**w**), loadings (**p**) and inner-coefficients are calculated sequentially as shown below. The PLS decomposition is started by selecting one column of **Y**, **y_j**, as the starting estimate for **u₁**. In the case of univariate **y**, **u₁** = **y**. Starting with the **X** data block which is a matrix of (*k*) absorbance data points with *n* samples (**x** is one spectrum):

$$\mathbf{w}_1 = \frac{\mathbf{X}^T \mathbf{u}_1}{\|\mathbf{X}^T \mathbf{u}_1\|} \quad \text{Eqn 2.52}$$

$$\mathbf{t}_1 = \mathbf{X} \mathbf{w}_1 \quad \text{Eqn 2.53}$$

In the **y** data:

$$\mathbf{q}_1 = \frac{\mathbf{u}_1^T \mathbf{t}_1}{\|\mathbf{u}_1^T \mathbf{t}_1\|} \quad \text{Eqn 2.54}$$

$$\mathbf{u}_1 = \mathbf{Y} \mathbf{q}_1 \quad \text{Eqn 2.55}$$

Convergence is monitored by comparing \mathbf{t}_1 in Eqn 2.53 with the value from the previous iteration. If they are equal within rounding error, proceed to Eqn 2.56. If they are not return to Eqn 2.52 and use \mathbf{u}_1 from Eqn 2.55. If the Y-block is univariate, Eqns 2.54 and 2.55 can be omitted, then set $\mathbf{q}_1 = 1$ and no iteration is required. The X data block loadings are calculated and the scores and weight rescaled accordingly:

$$\mathbf{p}_1 = \frac{\mathbf{X}^T \mathbf{t}_1}{\|\mathbf{t}_1^T \mathbf{t}_1\|} \quad \text{Eqn 2.56}$$

$$\mathbf{t}_{1 \text{ new}} = \mathbf{t}_{1 \text{ old}} \|\mathbf{p}_{1 \text{ old}}\| \quad \text{Eqn 2.57}$$

$$\mathbf{w}_{1 \text{ new}} = \mathbf{w}_{1 \text{ old}} \|\mathbf{p}_{1 \text{ old}}\| \quad \text{Eqn 2.58}$$

Find the regression coefficient \mathbf{b} for the inner relation:

$$\mathbf{b}_1 = \frac{\mathbf{u}_1^T \mathbf{t}_1}{\mathbf{t}_1^T \mathbf{t}_1} \quad \text{Eqn 2.59}$$

After the scores and loadings have been calculated for the first factor (latent variable (LV) in PLS), the X- and Y-block residuals are calculated as follows:

$$\mathbf{E}_1 = \mathbf{X} - \mathbf{t}_1 \mathbf{p}_1^T \quad \text{Eqn 2.60}$$

$$F_1 = Y - b_1 t_1 q_1^T \quad \text{Eqn 2.61}$$

This entire procedure is repeated for the next latent variable starting from Eqn 2.52. X and Y are replaced with their residuals E_1 and F_1 , respectively, and all subscripts are incremented by one. It can be shown that PLS forms the matrix inverse defined by:

$$X^+ = W(P^T W)^{-1}(T^T T)^{-1}T^T \quad \text{Eqn 2.62}$$

where the W , P , and T are as calculated above. It should be noted that although the scores and loadings calculated in PLS are not the same as those calculated in PCA and PCR, they correspond to these having been rotated to be more relevant for predicting y . Similarly to PCR, the PLS model converges to the MLR solution if all latent variables are included.

2.4.2.5. Artificial Neural Network Partial Least Squares (NN-PLS)

Artificial neural networks (ANNs) are simplified and idealised models of biological neural networks⁸⁸. An ANN (frequently shortened to neural network (NN)) approximates the function of multiple variables in terms of the function of one variable⁸⁹. One of the basic units for information carrying in NNs is the neuron. Neurons are arranged in a number of layers with weights linking them. The number of layers is dependent on model complexity but there is always an input and output layer with the number of hidden layers between these varying. The arrangement of the layers and the number of neurons in each is described as the neural network architecture. The input can be any multivariate signal, e.g., spectra, and the output is the predicted analyte value⁹⁰.

The output, $\hat{\mathbf{Y}}$, to an input vector (spectrum) \mathbf{x} , of a neural network with n_i input neurons, one hidden layer with n_h neurons and one output neuron with a linear transfer function, can be written

$$\hat{\mathbf{Y}} = \sum_{j=1}^{n_h} \mathbf{W}_j f \left(\sum_{i=1}^{n_i} w_{ji} x_i + bi_j \right) + \mathbf{Bias} \quad \text{Eqn 2.63}$$

where f is a linear, sigmoid or tangent hyperbolic transfer function, bi_j and \mathbf{Bias} are biases of the model and w_{ji} and \mathbf{W}_j are the weights of the hidden and output layers, respectively.

Like other multivariate techniques, NNs can also present small errors in the calibration data sets but large errors in validations sets. This is mainly due to the use of overly complex models which over-fit the model. A high level of operator expertise is required unless one of a increasing number of optimisation methods is used to prune the complexity. Optimum brain surgery (OBS) and optimum brain damage (OBD) are two available optimisations⁹⁰. Both these methods work by starting a neural network with an excessive number of neurons in the hidden layer(s) and cutting those connections which have little impact on the monitored residual error. Overfitting and complexity is therefore diminished by removing those neurons which have had all connections cut.

2.4.2.6. Pattern recognition

Pattern recognition techniques seek to identify regularities and similarities which are present in data. Mathematical pattern recognition is often confused with

optical pattern recognition, which seeks to teach machines to evaluate optical data. While these techniques do have some common bases, they are different in application, methodology and terminology. Many techniques are included in the category of pattern recognition.

There are two main categories of pattern recognition techniques: clustering (unsupervised pattern recognition) and supervised learning. Hierarchical clustering links all objects in a data set (one by one) by measuring their relative similarity in terms of Euclidean distance (ED). Mahalanobis distance (MD) can also be used in the same way to link similar populations by calculating the MD between the population means⁹¹ (see Appendix B for ED and MD calculation). Supervised pattern recognition methods can be further divided into either discrimination or class modelling techniques. Both incorporate a training set of objects of a known class, and a mathematical model is generated to predict the class of a newly presented object. Linear discriminant analysis (LDA), Quadratic discriminant analysis (QDA) and regularised discriminant analysis (RDA) are some examples of discrimination methods frequently used^{92, 93}. All these, however, use a global model to discriminate a class and an object must belong to one of the classes available.

In the case of LDA, the class of a next measurement can be predicted to a class membership K by:

$$cf_K(\mathbf{x}_i) = (\mathbf{x}_i - \bar{\mathbf{x}}_K) \mathbf{C}_{Pooled}^{-1} (\mathbf{x}_i - \bar{\mathbf{x}}_K)^T - 2 \ln \pi_K \quad \text{Eqn 2.64}$$

where $cf_K(x_i)$ is the classification score, C_{Pooled}^{-1} is the inverse of the pooled variance-covariance matrix of the different classes, x_i is the i th sample and \bar{x}_K is the absorption value at the centroid of the class K . $2\ln\pi_K$ is the prior probability which requires consideration if the number of elements in each class differs. The classification score is assessed against an F -tested critical value for acceptance to an appropriate class.

Another classification method is Soft Independent Modeling of Class Analogy (SIMCA). This method is based on making a PCA model (PCR and PLS models can be used but only the x variables will be influential) for each class in the training set. Unknown samples are then compared using the class models and assigned to classes according to their similarity to the training samples. SIMCA is a residual variance method which uses boundaries based on EDs between objects and the origin in PC residual space determined from PCA models⁹⁴. An equation describing this process is:

$$s_0 = \sqrt{\frac{\sum_{i=1}^n \sum_{j=1}^p e_{ij}^2}{(p-r)(n-r-1)}} \quad \text{Eqn 2.65}$$

where e_{ij}^2 is the squared residual of object i on the latent variable j , p is the number of dependent variables, n is the number of samples, r is the number of PCs and s_0 is the mean distance between all objects belonging to the class model. A new measurement is classified by projecting it towards PC space defined for the class and calculating its distance from the class model (s_j) using:

$$s_i = \sqrt{\sum \frac{e_{ij}^2}{(p-r)}} \quad \text{Eqn 2.66}$$

An F -test is applied to this value and a critical value calculated

$$s_{crit} = \sqrt{F_{crit} s_0^2} . \quad \text{Eqn 2.67}$$

If $s_i < s_{crit}$ the new measurement accepted as a class member otherwise it is considered to be an outlier. SIMCA, in contrast to the previously described methods, does not force new measurements into a class but will reject them.

In summary, the Mahalanobis technique is a distance method which covers the space defined by the significant PCs and the SIMCA model is a residual variance method covering residual space. Although these two techniques may be seen as competitors they are complementary and when used together can enhance the classification task.

Another major class of techniques, of great interest in recent years, is spectral library matching and comparison⁹⁵. These techniques seek to efficiently explain chemical structures from spectral data. They include nearest neighbour and distance (Mahalanobis or Euclidean) measures, correlation analysis, probability matching, Fourier and principal components analysis.

2.5. Standardisation of Instruments.

Generation of calibrations is time consuming and a complex procedure mainly because the acquisition of large data sets which are representative of a broad sample range is required. The inherent costs associated with such calibration development makes their transferability across a number of systems desirable. A predictive calibration model generated on spectra acquired from one instrument will generally give poor results when used on the spectra acquired from another instrument. This is due to small differences in instrumental response impacting on shape and position of spectral features. Individual spectrometer characteristics including, wavelength accuracy and photometric response, electronic noise, optical noise and temperature stability can all contribute to the failure of calibration transfer. Even during the use of a single spectrometer instrument drift or change in environmental conditions like a change in humidity may disrupt the performance of calibrations. The NIR spectrometric application for which calibration models have been generated may require transferability across a number of instruments and, possibly, locations. Some well known standardisation techniques, include.

1. Slope and Bias Correction (SBC)
2. Direct Standardisation (DS)
3. Piecewise Direct Standardisation (PDS)
4. Double Window Piecewise Direct Standardisation (DWPDS)
5. Orthogonal Signal Correction (OSC)
6. Finite Impulse Response filtering (FIR)
7. Wavelet Transform (modified) (WT)

8. Interpolation (Int.)
9. Interpolation with photometric correction (Int. and Mod.)
10. Model updating (MU)

A variety of standardisation techniques has been proposed which attempt to remove or minimise instrumental differences^{96, 97, 98, 99}. Most techniques require that spectral measurements to be made by both instruments of a standardisation sample set. In some cases this requirement may not be acceptable, e.g. instrument failure or instrument location, prompting many workers to develop alternatives.

2.5.1. Standardisation Techniques

In most standardisation methods, other than slope and bias correction, wavelength variables from a slave spectrometer, X_s , are transformed to appear as if originating from the other instrument X_m thus accommodating wavelength (x-axis) and photometric response (y-axis) variation. This is achieved by calculating standardisation parameters F which are applied in the following manner:

$$X_m = X_s \cdot F \quad \text{Eqn 2.68}$$

F can be calculated using any of the methods detailed below.

2.5.1.1. Slope and Bias Correction

One of the first standardisation approaches, a bias correction technique, was proposed by Osborne and Fearn¹⁰⁰ in 1983 to address the transfer question. Jones *et al.*¹⁰¹ modified this technique to one called slope and bias correction. The univariate slope and bias method is the simplest standardisation technique and has adequate performance when used where data sets have simple differences⁹⁹. Predictions are made on samples recorded on both spectrometers (Y_m and Y_s , master and slave respectively) using a predictive model generated on the master, then the results are regressed to provide

$$\hat{Y}_m = \text{slope} \cdot \hat{Y}_s + \text{bias} \quad \text{Eqn 2.69}$$

Each new prediction for the slave instruments is then transformed using this equation.

2.5.1.2. Shenk and Westerhaus patented standardisation technique

In 1989, Shenk and Westerhaus¹⁰² patented a standardisation technique which is currently incorporated in their chemometric software (WinISI, Infracsoft International, LLC., USA). This method is based on two main steps: wavelength matching and photometric response correction.

For wavelength matching, the data is firstly differentiated and the absorbance i th wavelength of the master instrument (x_m) is linearly correlated to absorbance at wavelengths in a spectral window ($i \pm w$) of the slave instrument (x_s). From these calculations, the wavelengths with the highest correlation (x_{mi} and x_{sk} , for the master and slave instruments, respectively) (k being in the interval $i \pm w$) are

identified. A quadratic function is fitted correlating these master and slave wavelengths, allowing new slave wavelengths to be defined by

$$i' = a + bi + ci^2 \quad \text{Eqn 2.70}$$

where i is the wavelength index, a , b and c are regression constants.

For photometric correction, raw absorbance data is used. Absorbance values are calculated for the new slave wavelengths using interpolation. The photometric responses, absorbances at the each wavelength, of the master instrument and the slave instrument are linearly regressed to identify the correlation between them. The regression is calculated from

$$x_{mi} = a(i) + b(i) \cdot x_{si'} \quad \text{Eqn 2.71}$$

are then used to adjust the absorbance values to new values using

$$x_{STDi} = a(i) + b(i) \cdot x_{si'} \quad \text{Eqn 2.72}$$

where x_{STDi} is the new absorbance value at the new wavelength and $a(i)$ and $b(i)$ are regression coefficients at the i th wavelength. Each new spectrum is treated with these wavelength coefficients to correct the wavelength scale and with the photometric response coefficients to correct the absorbance values.

2.5.1.3. Direct Standardisation

When the differences between instruments are simple an univariate approach which is based on slope and bias correction can be successful. However, when

more complex differences are present between instruments, more complex techniques are required. Such a method was proposed by Wang *et al.*¹⁰³ called direct standardisation (DS). The standardisation transformation matrix F is calculated by

$$F = \overline{R}_2^+ \overline{R}_1 \quad \text{Eqn 2.73}$$

where \overline{R}_1 is a matrix of absorbance values for a subset of standardisation samples measured on the master instrument and \overline{R}_2 is the matrix of absorbance values for the same subset of standardisation samples measured on the slave instrument. A new response vector of unknown samples, $r_{2,un}^T$, measured on the slave instrument is standardised by F to appear as a master response vector, $\hat{r}_{1,un}^T$ by using

$$\hat{r}_{1,un}^T = r_{2,un}^T F \quad \text{Eqn 2.74}$$

The previously generated predictive model can then be used on this standardised spectrum. In this method the whole spectrum acquired on the slave instrument is used to fit each spectral point on the master.

2.5.1.4. Piecewise Direct Standardisation

Wang *et al.*¹⁰³ developed the ‘piecewise direct standardisation’ (PDS) algorithm which is similar to the DS technique but incorporates the use of a moving window which steps across the variable range. For each wavelength of a sample spectrum collected on the master instrument, the absorbances are regressed

against the corresponding absorbances in a spectral window of neighbouring wavelengths from the slave instrument. For example, when the spectra from the master instrument are X_1 , and the slave instrument to be standardised are X_2 , and a window width of $2j+1$ is used, the model for the absorbance value of the i th variable (wavelength) b_i is identified by

$$b_i = X_2(:,i-j:i+j)^+ X_1(:,i) \quad \text{Eqn 2.75}$$

where $X_1(:,i)$ and $X_2(:,i-j:i+j)$ are columns identifiers used in the formation of the model b_i . The superscript '+' indicates a pseudo-inverse.

2.5.1.5. Double Window Piecewise Direct Standardisation

In cases where the spectral features are very narrow with regions of only baseline noise in between, as with some FTNIR spectra, transfer models developed with PDS do not perform well. Double window PDS (DWPDS) was developed by Wise¹⁰⁴, (personal communication, 2000) to address this issue. It does this by forming models based on data on both sides of the current window to be standardised. The second window defines the range data outside the original window to be used. The form of the model is identical to that of PDS, only the way in which the model is identified is different. In DWPDS, with a first window width of $2j+1$ and a second window width of $2k+1$, the model for the i th variable b_i is

$$b_i = X_{2DW}^+ X_{1DW} \quad \text{Eqn 2.76}$$

$$\text{where } \mathbf{X}_{2\text{DW}} = \begin{bmatrix} \mathbf{X}_2(:, i-j-k:i+j-k) \\ \mathbf{X}_2(:, i-j-k+1:i+j-k+1) \\ \mathbf{X}_2(:, i-j-k+2:i+j-k+2) \\ \dots \\ \mathbf{X}_2(:, i-j:i+j) \\ \dots \\ \mathbf{X}_2(:, i-j+k:i+j+k) \end{bmatrix}$$

$$\text{and } \mathbf{X}_{1\text{DW}} = \begin{bmatrix} \mathbf{X}_1(:, i-k) \\ \mathbf{X}_1(:, i-k+1) \\ \mathbf{X}_1(:, i-k+2) \\ \dots \\ \mathbf{X}_1(:, i) \\ \dots \\ \mathbf{X}_1(:, i+k) \end{bmatrix}$$

The model for the i th variable is based on a wider range of data, and therefore more data.

2.5.1.6. Orthogonal signal correction

Sjöblom *et al.*¹⁰⁵ investigated the use of orthogonal signal correction (OSC) for the standardisation of instruments. They proposed that OSC makes the spectra less dependent on instrument variation. OSC is a technique for the preprocessing of NIR spectra before they are subjected to multivariate calibration model generation. With OSC, the X-matrix (spectral data) is corrected by subtraction of variation that is orthogonal to the Y-matrix (concentration). This correction is then applied to new spectra that are going to be used in predictions. The main aim of OSC is to minimise the variation in the spectral data which is not correlated to the analyte concentration. This achieved by repeatedly orthogonalising the score vector, using principal component analysis (PCA), to

the analyte vector until stability is achieved. The spectral data is then PLS regressed against this resultant score vector and the B coefficients employed to construct new scores and loadings which transform spectral data to a new orthogonal signal corrected data set. Usually both spectral and analyte matrices are individually centred before orthogonalisation of the score vector.

2.5.1.7. Wavelet Transform

Walczak *et al.*¹⁰⁶ proposed standardisation of instruments in the wavelet domain. Wavelet theory can be described as the representation of a signal by the sum of analysing functions, achieved by an expansion of spectra into localised building blocks, defined by their scale and position¹⁰⁷. The spectra are essentially divided into ‘approximation/average’ and ‘detail/difference’ components, bandpasses of frequencies from 0 Hz to the Nyquist frequency (half the number of wavelengths)¹⁰⁸. Their mathematical basis stems from the familiar frequency analysis theory of Fourier transforms but instead of using the time-frequency variables of Fourier, wavelet transforms use a ‘scaling variable a ’ and the ‘position variable b ’ which closely resembles it.

Walczak’s procedure follows other standardisation steps by selecting a subset of spectra from the master and slave instruments to which wavelet transforms are applied using suggested filter and resolution criteria. The resultant wavelet coefficients for each are univariately, linearly regressed against each to obtain standardisation. This technique also can have the benefit of reducing spectral noise.

2.5.1.8. Finite Impulse Response

The Finite Impulse Response (FIR) function can be thought of as a moving window similar to the multiplicative scattering correction (MSC) function. In MSC, points of an average spectrum are regressed against corresponding points from an actual spectrum. The sample spectrum is corrected by multiplication and subtraction of the regression slope and bias values. The main purpose of the use of the MSC technique is to remove effects of scattering. The FIR function used as a standardisation technique was proposed by Blank *et al.*¹⁰⁹. A windowed (limited bandwidth) MSC is used to correct new spectra using one reference spectrum with only the centre channel of each window being corrected. This technique has the advantage of requiring only one spectrum from the master instrument to transfer spectra from a second instrument. A disadvantage of this technique is that if the reference spectrum has regions where the response is flat for a bandwidth corresponding to approximately the window size, artefacts (e.g. spikes) can arise in the corrected spectra making standardisation in that window poor.

2.5.1.9. Wavelength Selection

When samples cannot be measured on both instruments many of the commonly used techniques (DS, PDS, DWPDS and OSC) become useless. Swierenga *et al.*¹¹⁰ proposed an approach based on a wavelength selection technique as a data pretreatment prior to calibration model generation so that the model retains its predictive ability when it is transferred to another instrument.

Optimisation algorithms such as simulated annealing and the genetic algorithms have been applied to the wavelength selection but are very time intensive. Both these techniques require significant user input for their operational parameters therefore adding another labour consuming aspect to their use.

Brenchley *et al.*¹¹¹ demonstrated a simplified approach to wavelength selection by excluding wavelength regions known to be irrelevant to the analyte of interest rather than using time-consuming optimisation algorithms to select information carrying wavelengths. They demonstrated that certain PLS loading vectors were equivalent to correlograms of analyte to absorbance value and thus this type of analysis was useful for the determination of the primary regions responsible for spectral variations.

In 1999, McShane *et al.*¹¹² also proposed a simplified approach to wavelength selection, supporting its relevance as a useful alternative to the difficult-to-configure genetic algorithm approach. Their algorithm was a “peak-hopping” algorithm, which when used on glucose concentration in cell culture media and aqueous media determination improved the accuracy of the resultant predictions.

2.5.1.10. Interpolation and Photometric correction

The design of most modern post-dispersive NIR spectrometers incorporates the use of either linear PDAs or linear or area CCDs as photodetecting elements. The physical structure of these devices, when coupled to wavelength dispersion elements, means that a discrete number of intensity values (representing a spectrum) results. A calibration equation (often a fourth order polynomial) is

required to associate the spectral output of the dispersion elements (a continuous function) with the pixels of the photodetectors (discrete increments). Despite high engineering accuracy, small physical displacement of components means that each instrument will have slightly different wavelength/pixel assignment. The photometric response and noise characteristics of photodetectors, even from the same batch, can differ considerably compounding the problem of calibration transfer. The non-linear wavelength/pixel assignment of each photodetector can be re-assigned to a uniform, common (across instruments) wavelength/spectral position assignment, using an interpolation technique. The photometric response of one instrument can be mathematically modified to reproduce another instrument's response by ratioing a spectral measurement of a stable reference sample.

2.5.2. Sample Selection for Standardisation

The use of standardisation samples from a source different to those on which the calibration is to be used and which cover a larger spectral range, generally leads to poor results. Standardisation samples similar to the samples to be predicted can lead to good standardisation but will be applicable only to those samples^{113, 114, 115}. Bouveresse *et al.*¹¹³ investigated the effect of using three different standardisation sets for the transfer of calibrations, using Shenk's algorithm, between different spectrometers. One standardisation set contained samples very similar to the agricultural samples from the sets to be analysed, the second set contained generic standards, and the third set contained pure organic and inorganic chemicals. The accuracy of each standardisation was tested by assessing the root mean square errors and correlation coefficients before and

after standardisation. Predictive ability was also tested by assessing the standard error of prediction for the three different predictions before and after standardisation. They concluded that standardisation samples need to cover exactly the same absorbance value range as the samples on which prediction was intended, with the best predictions achieved following standardisation using like samples.

A frequently used algorithm for standardisation sample selection is the Kennard and Stone algorithm. This algorithm was proposed by Kennard and Stone¹¹⁶ in 1969 to assist experimental design. This method begins by removing a pair of samples in the 'master' calibration matrix ${}^m\mathbf{C}$ which are most different to each other and places these in a standardisation matrix ${}^m\mathbf{T}$. Then the following stepwise procedure is repeated until the desired number of samples is achieved. The Euclidean distance between the candidate sample and other selected samples is calculated and the minimum distance $d(u)$ is stored.

$$d(u) = \sqrt{\min_{s=1}^n \left(\sum \left({}^m\mathbf{C}(u,:) - {}^m\mathbf{T}(s,:) \right)^2 \right)} \quad \text{Eqn 2.77}$$

where s = index of selected spectra, n = number of spectra selected prior to this iteration, u = index of unselected spectra.

The unselected sample in the ${}^m\mathbf{C}$ matrix with the largest $d(u)$ value is removed and added to the ${}^m\mathbf{T}$ matrix.

2.6. Conclusion

Choice of spectrometer design can greatly impact on data quality and therefore predictive ability. Physical characteristics such as detection limit, signal to noise level, precision, and accuracy of spectrometric systems need to be carefully chosen for an application. Chemometric methods can unlock valuable information contained in data. Correct use and application of these techniques is the key to successful predictive model generation. Transfer of predictive models among systems is highly desirable to maximise cost efficiency. A number of chemometric methods are available to achieve this.

Design of the complete NIR spectroscopic fruit grading system, incorporating hardware and data analysis, requires extensive multi-disciplinary investigations.

3. Literature Review/Case Studies

3.1. Introduction

Consideration of the NIR region for spectroscopy followed from Coblenz's seminal work¹¹⁷ on fingerprinting of organic molecules using infrared (IR) (1000 – 15000 nm) spectra. Commercial NIR instrumentation became available in the 1950s. This instrumentation was usually based on filter or tilting diffraction grating dispersive elements used in a pre-dispersive format and was generally not suitable to in-line industrial applications due to the vibration sensitive nature of the componentry. Array spectrometers became available in the early 1990s with the advances in Si-based technologies, providing these photodetectors with rapid responses, high SNR and at a reasonable cost. In this section the criteria for the selection of appropriate hardware needed for the task of sorting fruit in an in-line application are reviewed.

3.2. Criteria Important to In-line Fruit Sorting System Design

3.2.1. Bandwidth

A large number of wavelengths in the NIR region 700 to 2500 nm have been assigned to sucrose and water. For example, the first overtone of CH₂ (sucrose) has been assigned to 1765 nm and 1725 nm, while the second, third and fourth overtone assignments are 1215 nm, 938 - 913 nm and 762 – 746 nm, respectively^{66, 118} (Appendix A). However, the surrounding matrix heavily influences band assignment. Further, the high absorbances of the first and second overtone regions results in shallow sample penetration of these

wavelengths in intact fruit, while absorbances in the third and fourth overtone regions (SW-NIR) allow far longer pathlengths. Thus, the practical application of fruit sorting requires use of third and fourth overtones (938 – 913, 762 – 746 nm).

On this basis, the recommended operational wavelength region is 760 – 940 nm. This region is covered by Si detectors. Wavelengths identified by Kawano *et al.*^{9, 68, 119}, Dull *et al.*^{56, 58, 120, 121, 122} and Ito¹²³ as being spectrally important in the wavelength range of Si are listed below (Table 3.1).

Table 3.1. Wavelengths (nm) in the SW-NIR region associated with sucrose or SSC in fruit samples. Kawano *et al.*^{9, 68, 119}, Dull *et al.*^{56, 58, 120, 121, 122} and Ito¹²³.

Kawano <i>et al.</i>	Dull <i>et al.</i>	Ito
745		
760		
769		
786		
796		
870	860	
878	884	
889	896	
904	907	900
906	913	905
914	918	910
935		918
950		
951		

3.2.2. Resolution

It is generally acknowledged that the instrument bandpass should be no greater than the absorber bandwidth. Spectra in the SW-NIR region generally have very low amplitude, broad (> 40 nm) absorption peaks¹⁴. This observation suggests that NIR instrumentation has a low resolution requirement.

In a study of glucose in an animal biological matrix, Ding and Small¹²⁴ transformed their original spectral data (with a point resolution of 2 cm^{-1} (0.8 nm) by de-resolving it to 4, 8, 16 cm^{-1} (1.6, 3.2 and 6.4 nm at 2000 nm, respectively). They found that the performance of the optimal PLS calibration models (based on the 2000 to 2500 nm range) obtained with the original spectra (0.8 nm resolution) was maintained with the lower resolution spectra of both 4 and 8 cm^{-1} (1.6 and 3.2 nm) point spacing. However calibration statistics were degraded when the spectra were computed with a point spacing of 16 cm^{-1} (6.4 nm). Similarly, Wang *et al.*¹²⁵ investigated the performance of multivariate analysis of pharmaceutical tablets with 14 different concentrations of aspirin (85 to 90%) as resolution was decreased from 2, 4, 8, 16 to 32 cm^{-1} (0.8, 1.6, 3.2, 6.4 and 12.8 nm at 2000 nm, respectively). In this study, a high resolution FT-NIR spectrometer (Brüker IFS 28/N, 2 cm^{-1} resolution, range 2000 to 2500 nm) was used in reflectance mode of operation. They found a roughly linear degradation in R^2 and RMSECV from 0.91 and 0.46% (respectively) at 2 cm^{-1} (0.8 nm) to 0.84 and 0.60% (respectively) at 32 cm^{-1} (12.8 nm). In a short follow-up study, the same spectrometer was used in transmission mode with a more sensitive InGaAs detector. They concluded from the statistical results ($R^2 = 0.96$ and RMSECV = 0.28%) of predictive models generated using spectra collected at a

resolution of 16 cm^{-1} (6.4 nm at 2000 nm) that higher resolutions are probably not required. A search for literature assessing the effect of resolution on the determination of SSC in intact fruit did not provide any material.

Thus, high resolution ($< 6\text{ nm FWHM}$) is probably unnecessary for predictive model generation in the SW-NIR region. Higher resolution often involves lower signal (due to use of a narrower slit) and thus lower signal to noise ratio (SNR). Determination of the requirements, specific to the application, are therefore necessary to the instrument design.

3.2.3. Noise and Sensitivity

Noise is inherent in low level light detection. It is often stated that quantitative NIR analyses requires high SNR, but the minimum level required has not been well defined in literature. One manufacturer of laboratory-based instruments (NIRSystems) benchmarks their instruments at 20 μA (micro-Absorbance units) standard deviation.

Noise on the spectral data limits the certainty prediction from calibrations generated using this data¹²⁶. By estimating these uncertainties an assessment of the robustness of each calibration model can be achieved. Theoretical estimation can be achieved using the following relationship:

$$\text{Lower Limit of RMSECV} = \sqrt{(\sigma^2 \times b^2)} \quad \text{Eqn 3.1}$$

where σ^2 = vector of variances of the spectral variables and \mathbf{b} is the calibration predictive coefficient vector.

Some workers have explored empirical validation of this estimation to a limited extent. For example, Lu and McClure¹²⁷ evaluated the performances of four calibration models: (1) stepwise multiple regression (SMLR); (2) classical least squares (CLS); (3) principal component regression (PCR) and (4) partial least squares (PLS) in NIR spectroscopy analysis when random noise was present in the spectral data of computer simulated and natural data sets. In these experiments the ZAP function in Grams/386 was used to add normally distributed random noise which specified as a percentage of the highest peak in each spectrum. The relative performance of each noise level was made using a simple numerical comparison without significance testing. It was concluded that for synthesised data, some full spectrum calibration methods “performed quite well for predicting the composition of a three-component mixture even in the presence of 99% noise” (i.e. addition of 99% noise, i.e. SNR of 600:1), although later in the same paper they report that when only one wavelength was used the “SEC and SEP increased as the noise level increased” (above 10%) and that “It is confirmed that random noise has an important effect on the performance of PLS”. They also found that for a natural product (tobacco), the level of added noise above which the prediction errors became unacceptable (SEP > 0.55) was 30% (i.e. SNR = 2000:1). These findings seem to suggest that if a full spectrum method were to be used on synthesised or natural spectra then, surprisingly, SNR is relatively unimportant in the development of calibrations if the correct

chemometric technique is used. This result could lead to greatly simplified instrument design if verified.

Norris¹²⁸ considered the effect of instrument noise on the measurement of narrow-bandwidth weak absorbers. This work was based on simulated spectra with Gaussian absorption bands and random white noise to a specified magnitude. He reported a steady increase in error with noise. Data pretreatments reduced these errors, but did not remove the trend for error to increase with increasing noise. This conclusion is contrary to that of Lu¹²⁷.

While a high count is required to maximise SNR, the twin issues of the optical density of fruit and the limited integration period available for assessment of moving fruit (ca. 50 ms) drives a requirement for a sensitive assembly. This can be achieved by maximising collection of light, use of large detector array pixel size and use of sensitive detector elements.

3.2.4. Light Detector Configuration.

Full transmission mode has limited application to optically dense fruit (ie. either large or optically dense flesh) or 'non-homogenous' fruit (e.g. fruit with a large seed). Most literature reports of the use of NIR spectroscopy for assessment of internal attributes have considered stationary fruit. These systems contacted the sample in order to exclude spectrally reflected light from the detector. Further, sample size, shape and surface texture differs greatly among fruit types (apple, rockmelon, mandarin and kiwifruit) necessitating specific instrument design for each.

Maeda⁶⁹ assessed a variety of illumination/detector configurations for use in an in-line setting. SSC was determined of thinned skinned fruit using reflectance mode of operation, in which the illumination source and detector were angled relative to each other at $< 90^\circ$, but the impact of fruit size and orientation on accuracy was too great to make this method successful. They concluded that, although measurements made in this mode could determine SSC of thin-skinned fruit (e.g. peaches, apples and pears) accuracy was poor due to light signal noise for specularly reflected light and wet chemistry inaccuracies due to ill-defined correlated sample regions. A non-contact, full transmittance detection method was also trialed, however, secondary and ternary reflected light degraded the quality of the acquired spectrum and limited its usefulness. An optical configuration which operates in transmission mode and requires contact with the fruit (oranges, small watermelons and thick rind melons) was therefore adopted.

Mechanical devices required for fruit-contacting measurements may introduce both system complexity and speed limitations. Non-contact spectral measurement is therefore desirable to eliminate these considerations.

3.2.5. Other Factors

Temperature stability and mechanical robustness (vibration tolerance) are primary design considerations of instrument manufacturers. In the application of in-line fruit sorting, where ambient temperatures can vary by 40°C and the instrumentation is subjected to long work periods (> 12 hours per day) in a mechanically harsh environment, these criteria become two of the major

considerations, in terms of impact on wavelength calibration stability and detector responsivity.

3.2.6. Summary

The major criteria for in an in-line fruit sorting application are:

- wavelength range,
- wavelength resolution,
- SNR (electronic and optical), sensitivity,
- optical geometry (lamp – sample – detector),
- temperature stability and
- mechanical robustness.

Non-contact spectral measurements are required to enhance processing speed capability of fruit sorting system.

Prior to the mid-1980s, patented NIR technology was used to distinguish damaged (bruised) vegetables or fruit using mainly reflectance methods (Table 3.2). These spectral measurements were limited in quality due to the use of unrefined dispersive elements (flat, ruled diffraction gratings) and early-technology photodetectors (e.g. photo-multiplier tubes). Also, although the work by Ben-Gera and Norris¹²⁹ had highlighted the benefits of the use of multivariate analysis (later, 1971, termed chemometrics⁷¹) to extract information from data and to develop efficient multivariate predictive models, high computational

Table 3.2. List of patents, presented in chronological order, relating to hardware for sorting of vegetables or fruit using NIR technology.

Country (Patent Number)	Year	Assignee	Title	Description
USA (US421379)	1973	Brown Segerlind ¹ 30	Method for detecting bruises in fruit.	Detection of bruises in fruit has been accomplished by measuring the reflectance of near infrared light from the fruit surface.
USA (US3867041)	1975	Brown Segerlind ¹ 31	Detection of bruises in fruit is accomplished by measuring reflectance of NIR light from the fruit surface.	Detection of bruises in several genera of fruit including apples, peaches, and pears by measuring the reflectance of NIR light from the fruit surface.
USA (US3930994)	1976	Conway Paddock ¹³ 2	Method and means for internal inspection and sorting of produce.	Evaluation of citrus fruits using transmission optics on a moving conveyor wherein the percentage of internal damage is computed for each fruit.
USA (US876085)	1978	Burford Henry ¹³³	Produce grading system using two visible and two invisible colours.	A method for sorting articles of a given produce according to a desired red colour and for sorting undesired nonvegetable articles such as dirt clods and rocks.
USA (US4204950)	1980	Burford ¹³⁴	Produce grading system using two visible and two invisible colours.	A sorting system, using two bands in the visible range and two in the NIR range, for undesired nonvegetable articles such as dirt clods and rocks.
Japan (JP8840740)	1988	Norinsho ¹ 35	Fruit and vegetable quality measurement by production of spectrum by irradiating fruit with NIR rays non-destructively.	A system to assess quality of fruit and vegetables non-destructively using NIR spectroscopy.

Literature Review/Case Studies

Table 3.2 (continued).

Japan (JP1301147)	1989	Mikio Masayuki Koji ¹³⁶	Method and device for measuring quality of vegetable and fruit.	A system to measure the quality of a vegetable or fruit for sugar and hardness non-destructively using reflected light from the vegetable or fruit of wavelengths e.g. 0.90 - 1.10, 1.11 - 1.31, 1.24 - 1.44, 1.35 - 1.55, 1.58 - 1.78, and 1.72 - 1.92 nm.
USA (US563170)	1990*	Birth Dull Leffler ¹³⁷	Nondestructive measurement of soluble solids in fruit by detection and measurement of NIR radiation scattered by internal structure of juice.	A system to determine SSC of fruit and vegetables using wavelengths in the range 700 – 1100 nm.
USA (US5089701)	1992*	Birth Dull Leffler ¹³⁸	Nondestructive measurement of soluble solids in fruits having a rind or skin.	An invention to non-destructively measure SSC of fruits having a rind or skin using NIR.
USA (US5164795)	1992	Conway ¹³⁹	Method and Apparatus for Grading Fruit	A method for grading the surface of fruit according to surface characteristics such as colour and blemish using three reflected NIR wavelength bands.
USA (US5324945)	1994*	Mutsuo Sumio ¹⁴⁰	Method of nondestructively measuring sugar content of fruit by using NIR transmittance spectrum.	A method of nondestructively measuring the SSC of fruit using NIR radiation; measuring the absorbance at a given wavelength; normalising the obtained absorbance; and predicting the sweetness of the fruit.
Japan (JP6186159)	1994*	Mutsuo Sumio ¹⁴¹	Nondestructive measurement method for fruit by using NIR transmittance spectrum.	A system to obtain an index for sweetness by irradiating fruits with NIR light, measuring absorbance at a specific wavelength with a spectroscope and correcting by the fruit size.

Table 3.2 (continued).

USA (5324945)	1994*	Iwamoto Mutsuo Kuno Sumio ¹⁴²	Method of nondestructively measuring sugar content of fruit by using NIR transmittance spectrum.	Same as US5324945
Japan (JP722983A)	1995	Toru Hideki ¹⁴³	Apparatus for measuring ripeness of fruit or vegetable on branch	Nondestructively measure ripeness of fruit or vegetables on the plant, using a measuring wavelength and detecting the reflected wavelength and correlating it to ripeness.
Belgium, Switzerland Germany, Spain, France, Great Britain Italy, Lithuania, Netherlands (EP736339)	1996*	Blanc ¹⁴⁴	Analysis device for automatically sorting products, especially fruit or vegetables.	A system using a multi-spectral-line laser, a near infrared collimated laser diode, an infrared collimated laser diode and associated mirrors, and polarising cubes to distinguish between outgoing and returning beams to automatically sort fruit.
USA (US5708271)	1998*	Ito Iida Terashima Kishimoto 123	Non-destructive sugar content measuring apparatus.	An apparatus to nondestructively measure SSC of vegetables or fruit to an accuracy of $\pm 1^\circ$ Brix using NIR lasers (860 - 880, 900 - 960 nm).
Australia (PP3652)	1998*	Salmond Greensill ¹⁴⁵	An Optical Device.	An optical apparatus for examining an object and in particular, an optical apparatus for examining carbohydrate constituents in a plant.
Japan (280171/98)	1998*	Salmond Greensill ¹⁴⁶	An Optical Device.	Same as previous example.

* = patents dealing with assessment of sugar content.

requirements restricted its application. When high-powered desktop computer power became readily available around the beginning of the 1980s, research accelerated in the field of chemometric methods. Chemometrics has proven to be the backbone of NIR spectrometric methods allowing more diverse application of NIR technology, for example rapid in-line fruit sorting.

After the mid 1980s, most patents employed high output (~ 100 W) QTH sources of illumination, post-dispersion by diffraction gratings and photodiode array-based detectors and reflectance mode of data acquisition. Blanc¹⁴⁴ continued to employ reflectance mode, but presented a novel use of mirrors and laser diodes for illumination of the sample and data acquisition. Transmission (body transmission) mode of spectral measurement has received preference in most of the patents from 1990 (e.g. Birth *et al.*¹³⁷).

The listed patents describe systems which manage interference from specularly reflected light by physical means (e.g light-tight cups). This arrangement, involving physical contact with the fruit, is cumbersome and will limit processing speeds (typical 3 fruit per second). A non-contact optical system would be far more appropriate to the task of in-line fruit grading.

A number of workers have reported the use of NIR spectroscopy for the non-invasive assessment of internal attributes of fruit and vegetables (Table 3.3). Although this is not an exhaustive list of publications in this field of research, it is representative (that is, temporally unbiased). Of a total of 54 listed, only 6 occurred before 1990 and 13 before 1995. It is obvious that a heightened interest

Table 3.3. List of publications relating to the determination of quality parameters in fruit, vegetables and fruit juice.

Year	Author	Fruit	Light Source Dispersive element	Detector (Number of pixels) [Manufacturer]	SNR [Scans averaged]	Resolution FWHM (nm) Range [nm]	RMSECV (STDEV) [R]	Comment
1965	Birth & Norris ¹⁴⁷	Peach Apple	QTH 150 W Filter Wheel	Photo-multiplier Tube	2000:1	[400 – 1000]	-	Categorised fruit into three classes on ΔOD .
1965	Yeatman & Norris ¹⁴⁸	Apple	QTH Filter Wheel	Photo-multiplier Tube [Dumont 6911]	-	690 nm (15) 744 nm (20)	[0.957]	60 fruit per minute sorting rate.
1978	Ballinger <i>et al.</i> ¹⁴⁹	Grape	Pre-dispersive Diffraction grating	Si and PbS [Cary 17]	-	0.1 [400 3000]	-	Feasibility of sorting small fruit like grapes or berries.
1989	Dull <i>et al.</i> ¹²¹	Honeydew	QTH 650 W Tilting Filter	Si photodiode [EG&G HUV-4000B]	-	0.5 [700 – 1000]	2.18	Detector angle determined (75°)
1989	Dull <i>et al.</i> ⁵⁶	Rockmelon	QTH 650 W Tilting Filter	Si photodiode [Biospect LT 7000]	-	0.5 [800 – 1000]	1.56 (1.95)	Detector angle determined (75°)
1989	Kawano <i>et al.</i> ¹¹⁹	Peach	-	- [Pacific Scientific 6250] [Technicon 500]	-	- [680 – 1235] [1100 – 2500]	0.42 (SEP) [0.96]	10 wavelengths identified for the assessment of SSC (887, 985, 1057, 1128, 1542, 1610, 1778, 2118, 2182 and 2242 nm). Bias = -0.01.
1990	Birth <i>et al.</i> ⁵⁷	Rockmelon Potato Onion	QTH 650 W Tilting Filter	Si photodiode [BioSpect LT7000]	-	6 [800 – 970]	2.18 (2.725)	Description of an instrument design
1990	Jaenisch <i>et al.</i> ¹⁵⁰	Date	QTH 50 W AOTF	Si photodiode [EG&G HUV-4000B]	-	9 [800 – 1050]	-	Focussed on AOTF description
1992	Dull <i>et al.</i> ¹²²	Honeydew	QTH (GE 1392) Tilting Filter	Si photodiode [EG&G HUV-4000B]	-	~ 0.7 [760 – 980]	1.85 (1.30)	Feasibility of assessment of SSC in honeydew melons.

Table 3.3 (continued).

1992	Kawano <i>et al.</i> ⁹	Peach	-	Si [Pacific Scientific 6250]	[50 scans]	[680 – 930]	0.50 (1.65)	4 wavelengths identified for assessment of SSC (870, 878, 889 and 906 nm)
1993	Bellon <i>et al.</i> ¹²	Peach	QTH 150 W Diffraction Grating	Si CCD (500 x 582) [Jobin Yvon CP200]	90000:1	1.8 [800 – 1000]	1.05 (1.83)	Feasibility of sorting peaches Best wavelength range was 767 1027 nm.
1993	Kawano <i>et al.</i> ⁶⁸	Mandarin	QTH 100 W Diffraction Grating (stationary) (600 l/mm)	Si [Pacific Scientific 6250]	-	0.4 [680 – 930]	0.32 (1.73)	4 wavelengths identified for assessment of SSC (745, 769, 786 and 914 nm)
1993	Shiina <i>et al.</i> ¹⁵¹	Pineapple	-	[Technicon 500]	-	- [700 – 2500]	1.29 (2.14)	Measurements were made of 3 cm slices of skin and flesh. Bias = -0.002
1995	Bellon-Maurel & Vigneau ¹⁵²	-	-	Si CCD	-	- [800 – 1050]	-	60 ms integration time
1995	Cho <i>et al.</i> ¹⁵³	Apple	- Filter [InfraAlyzer 400] Pre-dispersive	[InfraAlyzer 500 & 400]	-	-	1.07	Firmness of apples
1996	Aoki <i>et al.</i> ⁵⁹	Watermelon	QTH 16 lamps Diffraction Grating	Si PDA	9000:1	8.9	0.46 (0.61)	10 second measuring time
1996	Martinsen & Schaare ⁵⁰	-	QTH Diffraction Grating (400 l/mm, 850 blaze)	Si CCD (753 x 488) [Electrim EDC-1000HR] 11.5 x 13.5 µm pixel size. <i>rms</i> noise 140 electrons/pixel. Saturated signal 200000 electrons	~ 1400:1 [10 scans]	~6 [400 – 1100]	-	2 – 3 minutes scan time, 53 ms integration time

Table 3.3 (continued).

1996	Matsumoto <i>et al.</i> ⁸	Watermelon	QTH 16 x 100 W Diffraction Grating (600 l/mm)	Si PDA (1 x 64) Temperature controlled \pm 0.05° C.	9000:1 [32 scans]	8.9 [650 – 1070] accuracy \pm 3	0.38 (1.2)	10 ms integration time 6 wavelengths used for assessment of SSC (800, 820, 840, 860, 880 and 894 nm.)
1996	Osborne <i>et al.</i> ¹⁵⁴	Kiwifruit	QTH Diffraction Grating	Si PDA (1 x 256) [Zeiss MMS1]	30000:1 [5 scans]	9 [300 1100]	0.33 (1.46)	180 ms integration time
1996	Slaughter & Crisosto ¹⁵⁵	Kiwifruit	- Diffraction Grating Pre-dispersive	Si and PbS [NIRSystems 6500]	[250 scans]	10 [400 – 1100]	0.68 (SEC) (2.18)	Whole fruit scanned
1996	Tanabe <i>et al.</i> ¹⁵⁶	Mango	- Diffraction Grating Pre-dispersive	Si and PbS [NIRSystems 6500]	-	10 [400 – 1100]	0.48 (SEP) (0.73)	Assessment of variation of Focus on model performance across cultivars. Bias varied widely (-3.81 – 6) on predictive models originating from a different cultivar. MLR identified wavelengths for assessment of SSC (864, 920, 958 and 978 nm). Bias =-0.02
1997	Greensill & Newman ¹⁵⁷	Papaya	QTH 100 W Prism/s and Diffraction Grating	Si CCD (1 x 2048)	900:1	0.3 [600 – 1000]	-	Dispersion element comparison
1997	Guthrie & Walsh ¹⁵⁸	Pineapple Mango	QTH 200 W Diffraction Grating Pre-dispersive	Si and PbS [NIRSystems 6500]	-	10 [700 – 2500]	0.75 (3.354)	Feasibility of assessing SSC in pineapples and DM in mangoes.
1997	Guthrie & Walsh. ¹⁰	Pineapple Mango	QTH 200 W Diffraction Grating Pre-dispersive	Si and PbS [NIRSystems 6500]	-	10 [700 – 2500]	1.84 (3.477)	Robustness of predictive models for pineapples across seasons.

Table 3.3 (continued).

1997	Holland <i>et al.</i> ³¹	Berry Purée	-	Deuterated triglycine (DTGS) detector FT_IR [MonitIR & Bio-Rad FTS-7]	-	[2500 – 12500]	-	Classification success > 90%
1997	Osborne <i>et al.</i> ¹⁵⁹	Kiwifruit	QTH Diffraction Grating	Si PDA (1 x 256) [Zeiss MMS1]	30000:1	9 [300 1100]	0.445 (0.989)	Feasibility of sorting kiwifruit
1997	Peiris <i>et al.</i> ¹⁶⁰	Peach	QTH 50 W AOTF	Si photodiode [EG&G HUV-4000B]		0.5 [800 – 1050]	0.837 (1.79)	Calibrations malfunctioned when used on fruit from different time or cultivar.
1998	Akimoto <i>et al.</i> ¹⁶¹	Watermelon	QTH 16 x 100 W.	Si PDA (1 x 64) [NIRF2000]	9000:1	8.9 [640 – 1050]	0.46 (0.61)	10 second processing time
1998	Chang <i>et al.</i> ¹⁶²	Rockmelon Juice	- Pre-dispersive	[Hitachi U-3410]	-	1 [1000 – 2500]	0.485 (1.707)	2 wavelengths used 2270 and 2080 nm.
1998	Guthrie <i>et al.</i> ¹⁶³	Rockmelon	QTH 200 W Diffraction Grating Pre-dispersive	Si and PbS [NIRSystems 6500]	-	10 [400 – 2500]	1.84 (3.477)	Feasibility of assessing SSC in rockmelons.
1998	Kawano ¹⁶⁴	Pear Apple Mandarin	QTH 2 lamps Diffraction Grating	-	-	-	-	Grading 3 fruit per second
1998	Lammertyn <i>et al.</i> ⁶⁵	Apple	QTH 100 W Double diffraction Grating	Si & PbS [Optical Spectrum Analyser 6602]	4 scans	0.5 [380 – 1650]	SSC 0.61 (1.066)	Firmness, pH SSC stiffness factor elastic modulus of the flesh determined
1998	Lammertyn <i>et al.</i> ¹⁶⁵	Apple	QTH 100 W Double diffraction Grating	Si & PbS [Optical Spectrum Analyser 6602]	4 scans	0.5 [880 – 1650]	SSC 0.65 (1.318)	Focussed illumination geometry, 45° determined to be optimum.
1998	Maeda ⁶⁹	Apple Orange	QTH Diffraction Grating	-	-	-	0.56 (1.351)	Discusses illumination/detecting geometries.

Table 3.3 (continued).

1998	Martinsen & Schaare ¹⁶⁶	Kiwifruit	QTH Diffraction Grating (400 l/mm, 850 blaze)	Si CCD (753 x 488) [Electrim EDC-1000HR] 11.5 x 13.5 µm pixel size. <i>rms</i> noise 140 electrons/pixel. Saturated signal 200000 electrons	~ 1400:1	~5 [650 - 1100]	1.2 (2.4)	400 ms integration time
1998	McGlone & Kawano ¹⁶⁷	Kiwifruit	QTH 200 W Diffraction Grating Pre-dispersive	Si and PbS [NIRSystems 6500]	-	10 [800 - 1100]	0.42 (1.328)	Firmness and dry matter also assessed
1998	Mowat & Poole ¹⁶⁸	Persimmon	QTH Diffraction Grating	Si Array (1 x 1024) [Ocean Optics S1024]	~ 1000:1	0.5 [550 - 1000]	-	Segregation of fruit by cultivar and/or treatment.
1998	Peiris <i>et al.</i> ¹⁶⁹	Peach	QTH 50 W AOTF	Si photodiode [EG&G HUV-4000B]	~ 250:1	0.5 [800 - 1050]	1.11 (2.08)	Calibrations malfunctioned when used on fruit from different time or cultivar. Bias = -0.237
1998	Peiris <i>et al.</i> ¹⁷⁰	Tomatoes	QTH 65 W Diffraction Grating	Si PDA [OM - 2000 Onion Meter, Dual Ocean Optics spectrometers]	-	0.5 [650 - 1000]	0.52 (0.72)	Compared regression methods, e.g. PLS, MLR and NN.
1998	Ventura <i>et al.</i> ¹¹	Apple	QTH 6 W Diffraction Grating	Si PDA (1 x 1024) [Ocean Optics S1024 dual beam]	~ 250:1	[811 - 999]	1.14 (1.72) (SEP)	MLR determined wavelengths 819, 835, 859, 867, 875, 883, 891, 899, 939, 947, 971 and 987 nm. 10 scans averaged, 300 ms integration time. Bias = -0.13
1999	Greensill & Newman ¹⁷¹	Papaya	QTH 100 W Prisms	Si CCD (1 x 2048) [Larry2048]	900:1	0.3 [600 - 1000]	-	Wavelengths indicative of maturity identified (720, 745 and 815 nm)

Table 3.3 (continued).

1999	Guthrie <i>et al.</i> ¹⁷²	Pineapple	QTH 200 W Diffraction Grating Pre-dispersive	Si and PbS [NIRSystems 6500]	-	10 [400 – 2500]	1.84 (3.35)	Feasibility of assessing SSC in pineapples.
1999	Osborne <i>et al.</i> ¹⁷³	Kiwifruit	QTH 50W Diffraction Grating	Si PDA (1 x 256) [Zeiss MMS1]	30000:1	10 [300 - 1100]	0.27 (1.08)	50 ms integration time average 15 spectra
1999	Peiris <i>et al.</i> ¹⁷⁴	Rockmelon Honeydew	AOTF	Si Photodiode	-	6	0.978 (1.79)	Spatial variability of SSC.
1999	Sugiyama ¹⁷⁵	Andes melon	QTH	Si CCD [CV-0411, Industries] (16 bit A/D)	Mutoh	10 [400 – 2500]	-	Wavelengths (676 nm) determined by predictive models generated using a NIRSystems 6500 initially. Two dimensional spectral imaging. 500 ms integration time.
2000	Greensill & Newman ¹⁷⁶	Citrus	QTH 100 W Prism/s and Diffraction Grating	Si CCD (1 x 2048) [Larry 2048]	900:1	0.3 [600 – 1000]	-	Dispersion element comparison and identification of maturity indicative wavelengths (710, 730 and 805 nm).
2000	Greensill & Walsh ¹⁷⁷	Rockmelon	QTH 100W Diffraction Grating	Si PDA (1 x 256) [Zeiss MMS1]	30000:1	10 [300 - 1100]	0.636 (1.181)	New illumination/detector design assessment, assessment of light penetration (> 15 mm) and SSC distribution.
2000	Greensill & Walsh ¹⁷⁸	Rockmelon	QTH 100W Diffraction Grating	Si PDA (1 x 256) [Zeiss MMS1]	30000:1	10 [300 – 1100]	0.53 (1.077)	Assessment of calibration transfer techniques.

Table 3.3 (continued).

2000	Lammertyn <i>et al.</i> ¹⁷⁹	Apple	QTH 100 W Double diffraction Grating	Si & PbS [Optical Spectrum Analyser 6602]	[4 scans]	0.5 [880 – 1650]	SSC 0.61 (1.066)	Focussed on light penetration in fruit and illumination geometry, 45° determined to be optimum. Penetration depth determined to be ~ 4 mm at 500 – 1900 nm.
2000	Schmilovitch <i>et al.</i> ¹⁸⁰	Mango	QTH 75 W Diffraction Grating	PbS [Quantum 1200, LTI]	-	1 [1200 – 2400]	1.223 (1.545)	MLR gave best results wavelengths not given.
2000	Segtnan & Isaksson ¹⁸¹	Orange Juice	- Diffraction Grating Pre-dispersive	Si and PbS [NIRSystems 6500]	[32 scans]	10 [780 – 2500]	-	A new technique dry extract diffuse reflectance (DESIR) assessed against standard curvette methods in relative terms.
2000	Walsh <i>et al.</i> ¹⁸²	Rockmelon	QTH 50W x 4 Diffraction Grating	Si PDA (1 x 256) [Zeiss MMS1]	30000:1	10 [300 - 1100]	0.636 (1.181)	Focus on instrumentation and model generation for an at- line sorting application (45° light/detector angle).
2000	Wen & Tao ¹⁸³	Apple	-	Si [Hitachi KP-MI] Highpass filter (700 nm) PtSi (256 x 256) [ThermaCAM PM250]	-	Si [700 – 2500] PtSi [3400 – 5000]	-	Stem-end /calyx against true defect determination. ~ 100% classification rates.

has sparked a great deal of interest into hardware and software improvements since 1995. This appears likely to continue.

Much of the early melon work was based on assessment on samples excised from the fruit (e.g. Dull *et al.*, 1989a; Dull *et al.*, 1989b; Dull *et al.*, 1990^{56, 58, 121}) and hence are destructive measurements and not useful to an in-line sorting application. Aoki *et al.*⁵⁹ assessed whole watermelon fruit, but neither the apparatus (16 light surrounding the sample with the detector contacting the fruit) nor the required processing time (10 seconds) was conducive to the rapid in-line sorting.

Improvement in hardware technologies combined with improved chemometric techniques have contributed to better performance of predictive models e.g. for rockmelons, RMSECV has slowly decreased from < 2.1 to $> 0.6\%$ SSC through the 1990s.

3.3. Spectrometer Case Studies

3.3.1. Filter Based Instruments

Much of the early work undertaken in NIR spectroscopy employed filter-based instruments. These instruments were restricted to pre-selected wavelengths based on knowledge of relevant band assignments. Birth and Norris¹⁴⁷ reported the development of a portable filter-based instrument for determination of internal attributes of fruit and vegetables (e.g. hollow heart in potatoes, ripeness

of peaches, water core in apples). In 1965, Yeatman and Norris¹⁴⁸ presented an apparatus to sort apples by chlorophyll content. This instrument used a filter wheel monochromator (690 and 744 nm), allowing transmittance measurements which were differenced. Low chlorophyll content was associated with high eating quality (fruit maturity). This system could grade apples into 5 categories at a rate of 1 fruit per second. However, the relationship of chlorophyll to eating quality was cultivar and growing condition specific which degraded the instrument performance.

Ballinger *et al.*¹⁴⁹ automated a 'light sorting of fruit mechanism' based on the 'difference meter' which had been developed by Birth and Norris¹⁴⁷ ten years previously. The original instrument of Birth and Norris was capable of sorting blueberries at a rate of 2000 berries in a 10 hour period when operated by 6 workers. Ballinger *et al.*¹⁴⁹ achieved rates of 64 berries per minute whilst sorting into 5 grades and extended its use to other small fruit like grapes. These determinations were made in full transmission mode and detector technology (photo-multiplier tube) of this period was the fruit-size restricting parameter.

Burford and Henry¹³³ (Table 3.2) patented a 'Produce grading system using two visible and two invisible colours', which was based on filter technology designed to identify the presence of non-vegetative matter (e.g. dirt or rock) in produce in a process line. The basis of the patent was the relationship between four wavelengths (530, 660, 800 and 900 nm). No detail on the type or bandpass of the filters was provided.

Dull *et al.*¹²² employed tilting interference-filter technology for wavelength scanning and a Si detector with preamplifier to make non-destructive reflectance measurements to determine the percent SSC (SEC 0.82) in whole honeydew melons. This instrument had the advantage of flexibility due to wavelength range but the disadvantage of a number of moving parts which, generically, are prone to undesirable effects from temperature and vibration.

Filter-based technology thus offers a low-cost alternative in instrument design however, the disadvantages, in terms of mechanical robustness, speed of operation and wavelength selectability make it unsuitable to an in-line sorting application.

3.3.2. Gratings/Prisms Based Instruments

The advent of high quality semiconductor photodetector arrays (PDAs and CCDs) has led to a proliferation of commercially available stationary diffraction grating based instruments. Since no published work was discovered with respect to empirical comparison of the results of the prism versus diffraction grating designs, a gap exists in this body of knowledge. Currently no known instrument manufacturers employ prism-based technology despite some possible advantages, in terms of even efficiency distribution, high throughput and low cost.

3.3.3. AOTF Based Instruments

When this work was commenced the poor efficiency ($< 40\%$, unpolarised input light), high power consumption (and hence associated noise) and high cost of AOTFs (TeO_2 crystals) ($> \$20\text{K}$) limited application to the task of in-line sorting for fruit. However, Tran *et al.*⁴⁷ reported the development of a new acousto-optic tunable filter (AOTF) that had a wide spectral tuning range, high resolution, no sidelobes, and requires low RF powers. It required approximately 14 times lower driving power for a noncollinear AOTF with the same aperture, had a spectral range $> 600\text{ nm}$ with a relatively constant diffraction efficiency of $\sim 70\%$ (for polarised input light) for the entire tuned region and a resolution of $\sim 3\text{ nm}$ across the tuned spectral region.

AOTFs offer can offer scanning speeds $< 10\text{ }\mu\text{s}$ per wavelength, however the total spectral acquisition time required for good quality spectral data (high SNR) can be long. The integration time (spectral acquisition time) is dependent on the sensitivity and SNR characteristics of the photodetector used, for example, miniature, grating-based spectrometers using similar photo-detection systems to AOTFs frequently use integration times of $\sim 50\text{ ms}$ per scanned wavelength. This would mean that the total spectral acquisition time for an AOTF would be multiples of 50 ms (multiplied by the number of wavelengths used). Also, although transmission efficiency has improved ($\sim 49\%$) (Brimrose Corporation of America, 2000) it remains low therefore reducing sensitivity. Jaenisch *et al.*¹⁵⁰ (Table 3.3) designed a date sorting instrument based on AOTF technology which had a reported sorting capability for dates of 5 items per second. However, they concluded that this design would be restricted to small fruit due to

low AOTF efficiency. AOTF-based instruments are therefore unlikely candidates for rapid in-line sorting of fruit larger than dates.

3.3.4. LED Based instruments

An electronically scanned, small size 32 wavelength NIR spectrometer was developed for use as a handheld spectrometer and for a process application¹⁸⁴. The design relied on a linear light emitting diodes (LEDs) (200 mW, 13.3 nm FWHM) array light source and a fixed diffraction grating monochromator. A series of LED spectrometer modules was manufactured for short wave near infrared (SW-NIR) specifications, covering the range from 832 to 1048 nm. However, the range of this instrument is restrictive and may eliminate the assessment of certain fruits or attributes.

Schnable¹⁸⁵ reported the development of a portable instrument with a high-speed multiple-wavelength LED array source (range 420 – 950 nm), and simultaneous detectors for absorbance and 90 degree nephelometry. Absorbance values and simultaneous 90 degree-scatter intensities at six different wavelengths were determined and stored every 0.02 s. Rugged, laptop compatible, portable and inexpensive, the LED instrument was useful for discrete or on-line VIS-NIR absorption analysis and turbidity, or turbidity ratio, analysis. However, the slow scan rate of this instrument would exclude it from candidacy for a fruit sorting application.

LED technology offers potential for a fruit sorting application but suffers from similar restrictions to the filter based instruments in that their design may be

specific to a sample type and hence would not be optimised to all fruit types. If assessment were required for a different sample LED wavelength modification would be necessary. Further, it is doubtful whether LEDs emit sufficient light energy (200 mW diffusely emitted) to penetrate to depths considered useful to sort fruit rapidly and/or with thick optically dense exocarp.

3.3.5. Laser Based Instruments

Sample illumination by high intensity sources offers the possibility of obtaining constituent-descriptive data from greater fruit depths. For some fruit, full transmission may be possible. However, high intensity white light sources bring an inherent heat-load problem. Alternatively, laser light, at only the required wavelengths, offers the advantage of high illumination without the heat load. Another possible benefit, yet to be assessed, is that data may be cleaner due to fewer interactions between wavelengths because of the number of lasers used. Passively mode-locked titanium:sapphire laser provides new opportunities for acquiring spectral data in the near infrared, a region not commonly accessible to synchronously pumped dye lasers. A system designed along the lines of early pre-dispersive systems but incorporating tunable lasers or laser arrays as the monochromatic source instead of the traditional moving gratings is therefore possible. These systems would have the benefit of high power per wavelength, the possibility of high spectral scan rates if laser diode arrays were to be used, and low noise component (with use of a PIN detector).

Tunable lasers and laser diode arrays have become widely available since the mid-1990s and affordable (AU\$20K) for this project since the late 1990s.

Nakamura¹⁸⁶ implemented a non-destructive inspection method for the quantitative analysis of moulds inside soya beans. Three near-infrared lasers (150 mW 810 nm, 160 mW 1064 nm and 80 mW 1319 nm) were used for multispectral transmission imaging (Hamamatsu C2741-03 NIR Vidicon camera) of the beans. The results of these experiments were very successful, achieving discrimination between one species of old (green old) and 'good' beans.

Meurens and Moons¹⁸⁷ constructed and tested a system incorporating a 700 mW Titanium:Sapphire continuous wave laser and a sensitive CCD detector to spectrally examine solid samples such as apples using NIR spectroscopy for evaluation of internal attributes. A comparison of spectra taken by a CCD spectrometer (Ocean Optics S2000) on apples illuminated by this tunable laser (range 730 to 830 nm, in 5 nm increments) and a 150 W tungsten halogen lamp was undertaken with encouraging results. They concluded that the determination of optical density using transmitted light through whole apples in the range of 730 to 830 nm was better using the laser light than the white light source, based on the performance of predictive models (MLR) to determine SSC (e.g. $R^2 = 0.8$ and 0.5, laser and QTH data, respectively).

Blanc¹⁴⁴ (Table 3.2) patented a system employing an NIR laser diode and an IR laser diode associated with mirrors and polarising cubes which distinguish between outgoing and returning beams. Measurement time was reported to be $\sim 66 \mu\text{s}$ but few other details were given.

Ito *et al.*¹²³ (Table 3.2) patented an apparatus to non-destructively measure sugar content of a vegetable using three NIR lasers in the range 860 to 890 nm (specifically 910 – 915 nm (SSC), 860-890 nm and 920 – 925 nm non-SSC reference bands). An accuracy of $\pm 1\%$ SSC and R^2 of 0.85 was reported. This work formed the basis of a system marketed by Sumitomo Metal Mining Co. Ltd.

Sumitomo Metal Mining Co. Ltd. employs laser sample illumination instead of QTH. It offers systems to sort melons, apples, peaches, pears, nashi and watermelon at a maximum rate of 2 fruit per second (other performance results are unavailable). Very little system detail is available from this company so an in depth assessment is not possible. Again, the cost is > AU\$1M which makes it prohibitively expensive for most Australian customers.

The major drawback of these systems is their high overall costs (> AU\$20K) relative to the low cost (< AU\$6k) of miniature spectrometers and safety issues inherent in handling class III and IV lasers in Australia.

3.3.6. Detectors

Availability of Si based PDAs and CCDs with a range of pixel and array sizes, sensitivity, well capacity, peak wavelength efficiency and readout rates allows the detector to be optimised for each application. For example, Bellon *et al.*¹² reported the use of a spectrometer based on CCD technology (range of 800 to 1050 nm). Image acquisition time (20 spectra composed one image) for this instrument was 40 ms and a high SNR (> 27000:1) was reported. A predictive model generated on 54 and tested on 25 peaches of the population resulted in an

SEP of 1.04° (SSC). Despite the apparent potential usefulness of this instrument no further information was published on it.

No work has been published to date on an empirical comparison of a number of PDAs and CCDs for the design of an instrument for rapid in-line sorting of fruit. However, Godfrey¹⁸⁸ gives a useful theoretical comparison of a wide variety of photodetectors.

3.3.7. Optical Geometry

Another NIR fruit sorting spectroscopic system design was presented by Matsumoto *et al.*⁸ optimised many crucial aspects of the overall design of an NIR fruit sorting system including, sample illumination geometry and power, detector optics and electronic noise levels. The resultant system illuminated the sample with 16 x 100 W QTH lamps and achieved an SNR of $\sim 3000:1$ (at 3 Au). Spectral acquisition and processing time was 5.82 seconds which results in a very slow fruit processing rate of < 12 per minute.

Hiromu Maeda⁶⁹, representative director and president of Fantec Research Institute, presented a report on the ~ 1998 status of non-destructive measurement techniques for analysing internal attributes of fruit on-line using NIR spectroscopy which discussed the evolution of Fantec's research through many typical design questions related to on-line fruit grading. Reflectance spectroscopy was reported to be successful for small, thin skinned fruit (e.g. apples, pears, peaches) a decision was made to switch to transmittance measurements in 1996 in order to gain higher precision and accuracy. In

transmittance mode of operation, they examined the relative potential of a number of illumination technologies and geometries. For example, one system used opposed QTH light source and detector on the optical axis, and another used illumination by a battery of QTH light sources and detection through a light tight acceptance probe. The latter arrangement was adopted with good success in the determination of SSC and acid in oranges ($R = 0.96$, $SEP = 0.39$, and $R = 0.95$, $SEP = 0.12$, respectively) with a sorting rate of 3 fruit per second (maximum).

A number of other Japanese companies market fruit sweetness sorting systems. Mitsui Mining and Smelting Co. Ltd.¹⁶⁴ which first developed a sweetness sorting machine for peaches in Japan in 1986 (first marketed in 1989). This system operated in reflectance mode and a later version (released in 1990), concentrating on smaller fruit like peaches, pears, apples and citrus fruit used transmittance technology. Reflectance mode continues to be used for large fruit like melons with the sample being illuminated by an array of light sources (details not available) and can function on small fruit (apples, oranges, etc.). The process rate is 3 melons per second and 2 watermelons per second with an RMSEP 0.5° SSC for both fruit and similar rates for small fruit. This company also markets a full transmittance system to sort citrus fruit. This system can process a variety of citrus fruit at 6 samples per second with an RMSEP of 0.5° SSC and 0.2% acid. Details of the system components are, naturally, protected intellectual property. The assessment of these systems at a more fundamental level is not possible. This technology is not available outside Japan.

3.3.8. FT-NIR Based Instruments

Fourier transform (FT) spectroscopy has become a very successful analytical tool for some applications mainly due to their high frequency precision and high sensitivity characteristics. Their major drawbacks are their high sensitivity to vibration and temperature due to their delicate moving mirror instrumentation. This alone is sufficient to exclude them from candidacy for the application of fruit sorting in an in-line setting.

The principles of FTIR spectrometry are illustrated by the novel fibre-optic Fourier transform spectrometer described by Stelze⁴⁰. The optical retardation between the arms of a Mach-Zehnder-type interferometer made of single mode optical fibre is modulated by variation of the fibre temperature. Frequency shifts within the observed spectra was explained by the dependence of the refractive index on temperature, dn/dt . The bandwidth of this experimental system was 633 nm (due essentially due to the cutoff imposed by the fibre material) to 935 nm with a resolution of ~ 0.3 nm at 824 nm. This system alleviates many of the disadvantages of more traditional FTIR spectrometers (e.g. accurate positioning of moving parts) and its bandwidth was suitable for the application of SSC measurement in intact fruit. Its data acquisition rate, although not explicitly stated in terms of wavelengths or wavenumbers per second, is apparently greater than 40 nm per ms, making it unsuitable for assessment of moving samples as in an in-line setting.

Another variant on the design of a Fourier transform spectrometer was presented by Prunet *et al.*¹⁸⁹. The novelty of this work came from the interferometer

designed, with two identical Wollaston prisms. The interferogram, formed at infinity in the spatial domain, is independent of the size of the source and of its position. By associating the birefringent interferometer with a lens and a linear CCD sensor, they realised a spectrometer with a resolution about 19.5 nm at 580 nm and a range from 400 to 1100 nm. This system overcame some physical disadvantages of the traditional FTIR spectrometers but the effect of temperature variation and data acquisition rate was not assessed. The poor wavelength resolution is likely to preclude application to the sorting of fruit for SSC content.

3.4. Calibration Transfer

Although many workers (e.g. Bouveresse^{96, 99, 113, 114}; Dardenne *et al*¹⁹⁰; de Noord¹¹⁵; Despagne^{191, 192}; Dreassi¹⁹³; Duponchel¹⁹⁴; Geladi¹⁰⁸; Shenk and Westerhaus¹⁹⁵; Sjöblom¹⁰⁵; Sweirenga¹¹⁰) have researched calibration transfer techniques, only one researcher³¹ applied these techniques to fruit. They reported models using the first PC scores of the pre-treated spectra from one spectrometer were able to correctly assign the fruit species of between 91.1 and 96.4% of the pre-treated spectra of independent test sets. However, the data were of purées of berry fruits collected using FTNIR spectrometers and therefore the techniques may not be applicable to transfer of calibrations of intact fresh fruit across PDS or CCD based instruments used in an in-line setting.

Blanco *et al.*¹⁹⁶ discussed the problems potentially arising in transferring calibrations between diode array UV-Vis spectrophotometers. They highlight the

problem of wavelength differences between spectrophotometers in relation to the transfer of predictive models for binary mixtures of theophylline and doxylamine. They developed a method for aligning instrumental wavelengths on the basis of reference wavelengths and applied this to the transfer of predictive models developed from data collected from one spectrophotometer across four others (4 x Hewlett-Packard HP 8452A and 1 x HP8451A). Other literature has indicated that calibration transfer across instruments is likely to be seriously affected by changes in photometric responses of photodetectors and changes in illumination which was not discussed in this paper. Hence, these issues and other related additional complications when used with intact fruit in an in-line setting remain to be answered.

3.5. Conclusion

Instrumentation based on a QTH light source, post-dispersive spectrometer optics using dual prisms or holographic concave diffraction grating dispersion elements and Si or InGaAs array detector technology appears to be appropriate for the application of in-line sorting of fruit, in terms of wavelength range, wavelength resolution, SNR, speed of operation, mechanical stability and cost. This technology has been adopted in commercial fruit sorting operations in Japan. Technologies such as AOTF, tilting grating pre-dispersive, PbS and InGaAs offer specific advantages, but disadvantages of limited array size availability, cost and mechanical instability make them currently unsuitable. Technologies involving high intensity light sources (e.g. lasers) may have significant benefits, in terms of high SNR, but their high cost and safety requirements makes their use

challenging. Systems which use discrete wavelength illuminators in low numbers (e.g. filter-, LED-, laser-based instruments) may hamper their predictive efficiency by restricting their ability to employ powerful chemometric and data pretreatment methods (e.g. MLR, differentiation).

An emerging trend is that most companies are moving away from reflectance mode of detection to transmittance mode. Of those companies using transmittance technologies all require a detecting probe in contact with fruit, therefore limiting process rates. The process rate appears to be stalled at $\sim 2 - 3$ samples per second with the exception of one (Mitsui Mining and Smelting Co. Ltd) capable of 6 samples (citrus fruit) per second.

A number of issues continue to require clarification with respect to NIR fruit sorting design, for example

- What is the appropriate wavelength range to use?
- What is the appropriate wavelength resolution?
- What is the most efficient spectrometer optical design to use for this application?
- What photodetection system is most appropriate to this application?
- What level of SNR must be achieved for robust predictive model generation (considering noise-handling capabilities of chemometric techniques)?
- How will environmental conditions (e.g. temperature and vibration) impact system performance?
- What sample regions should be optically sampled to be representative of the entire fruit?

- How can predictive models generated on one system best be transferred to another?

The results of the research undertaken to answer these questions have been individually published and are presented in the following chapters. The aim of this thesis was to determine criteria important to the design of a NIR spectroscopic system used to automatically sort a variety of fruit ranging in size from 40 to 180 mm diameter for a variety of internal characteristics, e.g. SSC and DM.

4. An Experimental Comparison of Simple NIR Spectrometers for Fruit Grading Applications

This chapter has been accepted for publication under this title in the Journal of Applied Engineering in Agriculture, (2000).

4.1. Introduction

Due to increasing consumer demands, large-scale changes in both the production and retail sectors of the fresh fruit and vegetable industries in the developed countries of the world are resulting in increasing adoption of technology to maintain acceptable product quality. Ever more stringent standards which affect factors such as shelf life, appearance and flavour are being imposed on fresh produce by retailers. This is increasingly forcing the issue of quality control onto the individual producers and packing operations at 'farm gate' level. The sheer volume of produce passing through individual packing sheds means that the adoption of automated, uniform quality assessment procedures is becoming essential. One method that has received considerable attention is the use of near infrared (NIR) radiation to assess the level of ripeness and/or sweetness of the fresh product by relating the spectral response in the NIR region to constituents like total dissolved solids content^{66, 197, 198}. When used in conjunction with a visible (colour) sensor on a conveyor system, rapid and reliable grading of produce becomes a possibility. An NIR system would need to achieve sorting

Experimental Comparison of Simple NIR Spectrometers

rates of 3 to 15 fruits per second (dependent on commodity) to be considered financially viable.

Spectrometers designed for the NIR region have included instruments based on either pre- or post-dispersion optical geometries. Pre-dispersive instruments illuminate the sample with monochromatic light. They have limited illumination power to avoid dispersion element damage and have slow spectral acquisition times. Post-dispersive spectrometers can use an illumination source which contains all wavelengths and which is power-limited only by the criterion to avoid sample damage. When high rates of data acquisition (e.g. in-line fruit grading) are desired, post-dispersive spectrometers have the capability of processing all wavelengths simultaneously with the use of multi-element detectors. Both pre- and post dispersive designs have incorporated the use of interference filters¹⁹⁹, diffraction gratings with photodiode detectors²⁰⁰ and diffraction gratings with charge-coupled device detectors¹².

Much laboratory work has been performed in recent years to determine the internal attributes of many fruits using NIR radiation, e.g. data published for pawpaws^{171, 199}, mangoes and pineapples¹⁵⁸, honeydew melons¹²², peaches and citrus^{9, 68} and kiwifruit^{155, 201}. Measurements have been made using both the reflectance and transmission modes of operation. In the reflectance mode, instruments measure radiation scattered from a thin, near-surface layer of the fruit and presuppose a correlation between these measurements and the properties of interest in the bulk flesh. In transmission measurements, radiation is detected after passing through more of the body of the sample, dependent on illumination/detector geometry. Transmission mode possesses two major

Experimental Comparison of Simple NIR Spectrometers

advantages over reflectance; firstly, a direct measurement of the bulk flesh properties is undertaken and secondly, there is no specularly reflected background radiation interfering with the results. Reflectance data often requires mathematical pretreatment (e.g. second derivative) to remove interference of specular radiation which increases processing time⁶⁶. Absorption and scattering of the incident radiation is dependent upon physical and chemical characteristics of the fruit (density, size, water content, total soluble sugar (SSC) content, presence of seeds etc.). Due to long pathlengths, characteristic in transmission mode measurements, severe attenuation of the incident light occurs. High intensity light sources may be utilised to increase the transmitted signal but these may cause sample damage due to unacceptable heat loads. Alternatively, the inherent low signal level issue can be addressed by optimising instrument design factors for the application, such as dispersion element efficiency, light source configuration and detector sensitivity. The primary factors affecting the performance of the spectrometer operating in transmission mode are its sensitivity to extremely low light levels, rejection of background light, insensitivity to variable environmental conditions (e.g. temperature and humidity), linearity of response, effective bandwidth and data processing rate. Sensitivity, in terms of signal throughput, is the one of the main considerations for these systems. Resolution can be considered a secondary concern since spectral features in the NIR region are predominantly vibrational overtones or combination bands of fundamental molecular vibrations and hence are very broad (typically 40nm full width half maximum (FWHM)¹⁴).

High resolution, commercially available laboratory-based spectrometers are currently available but are generally expensive and unsuitable for integration into an industrial process line. This study focuses on the assessment three simple wavelength dispersion elements, in terms of spectral range, resolution, linearity and throughput, for the design of a simple, low-cost, robust NIR spectrometer for use in automated fruit grading systems.

4.2. Theory

The theory of wavelength dispersion by prisms and diffraction gratings is well documented in the literature (see, for example Demtröder²⁰²) so we confine this discussion to a brief overview of the relevant equations applicable in this instance. The terms used in the equations are defined in Figures 4.1 and 4.2.

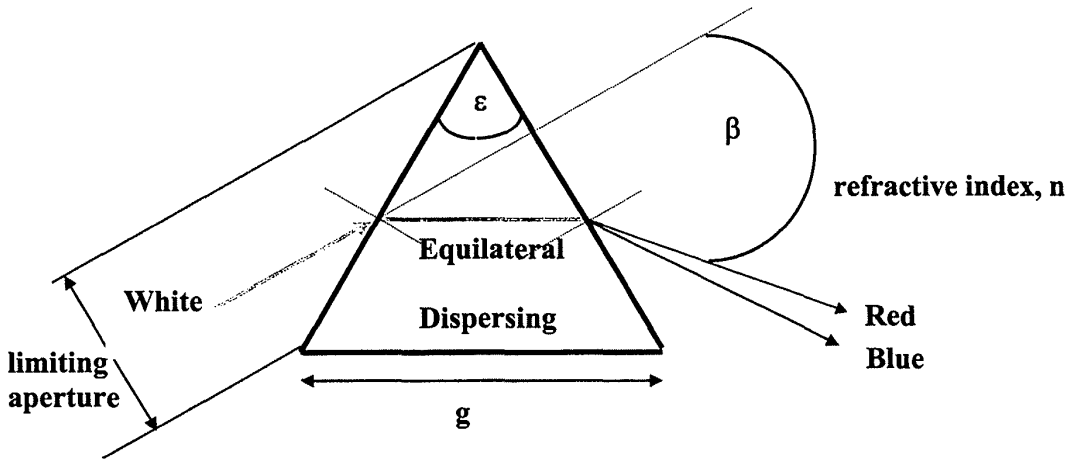


Figure 4.1. Defining terms for an equilateral prism.

4.2.1. Prism

When passing through a prism, light is deflected by an angle β according to its incident and exit angles, the angle of the prism, ε , and the refractive index, n , of the prism material (Figure 4.1). If the incident and exit angles are equal then the

Experimental Comparison of Simple NIR Spectrometers

light travels parallel to the base of the prism and β then defines the angle of minimum deviation. Under this condition, the angular dispersion, $d\beta/d\lambda$, is independent of the prism dimensions and a function of the prism angle and the dispersion, $dn/d\lambda$, through

$$\frac{d\beta}{d\lambda} = \frac{2 \sin(\epsilon/2)}{\sqrt{1 - n^2 \sin^2(\epsilon/2)}} \frac{dn}{d\lambda} \quad \text{Eqn 4.1}$$

The resolving power, $\lambda/\Delta\lambda$ is given by

$$\frac{\lambda}{\Delta\lambda} = g \frac{dn}{d\lambda} \quad \text{Eqn 4.2}$$

where 'g' is the base width of the prism and is related to the limiting aperture 'a' by straightforward trigonometrical manipulation.

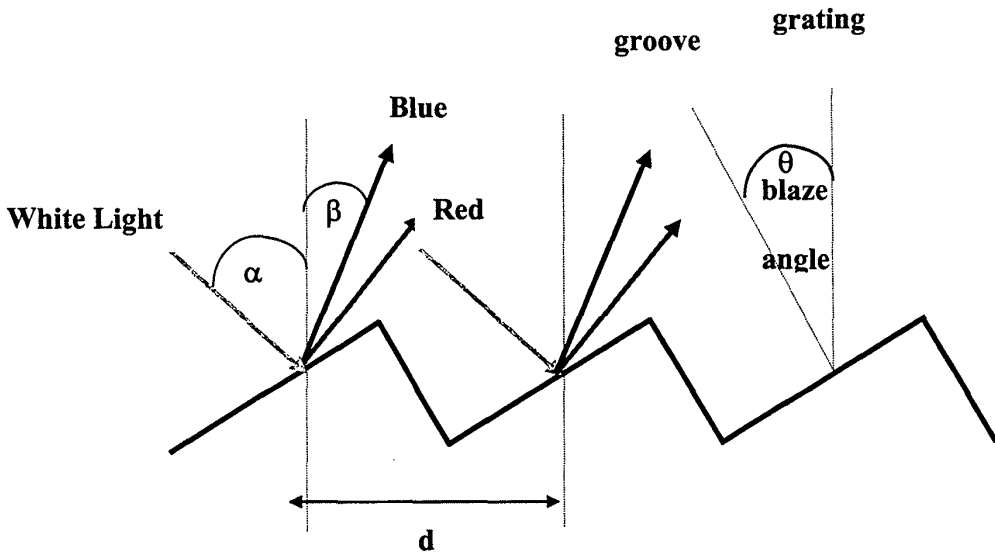


Figure 4.2. Defining terms for a diffraction grating.

4.2.2. Diffraction Grating

For a diffraction grating illuminated by a parallel beam of light of wavelength λ , incident at an angle α to the grating normal and reflected at an angle β on the opposite side of the normal (Figure 4.2), the grating equation is given by

$$d(\sin \alpha - \sin \beta) = m\lambda \quad \text{Eqn 4.3}$$

where m is the order of diffraction.

If the grating has N grooves, the intensity of diffracted waves, $I(\beta)$, is given by

$$I(\beta) = R(\theta, \beta) I_0 \frac{\sin^2(N\pi d \sin \beta / \lambda)}{\sin^2(\pi d \sin \beta / \lambda)} \quad \text{Eqn 4.4}$$

where I_0 is the incident light intensity and $R(\theta, \beta)$ defines the grating reflectivity.

A highly non-linear function results exhibiting a peak around the blaze angle of the grating.

The angular dispersion is independent of the number of grooves and is determined by the equation

$$\frac{d\beta}{d\lambda} = \frac{m}{d \cos \beta} = \frac{\sin \alpha + \sin \beta}{\lambda \cos \beta} \quad \text{Eqn 4.5}$$

The resolving power is given by

$$\frac{\lambda}{\Delta\lambda} = mN \quad \text{Eqn 4.6}$$

4.3. Experimental Method

4.3.1. Materials

4.3.1.1. Prisms

SF18 glass, used in the equilateral prism (25 mm sides, antireflective coated, Edmund Scientific Co. Barrington U.S.A) incorporated in the prism based designs, had a high transmission coefficient (> 0.95)(Fig. 4.3) and was highly linear in the spectral range of interest (650 to 1050 nm). The dispersion of the prism describes the effective change in the refractive index of the material for different wavelengths of radiation. The refractive index was a function of wavelength of the form

$$n(\lambda) = 1.6324304 + 2.0603786 \times 10^{-5} \lambda + 44.88937 / \lambda^2 \quad (\lambda \text{ in nm}).$$

The dispersion follows by a trivial differentiation yielding a weakly falling, linear function of wavelength in the NIR region. The characteristics of the glass were derived from commercial data (Sumita Optical Glass, Inc., Urawa, Saitama, Japan).

The first instrument design, utilizing a single prism, was based on traditional prism-based spectrometers, ie. collimated light was made incident on a single prism and the emergent beam focussed onto a detector. The second design incorporated an additional prism in the optical train of the first configuration to increase dispersion and therefore improved resolution (Figs. 4.4a and 4.4b).

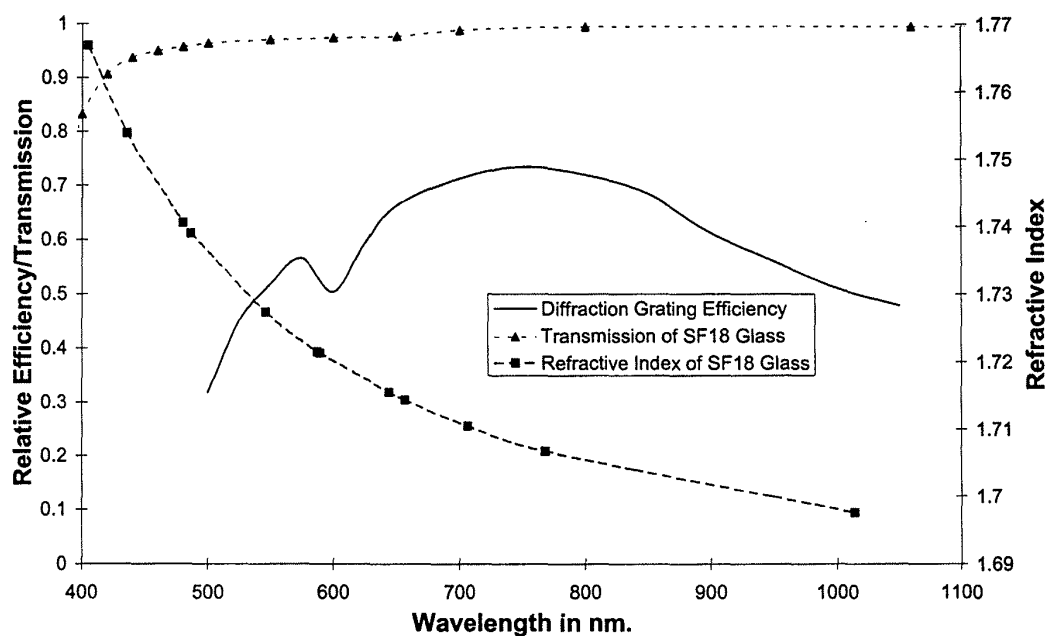


Figure 4.3. Illustration of the relationship between refractive index, optical transmission and diffraction grating efficiency and wavelength.

4.3.1.2. Diffraction Grating

For the assessment of a diffraction grating dispersion element, a unit based on traditional grating-based spectrometer designs used a diffraction grating (25mm square, ruled, 1200 l mm^{-1} , blazed at 750 nm, gold coated) supplied by Edmund Scientific Co. The grating normal was mounted at 17° to the incident radiation and first order wavelengths used for the assessment. The grating efficiency was non-linear peaking at the blazed wavelength (peak efficiency of $\sim 74\%$ at 750 nm) and decreasing in efficiency away to $\sim 66\%$ at 650 nm and 50% at 1050 nm (Figure 4.3). A diagram of the optical configuration is given in Fig. 4.4c.

4.3.1.3. Detector

The detector (Lastek, Adelaide, Australia, Larry, Model 2048) was purchased as a commercial package and incorporated a 2048 pixel, line element CCD (Sony ILX 503A) with a polymer window, a 500kHz, 12 bit ADC card and controlled by a custom data analysis and acquisition package (Lastek, Adelaide, Australia, SpectraSolve v 4.0). Manufacturer's specifications of this detector were: pixel size = $14 \times 12 \mu\text{m}$, well capacity = 95000 electrons, dark signal (25°C) = 185 electrons, sensitivity = 23 electrons per count and peak response at 550 nm.

4.3.1.4. Spectrometers

A vertical parallel slit S1 of width $10 \mu\text{m}$ was mounted approximately at the focal length of lens L1 to act as a real object and define the input beam to the spectrometer (Fig.4.5). Lens L1 provided a parallel beam of light incident on the dispersing element. The position of L1 relative to S1 was adjusted for optimum resolution and intensity for the particular dispersing element employed. Lens L1 comprised a combination of two plano-convex lenses (diameter = 38 mm, focal length = 68 mm) positioned to give a total focal length of 35 mm. Each lens was stopped to an f -number of 4, yielding an overall f -number of 2.1 for the combination. A lowpass filter ($< 550 \text{ nm}$ cutoff) was inserted into the optical path between lens L1 and the dispersion element to block second order effects characteristic of diffraction gratings. The dispersed radiation was focussed onto a CCD with an achromatic lens L2. Focal lengths for L2 of 250 mm and 60 mm were selected for the prism and diffraction grating configurations respectively to ensure a suitable linear dispersion of the spectrum across the CCD face. Typical integration times for the collection of spectra were in the range 10 - 100 ms.

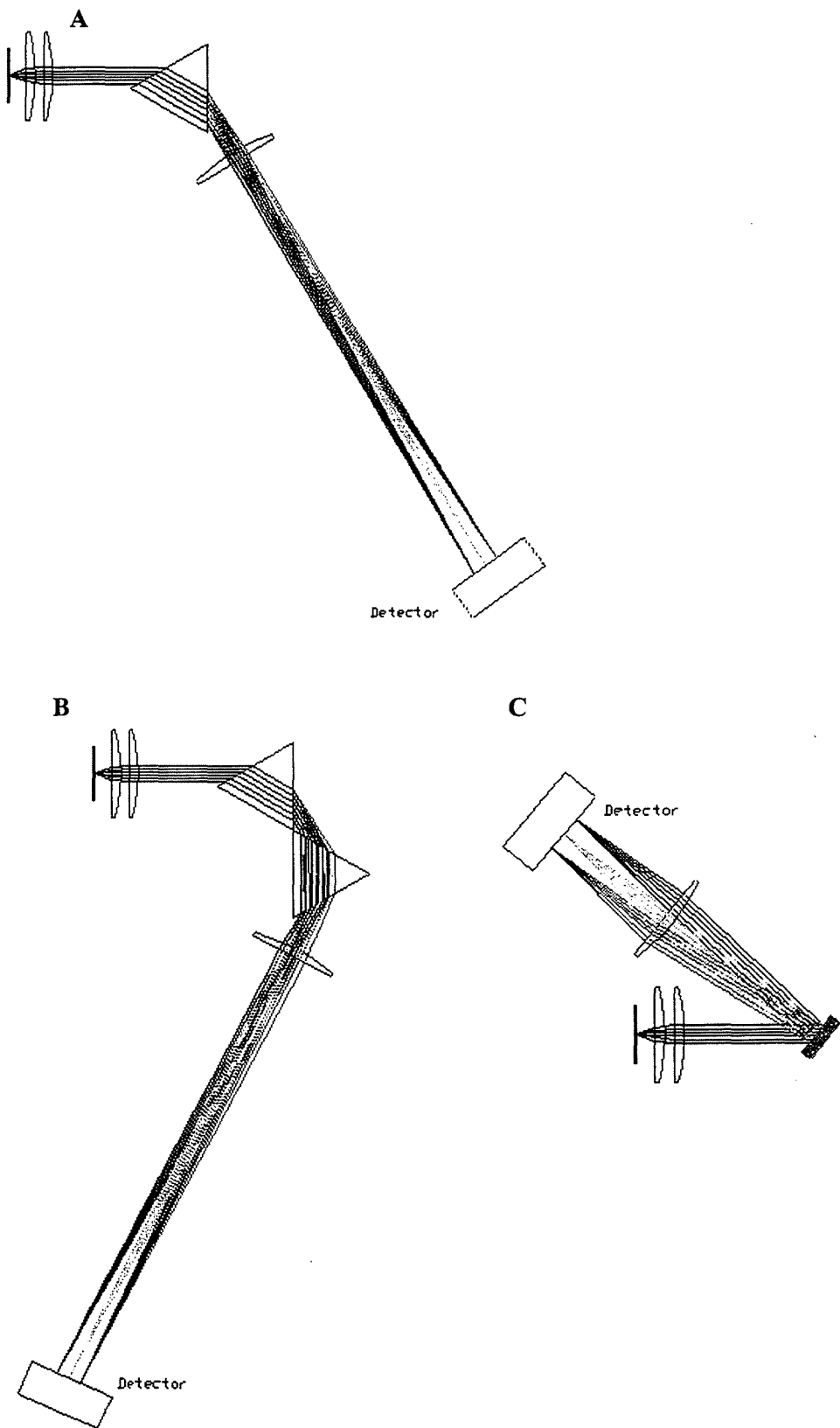


Figure 4.4. Diagrammatical representation of the optical geometries used for the single prism, two prism and diffraction grating spectrometers.

Experimental Comparison of Simple NIR Spectrometers

Initially, the stability of the light source was monitored using an optical fibre (500 μm diameter) positioned near the rim of the elliptical reflector and viewing the lamp. The monitored signal was attenuated using neutral density filters and recorded on a group of dedicated pixels on the detector via an optical fiber link. This signal could subsequently be used for intensity normalization to correct the spectrum for any possible fluctuations in the light source. This procedure was found to be unnecessary due to the stability of the power supply and light source and therefore not used any further.

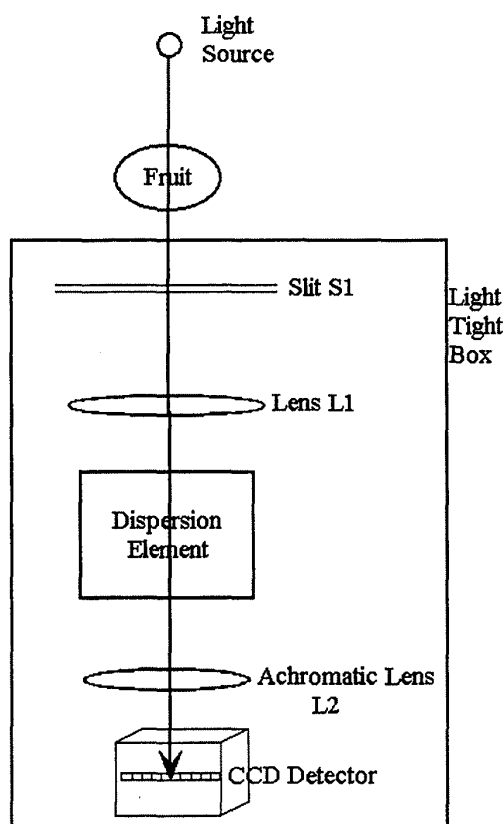


Figure 4.5. Diagrammatical representation of the NIR spectrometer.

The spectrometers (beam collimating and focussing optics, wavelength dispersion element and photodetector) were designed, constructed and housed in

Experimental Comparison of Simple NIR Spectrometers

a light tight box to eliminate the effects of stray light. An opaque test sample was placed in the sample position to test the system for this purpose. A diagram is shown in Figure 4.5.

Samples were illuminated using a 100 W tungsten halogen bulb powered at 12 V, 8 A by a low ripple DC power supply (Power House Pty. Ltd., Brisbane, Australia, L1288) mounted at the primary focus of a rhodium coated elliptical reflector (Melles Griot, Irvine, Ca., 02REM014). Electrical input power to the bulb was typically in the range 90 - 100W.

4.3.2. Method

4.3.2.1. Spectrometers

Measurements were made of light from a HgAr discharge source (Ocean Optics, Inc., Dunedin, FL, HG1) positioned 5 mm from S1. Spectral data were acquired using SpectraSolve v 4.0 with Larry addin detector driver package. Known spectral peaks (manufacturer supplied) were associated with pixel number and a calibration equation generated using TableCurve Windows v 1.10 (San Rafael, Ca.). Spectra were regenerated using calculated wavelengths to determine spectral range. Resolution was determined by full width at half maximum (FWHM) at 763 nm.

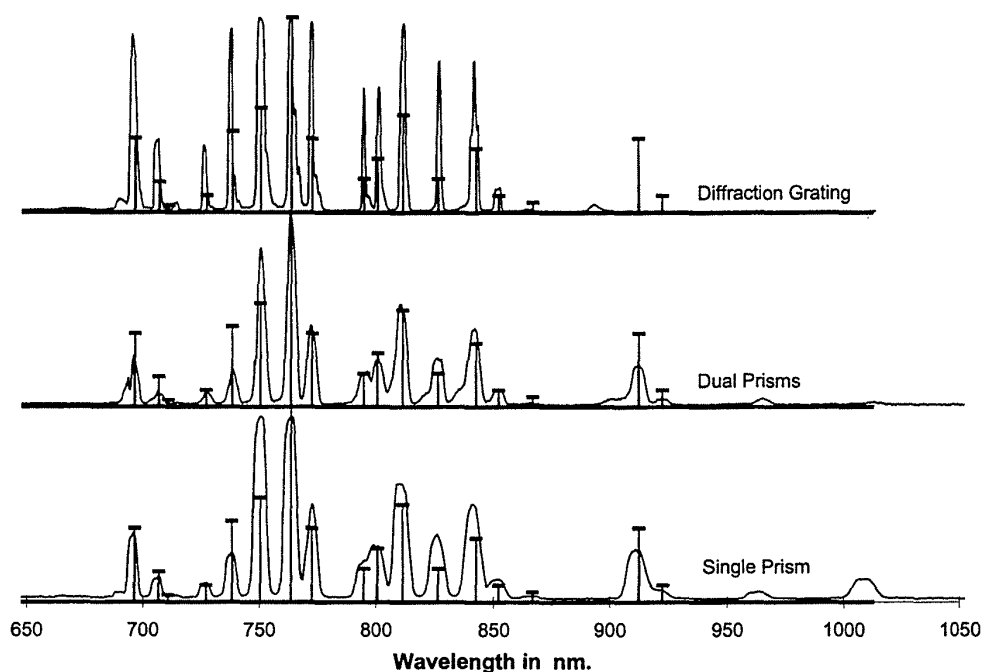


Figure 4.6. Comparison of the relative resolution and bandwidth of the diffraction grating, single prism and double prism spectrometers using a HgAr discharge source. Baselines have been displaced for clarity. Bars indicate manufacturer's specified peak intensity.

Throughput was assessed by comparison of peak heights of spectral responses to a 750 nm narrow bandpass filter (S10-750-F, Corion, Franklin, Ma.). Each configuration was exposed to direct illumination by the stabilised power supply attenuated by two neutral density filters (AD100F and AD30F, Corion, Franklin, Ma.) and passed through the 750 nm bandpass filter.

Linearity of response was visually assessed by comparing spectra of each system against the manufacturers specified peak intensities for the HgAr discharge source plotted as bars overlaying response plots for each system (Fig. 4.6).

4.3.2.2. Fruit Assessment

The fruit samples were positioned 5 mm from the slit on the optical axis with the light source. This position ensured full transmission mode was achieved and eliminated specular reflectance effects. The fruit under test was positioned at the secondary focus of the elliptical reflector, although positioning was found not to be critical as the fruit randomly scatters the incident radiation and acts as a diffuse, poorly defined object.

Representative batches of 18 limes at differing stages of maturity (assessed visually in the field) were collected from the authors' farms and stored in a refrigerator at approximately 5° C if same day experimentation was not possible. All fruit samples were allowed to equilibrate to room temperature (25° C) before measurements were made. The fruit samples (~ 47 - 60 mm diameter) were presented intact to each of the spectrometers in three orientations (ie. along the distal axis and along the equatorial axis in two orthogonal directions). Hence each sample produced three spectra increasing the total number of spectra recorded to 54. Each dispersing element configuration was optimized to maximize resolution and intensity using measurements of spectra of a commercial HgAr discharge source, positioned to illuminate slit S1 prior to sample spectral measurements to assess each at its individual optimum performance level.

4.4. Results and Discussion

4.4.1. Comparison of Spectrometer Performance

Spectra recorded by the single prism, double prism and diffraction grating spectrometer configurations when illuminated by the HgAr discharge source are shown on Figure 4.6. The resolution measured at 763 nm FWHM was 3 nm, 4 nm and 6 nm for the diffraction grating, dual prisms and single prism, respectively. Linear dispersion (0.53, 0.26, and 0.15 nm/pixel for the diffraction grating, dual prisms and single prism, respectively) of each system was in good agreement with the theoretical predictions as shown in Table 4.1.

Table 4.1. Observed and calculated resolution of the three spectrometer configurations.

Configuration	FWHM (nm)	linear dispersion	linear dispersion
	at 763 nm (observed)	nm / pixel (observed)	nm / pixel (calculated)
Single prism	6.04	0.56	0.53
Dual prism	4.43	0.23	0.26
Diffraction grating	2.96	0.16	0.15

Peak heights resulting from exposure to attenuated light from the stabilized power supply and passing through a 750 nm bandpass filter were 2500, 2400 and 1500 counts for diffraction grating, dual prisms and single prism, respectively. The band pass of this filter coincided with the peak efficiency for the grating so results for the grating may be slightly optimistic because grating efficiency deteriorates away from this high point. The lower than theoretically expected

Experimental Comparison of Simple NIR Spectrometers

efficiency of the prism based systems may be attributed to the design of the antireflective coating (MgF_2 , thickness optimized for 550 nm) and the high angle of incidence (60°) on the first interface. Reflectivity of the antireflective coating was calculated to be $\sim 7.5\%$ at 60° incident angle. Throughput for the prism based instruments may be improved by more appropriate antireflective design.

The most pronounced difference in the spectra arose in the effective useful bandwidth of operation. The prism configurations had a relatively uniform transmission function through the visible and NIR ($\sim 400 - 1050$ nm) and closely reproduced the HgAr discharge source intensity curve supplied by the manufacturer. The diffraction grating, however, had a non-linear, wavelength dependent efficiency which was a function of the blaze angle and the direction of reflected radiation relative to the grating normal. When optimized for maximum intensity and resolution, the useful bandwidth of the grating lay in the 650 - 900 nm range and spectral features in the region of the blazed angle were significantly enhanced. This may have a significant impact on the usefulness of the grating instrument for applications involving the analysis of raw spectral data unless additional signal processing to correct for the variation in efficiency is not performed. For example, physiological changes occurring in the fruit during the ripening process can lead to spectral signatures of maturity, for example variations, in the relative intensity of features and an increasing total transparency to radiation. In addition, the NIR spectra are generally characterised by broad spectral features, typically 40 nm wide¹⁴ making band assignment difficult if distortion of the spectra by the instrument function occurs. Greensill and Newman¹⁷¹ have discussed this effect on spectra of pawpaw

(*Carica papaya*) and similar effects are evident in the spectra of limes in this study.

4.4.2. Radiation Transmission by Limes

Citrus fruit exhibit a gradual decline in their respiratory pattern during ripening which classifies them as non-climacteric and requires that they must be allowed to mature on the tree before harvesting. The peel comprises two layers, the thin, outer, pigmented exocarp and the thicker, inner mesocarp which is a colourless tissue with many large air spaces. The endocarp or pulp of the fruit is a complex, segmented structure built up of many juice sacs which contain essentially all of the soluble solids responsible for flavour and some pigments²⁰³.

The spectra recorded by each spectrometer demonstrated a similar trend of increasing transmission towards shorter wavelengths as ripeness develops. As the ripening process proceeds, the exocarp of the lime changes from green to yellow due to the degradation of chlorophyll and increased biosynthesis of carotenoids whereas the endocarp remains green. Chlorophyll is known to absorb radiation over the ranges 550 - 590 nm, 620 - 630 nm and 710 - 740nm¹⁹⁹ so that the increasing transmission observed in the spectra in the region of 700 - 720 nm can be attributed to a falling concentration of chlorophyll in the exocarp. Band assignment for the 805 nm peak could not be confidently made because a comprehensive listing of band assignments for the 700 -1050 nm region was not available. The 850 nm band may correspond to C-H unsaturated fats peaks⁶⁶.

Experimental Comparison of Simple NIR Spectrometers

A typical transmission spectrum for immature (green) and mature (yellow) limes, believed to be the 'West Indian' cultivar, was obtained with the diffraction grating, dual prism and single prism spectrometers are shown in Figures 4.7, 4.8 and 4.9, respectively. All spectra were smoothed using a boxcar smoothing algorithm with a window size dependent on their relative resolution (3 nm, 6 nm and 4 nm, for diffraction grating, one prism and two prisms, respectively). These spectra were normalized to maximum intensity for clarity.

The features present in these spectra are listed and compared in Table 4.2. Although inferior resolution of the single prism spectrometer resulted in a loss of detail, the spectra demonstrated a shift in the intensity of peak transmission with ripening from about 805 nm to 720 nm in agreement with the dual prism instrument. A comparison of the higher resolution dual prism and diffraction grating results highlighted features which were common to both sets of spectra, but which had marked differences in intensities. Raw spectral data for the three spectrometers, with a simple linear background subtraction, yielded a useful threshold signature of fruit maturity (Table 4.3). The dual prism results demonstrated a capability of using these features to discriminate for maturity using the intensity ratios I_{720} / I_{750} or I_{720} / I_{805} directly from the raw data, however for the grating the structure at 720 nm was not as well defined. The grating spectra exhibited shoulders at 745 nm and 805 nm which changed in intensity relative to the maximum transmission peak but, as this did not occur at a fixed wavelength for the green and ripe limes, an additional computation would

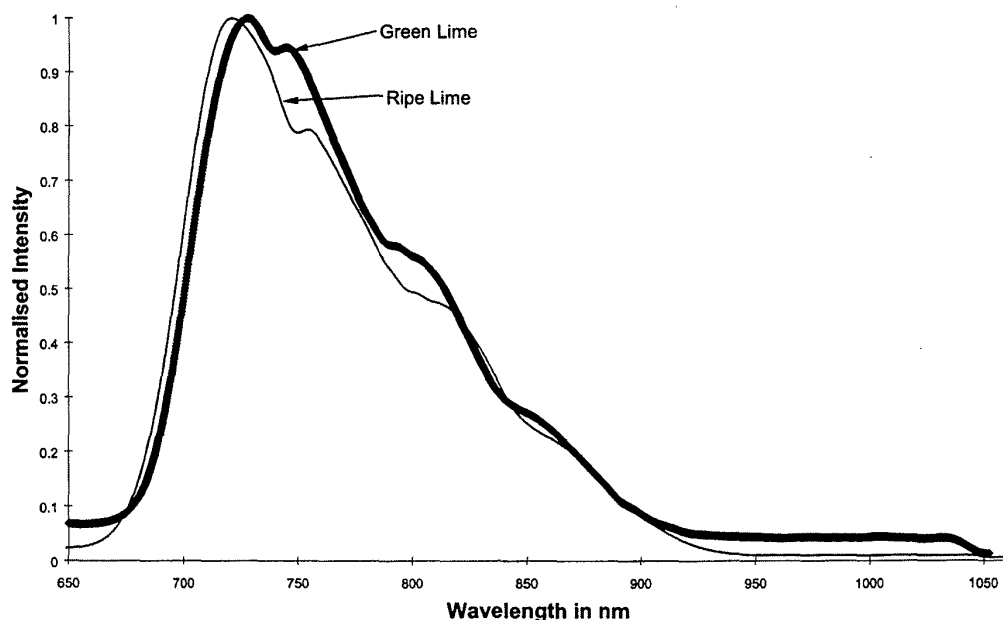


Figure 4.7. Transmission spectra of limes at two stages of ripeness using the diffraction grating spectrometer. Normalisation factors $\cong 3.5 \times 10^{-4}$ for ripe and 1.5×10^{-3} for green states.

be required to determine its position. Although this would be a trivial task, it would have consequences for the ultimate throughput of a machine in practical use. The dual prism spectrometer had an advantage over the diffraction grating based instrument since it could identify two relationships (I_{720} / I_{750} and I_{720} / I_{805}) for prediction purposes whereas the diffraction grating instrument could only reliably identify one (I_{710} / I_{805}). Although, attenuation of transmitted radiation through fruit is extremely high (dependent on the sample), the relationship among spectral peak amplitudes can remain constant, despite variation in attenuation due to different pathlengths, if appropriately selected.

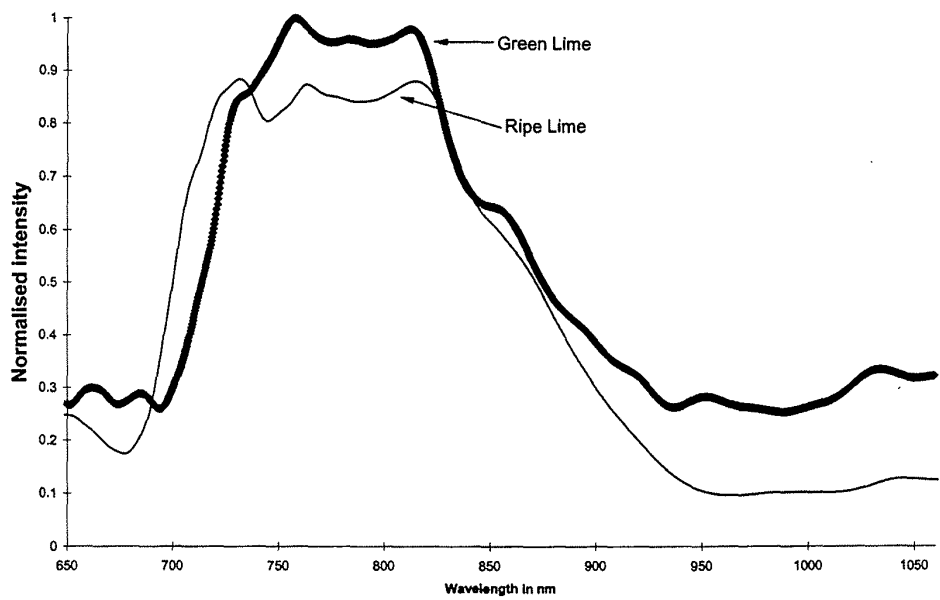


Figure 4.8. Transmission spectra of limes at two stages of ripeness using the dual prism spectrometer. Normalisation factors $\cong 3 \times 10^{-3}$ for ripe and 9×10^{-3} for green states.

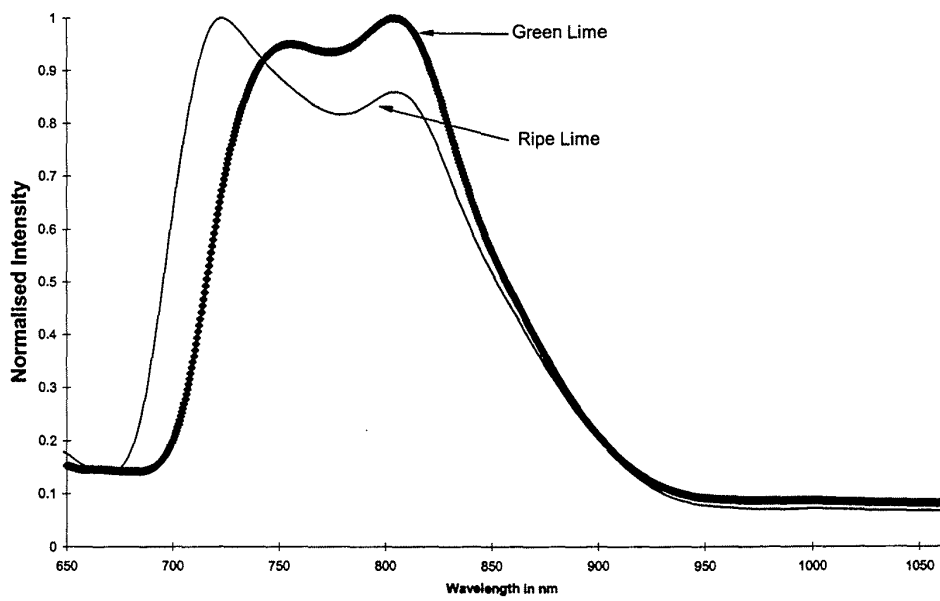


Figure 4.9. Transmission spectra of limes at two stages of ripeness using the single prism spectrometer. Normalisation factors $\cong 1.5 \times 10^{-3}$ for all spectra.

Table 4.2. Summary of features observed in the transmission spectra of limes taken with the prism and diffraction grating spectrometer configurations. The following abbreviations apply; fruit maturity, R : ripe, G : green; spectrometer configuration, SP : single prism, DP : dual prism, DG : diffraction grating.

λ (nm)	Structure	Maturity	Configuration
710	transmission peak	R	DG
720	transmission peak	R	DP, SP
730	transmission peak	G	DG
745-750	peak	G, R	DP
	pronounced shoulder	G	SP
	shoulder	G, R	DG
805	peak	G, R	DP, SP
	shoulder	G, R	DG
845-850	weak shoulder	G, R	DP, DG

Table 4.3. Intensity ratios as indicated of selected features according to lime maturity for the prism and diffraction grating based spectrometer configurations.

	Single Prism	Double Prism	Diffraction Grating
Ripe	1.13 ± 0.01 (I_{720} / I_{805})	1.06 ± 0.01 (I_{720} / I_{805}) 1.03 ± 0.01 (I_{720} / I_{750})	2.13 ± 0.05 (I_{710} / I_{805})
Green	0.73 ± 0.02 (I_{720} / I_{805})	0.76 ± 0.02 (I_{720} / I_{805}) 0.69 ± 0.02 (I_{720} / I_{750})	1.62 ± 0.07 (I_{730} / I_{805})

Figures 4.7 to 4.9 highlighted the efficiency differences between the two types dispersive elements. The spectral response of the grating based system was

wavelength dependent; hence the resultant spectra displayed a reduced sensitivity in the regions away from its blazed wavelength (750 nm) or region of peak efficiency (650 to 850 nm) when compared to those of the prism based systems. Since spectral features outside this region are frequently used for fruit quality assessment⁶⁸ the performance of the grating based instrument may be less than desirable.

4.5. Conclusion

Three simple near infrared (NIR) spectrometers, incorporating differing dispersion elements (single equilateral prism, two equilateral prisms in series and ruled diffraction grating) were constructed to compare performance for suitability for fruit sorting in an in-line setting. Performance, in terms of resolution, spectral range, efficiency and linearity across the spectral range, was characterised using a HgAr discharge source. Further, practical application was assessed by comparison of spectra from transmitted radiation of whole immature and mature limes (*Citrus aurantifolia*) over the wavelength range 650 - 1050 nm.

The resolution of each spectrometer configuration was estimated from the full width at half maximum of the 763 nm line from a HgAr discharge source. Results yielded 3.0 nm, 4.4 nm and 6.1 nm for the diffraction grating, dual prism and single prism configurations, respectively. The results of measurements on limes indicated that, on the basis of the performance criteria above, the configurations ranked in order of suitability are: dual prism, diffraction grating and single prism. The dual prism configuration exhibited uniform efficiency and

Experimental Comparison of Simple NIR Spectrometers

dispersion characteristics over a wider spectral range than the diffraction based instrument resulting in markedly different effects on the intensities of common features in the raw data of each. The characteristics of the dual prism may facilitate the generation of predictions relationships from appropriately selected features over those of the grating based instrument. Throughput was found to be slightly lower for the prism based than the grating based instruments although this relationship could be reversed by more appropriate antireflective coating design.

Radiation transmitted through whole limes in the unripe (green peel) and ripe (yellow peel) states was measured over the wavelength range 650 - 1050 nm in order to ascertain whether spectral signatures existed to allow the maturity of the samples to be identified from the raw data with minimal further processing. The results demonstrated an apparent correlation between the degradation of chlorophyll in the outer peel, observed through an increase in transmission at about 720 nm, with respect to the intensity of spectral features, possibly related to the concentration of sugars in the pulp, at 750 nm and 850 nm. Further experiments are now in progress to determine whether a quantitative relationship can be established between particular intensity ratios of these spectral features and the degree of fruit maturity.

5. An Investigation into the Determination of the Maturity of Pawpaws (*Carica papaya*) from NIR Transmission Spectra

This chapter has been published under this title in the Journal of Near Infrared Spectroscopy, 7 (1999), pp. 109-116.

5.1. Introduction

The increasing demands of volume production and the need for quality assurance in the fresh fruit and vegetable industry are resulting in food processors looking towards technological solutions for rapid, non-invasive assessment of produce. One method that has been receiving considerable attention is the use of near infrared (NIR) radiation to indicate the level of maturity and/or ripeness of the primary product. Optical spectrometers have been employed that detect radiation that is either scattered from the skin and near surface layer (reflectance mode) or scattered by the bulk flesh (transmission mode) of the product before detection. In transmission measurements, radiation is detected after passing through the body of the fruit where absorption and scattering occurs dependent upon various physical and chemical characteristics of the fruit (dimensions, density, water content, sugar content, presence of seeds etc.). Many laboratory studies have been performed that have determined the existence of correlations between the spectral response and the total dissolved solids content of various fruits in the NIR region. For example, work has been reported for mangoes^{10, 156,}

An Investigation into the Determination of Maturity of Pawpaws

pawpaws¹⁹⁹, melons^{59, 122} and peaches⁹. Knowledge of the ripening properties of fruit can have considerable advantages in practice, especially with regard to optimal harvesting times to minimise damage to produce from environmental pests. The capability to assess the maturity of the fruit before harvest would have definite advantages.

Pawpaws are susceptible to attack by a variety of insect pests. For example, in Hawaii they are infested by the Oriental fruit fly (*Dacus dorsalis*), the melon fly (*Dacus cucurbitae*) and the Mediterranean fruit fly (*Ceratitidis capitata*)^{204, 205}. Pests of significance to Australia include the Queensland fruit fly (*Dacus tryoni*) and the Papaya fruit fly (*Bactrocera papayae*) which made its first appearance on the mainland in the Cairns district in 1995 followed by a more serious outbreak in 1997 along the eastern seaboard of northern Queensland down to the Townsville area. Harvesting pawpaws at an early stage in their development can minimise the incidence of fruit fly infestation. Previous work by Seo *et al.*²⁰⁶ and Couey *et al.*²⁰⁷ has shown that pawpaws more mature than the half ripe stage are most susceptible to attack.

The pawpaw is a climacteric fruit in that it demonstrates a peak in its respiratory pattern during ripening. Several physical and chemical changes occur during the development of the fruit but between 110-120 days after flower fertilisation, two useful indicators to maturity become apparent. In an immature green pawpaw, the seeds and the flesh surrounding the central cavity are both white, for a mature green pawpaw, the seeds are turning black and the flesh begins to yellow. At a certain stage of maturity, a green pawpaw can be picked and will continue to

An Investigation into the Determination of Maturity of Pawpaws

ripen off the palm to achieve its full flavour; this is not the case for an immature green fruit²⁰⁷. However, these internal indicators of maturity are not accompanied by any visible change to the exterior of the fruit so that a reliable, non-invasive indication of the maturity status of the fruit could be of considerable benefit to the industry.

Experiments have been conducted by the United States Department of Agriculture in an effort to determine the maturity status of green pawpaws in a quantitative and non-destructive fashion. These include the body reflectance and transmittance work of Birth *et al.*¹⁹⁹ and the delayed light emission studies of Forbus *et al.*²⁰⁴ and Forbus and Chan²⁰⁵. Birth *et al.*¹⁹⁹ used a scanning monochromator and a tilting filter spectrometer to measure the change in relative optical density of immature and mature green pawpaws over the wavelength range of 500 - 900nm. They presented their data in terms of a relative optical density (ROD) of the fruit as a function of wavelength (where they defined ROD as the logarithm of the ratio of the transmission of a standard to the sample) and based their maturity predictions primarily on measurements from the visible region of the spectrum where the ROD was yielding a transmission of about 0.1% of that in the near infrared. Their spectra did generally show, however, identifiable trends in the wavelengths over the 700-800nm range but as the resolution of their instrument appeared to be low (> 4 nm FWHM at 700 nm), they were unable to resolve sharp features which limited their findings.

Forbus *et al.*²⁰⁴ employed the technique of delayed light emission to measure pawpaw maturity and later, Forbus and Chan²⁰⁵ extended the method to predict

the susceptibility of pawpaw to fruit fly infestation. Delayed light emission occurs for several seconds after chlorophyll containing material is illuminated by a light source and then placed in the dark. The work indicated a high correlation between the intensity of delayed light emission and colorimetric methods (Hunter 'b' values) of determining the ripeness of the fruit from the yellowing of the skin. However, the physical requirements of this technique limit its usefulness for incorporation into a small portable instrument.

This paper reports on some of our investigations into NIR transmission spectra of pawpaws in various states of maturity ranging from immature green through to skin colour break. The main aim of our work is to determine and identify whether any features or trends exist in the NIR spectra which can be used to assess the level of maturity of pawpaws using a simple correlation between the observed features and the level of maturity without the need for time consuming and expensive calibrations that are frequently used in other similar horticultural applications at the present. Success in this endeavour would illustrate the utility of a simple instrument for this determination which would be of interest to those workers in the field.

5.2. Experimental Method

5.2.1. Spectrometer

The NIR optical spectrometer, designed and constructed at this research facility for the purpose of these experiments, is comprised of a light source, beam

collimating and transport optics, a wavelength dispersion element and a photodetector as shown diagrammatically in Figure 5.1.

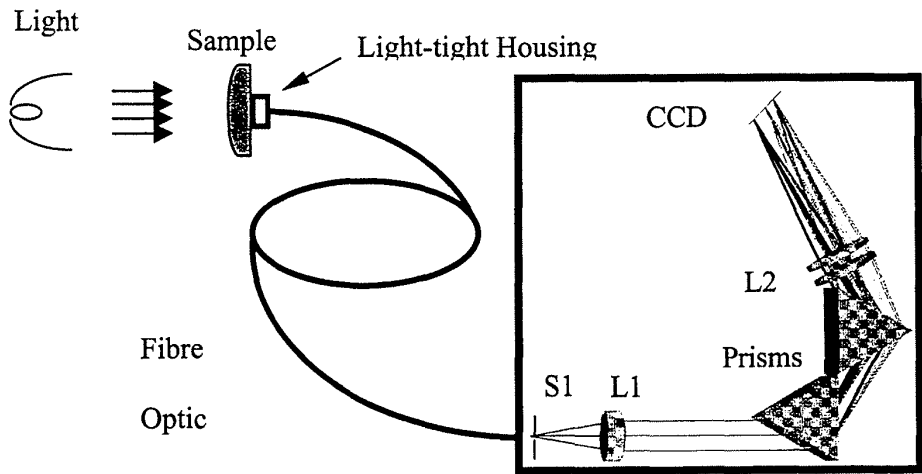


Figure 5.1. Diagrammatical representation of the NIR spectrometer.

All elements of the optical train, after the light source, were mounted in a blackened light tight box to eliminate any interference from environmental background radiation and reflections from optical surfaces. The light source consisted of a tungsten halogen bulb, mounted at the primary focus of an elliptical reflector and powered by a low ripple DC power supply at a typical electrical input power of about 90 - 100W. The fruit sample under test was positioned in the region of the secondary focus of the reflector, although this was not found to be a critical consideration as the fruit randomly scatters the incident radiation and acts as a diffuse, poorly defined object. Radiation transmitted through the sample was collected by a 500 μ m diameter optical fibre with an 11° numerical aperture mounted on the optical axis of the reflector. The receiving end of this fibre optical cable was positioned at a fixed distance of 5mm from the

An Investigation into the Determination of Maturity of Pawpaws

sample inside a blackened cavity which contacted the sample thereby eliminating stray light. The other end of the fibre was positioned before a vertical parallel slit, S1, of 10 μ m width mounted approximately at the focal length of a collimating lens, L1 (achromat of 30mm diameter and 50mm focal length), to define a parallel input beam to the spectrometer. The precise position of L1 relative to S1 was adjusted to optimise the resolution and intensity of the spectrometer.

Dual equilateral prisms of SF18 glass were employed for the wavelength-dispersing element. The dispersed radiation was focussed onto a charge coupled device (CCD) detector with lens L2, comprised of a combination of two plano-convex lenses (40mm diameter and 200mm focal length) positioned to give a total focal length of 100mm which ensured a suitable linear dispersion of the spectrum across the CCD face. The detector was purchased as a commercial package and consisted of a 2048 pixel, line element CCD (Larry™) with a 500kHz, 12 bit ADC card. The CCD was supplied with a polymer window and had pixel dimensions of 14 μ m (h) by 12 μ m (w) on a 14 μ m spacing. The spectrometer was controlled by a PC running a custom data analysis and acquisition package (Spectrasolve™).

Calibration of the wavelength scale was accomplished using a commercial mercury - argon discharge source (Ocean Optics HG1) coupled to the optical fibre input of the spectrometer. The resolution of the system was estimated from the full width at half maximum (FWHM) of selected peaks in the discharge spectrum.

5.2.2. Materials

Pawpaws at differing stages of maturity (assessed visually in the field by experienced personnel) were sourced from local farms from the Yarwun area of Central Queensland and stored in a refrigerator at approximately 10°C until the experiments were performed. All fruit samples were allowed to reach room temperature (about 20°C) before commencing any measurements. Individual pawpaws were sectioned into thirds perpendicular to the polar axis, the seeds were removed and their maturity assessed from flesh and seed colouration. For the purposes of this work, four grades of apparent maturity were noted as follows: (i) immature; skin green, flesh and seeds white (ii) transition; skin green, flesh white overall with a slight orange colouration around the seed cavity, seeds grey to black (iii) mature green; skin green, flesh demonstrating definite orange colouration (iv) colour break; skin pale green to patchy yellow, flesh uniform orange/yellow. Each third was further sectioned longitudinally into approximately 60 degree segments and three alternate segments were selected for the experiments and trimmed to approximately 20 - 25mm thickness. This process created nine samples from the one fruit but characteristic of that fruit. The flat, cut surface of the sectioned fruit was placed in contact with a light-tight housing which was connected to the fibre optic probe of the spectrometer. In this arrangement the sample to fibre optical cable distance was maintained at 5 mm and since the internal diameter of the housing was 25mm diameter and the N.A. of the fibre was 11° stray light was eliminated. Spectra were recorded with light incident on the skin surface using a CCD integration time of 50ms. A total of 30 pawpaws were sectioned in the above the manner to provide 270 samples to

determine whether any correlation exists between the observed spectral features and the assessed fruit maturity.

5.3. Results and Discussion

5.3.1. (a) Characteristics of the Spectrometer

The spectrometer transmission results using the HgAr discharge source are shown in Figure 5.2. The resolution of the system was estimated from the full width at half maximum of selected peaks and yielded the values of 3.5nm FWHM at 436nm, 4nm FWHM at 696nm and 9nm FWHM at 965nm. The relative intensities of the spectral lines were also in good agreement with the expected intensity distribution estimated from radiative transition probability data and the instrumental response of the spectrometer. Some instrumental effects were observed on the data but since they did not appear to complicate the determinations they were not removed and so the spectra presented herein are the raw transmission data.

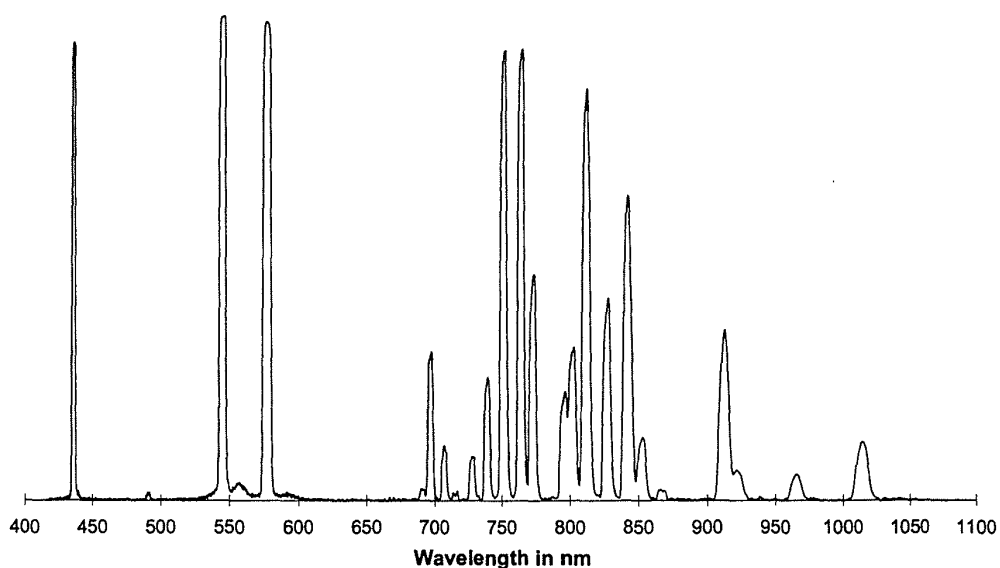


Figure 5.2. Spectrometer transmission results using a HgAr discharge source.

5.3.2. (b) Radiation Transmission by Pawpaw

Visual inspections of the flesh and skin colour of each segment were made before experimentation to allow an estimation of the maturity status. For grades (i) - (iii), described earlier, there was no external visual difference between the fruit.

In order to minimise possible effects on the results arising from the (unknown) field conditions of the fruit such as exposure to sun and shade, summed spectra were calculated for the stalk, central and blossom sections from the spectra of their three respective segments. In general the blossom and central thirds provided similar indicators of the maturity status whereas the stalk third indicated a less mature fruit. In addition an overall total summed spectrum was calculated from all nine segments to simulate data that would be collected from a

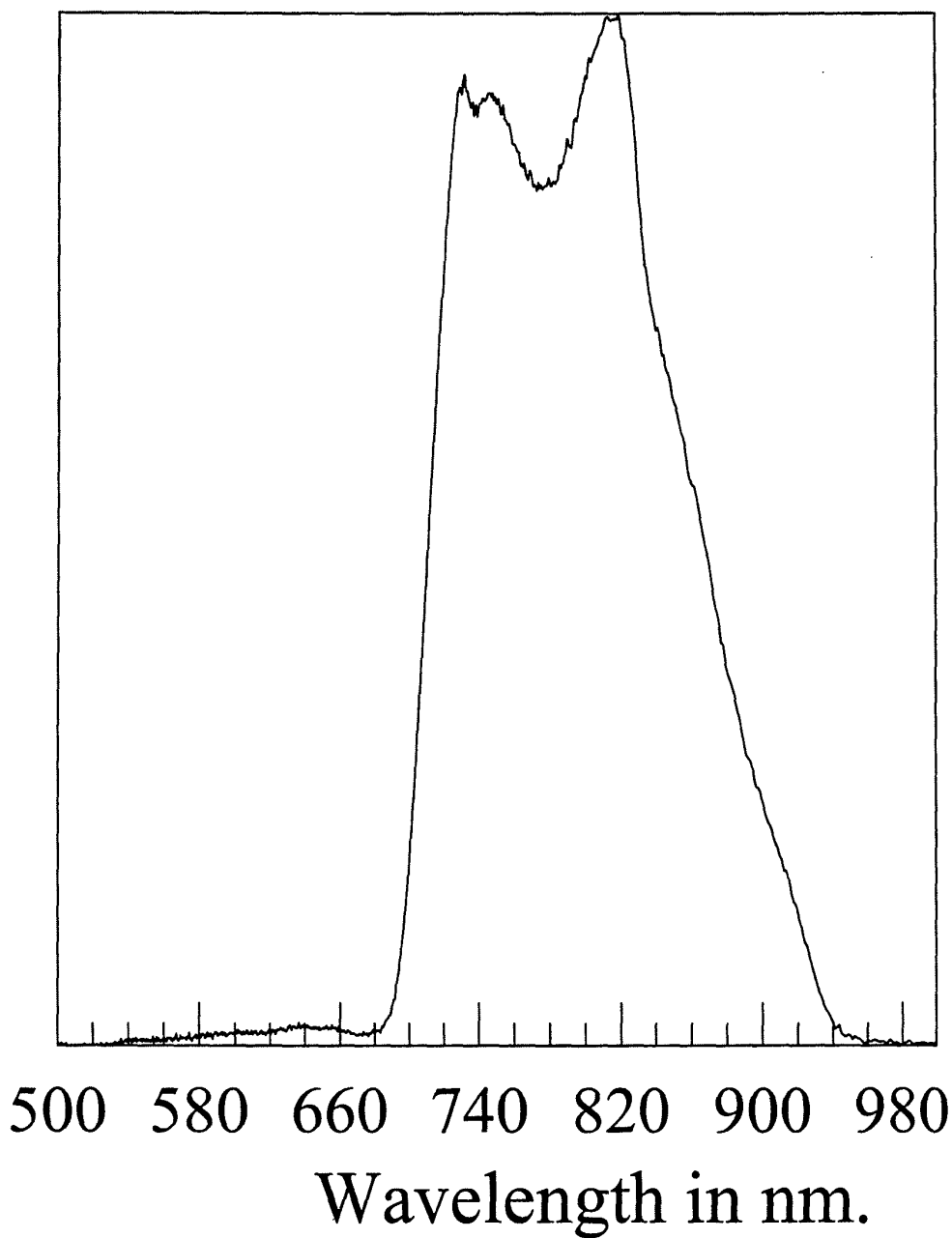


Figure 5.3. Typical averaged transmission spectra of pawpaw at an immature stage of maturity. Grade (i)

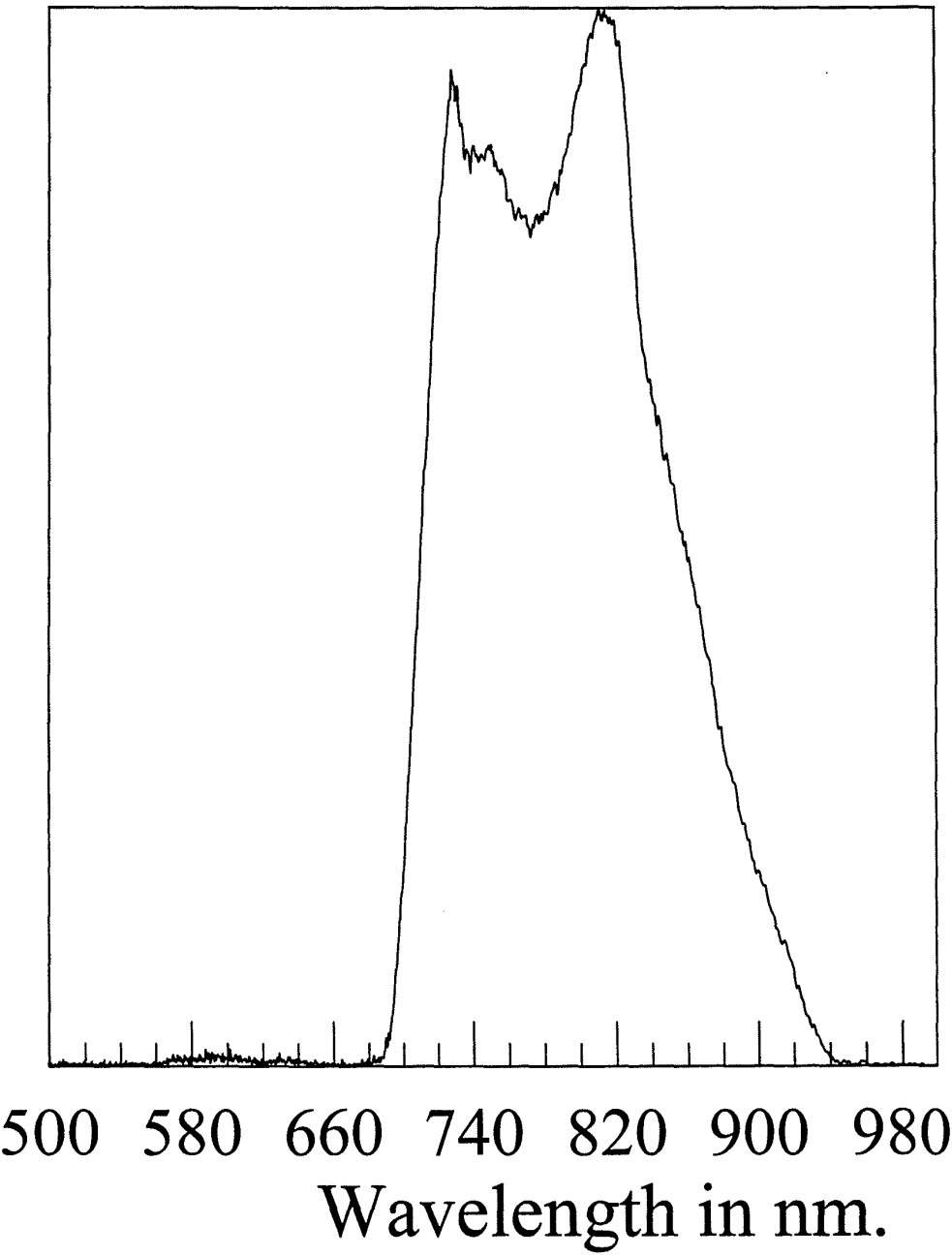


Figure 5.4. Typical averaged transmission spectra of pawpaw at the transition stage of maturity. Grade (ii)

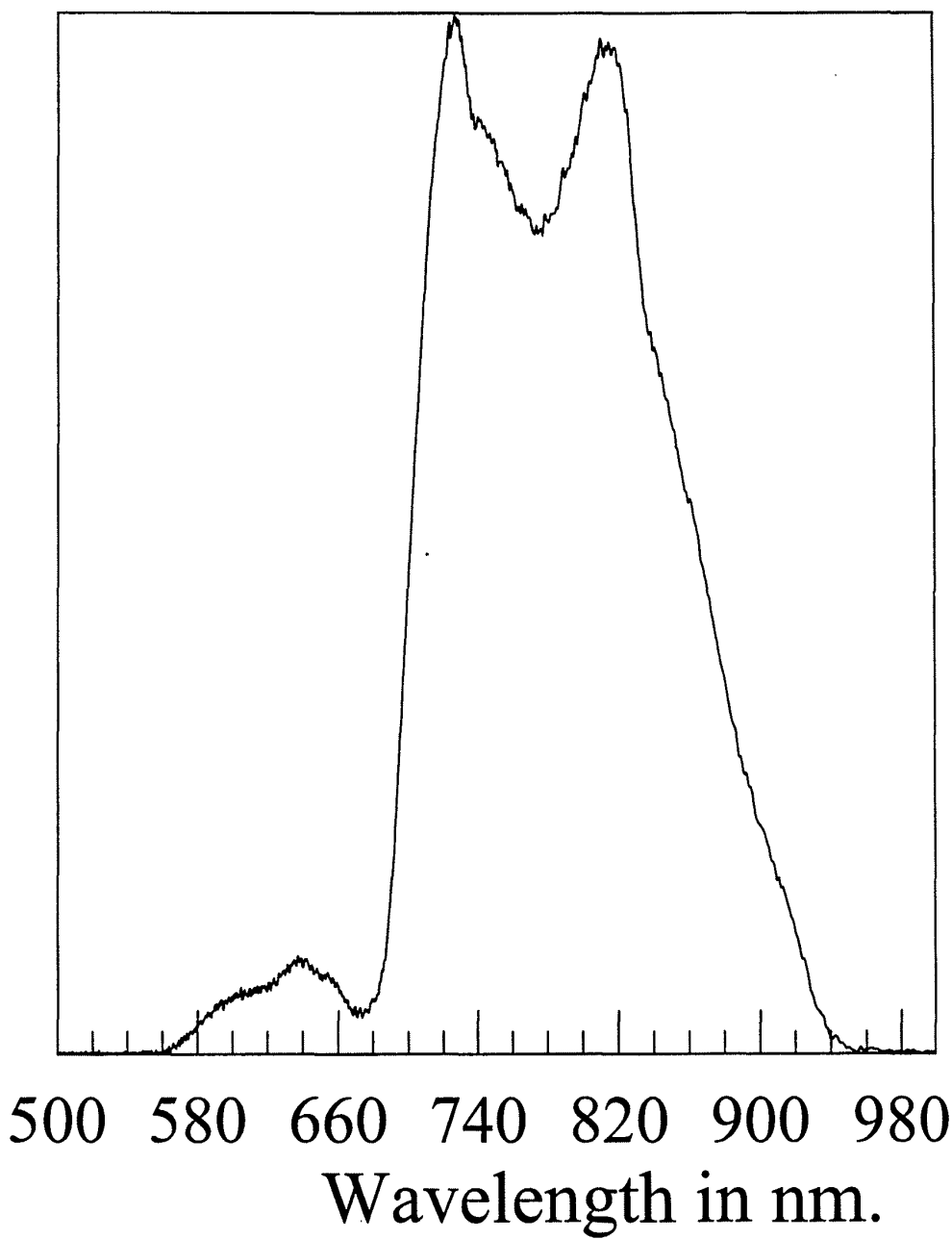


Figure 5.5. Typical averaged transmission spectra of pawpaw at late mature green stage of maturity. Grade (iii).

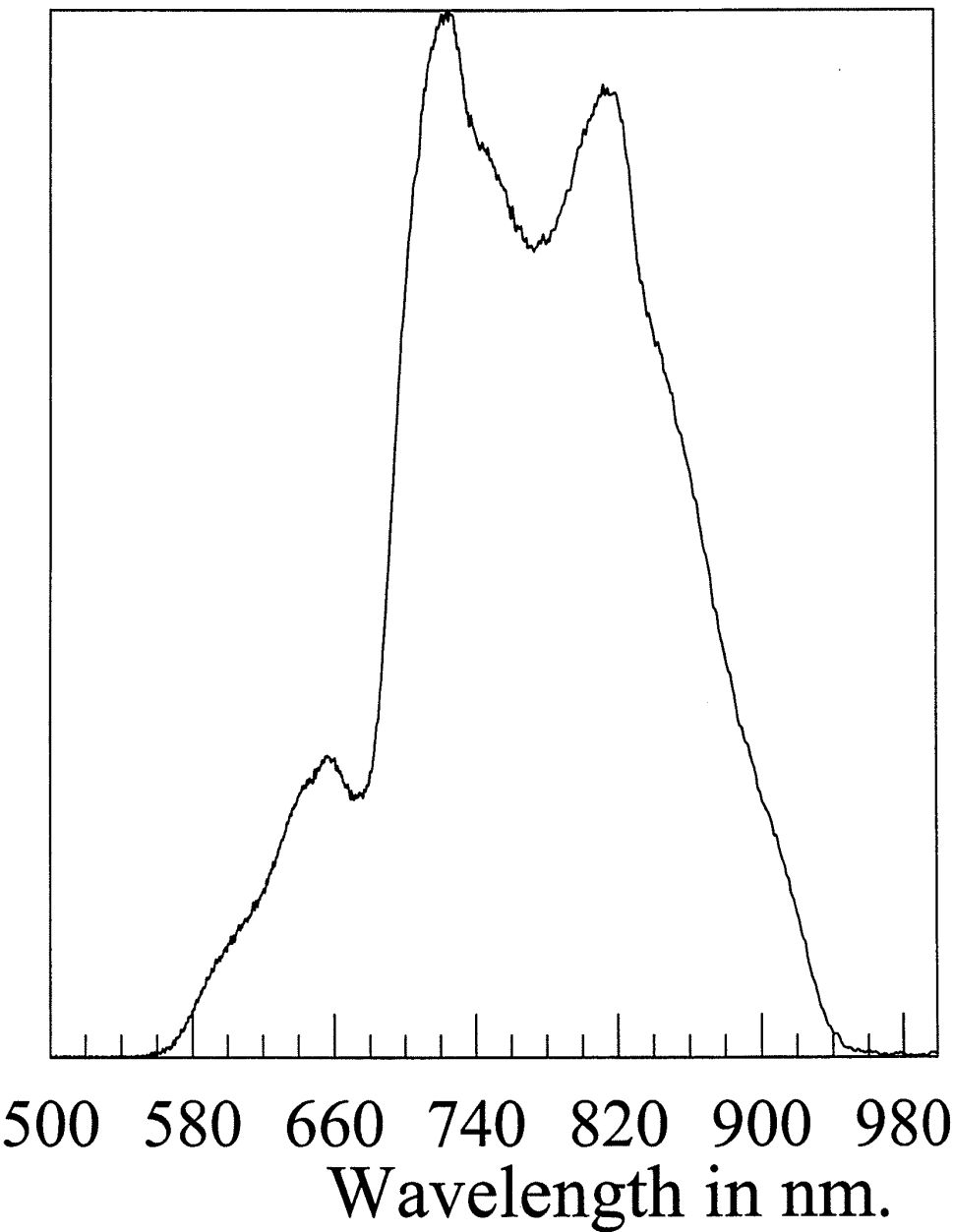


Figure 5.6. Typical averaged transmission spectra of pawpaw at the colour break stage of maturity. Grade (iv).

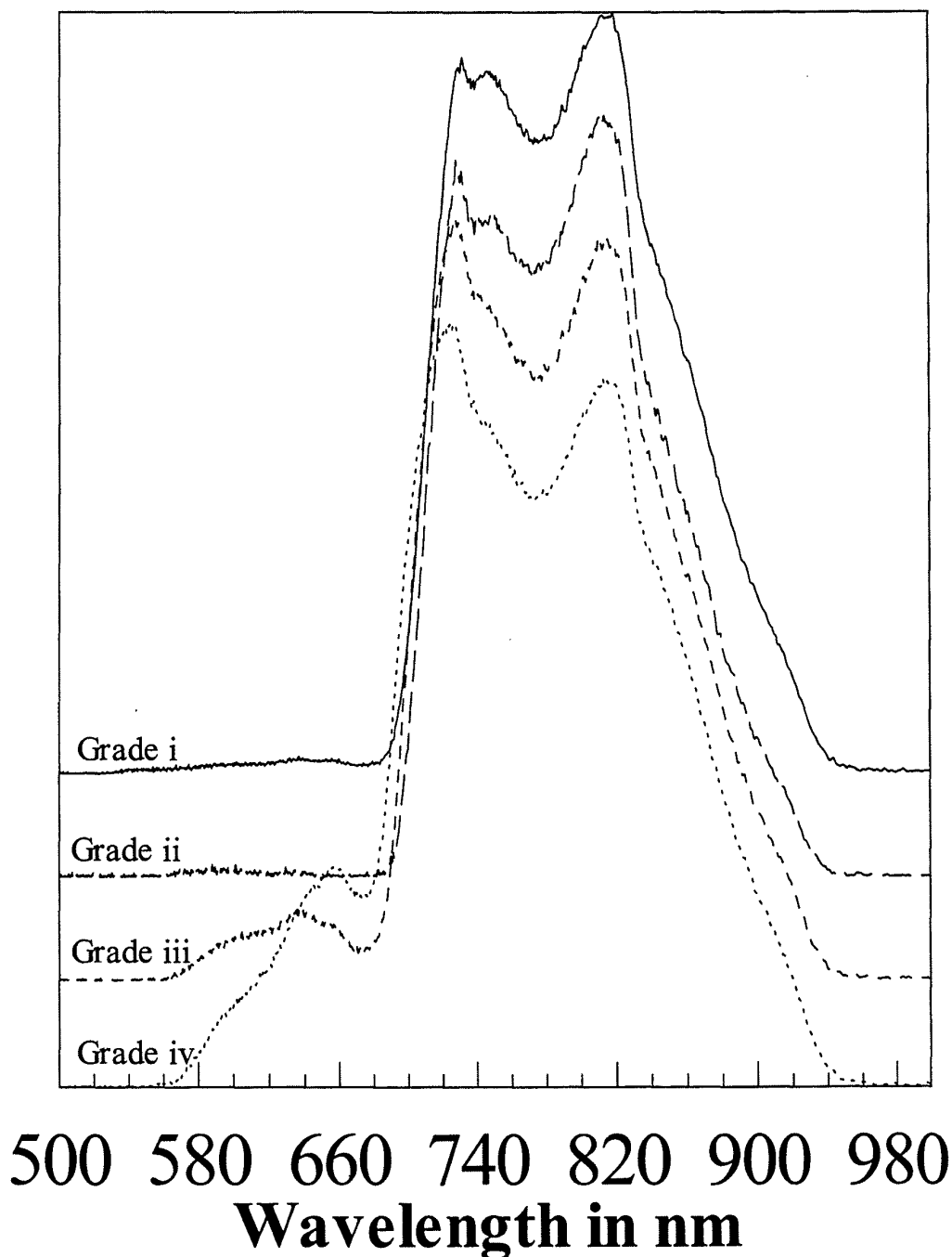


Figure 5.7. Typical averaged transmission spectra of pawpaw at the four stages of maturity. Grades (i).(ii), (iii), and (iv). The respective spectra have been displaced vertically for clarity and no ordinate axis is used since these spectra are viewed as self-calibrating.

whole fruit by an instrument operating in a scanning situation. Comparing all of the summed spectra, there appeared to be little difference between the whole fruit spectrum and the central and blossom end spectra apart from an improvement in the signal to noise ratio. Hence Figures 5.3 to 5.6 inclusive are typical summed transmission spectra for whole pawpaws representative of the four grades of maturity outlined above. Transmission mode was used in making these measurements to determine if a correlation among features of each sample's spectrum and their corresponding maturity level could be achieved.

Taking the spectra in Figures 5.3 to 5.6 as a whole, there are up to four distinct features in the transmission functions of which two demonstrated variability with sample maturity. No ordinate axes are defined in these figures since these spectra are viewed as self-calibrating and hence independent of the intensity of the transmission measurement. The individual spectra from Figures 5.3 to 5.6 are combined in Figure 5.7 and have been displaced vertically for clarity. All spectra showed a prominent peak at about 815nm after which the transmission fell rapidly to zero with increasing wavelength. This was most likely due to a combination of factors arising from the falling efficiency of the spectrometer at long wavelengths and the onset of absorption by water and to a lesser extent by carbohydrate (starch and cellulose)¹⁸ in this region. Further structures at 720nm and 745nm demonstrated interesting behaviour as ripening proceeded. In the immature green fruit, (Fig. 5.3), the 745nm peak was clearly seen with a distinct shoulder at 720nm. However once the fruit had ripened to the transition stage and beyond, the structures reversed in appearance, a prominent peak was observed at 720nm with a shoulder at 745nm (Fig.5.4). In addition the

magnitude of the 720nm peak showed a correlation with the maturity of the fruit, its intensity increased to a similar order as that of the 815nm peak as the fruit developed to the mature green stage (Fig. 5.5). For all of these maturity states, the threshold of increasing transmission remained constant at about 700nm. Once the fruit had reached the colour break stage (Fig. 5.6), the intensity of the 720nm peak exceeded that of the 815nm peak and it became the dominant feature in the NIR spectrum. At this stage the transmission threshold of the 720nm peak also shifted down to about 670nm and increasing transmission at lower wavelengths peaking around 660nm was also apparent.

As the ripening process proceeds, the chlorophyll content of the fruit falls to one sixteenth of its value at the immature stage and the carotenoids that result in the yellow colouration rise by a factor of about fourteen²⁰³. The measurements of Birth *et al.*¹⁹⁹ showed that both chlorophyll and carotenoids absorb radiation in the ranges of 550-590nm and 620-630nm but chlorophyll also absorbs over 710-740nm. Therefore the increase in intensity of the 720nm peak observed in the present spectra was attributed to a reduction in absorption by a falling concentration of chlorophyll.

The spectra for the immature, transition and mature green fruit all demonstrated a reasonably constant transmission bandwidth with a threshold of transmission occurring at about 700nm. For the colour break fruit, inspection of Figure 5.6 shows that the equivalent threshold has shifted down in wavelength to about 670nm though this has been masked to some extent by a rapidly increasing transmission of visible radiation giving rise to a small peak at about 660nm.

Some visible radiation was also observed in the mature green fruit spectra (Fig. 5.5). Although the increase in visible transmission was a real effect for ripening fruit, any attempt to link it to maturity offered fewer categories and more uncertainty. In contrast, the features observed in the NIR range, though attenuated to some degree by sample dimensions, always demonstrated the same relative intensity behaviour irrespective of reasonable experimental geometries.

In this work no attempt was made to reference the sample transmission to a standard as a primary interest of the investigation was the possibility of self-calibration by the sample using its own spectral signature.

The only other optical determination of pawpaw maturity of which the authors are aware that attempts similar measurements to those described in this paper was performed by Birth *et al*¹⁹⁹. Their spectra generally showed similar trends to the present work over the 700-800nm range but as the resolution of their instrument appeared to be somewhat less than that employed here, they were unable to resolve the sharp features seen in Figures 5.3-5.6. Their data for the immature green fruit yielded a smooth curve exhibiting lower transmission at about 730nm compared to 800nm whereas the mature green fruit demonstrated a similar intensity of transmission across this range. This can be compared with the present observations regarding the intensity shifts of the sharp feature at 720nm compared to that at 815nm. Both experiments observed a transmission threshold at about 690nm followed by increasing transmission with similar gradient as a function of wavelength irrespective of the maturity status of the fruit. Birth *et al*'s¹⁹⁹ data also showed a broad maximum at about 780-800nm

which overlapped for the immature and mature green fruit which probably corresponds to the 815nm feature observed in this work.

In contrast to the present work, Birth *et al*¹⁹⁹ based their maturity predictions primarily on measurements from the visible region. The experimental technique that they employed would have enabled data to be collected at low light levels in a straightforward fashion by varying the counting period to obtain an acceptable signal to noise ratio. In the presented method which collected light at all wavelengths simultaneously, the counting period was limited by the time taken to saturate the detector by the most intense transmission feature in the near infrared, often resulting in a poor signal to noise ratio for weak features in the visible region. Therefore given our earlier comments regarding visible light transmission, no conclusions concerning the maturity of fruit at less than the colour break stage could be reliably drawn from observations in this wavelength region with the present apparatus.

5.4. Conclusion

Samples of pawpaws (*Carica papaya*) were illuminated by a focussed 100W tungsten halogen light source and the transmitted radiation coupled to the entrance slit of the spectrometer by an optical fibre probe. Data acquisition times were typically 50ms per spectrum. Transmission spectra over the wavelength range of 500 - 1000nm were recorded from 270 samples taken from 30 fruit at varying stages of development ranging from an immature green state to beyond skin colour break. Distinct spectral features were observed at 720nm, 745nm and

815nm in the raw data. As ripening proceeded the 720nm feature gained in intensity and changed from an indistinct structure in the immature green fruit to a prominent peak of similar magnitude to the 815nm peak in the mature green fruit. At the skin colour break stage, the 720nm peak dominated the spectrum and increasing transmission was also observed in the 550 - 700nm wavelength range. Previous work by Birth *et al.*¹⁹⁹ linked the region of 710-740nm to absorption by chlorophyll and the wavelength of the feature at 720nm and the changes in its spectral behaviour appeared to be indicative of the degradation of chlorophyll in the maturing fruit.

This work has demonstrated that direct observation of the near infrared optical transmission function can provide a non-invasive method for determining the maturity status of green pawpaws. If the maturity status of the green fruit is known, this could permit early harvesting, helping to minimise the likelihood of pest infestation. The results could potentially be exploited in the development of a portable instrument for use in the field and/or an in-line instrument for grading on a conveyor belt.

6. Optimisation of Instrumentation Precision and Wavelength Resolution for the Performance of NIR Calibrations of Sucrose in a Water-Cellulose Matrix.

This chapter has been published under this title in the Journal of Applied Spectroscopy (2000), 54, (3), 426-30.

6.1. Introduction

Since the early 1970s the interest in and the use of *near infrared* (NIR) spectroscopy has grown enormously in the food related industries. Technological progress has seen the instrumentation evolve from instruments incorporating the use of single photomultiplier tubes and changeable filters¹⁹⁹ to those with scanning diffraction gratings as the wavelength selection mechanism, and the use of a single semiconductor (e.g. Si, InGaAs, PbS)²⁰⁰ in place of the photomultiplier tube. The next step in this evolutionary process was the transition to instruments using arrays of photodetectors in combination with stationary wavelength dispersion elements like diffraction gratings to capture entire spectra simultaneously. This step allowed the possibility of near-realtime processing in analytical process control applications. Technological progress has also provided the instrument designer with a choice of types of photodetector. For example, the use of *photodiode arrays* (PDA) allows higher signal precision (or signal to noise ratio, SNR) whereas the use of *charge-coupled devices* (CCD)¹² offer higher sensitivity but reduced precision. Since CCDs generally

Optimisation of instrumentation precision and wavelength resolution.

have smaller pixel dimensions than the PDAs, the wavelength resolution available in CCDs is generally higher than PDAs for a given instrument size. All of these types of instrumentation have been used for the NIR spectroscopic assessment of fruit for soluble sugar content (e.g. scanning grating¹⁶³, CCD¹², PDA¹⁷³).

The primary performance characteristics of a spectrometer operating in body transmittance mode are its precision, wavelength resolution, sensitivity to light, stray light, sensitivity to environmental variables (e.g. temperature and humidity fluctuations), bandwidth and rate of processing data. These criteria together with the manufacturing simplicity and cost of the instrument need to be defined in order to design an instrument for a specific commercial application.

Quantitative data analysis requires that the precision (SNR) of an instrument be of an acceptable level. This criterion is influenced by the various noise contributions associated with the detector type, associated electronics and signal level. Digital filtering has been demonstrated to improve the SNR and hence improve the performance of resultant calibrations²⁰⁸. Lu and McClure¹²⁷ report that when calibrating on synthesised data some full spectrum calibration methods “performed quite well for predicting the composition of a three-component mixture even in the presence of 99% noise” (CV ~ 0.17). However, later in the same paper they report that when only one wavelength was used the “SEC and SEP increased as the noise level increased” (> 10%). They conclude that “it is confirmed that random noise has an important effect on the performance of PLS”. In these experiments the ZAP function in Grams/386 was used to add the

Optimisation of instrumentation precision and wavelength resolution.

random noise which was normally distributed and specified as a percentage of the highest peak in each spectrum. Assuming this noise is distributed within 6 standard deviations around a zero mean, one standard deviation can be used for the CV determination. When Lu and McClure tested these findings (using PLS, PCR and CLS) on spectra of natural products (nicotine in flue cured tobacco), the level of noise above which the prediction errors became unacceptable ($SEP > 0.55$) was 30% ($CV \sim 0.05$). These findings suggest that, surprisingly, SNR is relatively unimportant in the development of calibrations if the correct chemometric technique is used.

The wavelength resolution of an instrument can be considered a secondary concern because spectral features in the NIR region are predominantly broad (around 50-100 nm FWHM) vibrational overtones or combination bands of fundamental molecular vibrations. These features are often shifted from their theoretically predicted positions by the influence of local environmental factors of the molecule such as hydrogen bonding⁵. As such, the spectral assignment of the features themselves is not particularly important and often not possible without supporting data collected at longer wavelengths to measure the fundamental vibrational spectra. Yet, higher resolutions would be expected to assist in the identification of subtle changes in the slopes of absorption spectra, and thus in the identification of overlaid spectral features.

Wang, Conzen, Schmidt and Weiler¹²⁵ reported that relatively high spectral resolution was necessary to achieve satisfactory NIRS-PCA analyses involving FTNIR analysis (Bruker IFS28/N) of multi-component systems (pharmaceutical

Optimisation of instrumentation precision and wavelength resolution.

tablets – AspirinTM) with heavily overlapping spectral features. Spectral resolution of 2 cm⁻¹ (0.9 nm at 2173 nm) was required to differentiate tablets of different amounts of active ingredients in the 400 to 7000 cm⁻¹ (1430 to 25000 nm) spectral region and 16 cm⁻¹ (1.8 nm at 1050 nm) in the 7100 to 12000 cm⁻¹ (830 to 1410 nm) spectral region. This result suggests that resolution of ca. 1-2 nm is required for optimal instrument performance, for this application.

In this manuscript we adopt an empirical approach to variation of the precision and wavelength resolution of a spectrometer in terms of the performance of calibrations for the prediction of sugar content against a water-cellulose matrix. This work is undertaken with a view to specifying instrumentation parameters for the application of non-invasive assessment of fruit soluble sugar content.

6.2. Experimental

6.2.1. Instrumentation.

An MMS1 VIS/NIR spectrometer and associated 15 bit electronics from Carl Zeiss Pty. Ltd. (Jena, Germany) was used in conjunction with an LG1 tungsten halogen light and reflectance probe (R400-7-VIS/NIR) (Ocean Optics, Dunedin, FL, USA). The probe end was housed in a light tight tube and a fixed position maintained at a distance of 2 mm above the sample. Aspect Plus® (Carl Zeiss) software was used for data acquisition.

Optimisation of instrumentation precision and wavelength resolution.

The MMS1 spectrometer and LG1 light source required, at minimum, 30 and 60 min operation, respectively, before being considered stable for the purpose of the experiments described in the following paragraphs. Both these instruments were powered up two hours before any work began. In an attempt to minimise the possible effects of the Windows95 operating system on the tight timing schedule of the MMS1 spectrometer, the resource management software UPD32, (shareware, Uwe Buenting), was employed in 'real-time' mode thereby allocating top priority to this selected task. The above conditions apply to all the blocks of experiments described below.

A Hamamatsu S4874Q photodiode array was incorporated into the spectrometer design of Greensill and Newman¹⁷¹. The spectral range of this instrument was 500 to 1050 nm. The probe end was maintained at a fixed distance from the upper most sheet of filter paper, as described above. Resolution of the spectrometer was altered by adjusting the slit width, and estimated from the full width at half maximum of the 750, 763, 811 and 912 nm peaks of the HgAr lamp using SpectraSolve® (Therbaron, SA, Australia) spectroscopic software. Five levels of resolution varying between 8 and 20 nm (estimated of the 912 peak of the HgAr lamp) were used, while adjusting integration time to maintain a constant signal.

6.2.2. Determination of Coefficient of Variation.

The precision of an MMS1 spectrometer was assessed by determining the coefficient of variation (CV) at 12 different settings for the maximum signal level and number of scans averaged, using a white Teflon tile as the sample

Optimisation of instrumentation precision and wavelength resolution.

(Table 6.1). To vary the maximum count level, the detector height was adjusted to a suitable distance whilst keeping the integration time (100 ms) constant. In this way all environmental variations were considered ‘rendered negligible’ from the CV determination.

At each of these settings, 50 sets of 50 spectra were acquired. Initially 2500 spectra were acquired sequentially over a five hour period to make the determination of the CV at each wavelength but the variation in the light source grossly distorted the determination. This result prompted the decision to acquire sets of 50 spectra over short periods (< 4 minutes) in order to reduce the effect attributed to the light source to a negligible level. A CV was calculated as the mean divided by the standard deviation of measurements of each wavelength for each group of 50 spectra. The CV of all groups was then averaged to arrive at a mean CV for each wavelength for a total of 2500 spectra.

6.2.3. Determination of the Number of Layers of Filter Paper.

For the reflectance studies employing filter paper it was necessary to determine the apparent absorption and scattering coefficients of filter paper saturated with sucrose solution, so that sufficient layers could be used to limit the reflectance data to that of the sample only and not from any underlying material. The MMS1 spectrometer was coupled (0.5 mm distance from fibre optic probe to filter paper) to a 100 mm platform on which filter paper (Whatman #1004, 150 mm diameter) wet with distilled water, rested. Incident light was delivered by the Ocean Optics reflectance probe to the opposite surface of the filter paper to the surface on which measurements were made. The light source and the

Optimisation of instrumentation precision and wavelength resolution.

detecting optical fibre were aligned on their optical axis. The vertical position above the upper-most sheet of filter paper was maintained at 2 mm so as to provide an area of illumination which would not vary with increasing numbers of filter paper. To reduce the counts to a level of <10 counts, 42 filter paper layers were sufficient. In subsequent work, 50 layers were used, with the filter papers placed on an optical dump constructed from a 100 mm metal ring with the underlying cavity lined with black cloth to minimise the contribution of the underlying material.

6.2.4. Calibration of Sucrose Solutions on Filter Paper.

Sixteen concentrations of sucrose, varying between 0 and 20% w/v, were prepared by the dissolution of refined white cane sugar in distilled water. Each solution was used to saturate a bundle of 50 sheets of filter paper. These bundles were presented in a random order to minimise experimental method error. The vertical position of the reflectance probe was maintained at a constant height above the upper-most sheet of filter paper for the measurements involving the maximum number of counts (32000). For the two sets of measurements at lower numbers of counts the probe was elevated above the upper-most sheet to a vertical position. The reflectance measurements were made at four separate positions, within a 40 mm diameter area, of the centre of each sample and at five levels of CV (achieved by varying the integration time or the number of scans, see Table 6.1). Wavelength resolution was changed by alteration of entrance slit width (Table 6.2).

Spectra were acquired using Tec5® software but since this software did not offer group calculation of absorbance values, each spectrum was individually imported

into Excel where an absorbance value was calculated using the first zero sugar (ie. filter paper and distilled water) measurement as the reference.

Calibrations were generated from absorbance data using The Unscrambler® (v. 7.1, Camo ASA). Data were not pretreated before PLS calibrations were developed, although the centring and 1/STD weighting option offered during the calibration phase were applied. The spectral window investigated was 700 to 1050 nm. Although outliers existed and better calibrations were achievable for all data sets, in order to make equivalent comparisons only a minimum level of processing was applied to all cases to give each data set equal opportunity. These resultant *standard error of cross validation* (SECV) and *coefficient of correlation-validation* (R_v) were used to make an assessment of the effect of the resolution on the performance of calibrations. SAS® software was used to analyse and compare (at $\alpha=0.05$) the SECV and R_v of the generated calibration equations.

6.3. Results and Discussion

6.3.1. Signal Coefficient of Variation.

A range of % CV values was achieved (0.156 to 0.0031; SNR 707 to 30303) by altering signal level and the number of scans averaged per spectrum (Table 6.1). Variation in signal level will include contributions from a (constant) dark current value, a (variable) readout noise from the electronic components and variation attributed to the signal uncertainty (Shot noise with a Poisson distribution). The

expected Shot noise variation, calculated as the square root of number of incident photons using the available photon to electron to count conversion rate (supplied by the detector manufacturer, Hamamatsu Photonics) was close to the observed values (Table 6.1). Further, the CV can also be expected to demonstrate a square root proportionality to the number of scans. The calculated CV was in general agreement with the observed value, except for the conditions of above 16 scans averaged per spectrum. This poor result is attributed to a limitation in software timing.

6.3.2. Number of Layers of Filter Paper.

An inverse ~ 2 order relationship ($y = 36907 x^{-2.1954}$) existed between the number of counts and the number of filter paper layers (Fig. 6.1). In this case 42

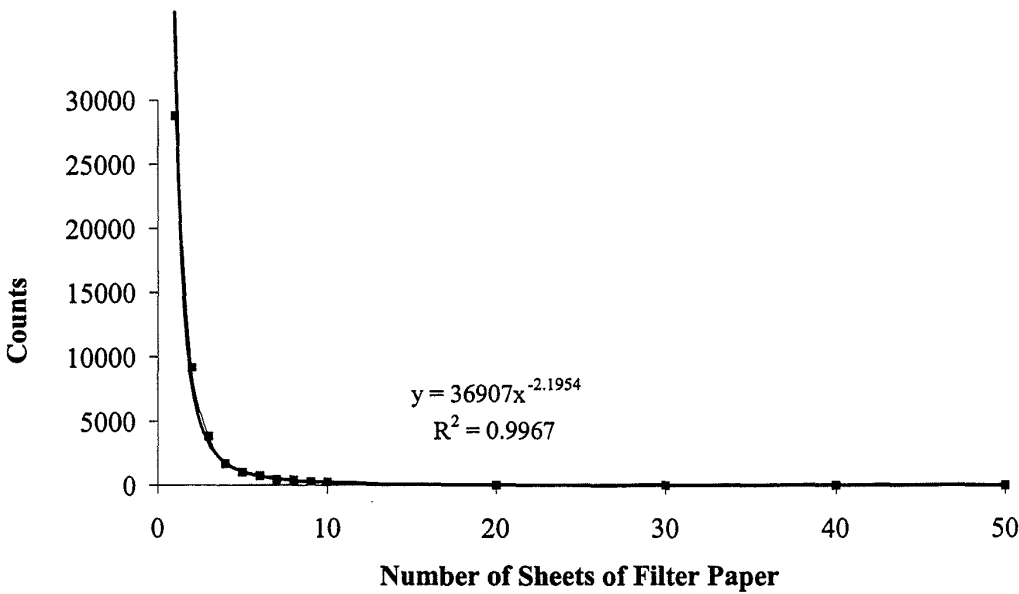


Figure 6.1. Transmission of light through water soaked filter paper at ~ 800 nm. The integration time (45 ms) was set so that a maximum number of counts were available when one sheet of filter paper was placed on the optical axis between light source and detector.

Table 6.1. Effect of signal precision on calibration of sucrose solutions (0-20% w/v) on cellulose. Signal precision, measured as Coefficient of Variation (standard deviation of 50 spectra divided by mean), and quoted for maximum signal in spectrum was varied by alteration of signal level and number of scans averaged per spectrum. When the number of scans is varied the number of counts is 32000. The expected CV is that calculated from theoretical considerations, from the CV of the 1 scan measurement. Those settings marked '*' were used for the development of calibrations. PLS calibration performance is reported in terms of RMSECV and R_v , with a General Linear Models Procedure T test (Alpha = 0.05) on the significance of these variables. An associated Least Significant Difference (LSD) is provided. Note that this test controls the type I comparison wise error rate and not the experiment wise error rate. Within a column, means with the same letter are not significantly different.

Treatment	CV (%)	Expected CV (%)	RMSECV	T tests (LSD) for variable: df= 20 MSE= 0.104561 Critical Value of T= 2.09 LSD = 0.3894.	R_v	T tests (LSD) for variable: df= 20 MSE= 0.000261 Critical Value of T= 2.09 LSD = 0.0194
1K Counts	0.1415	0.1190	2.017	A	0.925	A
*2K Counts	0.0729	0.0729				
4K Counts	0.0379	0.0446				
*8K Counts	0.0216	0.0273				
16K Counts	0.0146	0.0167	1.289	B	0.966	B
*1 Scan	0.0103	0.0103				
*2 Scans	0.0063	0.0073				
4 Scans	0.0045	0.0052				
8 Scans	0.0042	0.0036	1.294	B	0.972	B
*16 Scans	0.0033	0.0026				
32 Scans	0.0031	0.0018				
64 Scans	0.0044	0.0013				
			1.459	B	0.964	B
			0.955	B	0.955	B

Table 6.2. Effect of wavelength resolution, reported for four emission lines of a HgAr calibration lamp, on calibration of sucrose solutions (0-20% w/v) on cellulose. Wavelength resolution was altered by setting of the entrance slit width, and signal level maintained by adjusting integration time. PLS calibration performance is reported in terms of RMSECV and R_v , with a General Linear Models Procedure T test (Alpha = 0.08) on the significance of these variables. An associated Least Significant Difference (LSD) is provided. Note that this test controls the type I comparison wise error rate and not the experiment wise error rate. Within a column, means with the same letter are not significantly different.

Slit width (μm)	Integration Time (ms)	Wavelength (nm)	FWHM (nm)	RMSECV	T tests (LSD) for variable: df= 20 MSE= 0.005211 Crit. Tcal Value of T= 2.09 LSD = 0.0869	R_v	T tests (LSD) for variable: df= 20 MSE= 9.316E-6 Critical Value of T= 2.09 LSD = 0.0037
48	500	578	7.2	1.04	A	0.979	A
		750	6.2				
		826	6.5				
		912	7.7				
60	350	578	7.4	0.966	A B	0.981	A
		750	7.3				
		826	8.2				
		912	10.6				
73	250	578	7.7	0.932	B	0.983	A
		750	9.2				
		826	10.9				
		912	13.8				
89	220	578	7.9	0.923	B	0.982	A
		912	16.7				
107	200	578	8.3	0.982	A...B	0.980	A
		912	20.0				

layers are required to reduce the number of counts to 10 (ie. near to dark count level), and we accepted 50 layers as a convenient number in excess of this value.

6.3.3. Calibration of Sucrose Solutions.

Martens & Dardenne (1998) define the coefficient of correlation, R , in terms of RMSEP (which closely corresponds to SEC) and the variance of the population (σ) (Eqn. 6.1). RMSEP is a measure of the variation between the predicted and actual values (Eqn. 6.2).

$$R^2 = 1 - \frac{RMSEP^2}{\sigma} \quad \text{Eqn 6.1}$$

$$RMSEP = \sqrt{\frac{\sum_{i=1}^I (\hat{y}_i - y_i)^2}{(I-1)}} \quad \text{Eqn 6.2}$$

where \hat{y}_i is the predicted value for sample 'i', y_i is the actual value for sample 'i', and I is the number of samples. Thus RMSECV and R^2 values should be closely correlated, as should SEC and R_C , based on the inter-relatedness of these measures. However, The Unscrambler chemometric package employs a different definition for the coefficient of correlation (Eqn. 6.3).

$$R = \frac{\sum_{i=1}^I (\hat{y}_i - \bar{y}) \cdot (y_i - \bar{y})}{(I-1) \cdot S_y(\hat{y}) \cdot S_y(y)} \quad \text{Eqn 6.3}$$

where S_y is the standard deviation (Eqn. 6.4).

$$S_y(y) = \sqrt{\frac{\sum_{i=1}^I (y_i - \bar{y})^2}{(I-1)}} \quad \text{Eqn 6.4}$$

In consequence, the RMSECV and R^2 values were not directly correlated (Tables 6.1, 6.2). However, statistical analyses (Least Significant Difference or Protected t test) using SAS® software indicated that the results for SECV and R_y have similar trends in terms of the performance of the calibrations (Table 6.1, 6.2). SEC and R_C values were not significantly different between any of the calibrations performed (data not shown).

Calibration performance was significantly poorer, in terms of SECV and R_y , using spectra with maxima of below 8000 counts than for those above this threshold, i.e. a precision plateau was reached at around 8000 counts ($CV = 0.022\%$ or $SNR \sim 5000:1$) beyond which no significant increase was evident. The maximum achievable SNR for a CCD or a photodiode can be estimated by the ratio of the well depth of each pixel to the combined dark current, readout noise and shot noise. For example a typical CCD may have a well depth of ~ 810000 electrons, and thus an expected shot noise of 900 electrons, a readout noise of 13 electrons and a dark current of 13 electrons. Therefore the maximum SNR expected is $\sim 900:1$. The same calculation for a typical photodiode array which would have a well depth of 125000000 electrons and thus a shot noise of 11180 electrons, a readout noise of 3000 electrons and a dark current of 4000 electrons would result in a SNR of $\sim 12250:1$. However, various techniques (vertical and horizontal binning) can augment the SNR of a CCD array to a value near to that of a PDA. We conclude that PDA linear arrays, or CCD two dimensional arrays using binning, can be employed for the application of sucrose

Optimisation of instrumentation precision and wavelength resolution.

assessment, with scope for operation in single scan mode and at signal strengths significantly below saturation.

Resolution (FWHM) was not constant across the spectral range, a result of the dispersion mechanism employed (prisms), the wavefront geometry and the planar surface of the detector. Variation of the slit-width from 47 to 107 μm achieved a range of resolutions from ~ 8 to 20 nm at 912 nm. The resolution at slit openings 89 and 107 μm was too low (>12 nm) to allow the values of FWHM to be determined for those peaks with close neighbours, i.e. 750 and 826 nm (Table 6.2).

There was insignificant difference in the performance of calibrations (as judged in terms of SECV and R_V) when the slit opening was in the range 60 to 107 μm (resolution from 11 to 20 nm at 912 nm). The highest resolution (8 nm, slitwidth 48 μm) supported a significantly poorer calibration than that developed at a resolution of 14 and 17 nm (Table 6.2) (SECV only), a result attributed to diffraction effects of the narrow slit.

6.4. Conclusion

The future of NIR spectroscopy lies in the design of cost effective, application specific, instrumentation. On the basis of the work presented here, we suggest instrumentation for the application of grading cellulose based (plant) products for sugar content can involve a resolution as low as 16 nm (at 912 nm) and a CV of 0.022 (SNR $\sim 5000:1$). These criteria impact on detector choice and electronic design of the spectroscopic instrument design for this application. The design of

Optimisation of instrumentation precision and wavelength resolution.

an instrument with a relatively low resolution, when compared to most currently available array spectrometers, may be advantageous in terms of instrument cost and higher speed of operation (increased throughput).

7. A Remote Acceptance Probe and Illumination Configuration for Spectral Assessment of Internal Attributes of Intact Fruit

This chapter has been accepted for publication under this title in the Journal of Measurement Science and Technology, (2000), in press.

7.1. Introduction

Fruit can be non-invasively assessed for internal quality attributes such as sugar content through chemometric analysis (typically using partial least-squares (PLS) and multiple linear regression (MLR) or other multivariate techniques) of near infrared (NIR) spectra. We have previously reported on characteristics of the spectrometer which impact on the calibration performance for this task (e.g. signal precision, wavelength resolution¹⁷⁸). Application of this technology in a commercial pack-line setting (operating at a belt speed of up to 1 m s^{-1}), however, requires the optimisation for a given fruit type of a non-contact illumination and detector configuration. The sample illumination and detector system must allow rapid spectral data acquisition of regions representative of the whole sample for the attribute of interest.

Both transmittance (where light penetrates the sample and is re-emergent into a non-illuminated area of detection) and reflectance (where light also penetrates the sample and is re-emergent but where specularly reflected light is often a

Remote acceptance probe and illumination configuration.

significant portion of the detected signal) optical configurations have been applied to in-line fruit sorting. Transmittance spectral data is expected to carry significantly more attribute information, since the detected light will have a longer path length within the sample, than reflectance spectral data. However, while full transmittance optics (where the illumination and detection systems are at 180° with reference to the centre of the fruit) will be possible only with fruit of relatively high transmittance (e.g. citrus fruit, but not seeded mangoes). In full transmittance mode, the amplitude of the measured signal is relatively low, and, by association, the signal-to-noise ratio (SNR) is also low. SNR below 5000:1 has been shown to give relatively poor calibration performances for sucrose in a water-cellulose matrix¹⁷⁸ and is expected to have the same impact on performance for rockmelon fruit. Partial transmittance (where the angled axis of illumination and detector with respect to the centre of the fruit is other than 180° , but designed to optically eliminate specular reflectance) has advantages in terms of increased signal level, although path length is ill-defined. However, optical path-length can be estimated through the measure of absorbance of a wavelength not readily absorbed by the sample, and not relevant to the constituent of interest. For example, Kawano⁶⁸ measured absorbance at 844 nm to determine the path length of light in Satsumo mandarins when determining soluble solids content.

For a fruit pack line, where fruit are moving with respect to the light source and detector, the optical system should also be designed to minimise secondary specularly reflected light reaching the detector, and to prevent possible detector damage from frequent full saturation of the detector by the primary light beam between samples (ie. as would occur in full transmittance mode without

Remote acceptance probe and illumination configuration.

additional shuttering hardware). Also, the optical system should not require physical contact with the sample. Some of the most important design considerations will therefore include the desired range of operation between detector assembly and fruit, the collimation of the light source, size of sample and the field of view of the detector.

Reflectance mode optics have been used for several decades in commercial spectrometers designed for non-contact process control applications of optically dense materials (e.g. grain, NIRSystems, Silver Springs, USA; DA7000, Perten, Huddinge, Sweden). Mitsui Mining (Japan) introduced a non-destructive (peach) fruit sweetness sorter operating in non-contact reflectance mode in 1989, using two focussed tungsten halogen lamps to illuminate the sample¹⁶⁴. However, variations in surface roughness greatly impact on the amount of specular radiation received by the detector, and thus on calibration performance. For example, Walsh *et al.*²⁰⁹ reported an improved calibration for soluble solids content of melon fruit for a lamp-fruit-detector angle of 40° when a light excluding shroud was used between the detector and the fruit surface. This result was ascribed to the reduction of detected specular radiation. Alternatively additional chemometric manipulation (e.g. derivatives) can be applied to remove the effect of specular reflectance when using the reflectance technique¹⁶⁴.

Maeda⁶⁹ employed a non-contact, full transmittance method in an in-line setting with citrus fruit, with an electronic shutter used to prevent saturation of the detector between samples. However, secondary and tertiary reflected light (due to reflective surfaces of componentry) was reported to degrade the quality of the

Remote acceptance probe and illumination configuration.

received signal and limit the application of the system in the determination of low concentration constituents. Full transmittance optics are also not appropriate for dense or seeded fruit (e.g. melons or mangoes).

With partial transmittance optics, the illuminated and detected areas of the fruit are not at 180° relative to the centre of the fruit. A sample cup is generally used to eliminate specularly reflected light from the field of view of the detector (e.g. Ballinger¹⁴⁹ and Yeatman¹⁴⁸ illuminated fruit through an aperture in the base of a cup in which the sample rested, and collected spectral data from a non-illuminated area of the fruit). In these systems, the benefit of higher signal (higher signal to noise ratio) must be balanced against the need to optically sample a representative region of the fruit. For example, Walsh *et al.*²¹⁰ employed four 50 W lamps positioned at various angles with reference to the centre of melon fruit and to the detected region (with a sample cup between the fruit and the input fibre optic to the detector).. For a given integration time, calibration statistics for prediction of SSC of edible flesh was improved using a lamp-fruit-detector angle of 40° or 60°, relative to 20°, despite the reduction in signal intensity. The greater angles presumably a better optical representation of the tissue of interest (inner mesocarp). Fantec Research Institute Co. Ltd.⁸ employed 16 lamps evenly spaced radially around the fruit, and orthogonal to the axis of the fruit and detector for the same application (melon SSC evaluation), again ensuring optical sampling of a representative region of the fruit. . In this case, the detector was located below a light excluding cup. However, the 'cup' concept is not particularly appropriate for use in high speed pack lines. Location of either light source or detector optics below the transport system is also

Remote acceptance probe and illumination configuration.

disadvantageous in terms of falling debris. Further, a 90° placement of detector to light source, relative to fruit centre still involves a relatively long optical path, and thus requires high illumination load to provide an adequate signal level from large, dense fruit such as melons. Osborne *et al.*¹⁷³ aligned the light source behind a detector probe, with this probe placed in contact with the (kiwi) fruit. This arrangement prevented specular light from reaching the detector, and while most light received by the detector is expected to have derived from the upper layers of the fruit, acceptable PLS derived correlation was obtained between the absorption spectra and the soluble solids content of juice extracted from the whole fruit.

A basis for the theoretical description of light scattering in food produce was laid by Birth, and developed by other workers in the last two decades. Birth^{24, 211} reported a diffuse thickness (the depth after which no light directionality remains) of 25 μm and ~2.5 mm for dry, white paper and potato tuber respectively (absorption and scattering coefficients of $S = 2.75$ and $K = 0.37$, respectively, reported for white potato flesh). From this theoretical base, we expect that light will be totally diffuse within a few millimetres of entry into a product such as a melon fruit. However, this prediction remains to be empirically validated.

Another spatial-geometrical problem in the application of NIRS sorting of moving fruit on a pack-line relates to the assessment of consistent regions of the fruit, as fruit are not homogeneous in relation to the assessed criteria. For example, Peiris *et al.*¹⁷⁴ described the spatial variation in SSC of a number of

Remote acceptance probe and illumination configuration.

fruit types, including cantaloupe (*Cucumis melo* L. Cantaloupensis group). SSC was noted to increase along the proximal-distal axis, and towards the seed cavity. Little variation was noted circumferentially at the equator.

In this study we assess a novel illumination/acceptance probe configuration which allows non-contact spectral acquisition from moving rockmelon fruit, for the assessment of fruit SSC. The system was designed with reference to light penetration through the sample and the distribution of SSC within the sample. The non-contact configuration was assessed in terms of PLS calibration performance for assessment of SSC in rockmelons, relative to calibrations developed using a configuration in which optical probe and sample were in contact, eliminating specular reflectance (as used by Walsh *et al.*²⁰⁹).

7.2. Materials and Methods

7.2.1. Distribution of SSC within a rockmelon fruit

Five rockmelons were sliced at 10 mm intervals along the length of the fruit (from flower to peduncle end) to provide 12 slices from each fruit. Cores (8 mm diameter) were excised from twelve points from each slice and assessed for soluble solids content. These points were positioned with reference to the major vascular networks associated with the seed masses, and with reference to distance from the exocarp (Fig. 7.1). The inner mesocarp was not represented in the extreme two slices (from each end of the fruit), which represented tangential

Figure 7.1. Sampling positions (grey circles) in relation to fruit anatomy. Twelve slices were taken along the distal proximal axis, per fruit. Six paired samples of inner and outer mesocarp were taken per slice, with three sets located adjacent to the vascular tissue - seed masses, and three sets located between these points.

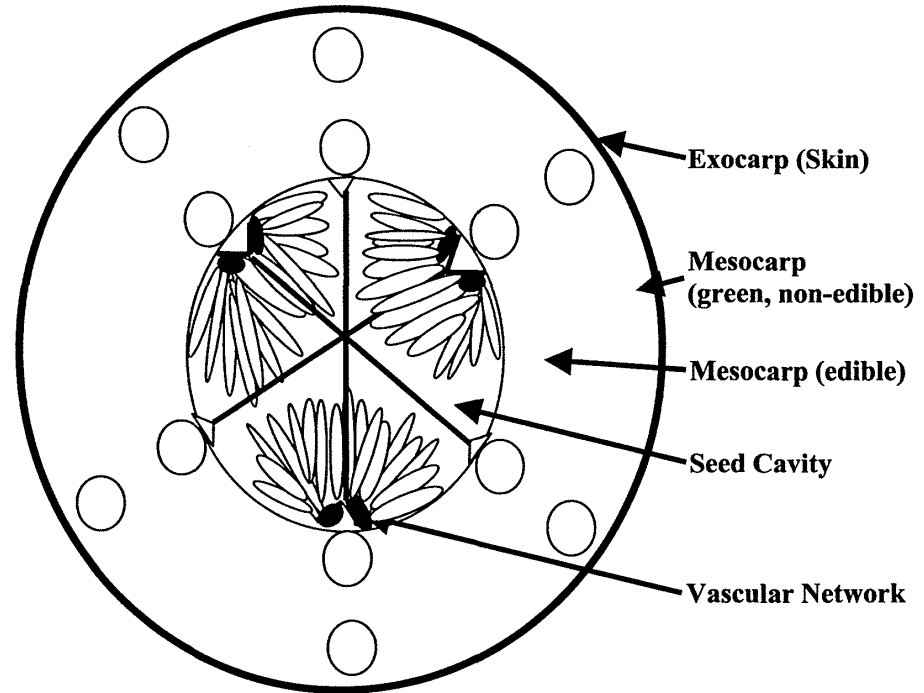
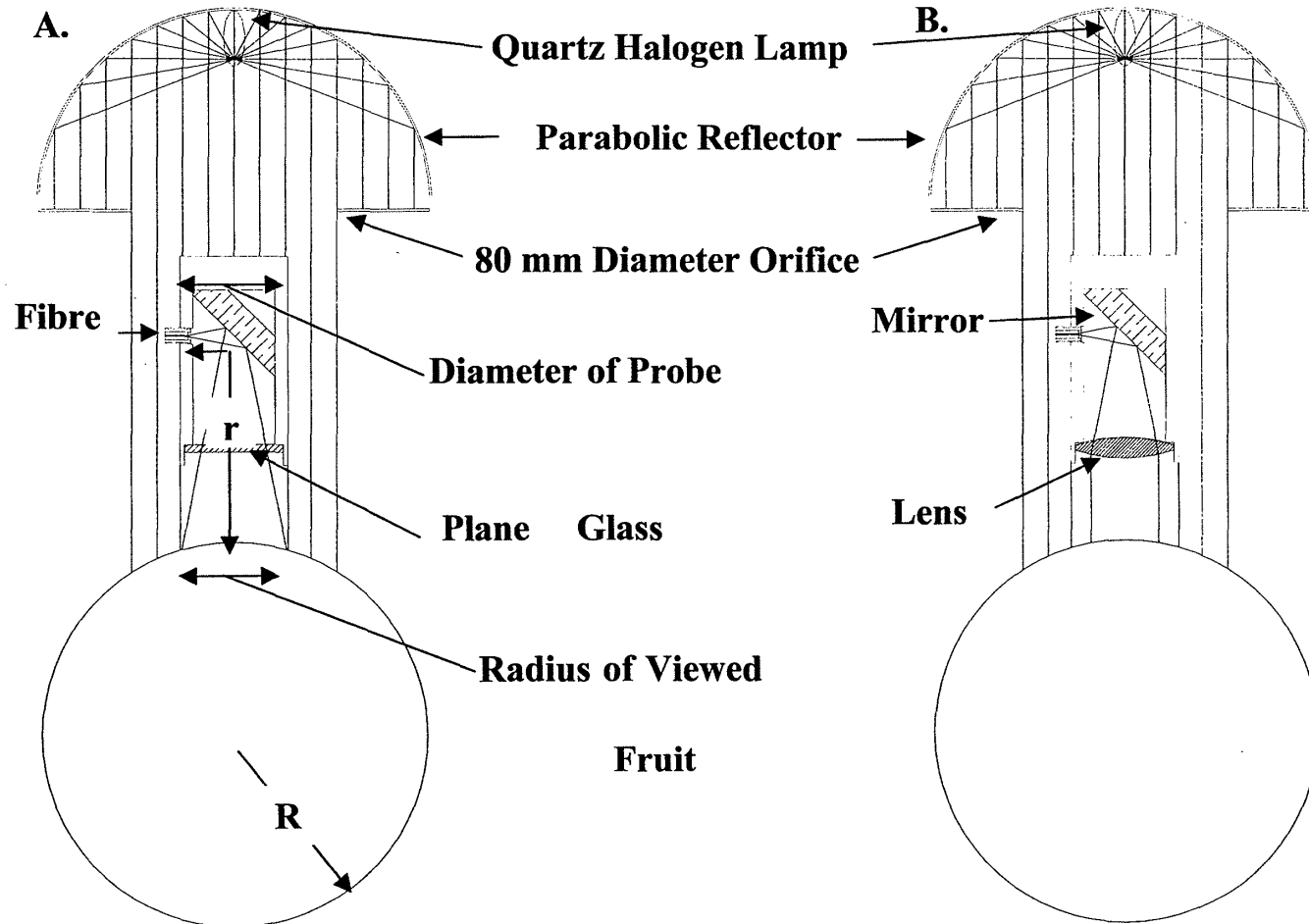


Figure 7.2. Schematic of illumination and detector probe configurations assessed for the non-contact assessment of fruit. (A) Without front lens; (B) With front lens. A collimated light source illuminates the fruit. The detector probe acts as an optical spot of diameter 'd', casting a shadow onto the fruit surface. The end of the detector fibre optic is a distance 'r' from the fruit surface, with a detected area of 'a' radius of the fruit surface. The fruit has a diameter, 'R'.



sections through the outer mesocarp only. Each core was crushed with a hand operated garlic press and a soluble solids content assessed of the resultant juice using an Erma digital refractometer (accuracy 0.2% SSC), against sucrose reference standards. SSC distribution within rockmelon fruit highlighted the need for a comparison of tissue sampling techniques used in the reference measurement of SSC by refractometry for the NIR calibration. One population of fruit (~ 290 spectra) was sampled using three sampling methods : (A) four 10 mm cores taken from a 50 mm diameter area covering the region identified to have been spectrally scanned from a stationary perspective, inclusive of the exocarp; (B) as previously but with the outer 8 mm of exocarp and outer mesocarp removed; and (C) a section of fruit ~ 40 mm wide and 70 mm long excised from the samples in the region determined as having been spectrally scanned, with 8 mm of exocarp and outer mesocarp removed.

SSC data is presented in the text as mean \pm standard error. Microsoft Excel analysis of variance routines were used to assess significance of differences in SSC across slice and radial position, reported at 95% confidence limit.

7.2.2. Optical design

A collimated light source illuminated the sample, with the centre of this beam obscured by a stop (the detector acceptance probe) (Fig. 7.2). The stop formed a shadow on the sample surface, and radiation emergent from this region must represent radiation that has interacted with the sample, being diffusely scattered and absorbed within the fruit. A light source consisted of a 100W quartz-tungsten-halogen automotive spot light supplied by ARB Pty. Ltd. Australia for

Remote acceptance probe and illumination configuration.

those experiments involving comparison of optical configurations, and a 100 W focusable RMDL 170 Striker spotlight from Light Force Australia Pty. Ltd, Cleve, Australia for all other work. However, the output beam of this source was not fully collimated across its entire width due to the finite spatial extents of the components making up the source (e.g. the filament is not a point source). For this reason an orifice was used on the light source (Fig. 7.1), reducing the level of non-collimated light impinging on the shaded region. This assembly provided an 80 mm diameter beam of collimated light to the sample.

The acceptance probe was positioned 65 mm from the lens of the light source and on the optical axis between the light source and the centroid of the sample (Fig. 7.2). The acceptance probe housed a mirror (gold coated front surface, Edmunds Scientific Company, Barrington, NJ USA) to direct incoming light to the fibre optical cable of a Zeiss MMS1 spectral sensor (a bundle of 30 fibres, each 70 μm in diameter, total diameter of 500 μm ; NA 0.22) (Fig. 7.2). Gold has a high (> 0.95) reflectance in the region 600 to 2500 nm (CRC Handbook, p. E379). The probe was designed to minimise refraction losses at interfaces and transmittance losses. Direct specular light entering the probe assembly will not fall within the angle of acceptance of the fibre optic, and will thus not be transmitted to the detector. The interior of the probe assembly was painted in a matt black to minimise further secondary reflections. The front of the probe was sealed with either a flat glass plane (BK7) or a lens of focal length (87 mm).

7.2.3. Light penetration through rockmelon fruit

The 'non-contact' system was used to illuminate an area in the 'equatorial' region of a rockmelon fruit, with the detector probe positioned 40 mm from the fruit surface. A grid consisting of 100 equally spaced (15 mm centres) 12.5 mm diameter holes in a 10 x 10 array constructed from 20 mm thick acrylic was positioned over the fruit on the side opposite to the light source. Grid orientation was maintained, relative to the sample, by two locating guides. Spectra were acquired via a 1 metre fibre optical cable, connected using a SMA connector to the fibre optical input of the Zeiss MMS1 spectrometer and a 12 mm diameter probe at the input end. This probe was inserted in the grid holes and contacted the sample under its own weight. This arrangement ensured a constant distance of 25 mm between fibre end and fruit surface, giving a constant field of view ($\sim 79 \text{ mm}^2$). Integration time was set to 250 ms. The holding frame and fruit was covered in black cloth to exclude ambient light from spectral measurements. Spectral data was collected from each grid point. Once 100 measurements had been made, a 10 mm thick slice of fruit was removed and the process repeated until all the fruit was sliced (generally 12 slices, with the final slice ~ 15 mm thick). Ten fruit were processed in this manner.

Spectral data was processed in Matlab V5.3 to extract the transmitted light intensity level at 812 nm (relative maximum value) for all collected spectra and to format to a configuration acceptable to Slicer Dicer (Visualogic).

7.2.4. Comparison of optical configurations

The performance of calibrations generated against SSC of fruit mesocarp tissue was assessed for spectra collected by two optical configurations. The 'non-contact' optical configuration described above was compared to those from a system in which the detector assembly was placed in contact with the fruit surface, excluding specular light from the detector. The 'contact' system was described by Walsh *et al.*²¹⁰, and is similar to that of Osborne *et al.*¹⁷³ This system was developed for the acquisition of spectral data of stationary fruit²¹⁰ and used to examine the effects on the performance of calibrations of different cultivars and growing districts¹⁶³. The illumination/detector configuration of this assembly was based on 4 x 50 W QTH lamps illuminating the sample at 45° to a 50 mm diameter probe sample (relative to the centroid axis) and positioned at 90° to each other. The acceptance probe contacts the sample, thereby excluding all external light.

In both configurations, spectral measurements were made with a MMS1 NIR-enhanced spectrometer from Carl Zeiss Pty. Ltd. (Jena, Germany) using Tec5 (15 bit resolution) electronics. Labview based software was developed for data acquisition and spectrometer control. The light sources and spectrometers were powered up two hours prior to commencement of experimentation to ensure stable operation. The reference used for all measurements was a 6 mm thick, white teflon tile positioned so that the maximum (reflectance) count level was ~ 80% of the dynamic range.

Remote acceptance probe and illumination configuration.

Single scans of 50 ms integration time were taken for the 'non-contact' system. Four scans of 200 ms integration time were averaged per spectrum acquired when using the 'contact' system (as per Walsh *et al.* 2009). This level of signal averaging should, theoretically, reduce noise by ~ 1.4 times and therefore potentially enhance calibration performance. However, Greensill and Walsh¹⁷⁸ demonstrated that calibration performance for the prediction of sucrose concentration in water-cellulose matrix was not improved by improvement in signal precision above a SNR of 5000:1. This level of precision was achieved at a count level of 8000 counts with the Zeiss MMS1 detector system. A maximum count of 10000 was accepted in the present study, and thus the spectral averaging used with the 'non-contact' system should not have influenced the calibration result.

Spectral data were pre-treated and used in PLS (partial least squares) multivariate linear regression calibrations generated against mesocarp soluble solids content (see below) using The Unscrambler v7.5 (Camo ASA). For each population of fruit, calibrations were generated using absorbance data from two spectral windows (700 to 1050 nm and 600 to 970 nm), and transmittance and derivatisation of absorbance for the 700 to 1050 nm spectral window. Calibrations were generated using mean centring and autoscaling. Second derivative pre-treatment used a Savitzky-Golay method with a half width set to 4 units and a second order polynomial fitting function. Calibration performance was recorded in terms of Root Mean Square Error of Cross-Validation (RMSECV; 6 segments with random selection), Correlation Coefficient (Validation) (R_v), and Standard Deviation Ratio (SDR) and population statistics,

Remote acceptance probe and illumination configuration.

number of sample population and Standard Deviation (STDev) of soluble solids content.

Root mean squared error of cross validation (RMSECV) is calculated by:

$$RMSECV = \sqrt{\frac{\sum_{i=1}^I (\hat{y}_i - y_i)^2}{I-1}} \quad \text{Eqn 7.1}$$

where \hat{y}_i is the predicted SSC value, y_i is the actual SSC value and I is the number of samples.

The Standard Deviation Ratio (SDR) is calculated by:

$$SDR = \frac{\sigma}{RMSECV} \quad \text{Eqn 7.2}$$

where σ is the standard deviation of the SSC of the population.

The correlation R_v between two variables k_1 and k_2 is calculated by:

$$R_v = \frac{\sum (y_{ik_1} - \bar{y}_{ik_1}) \cdot (y_{ik_2} - \bar{y}_{ik_2})}{(I-1) \cdot \sigma_{k_1} \cdot \sigma_{k_2}} \quad \text{for } k_1, k_2 = 1 \dots K. \quad \text{Eqn 7.3}$$

where i is the sample identifier, I is the number of samples, k is the variable identifier and σ_k is the standard deviation of the variable.

Remote acceptance probe and illumination configuration.

The primary assessment for performance of calibrations was made on the significance of the variation in the RMSECV as recommended by Fearn²¹² ($\alpha = 0.05$, and assuming bias negligible since bias is minimised by the calibration ‘intercept’ coefficient, B_0) (see also Snedecor and Cochran²¹³). For each comparison of two calibrations, the R^2 of the correlation between residuals (predicted – actual SSC) and the 95% confidence limits on RMSECV are reported. Briefly, Fearn’s method involves comparison of prediction errors (root mean square error, RMSE) for two calibrations, predicting analyte concentration from spectral data for a single validation set of n samples (for which analyte concentrations have been determined by a primary analytical method). Since both calibration models have been tested on the same samples, the calculated errors are correlated, that is, laboratory error will appear in both methods. The correlation coefficient (R) between the two sets of errors is calculated and used in the following manner:

$$F_K = 1 + \frac{2(1 - R^2)t_{n-2,0.025}^3}{n-2} \quad \text{Eqn 7.4}$$

where $t_{n-2,0.025}$ is the upper 2.5% point of a t distribution on $n-2$ degrees of freedom.

Then calculate

$$F_L = \sqrt{\left(F_K + \sqrt{(F_K^2 - 1)}\right)} \quad \text{Eqn 7.5}$$

The upper and lower limits of a 95% confidence interval for the ratio of the RMSEs the equations are

Remote acceptance probe and illumination configuration.

calculated as

$$\frac{RMSE_1}{RMSE_2} \times F_L \quad \text{Eqn 7.6}$$

and

$$\frac{RMSE_1}{RMSE_2} \times \frac{1}{F_L} \quad \text{Eqn 7.7}$$

respectively. If the compared value falls between these two values it is not significantly different at $\alpha=0.05$.

Note that in order to achieve comparative results for all data sets, calibrations generated used equivalent calibration parameters (in terms of the exclusion of outliers above the set threshold) which were not optimised for any individual set. Therefore RMSECV and SDR should not be assessed in an individual context. A ‘working’ calibration would also require attention to the selection of samples used in the calibration set.

Eleven populations of rockmelons (*Cucumis melo*, L. *Cantaloupensis* group), comprised of four different cultivars and sourced from four different growing localities (total population of 1764 melons), were used to compare performance of calibrations generated on both the ‘non-contact’ and ‘contact’ (with or without front lens) systems. Spectra were acquired of stationary fruit samples, placed manually below the detector, for both the ‘non-contact’ and ‘contact’ system. However, for two populations, spectra were also collected of fruit moving past the detector on a conveyor at 0.5 ms^{-1} . These spectra were acquired on a trigger from an optical sensor.

7.3. Results and Discussion

7.3.1. Variation of Soluble Solids Content within Rockmelon Mesocarp

The SSC of tissue within a given rockmelon fruit varied with position of sampling along the fruit (from blossom to peduncle end, Fig. 7.3), around the fruit (Fig. 7.4), with respect to the depth of sampling into the mesocarp (Figs. 7.3 and 7.4). The average ($n=5$ fruit) standard deviation for SSC (% w/v) within each rockmelon fruit (across 12 slices of fruit from distal to proximal ends, and around the fruit, see Fig. 7.2 for sampling strategy) was 1.66 for mesocarp (inner and outer) tissue ($n=144$), 1.05 for inner mesocarp only ($n=72$), 0.72 for outer mesocarp only ($n=72$), 0.52 for the inner mesocarp tissue of only the three centre or 'equatorial' slices ($n=18$), and 0.47 for outer mesocarp of only the three centre or 'equatorial' slices ($n=18$).

SSC varied significantly along the distal axis of the fruit, with the average maximum difference in SSC 1.86 ± 0.01 and $2.51 \% \text{ w/v} \pm 0.01$ ($n=5$ fruit) for inner and outer mesocarp respectively. Most of the variation occurred in the extreme two slices (ie. the first and last 30 mm of fruit), with little variation in the central region. Peiris *et al.*¹⁷⁴ reported a similar result for soluble solids content variation along the proximal-distal axis when measurements were made close to the skin. We conclude that spectral data should be acquired from the equatorial region to best represent average fruit eating quality.

The average difference in SSC between tissue from the inner and outer mesocarp was $2.82 \% \text{ w/v} \pm 0.06$ ($n=5$ fruit). This difference was larger than differences observed with respect to the proximal-distal axis of the fruit (ie. 'latitude'), or

Remote acceptance probe and illumination configuration.

with respect to position 'around' the fruit (ie. 'longitude'). The correlation of outer to inner mesocarp data was very poor ($R^2 \sim 0.16$, $n = 60$; data not shown). Similarly, SSC varied between different sampling methods for the same area of fruit, principally representing variation in the relative proportion of inner and outer mesocarp in the sample. The relationship between the SSC measure of four cores with skin, relative to four cores without skin was $y = 0.91x + 0.36$ ($R^2 = 0.85$, $n = 284$). The relationship between the SSC of a section of fruit (40 by 70 mm, without skin) and four cores from the same area of fruit, with and without skin, was $y = 0.82x + 1.19$ ($R^2 = 0.73$) and $y = 0.84x + 2.31$ ($R^2 = 0.75$) ($n = 284$), respectively.

We recommend that attention be given to the variation in SSC across a sample in the development of calibrations. For example, the attribute of exocarp thickness may vary in fruit grown under different agronomic conditions. As optical data will be derived principally from the outer layers of the fruit, the performance of a calibration may be degraded if exocarp thickness is changed. It is also important that a consistent thickness of skin is removed from the cored sample, with the lower soluble solids content of the outer mesocarp averaged with the higher content of the inner mesocarp.

The average difference between tissue from between vascular bundles relative to adjacent to vascular bundles was $0.10\% \text{ w/v} \pm 0.03$, and $0.0\% \text{ w/v} \pm 0.04$ ($n = 5$ fruit) for inner and outer mesocarp tissue, respectively. The average difference between tissue from between vascular bundles and close to the ground-spot relative to that away from the ground-spot was $0.02\% \text{ w/v} \pm 0.37$ and 0.40%

Remote acceptance probe and illumination configuration.

$w/v \pm 0.42$ ($n = 5$ fruit) for inner and outer mesocarp tissue, respectively. These differences are small relative to the variation between fruit, and hence the fruit orientation with respect to these characteristics can be ignored.

We conclude that edible mesocarp tissue (sample regions with consumer importance) sampled from the equatorial region of the fruit should be used without skin for a SSC estimation of the whole fruit that is relevant to the consumer importance (ie. fruit flesh which is consumed). The spectral assessment system described below is similarly targeted at the equatorial region of the fruit.

7.3.2. Light Scattering within Rockmelon Fruit

When an annular illumination beam was used to illuminate the fruit surface (collimated 80 mm diameter beam interrupted by 42 mm diameter stop), the light intensity assessed through 15 mm of fruit exocarp and mesocarp was equivalent under the stop and under the area of direct surface illumination (Fig. 7.5). This result is attributed to scattering of light by the fruit tissue, and is consistent with the estimate of diffuse thickness of 2.5 mm for potato tissue²¹¹. Light intensity (y) rapidly decreased (exponential relationship, e.g. $y = \exp(11.002412 - 0.78879785 x)$, $R^2 = 0.999$) (averaging signal at position adjacent to seed cavity over 10 fruit) with increasing thickness of fruit (where x is the slice number, each slice $\cong 10$ mm thickness). Thus ca. 25% of incident light was transmitted through 10 mm of fruit tissue.

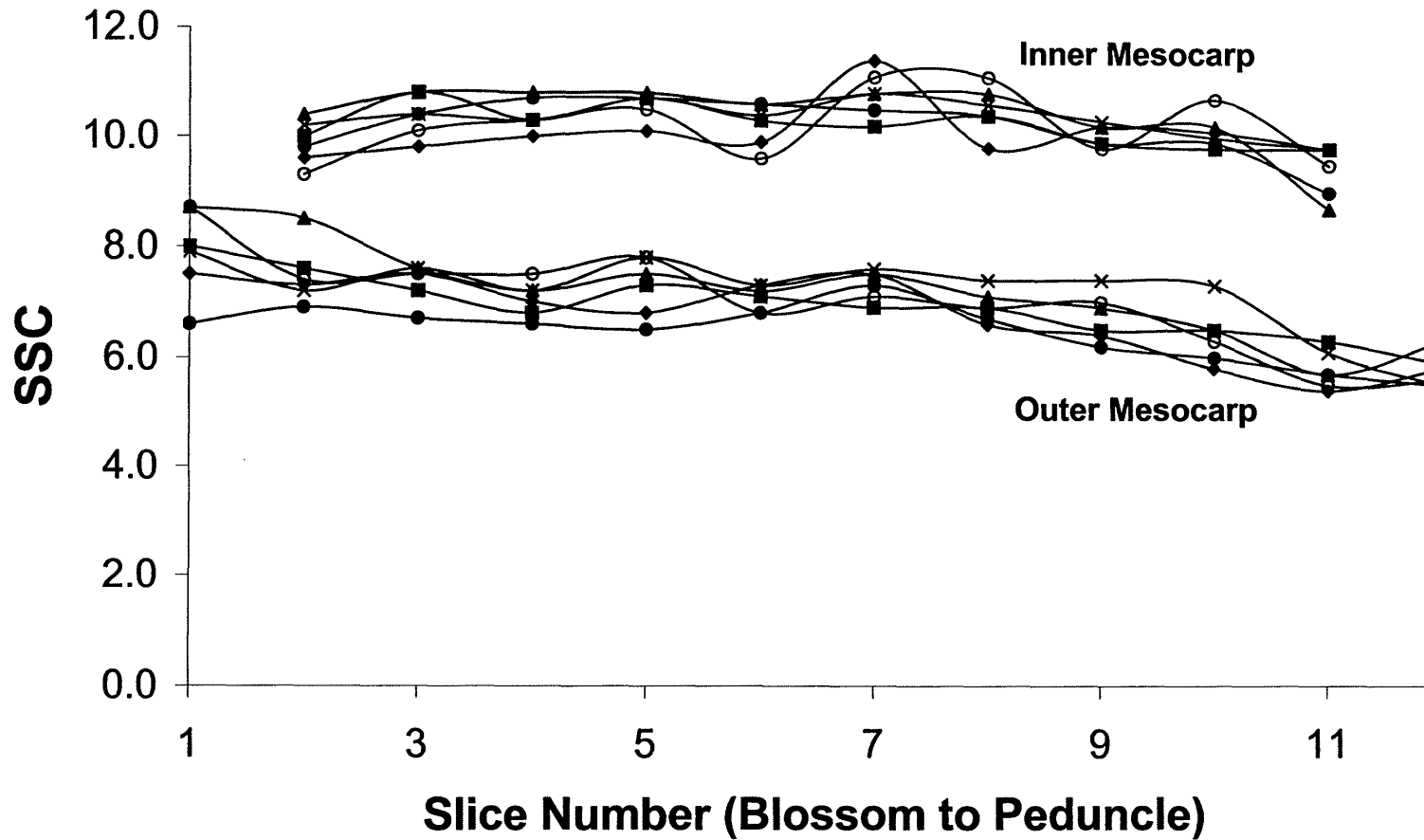


Figure 7.3. Soluble solids content of inner and outer mesocarp tissue of twelve equidistant slices of a fruit, numbered distally from blossom to peduncle end of the fruit. Six samples were assessed per slice, representing circumferential variation. Data is representative of all (n=5) fruit assessed. Lines connect a given symbol type, representing a given sampling location within a slice.

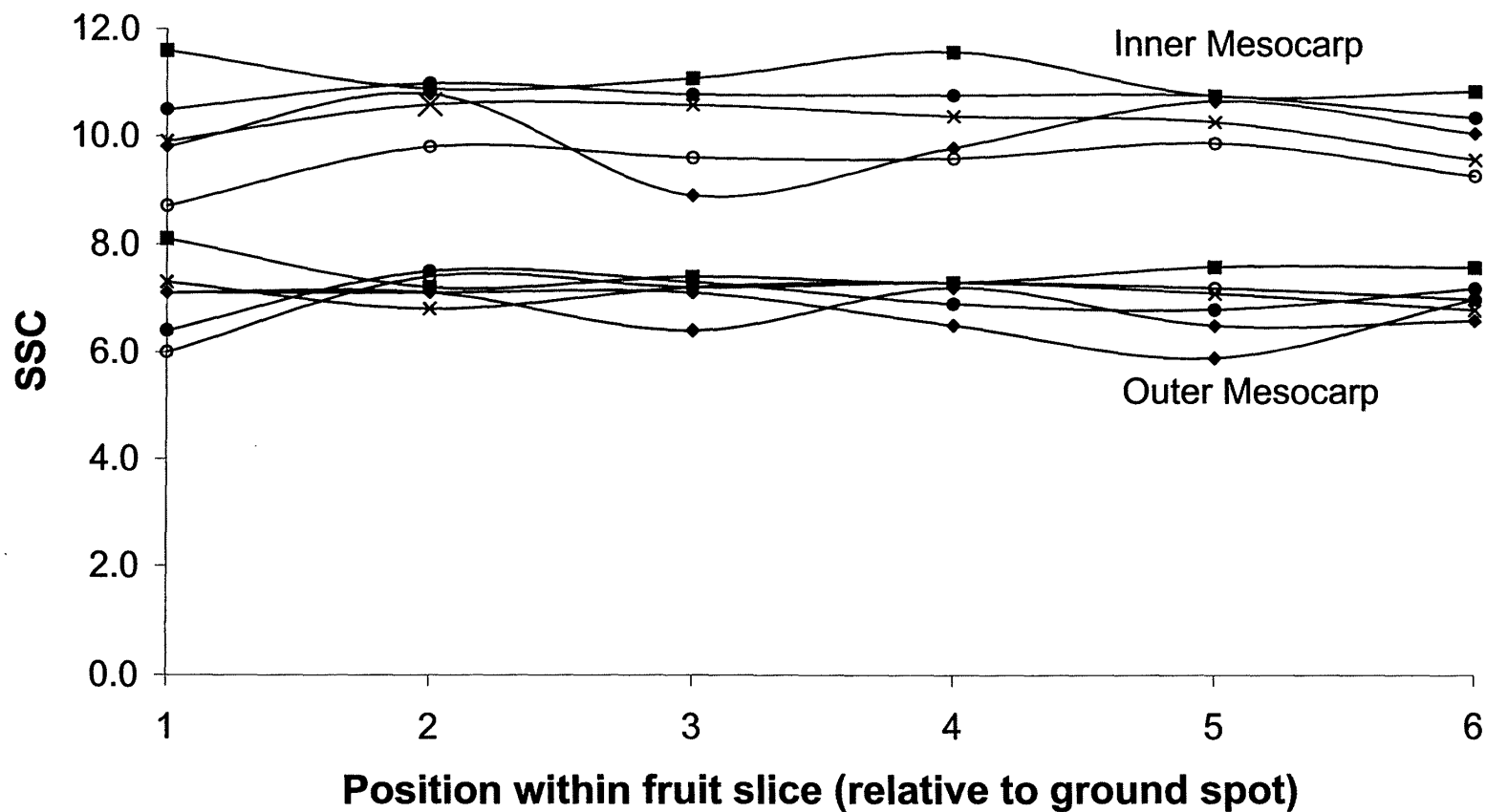


Figure 7.4. Soluble solids content of inner and outer mesocarp tissue of median slices (slice #6 in Fig. 7.3) from five fruit, with respect to the position of sampling within the slice (see Fig. 7.1). The position of sampling is numbered in clockwise sequence (viewed from distal end of fruit) from the groundspot (part of fruit in contact with the ground during growth) except for one fruit (ground spot identified by enlarged data point symbol). Lines connect a given symbol type, representing a given fruit.

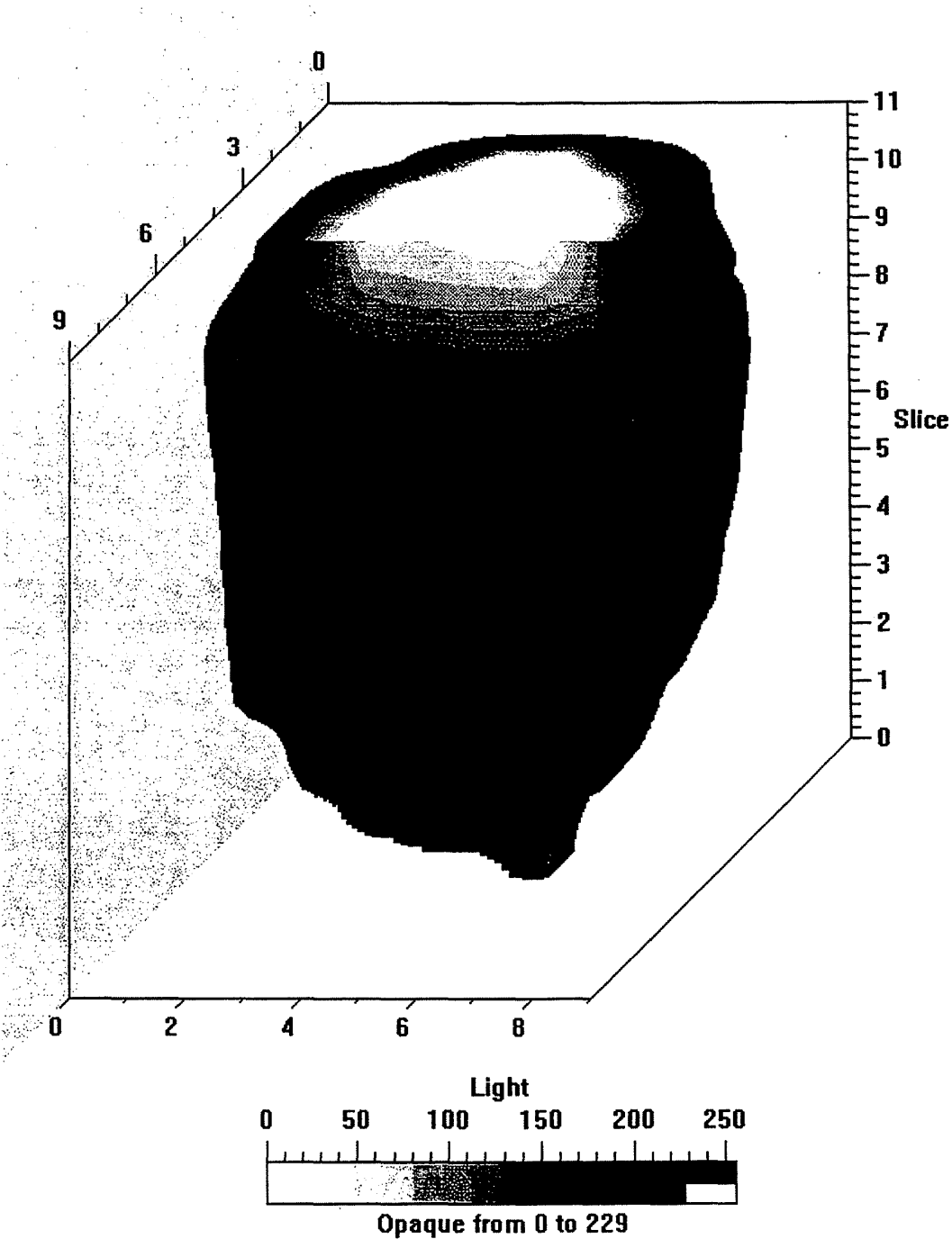


Figure 7.5. Three dimensional representation of light penetration through a fruit. The data set consists of twelve slices (z axis), with 100 (10 by 10 matrix) values per slice. Data is presented in raw AtoD counts, ranging from a maximum of 32000 in 15 equal steps (225 counts).

Remote acceptance probe and illumination configuration.

A light ray reaching any given depth can be scattered back towards the illuminated surface. Approximately 25% of the diffuse light at 10 mm depth is expected to re-emerge from the fruit surface (ie. ca. 6.25% of incident light reaches this depth and is returned to the surface). Diffusely scattered light re-emerging within the shadowed region will be collected by the detector system if the ray is within the angle of acceptance of the fibre optic. Thus the detected light will have primarily originated within the upper layer (first 10 mm depth) of fruit, although some of the signal will have been contributed from depths as far as the seed cavity. Increasing incident light intensity will not proportionally increase the level of signal received from deeper layers of the fruit, but the absolute level of such signal should be increased, and thus SNR should be improved. The soluble solids content of inner mesocarp tissue, however, is poorly correlated to that of the outer mesocarp. Thus calibration against SSC of the inner tissue should be possible only to the level of the correlation between inner and outer mesocarp soluble solids content, or to the level of a secondary correlation involving spectral characteristics of another attribute of the outer mesocarp and the SSC content of inner mesocarp.

7.3.3. Design of illumination and detection system

The diameter and length of the probe were matched to the characteristics of the fibre (numerical aperture, NA, 0.22) and the desired range of operation. With a diameter of the probe of 42 mm, the detected field of view reached 42 mm (the diameter of the probe shadow) at a fibre to sample distance of 40 mm. Given that the light source was not perfectly collimated, it was useful to limit the

Remote acceptance probe and illumination configuration.

detected area diameter to a value less than the diameter of the detector probe / shadowed region.

This optical assembly was most easily adapted to the in-line sorting of fruit moving on a conveyor belt by viewing the fruit from above (as shown in Fig. 7.1). However, this orientation will involve a change in the distance from detector probe to the fruit surface with change in fruit diameter. Smaller fruit are positioned more distant from the probe, and thus have a reduced surface radiance. However, the field of view of the fibre optic (without lens) is increased with distance between probe and fruit surface, and should result in a compensatory increase in signal intensity as distance increases. The balance of these factors is considered below.

The following calculations attempt to describe, using the frequently used reversed optics technique, the effect of distance from the fibre cable end and curvature of fruit on the signal level emerging for a shadowed region on the fruit sample, assuming uniform radiance across the region.

A fibre optic cable with a cross-sectional fibre area $A_{IF} = 7.854 \times 10^{-7} \text{ m}^2$ was used to image an area on the (flat) sample defined by $A_{2F} = \pi a_s^2$, where a_s = the radius of the segment viewed by the fibre with a numerical aperture of 0.22. Thus :

$$a_s \sim 0.2r_{ff} \quad \text{Eqn 7.8}$$

where r_{ff} is the distance between the fruit and the fibre (Eqn. 7.8.).

Remote acceptance probe and illumination configuration.

Given that Radiant Flux (Φ) represents the change in radiant energy per unit area, per unit time, and that the Radiant Intensity (L) is defined as the radiant flux emitted per unit area of solid angle by a point source, it follows that :

$$\Phi = \int_{A_{1F}} \int_{A_{2F}} \frac{L \cos\theta_1 \cos\theta_2 dA_{1F} dA_{2F}}{r_p^2} \quad \text{Eqn 7.9}$$

where θ_1 and θ_2 represent the angles of the planes of the illumination source and the illuminated area, respectively, to the optical axis, and r_p is the distance separating the two planes. Assuming that both these planes are flat and orthogonal to the incident light, $\cos \theta_1 = \cos \theta_2 = 1$. This equation can be simplified to:

$$\Phi = \frac{L A_{1F} A_{2F}}{r_p^2} = \frac{1.963 \times 10^{-7} \times L \times 0.126 r_p^2}{r_p^2} = 2.467 \times 10^{-8} L \quad \text{Eqn 7.10}$$

Thus, for the current application, as the distance between the fibre (probe) and sample surface is increased, the radiance of the viewed area (Φ) will increase but the assessed radiance of the fruit would remain close to constant.

However, these calculations have not allowed for curvature of the surface of the sample as encountered with fruit. In such cases, the illuminated area and radiant flux on the fruit surface is a function of both the distance between the fruit and the fibre and the radius of the fruit (R_oF). The half segment angle of the viewed area on the fruit θ_b , relative to the centre of the fruit, is defined as :

$$\sin \theta_b = \frac{0.2r_p}{RoF} \quad \text{Eqn 7.11}$$

$$\cos \theta_b = \frac{\left(RoF^2 - (0.2r_p)^2 \right)^{\frac{1}{2}}}{RoF} \quad \text{Eqn 7.12}$$

where θ_b is half the segment angle of the viewed area on the fruit and RoF is radius of the fruit.

The surface area of the illuminated curved segment on the fruit is determined as :

$$\text{Area} = 2\pi R^2 \int_0^{\theta_b} \sin \theta \, d\theta \quad \text{Eqn 7.13}$$

$$= 2\pi R^2 [\cos \theta]_{\theta_b}^0 \quad \text{Eqn 7.14}$$

$$= 2\pi R^2 (1 - \cos \theta_b) \quad \text{Eqn 7.15}$$

$$= 2\pi R^2 \left(1 - \frac{\left(R^2 - (0.2r)^2 \right)^{\frac{1}{2}}}{R} \right) \quad \text{Eqn 7.16}$$

$$= 2\pi \left(R^2 - R \left(R^2 - (0.2r)^2 \right)^{\frac{1}{2}} \right) \quad \text{Eqn 7.17}$$

Substituting into Eqn. 7.9, Radiant Flux can be defined as :

$$\Phi = \frac{1.963 \times 10^{-7} L \cdot 2\pi \left(R^2 - R \left(R^2 - (0.2r_p)^2 \right)^{\frac{1}{2}} \right)}{r_p^2} \quad \text{Eqn 7.18}$$

Remote acceptance probe and illumination configuration.

When a collimated light source is used, as the distance to the sample is increased, radiance of the fruit surface is therefore expected to increase. When a fruit surface is moved from 25 to 35 mm from the end of the probe, radiance is calculated to increase by 0.8% and 0.3% for a 100 mm and 150 mm diameter fruit respectively. At a given distance from light source to sample, the radiance of a smaller diameter fruit will be less than that on a larger diameter fruit due to the increased area of illumination of the smaller fruit, and the average distance from the illuminated region to the detector is increased. Thus the amplitude of the detected signal will decrease. However, it is expected (Eqn. 7.18) that the overall effect will be that radiance will be slightly increased with increased distance between light source and fruit due to decreased fruit size. At a fixed distance of 25 mm from the probe end, the difference in radiance for 100 mm and 150 mm diameter fruit is expected to be 1.5% higher (or 450 counts on a near saturation signal of 30000 counts) for the smaller fruit. This variation in signal level is within the signal to noise (SNR) limit of 5000:1 (~0.025% variation in signal, count level maintained > 8000 counts) shown to effect the calibration of sucrose in water on a cellulose matrix, using absorbance data from a Zeiss MMS1¹⁷⁸.

If a lens is used in this design, the area of the viewed segment is only affected by the curvature of the fruit since the lens is set at its focal length from the fibre. Signal level will decrease with increased distance from fruit to probe (e.g. smaller fruit) due to the decreased radiance. Empirically this has been found to be as high as ~ 25% signal level over 100 mm range (probe to sample). Providing the signal level is maintained above the previously determined critical

level (8000 counts²¹¹) the SNR is sufficiently high to allow the generation of reliable predictive models.

7.3.4. Optimisation of optical geometry and sampling strategy with respect to calibration performance

A comparison was made of calibration development for the wavelength range 700 – 1050 nm, using either transmittance, absorbance or second derivative data, and for the wavelength range 630- 980 nm, using absorbance data (Table 7.1). Calibration performance (RMSECV) was not significantly different at the 95% confidence interval, using Fearn's' criteria. Nonetheless, RMSECV results for each technique for each of the 11 data sets was assigned a value (0 to 3, 3 being best), commensurate with their performance relative to the others of the same set. Weighted sums of all results were calculated for each technique to determine the optimal technique. A optimal RMSECV value was obtained for the 'contact' configuration using d^2A data in 43% of the cases ($n= 11$), with optimal RMSECV attributed to each of the other three techniques in ca. 20% of cases each. Optimal RMSECV was obtained for the 'non-contact' configuration using absorbance data from the wavelength range 630 – 980 nm in 29% of cases. Derivatisation of data is commonly employed to remove background effects from spectra, such as those introduced by specular light. Given that the optical configurations effectively eliminated specular light from the detector, the lack of effect of this data pre-treatment is not surprising. Little information is carried in

Table 7.1. PLS calibration performance for spectra collected using the ‘contact’ and ‘non-contact’ (without lens) illumination/detector optical configuration, across eleven populations of differing cultivars and growing districts. Data was processed as absorbance data (A), transmittance data (T), second derivatised absorbance data (d²A) and lowered spectral window using absorbance data (LA). Calibration performance is reported in terms of number of samples in the calibration set, standard deviation of refractometer assessed soluble solids content in the population (SD), RMSEC, RMSECV, R_v, the ratio of SD to RMSECV (SDR). Calibration performance of the two optical configurations is reported in terms of Fearn’s criteria (R² and RMSECV values for a 95% confidence interval). Differences in RMSECV which were significantly different at a 5% confidence interval using Fearn’s criteria are indicated by bold type.

Cultivar - Site (Number of Samples)	Optical Configuration	Data Type	Standard Deviation	R _v	SDR	RMSECV	Fearn R ² Low - High RMSECV
Dubloon - A (n = 178)	contact	A	1.01	0.74	1.51	0.67	0.17
	contact	T	1.03	0.78	1.58	0.65	0.56 - 0.75
	contact	d ² A	1	0.77	1.52	0.66	
	contact	LA	0.96	0.59	1.26	0.76	
	non-contact	A	0.9	0.64	1.30	0.69	
	non-contact	T	0.91	0.64	1.30	0.7	
	non-contact	d ² A	1.04	0.71	1.41	0.74	
	non-contact	LA	0.91	0.66	1.34	0.68	
Dubloon - A (n = 172)	contact	d ² A	1.24	0.82	1.77	0.7	0.16
	non-contact	LA	1.28	0.79	1.64	0.78	0.60 - 0.82
Highline - A (n = 180)	contact	A	1.13	0.86	1.95	0.58	0.13
	non-contact	A	1.1	0.81	1.72	0.64	0.50 – 0.67
Dubloon - B (n = 140)	contact	d ² A	0.78	0.7	1.44	0.54	0.15
	non-contact	T	0.84	0.76	1.50	0.56	0.45 – 0.64

Table 7.1. (continued)

Cultivar - Site (Number of Samples)	Optical Configuration	Data Type	Standard Deviation	R_v	SDR	RMSECV	Fearn R^2 Low - High RMSECV
Eastern Star - B (n = 72)	non-contact	d ² A	0.89	0.68	1.37	0.65	0.16
	non-contact	T	0.95	0.67	1.32	0.72	0.51 – 0.83
Eastern Star - B (n = 142)	contact	d ² A	1.07	0.74	1.47	0.73	0.21
	non-contact	T	0.99	0.77	1.46	0.68	0.62 – 0.87
Eastern Star - Domenico (160)	contact	A	1.01	0.72	1.49	0.68	0.42
	non-contact	LA	1.02	0.72	1.44	0.71	0.59 – 0.79
Eastern Star - B (n = 180)	contact	d ² A	1.02	0.85	1.92	0.53	0.18
	non-contact	LA	1.01	0.77	1.55	0.65	0.46 – 0.61

Table 7.2. PLS calibration performance for spectra collected in stationary and moving (0.5 m s^{-1}) modes of the 'non-contact' illumination/detector system (without lens) configuration, across two populations. Calibration performance parameters are described in the legend to Table 1. Differences in RMSECV values for spectra collected of moving and stationary fruit were not significantly different at $\alpha = 0.05$, using Fearn's criteria.

Cultivar - Site (Number of Samples)	Sample presentation	Data Type	Standard Deviation	R_v	SDR	RMSECV	Fearn R^2 Low – High RMSECV
Eldorado - B (n = 196)	stationary	LA	1.69	0.83	1.80	0.94	0.52
	moving	LA	1.67	0.81	1.72	0.97	0.83 – 1.06
Eldorado - B (n = 788)	stationary	T	1.69	0.87	2.38	0.71	0.49
	moving	T	1.69	0.87	2.38	0.71	0.68 – 0.76

Table 7.3. Results of calibration of spectra collected in moving (0.5 m s^{-1}) mode of operation of the ‘in-line’ illumination/detector system with and without a lens across one population. Performance of calibrations using spectral data acquired using the at-line configuration from another population (ABZ) were assessed against spectral data acquired using the illumination/detector probe with lens when fruit were moving at 0.5 ms^{-1} (neither significant at 5% confidence level). In-line moving data with out window is indicated by ILMNW and in-line moving data with lens by ILML.

Cultivar - Grower (Number of Samples)	Optical Configuration	Data Type	Standard Deviation	R_v	SDR	RMSECV	Fearn R^2 Low – High RMSECV
Eastern Star - D (286)	No lens	d^2A	1.16	0.72	1.49	0.78	0.14
	Lens	d^2A	1.20	0.77	1.58	0.76	0.69 – 0.88
Eastern Star - E (238)	non-contact	A	1.43	0.77	1.59	0.90	0.11
	Lens	LA	1.45	0.83	1.77	0.82	0.79 – 1.03

Table 7.4. PLS calibration performance for spectra collected of one population of fruit, with three sampling procedures employed in the extraction of a juice sample for SSC determination. Fruit were sampled by extraction of four 10 mm diameter cores, with either removal or retention of the 'skin' (outer 8 mm of mesocarp and exocarp) or of a 'scoop' (40 by 70 mm) of tissue. Data presented is from spectra were collected using the 'non-contact' configuration operated with moving samples (0.5 m.s^{-1}) with and without a front lens. Calibration performance parameters are described in the legend to Table 1. Differences in RMSECV values for spectra collected with and without the front lens were not significantly different at $\alpha = 0.05$, using Fearn's criteria.

Cultivar - Grower (Number of Samples)	System	Tissue Sampled	Standard Deviation	R_v	SDR	RMSECV	Fearn R^2 Low – High RMSECV
Eastern Star - D (n = 215)	no lens	No skin	1.22	0.69	1.39	0.88	0.23
	lens	No skin	1.24	0.76	1.53	0.81	0.77 – 1.01
	no lens	Skin	1.16	0.70	1.40	0.83	0.30
	lens	Skin	1.21	0.78	1.57	0.77	0.73 – 0.95
	no lens	Scoop	1.29	0.67	1.36	0.95	0.18
	lens	Scoop	1.28	0.73	1.41	0.91	0.83 – 1.09

Remote acceptance probe and illumination configuration.

wavelengths below 700 nm with respect to vibrational and stretching modes associated with sucrose. However, this region is significant for absorption of wavelengths related to transitions within the chlorophyll molecule. Chlorophyll content of a fruit can act as an index of maturity, and thus for sugar content within a given population. Thus it was anticipated that the lower wavelength window might support superior calibrations. Probability plots reveal slightly non linear curves of both absorbance and transmittance data, with transmittance slightly worse in most cases. Often the observed non-linearities can be accommodated by PLS by the use of additional principal components (PCs). Hence, in some cases, transmittance data can achieve a better predictive model than absorbance data despite the assumption, based on the Beer-Lambert law, that a logarithmic proportionality should exist between concentrate and spectral measurement. Without clear differences between the data types, absorbance data over 700 –1050 nm range was accepted as the default for chemometric analysis (e.g. Table 7.4).

In two of 11 populations, the RMSECV of the non-contact system was significantly different from that of the contact configuration, one being poorer and one improved (Table 7.1). We conclude that the ‘non-contact’ system did not perform significantly better than the ‘contact’ system for these data sets. Walsh *et al.*²⁰⁹ demonstrated superior calibration performance for data sets collected using the contact assembly, which totally excludes specular light, relative to optical arrangements which permitted specular light to be detected. The present result indicates that if any specular light is detected using the non-

Remote acceptance probe and illumination configuration.

contact probe, it must be at levels sufficiently low level that calibration performance is not affected.

As noted earlier, the SSC of this tissue is poorly correlated with that of the deeper, edible mesocarp. Surprisingly, given that the ‘non-contact’ probe used in this study detected light returned primarily from the upper layers (ca. 10 mm), a superior correlation was developed using optical data from the ‘non-contact’ probe (predicted on actual SSC). Therefore, it is likely that the PLS calibration is based on a secondary attribute of the outer layers, which is in turn is correlated to inner mesocarp SSC. This relationship may be population specific, and we propose further work to examine the robustness of the calibration.

For the two populations assessed, calibration performance was not significantly different in terms of Fearn’s criterion for RMSECV comparison for spectra collected of either stationary fruit, or fruit moving on a conveyor at 0.5 ms^{-1} , using the ‘non-contact’ configuration (Table 7.2). At a belt speed of 0.5 m.s^{-1} , fruit will have moved 25 mm with respect to the detector, during the period of signal integration. This movement is not significant with respect to the overall size of a rockmelon, with the optical signal collected within the equatorial region of the fruit. This region has a consistent soluble solids content. Faster belt speeds, leading to integration of signal over greater areas of the fruit, are expected to result in a decreased calibration performance.

Inclusion of a front lens in the optical train of the ‘non-contact’ configuration was anticipated to improve signal stability with respect to variation in fruit size.

Remote acceptance probe and illumination configuration.

However, calibration performance was not significantly improved by inclusion of the lens, as judged using Fearn's criterion (Table 7.3). The diameter of the rockmelon fruit size in this population assessed ranged from 115 to 150 mm. The use of the lens may have more impact with fruit spanning a larger size range.

Three fruit sampling protocols were trialed. Two protocols involved removal of cores of the fruit, with either removal of the outer green mesocarp and skin, or inclusion. The third protocol involved removal of a larger segment of the fruit, and removal of the skin and green mesocarp. Calibrations developed for SSC derived from juicing of any of the three sample types were not significantly different, using Fearn's criterion. Evidently, the three sampling techniques are equivalent in assessing SSC of a tissue area relevant to that optically sampled.

7.4. Conclusion

The rockmelon fruit used in these experiments had a range of 5 to 13.1 % SSC with a mean of 8.4 and standard deviation of 1.7 % (the threshold for acceptable tasting fruit is 10 % SSC). The 'non contact' system was capable of grading rockmelons to an accuracy of ca. 1.5 % SSC (estimated as two times RMSECV ca. 0.7 achieved). The non-contact detector/illumination configuration is therefore recommended as appropriate for the application of non-invasive, spectroscopic determination of SSC of rockmelon, using PLS regression techniques based on absorbance data. Optical and related tissue juice SSC sampling from the equatorial region of the fruit is recommended to best represent 'whole fruit' quality.

8. Calibration Transfer between NIR Spectrometers in the NIR Assessment of Melon Soluble Solids Content.

This chapter has been submitted for publication under this title in the Journal of Applied Spectroscopy, (2000).

8.1. Introduction

NIR spectrometers using low cost photodiode array (PDA) or charged-coupled device (CCD) using either silicon (Si) (400 to 1100 nm) and/or indium gallium arsenide (InGaAs) (800 to 1700 nm) technologies are finding application in an ever increasing number of process line applications. Commercial applications demand transferability of calibrations rather than calibration generation for each installation.

The design of most modern post-dispersive NIR spectrometers incorporates the use of a dispersive element and either PDA or CCD photo-detecting elements. These units will vary in wavelength calibration and photometric response, even within one model and batch of manufacture. The spectral alignment of the detector array (commonly associated using a fourth order polynomial calibration equation between pixel number and wavelength) will differ between spectrometers due to small physical displacements of components. Pixel related photo-detector output can be interpolated to yield a common wavelength related assignment across instruments. Correction of differences in photometric

response between instruments is more difficult. The use of absorbance units, with referencing to a stable standard, allows comparison of spectra collected on different detecting units, however this strategy can not correct for differences in the signal to noise ratio associated with the raw count across the spectral range of the units. Slight differences in illumination geometries associated with sample orientation relative to light source and detector will contribute to differences in the recorded absorbance spectra of a given sample from two instruments. To correct for this difference, the absorbance spectra obtained on the slave instrument can be modified to reproduce that of another instrument by use of a correction factor for each pixel, relative to an absorbance spectrum for the same sample, collected on the master instrument. The standardisation samples used in such an exercise must be similar to the samples on which the predictions are to be used¹¹³. Model failure will occur when the response of the master and slave instruments is very different, or when the standard sample does not represent the samples to be analysed.

8.1.1. Standardisation Techniques.

Transfer of predictive models from one (master) instrument to another (slave) instrument is commonly accomplished using either calibration model correction or spectral response correction¹¹³. In the ‘calibration model’ approach, the predictive model, generated from spectra collected on a master instrument, is corrected to predict on spectra collected on a slave instrument (e.g. slope and bias correction). This method relies on the assumption that a linear relationship exists and will remain stable between both instruments¹⁰³. In the ‘spectral response correction’ approach, spectra collected on one instrument are modified

to appear as if originating from the other instrument^{103, 214}. This procedure has advantages over the 'calibration model correction' approach because estimation errors in the model transformation process can be eliminated from the new model. In one variant of this approach, spectra acquired on the slave instrument are modified to appear as if having originated from the master instrument. Thus, a predictive model generated on 'master instrument' spectra can be used on data from all transformed slave instruments. This method has the advantage that once a standardisation calibration has been developed between instruments, no further development is required on samples of the same genre¹¹⁵. The second variant modifies spectra of the master instrument to appear as if originating from the slave instrument and generates a new predictive model. This approach is not dependent on maintenance of a central master instrument and thus new spectra may be added to the model thereby evolving it to one comprised exclusively of slave instrument spectra¹¹⁵. However predictive model development is required for each instrument.

In NIR spectroscopy, calibration transfer has been accomplished using various chemometric techniques, for example slope and bias correction (SBC), direct standardisation (DS), and application of neural networks. When the differences between instruments are simple, an univariate approach based on SBC may prove successful¹⁰⁰. However, when more complex differences between instruments are present, more complex techniques are required. Detailed explanations of the relative procedures can be found in the references and only an overview is given here.

Wang *et al.*¹⁰³ proposed a method called direct standardisation (DS), which transforms spectra collected from a slave instrument to appear as though collected from a different (master) instrument. In this method, multiple linear regression is performed for the entire spectrum collected of a set of standardisation samples using the slave instrument, against each data point of the master instrument. Wang *et al.*¹⁰³ also developed the piecewise direct standardisation (PDS) algorithm which is similar to the DS technique but incorporates the use of a moving window which steps across the variable range. For each wavelength of a sample spectrum the absorbances for the slave instrument are regressed against the corresponding absorbances in a spectral window of neighbouring wavelengths from the master instrument.

PDS models may perform adequately where features are present in the transfer spectra but not very well when featureless regions are frequent. A further modification extended the PDS algorithm incorporating a double window (DWPDS) (personal communication, Wise¹⁰⁴). The second window extends the window range and flexibility allowing for Fourier Transform NIR (FTNIR) spectra of gas samples with very narrow spectral features and regions of only baseline noise in between. DWPDS addresses this problem by forming models based on data on both sides of the current window used in the standardisation. The second window defines the data range outside the original window to be used. The form of the model is identical to that of PDS, with difference in the way in which the model is identified.

Orthogonal signal correction (OSC)^{80, 86} is a technique that can be used for the preprocessing of NIR spectra by the subtraction of variation that is orthogonal to the analyte concentration before they are subjected to multivariate calibration. To achieve calibration transfer, standardisation sample spectral data are collected on master and slave instruments and corrected by subtraction of variation that is orthogonal to the analyte concentration (e.g. instrumental differences). Predictive models are generated on corrected spectra from the master instrument and applied to corrected spectra from the slave instrument.

In 1997, Walczak¹⁰⁶ proposed a wavelet transform-based standardisation technique (WT). In this method, the wavelet transform coefficients of selected standardisation sample spectra from both instruments are univariately and linearly regressed to achieve a correspondence by which new spectra may be modified to appear as though originating from the master instrument. This technique also can have the benefit of removing noise from the spectra.

When the same set of samples cannot be measured on both instruments, many of the commonly used techniques (e.g. DS, PDS, DWPDS and OSC) become useless. The Finite Impulse Response (FIR) technique, proposed by Blank *et al.*¹⁰⁹ does not require spectra to be measured on both instruments. This technique can be thought of as a moving window similar to the multiplicative scattering correction (MSC). This moving window is used to correct spectra from master and slave using one reference spectrum (e.g. mean spectrum of the calibration set from the master instrument) with only the centre channel of each window being corrected. It uses corrected spectra from the master to develop a

calibration model which is then applied to corrected slave spectra. A disadvantage of this technique is that artefacts arise when the FIR transfer produces very small regression coefficients in the corrected spectra, making standardisation in that window poor.

An alternative method, model updating (MU), provides an evolving model which, when performance monitoring data are routinely added and a corresponding number of old data are deleted, will eventually contain data solely from the new system. It has the benefit of not requiring samples to be measured on both instruments but the disadvantage of requiring individual predictive model generation for each instrument.

8.1.2. Sample Selection.

Sample selection is critical to success for those methods requiring standardisation samples to be measured on both instruments. The use of standardisation samples from a source different to those on which the calibration is to be used and which cover a larger spectral range generally leads to poor results¹¹⁴. Use of standardisation samples similar to the samples to be predicted can lead to good standardisation, but the transfer will be applicable only to that sample genre¹¹⁴,
115.

A frequently used standardisation sample selection technique comes from an algorithm that Kennard and Stone proposed in 1969¹¹⁶ to assist experimental design. This method begins by removing a pair of samples in the 'master' calibration matrix (mC) which are most different to each other, based on the

Euclidean distance of absorbance spectra and places these in a standardisation matrix (mT). The following stepwise procedure is then repeated until the desired number of samples is achieved. The Euclidean distance between the candidate sample and other selected samples is calculated and the minimum distance $d(u)$ is stored.

$$d(u) = \sqrt{\min_{s=1}^n \left(\sum \left({}^mC(u,:) - {}^mT(s,:) \right)^2 \right)} \quad \text{Eqn 8.1}$$

where s = index of selected spectra, u = index of unselected spectra and n = number of spectra selected prior to this iteration. The unselected sample in the mC matrix with the largest $d(u)$ value is removed and added to the mT matrix.

8.1.3. Technique Selection.

There is no clear choice for a calibration transfer methodology to suit all applications. For example, NIR spectrometry has been extensively applied to the quantitative analysis of a range of agricultural products (particularly grain) since the 1970s, for which calibration transfer between instruments has been a major goal. Many workers (for example, Park *et al.*²¹⁵, Osborne²¹⁶, Tillman²¹⁷, and Shenk and Westerhaus¹⁹⁵) have reported standardisation results achieved between NIRSystems instruments, using propriety software and techniques (for example, use of 'single sample standardisation', a photometric response correction method, or 'repeatability files', a model updating method, WinISI, Infrasoft International, LLC., USA). However, other instrument manufacturers advocate different calibration transfer methodologies for the same sample type.

In another application area, Geladi¹⁰⁸ assessed a number of techniques, including Savitzky-Golay Transform (SGT), FIR, PDS, OSC and WT, for the transfer of NIR calibrations developed to predict the pH of lake sediment between five different spectrometers (four NIRSystems 6500 and one NIRSystems 5000). It was concluded that, for these data, OSC filtering worked best and adequate calibration transfer resulted.

Swierenger *et al.*¹¹⁰ considered the case where measurement of standardisation samples on both instruments was not possible. This approach makes the model robust with respect to transfer by data preprocessing during the development of the model. They found that variable selection by simulated annealing (SA) of NIR spectra from NIRSystems 5000 and 6500 spectrometers enhanced the model's robustness with respect to transfer and also improved its predictive ability when used on models of water content of tablets (unspecified ingredients). This improvement was comparable with that obtained by PDS.

In the current study we explore the capabilities of seven well-known standardisation techniques, one simple new method and a model updating method for the application of calibration transfer between Zeiss MMS1 PDA spectrometers used in the application of non-invasive assessment of SSC of intact melon fruit¹⁷⁷. In this application a RMSEP of < 1% SSC is required.

8.2. Experimental Method:

8.2.1. Data Sets.

The performance of standardisation of calibrations, generated against soluble solids content (SSC) of fruit mesocarp tissue, was assessed for two data sets from two populations of rockmelons (designated A and B). Set A comprised spectra of one population of 201 fruit (Dubloon, from a commercial property near St. George, Southern Queensland) collected using four MMS1 spectrometers (designated 155, 726, 730, and 738) and set B using a subset of two MMS1 spectrometers (726 and 738) on a separate population of 198 rockmelons (Navajo, from a commercial property near Kingaroy, Southern Queensland). All samples were allowed to equilibrate to room temperature (27° C) overnight before spectral measurements were made. Wet chemistry was performed on the juice extracted from four 8 mm diameter cores of representative mesocarp from each fruit using a garlic press and an Otago refractometer (~ 0.2% SSC accuracy) to determine associated SSC values. The means of the SSC value for each population were 10.67 and 10.02 while the standard deviations were 0.890 and 1.181 (for the A and B data sets, respectively).

8.2.2. Instrumentation

All spectrometers were MMS1 NIR-enhanced spectrometers from Carl Zeiss Pty. Ltd. (Jena, Germany) using Tec5 (15 bit resolution) electronics. Labview based software was developed for data acquisition and spectrometer control. The light sources and spectrometers were powered up two hours prior to commencement of experimentation to ensure stable operation. The reference used for all

measurements was a 6 mm thick, white teflon tile positioned so that the maximum (reflectance) count level was $\sim 80\%$ of the dynamic range. A collimated light source (100 W quartz tungsten halogen (QTH), focusable RMDL 170 Striker (Light Force Australia Pty. Ltd, Cleve, Australia)) illuminated the sample with an 80 mm diameter beam. An acceptance probe¹⁷⁷ housed a mirror (gold coated front surface, Edmunds Scientific Company, Barrington, NJ USA) to direct incoming light to the fibre optical cable of a Zeiss MMS1 spectral sensor (a bundle of 30 fibres, each 70 μm in diameter, total diameter of 500 μm ; NA 0.22).

8.2.3. Spectral Data Treatment.

Single scans of 50 ms integration time were taken for each spectrum. A maximum count level > 10000 was maintained to minimise any variation in performance due to changing signal to noise ratio (SNR) of each system¹⁷⁸. Spectral absorbance data were pre-treated by subtraction of the mean absorbance spectrum of the population (mean centring). Partial least squares (PLS) multivariate linear regression calibrations were generated against mesocarp SSC using Matlab v5.3 (The Mathworks, Inc., USA.) and PLS Toolbox, v 2.0 (Eigenvector Research, Inc., ASA). For each system, calibrations were generated using absorbance data from the spectral window 630 to 1030 nm. Calibration performance was recorded for the master instruments in terms of Root Mean Square Error of Calibration (RMSEC), Root Mean Square Error of Cross-Validation (RMSECV using leave-one out (LOO) cross validation segment selection), and Standard Deviation (STDev) of SSC. Calibration

performance in terms of prediction on standardised slave spectra was recorded in terms of Root Mean Square Error of Prediction (RMSEP).

RMSEP was calculated as:

$$\text{RMSEP} = \sqrt{\frac{\sum_{i=1}^I (\hat{y}_i - y_i)^2}{I - 1}} \quad \text{Eqn 8.2}$$

where \hat{y}_i is the predicted SSC value, y_i is the actual SSC value and I is the number of samples.

The primary assessment for performance of calibrations was made on the significance of the variation in the RMSEP following the approach of Fearn²¹² ($\alpha = 0.01$, and assuming bias negligible) (see also Snedecor and Cochran²¹³). For each comparison of two calibrations, the R^2 of the correlation between residuals (predicted – actual SSC) and the 95% confidence limits on RMSEP are reported. Briefly, Fearn's method involves comparison of prediction errors (root mean square error, RMSE) for two calibrations, predicting analyte concentration from spectral data for a single validation set of n samples (for which analyte concentrations have been determined by a primary analytical method). Since both calibration models have been tested on the same samples, the calculated errors are correlated, that is, laboratory error will appear in both methods. The correlation coefficient (R) between the two sets of errors is calculated and used in the following manner:

$$F_K = 1 + \frac{2(1-R^2)t_{n-2,0.025}^3}{n-2} \quad \text{Eqn 8.3}$$

where $t_{n-2,0.025}$ is the upper 2.5% point of a t distribution on $n-2$ degrees of freedom.

Then calculate

$$F_L = \sqrt{\left(F_K + \sqrt{(F_K^2 - 1)}\right)}. \quad \text{Eqn 8.4}$$

The upper and lower limits of a 95% confidence interval for the ratio of the RMSEs the equations are

calculated as

$$\frac{RMSE_1}{RMSE_2} \times F_L \quad \text{Eqn 8.5}$$

and

$$\frac{RMSE_1}{RMSE_2} \times \frac{1}{F_L} \quad \text{Eqn 8.6}$$

respectively. If the compared value falls between these two values it is not significantly different at $\alpha=0.05$.

Algorithms to test each standardisation technique were implemented using Matlab v 5.3 scripting (The Mathworks, Inc., USA) and the parameters relevant to each technique were incremented to achieve optimisation. Scripts assessing

DS, PDS, DWPDS, FIR standardisation techniques used algorithms available in PLS_Toolbox software (Eigenvector Research, Inc., USA) for these standardisation assessments. A new OSC algorithm⁸⁰ was used for the OSC technique assessment. Assessment of the wavelet transform technique (WT) was based on a method proposed by Walczak¹⁰⁶, but differed by the use of DS on the wavelet coefficients instead of directly univariately and linearly regressing one on the other. Wavelet coefficients from the first level decomposition were used in the DS association.

In all cases, except FIR which did not require this parameter, the number of samples used in the standardisation was varied between 3 and 25 to allow a optimum number to be determined. These were selected using the Kennard-Stone algorithm available in the PLS_Toolbox V 2.0. Window sizes for PDS and DWPDS was varied between 3 and 21 (increments of 2). The window size for FIR was ranged from 3 to 41 in increments of 4. The number of OSC components was varied from 1 to 5.

Zeiss MMS1 NIR Enhanced miniature spectrometers were used in this application (Carl Zeiss GmbH, Jena). The resolution is ~ 10 nm across the instrument range, quoted using the Rayleigh criteria, and calculated as three times the pixel dispersion (3.3 nm). The bandwidth of absorption peaks in the short wavelength NIR (SW-NIR) (600 to 1100 nm) has often been reported to be greater than 40 nm¹⁴ and the resolution of a suitable instrument need not exceed 16 nm at 912 nm for characterisation of sucrose content in a cellulose/water matrix¹⁷⁸. The guaranteed wavelength accuracy for this instrument is 0.3 nm

Calibration transfer between NIR spectrometers.

across its range (~305 to 1150 nm). However, wavelength range varies slightly among instruments due to small variations in the optical alignment of components. Interpolation to a common wavelength scale was achieved using a cubic spline interpolation technique.

Although the photometric response of these instruments is similar due to this company's rigorous photodiode selection criteria, differences between instruments with long periods between manufacture dates was observed. The photometric response (mean absorbance spectrum of standardisation sample set) of slave and master was ratioed. A comparison of this transfer technique is made against other proposed transfer techniques.

A technique generally used for updating calibration models with new spectra considered to encompass new variables (e.g. new cultivars or growing districts) was used to adapt to new instrumental variables. To assess the capabilities of model updating, increasing numbers of Kennard - Stone selected samples were added to the master data and new models generated. The new model was tested on the original slave data set.

The performance of a calibration across population of fruit varying in time of harvest or variety is a significant issue, suggesting that significant spectral variation exists between such groups¹⁶³. The performance of the best transformation procedure (WT) was therefore tested by comparing the performance of a calibration developed using a given spectrometer and

population of fruit on another population of fruit assessed using either the spectrometer used for the calibration set or another unit.

All data sets were subjected to the same data pretreatments (mean centring) and predictive modelling (PLS) with the relevant parameters for both predictive model generation (principal components) and standardisation method implementation (number of samples and/ or window size) optimised for each. Calibrations generated used equivalent data pretreatment methods which were not optimised for any individual set. Therefore RMSECV and RMSEP should not be assessed in an individual context. A 'working' calibration would also require attention to the optimisation of data pretreatment techniques.

8.3. Results

8.3.1. Comparison of Spectrometers.

The four spectrometers differed in photometric response, not only as an overall response but also in terms of spectral sensitivity as illustrated by spectra of a white reference (Fig. 8.1). Although the manufacturer (Carl Zeiss GmbH) selects photodetectors (Hamamatsu Q4874) on uniformity to minimise this type of variation, an obvious difference prevailed which is expected to impact on transferability of calibrations. For example, the photometric response (18591, 17942 and 10457, for spectrometers 726, 738 and 155, respectively) varied by 3.5% in terms of raw digital counts for spectrometers 726 and 738, respectively, at 912 nm (significant wavelength for SSC determination).

If no differences existed between two spectrometers, a plot of the mean spectrum of one against mean of other would result in a straight line with the intercept at zero and a slope of 1. Hysteresis in a plot of the mean spectrum of the master (Set A, #726) versus the mean of the slave spectra (Set A, #738) for 201 spectra (Fig. 8.2) is indicative of wavelength shift. The variation in the slope of this relationship indicated a difference in photometric responses between the detectors used in these spectrometers. The remaining difference between spectrometers following interpolation to a common wavelength scale is ascribed solely to difference in photometric responses, (Fig. 8.2, line shifted 0.1 absorbance units on the Y axis for clarity).

8.3.2. Comparison of Standardisation Techniques.

The residuals of six methods from Set B were highly correlated (Fig. 8.3, see also Table 8.3) between these techniques indicating that any remaining residual can probably be attributed to the error in the reference method. The highest correlation ($R^2 = 0.98$, $n = 198$) was achieved existing between PDS, a frequently referenced standardisation technique and DWPDS (variant of PDS) (Fig. 8.3). The performance of seven standardisation techniques SBC, DS, PDS, DWPDS, OSC, FIR, and WT, a wavelength interpolation method (with and without photometric correction) and a MU procedure were compared using the respective RMSEPs (Table 8.1). No one technique prevailed in all cases (seven calibration transfer exercises attempted), although MU performed best in the majority of cases (6 of 7). Ignoring the MU method, WT and OSC each prevailed in 3 of 7 cases (Table 8.1).

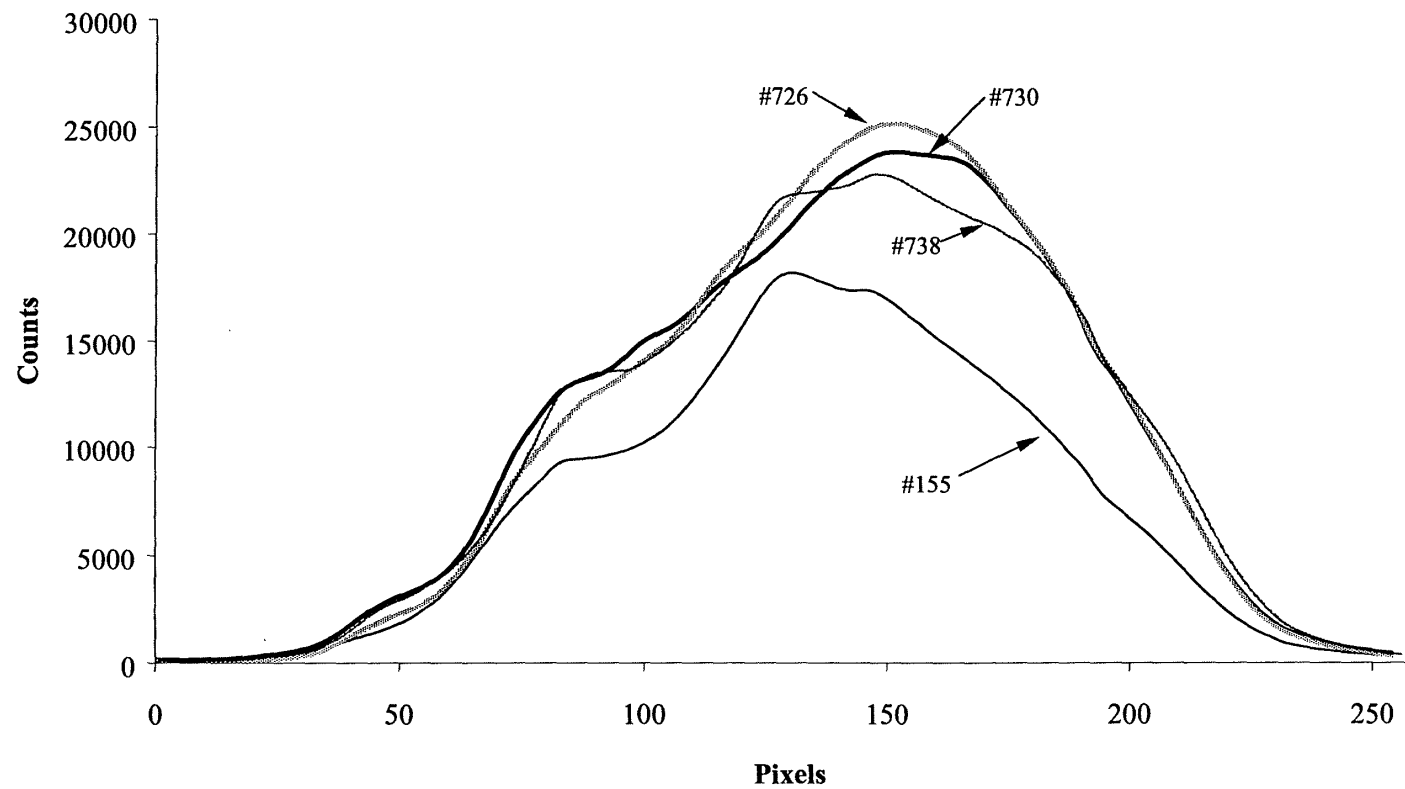


Figure 8.1. White reference spectra representative of differences observed between MMS1 spectrometers (155, 726, 730 and 738).

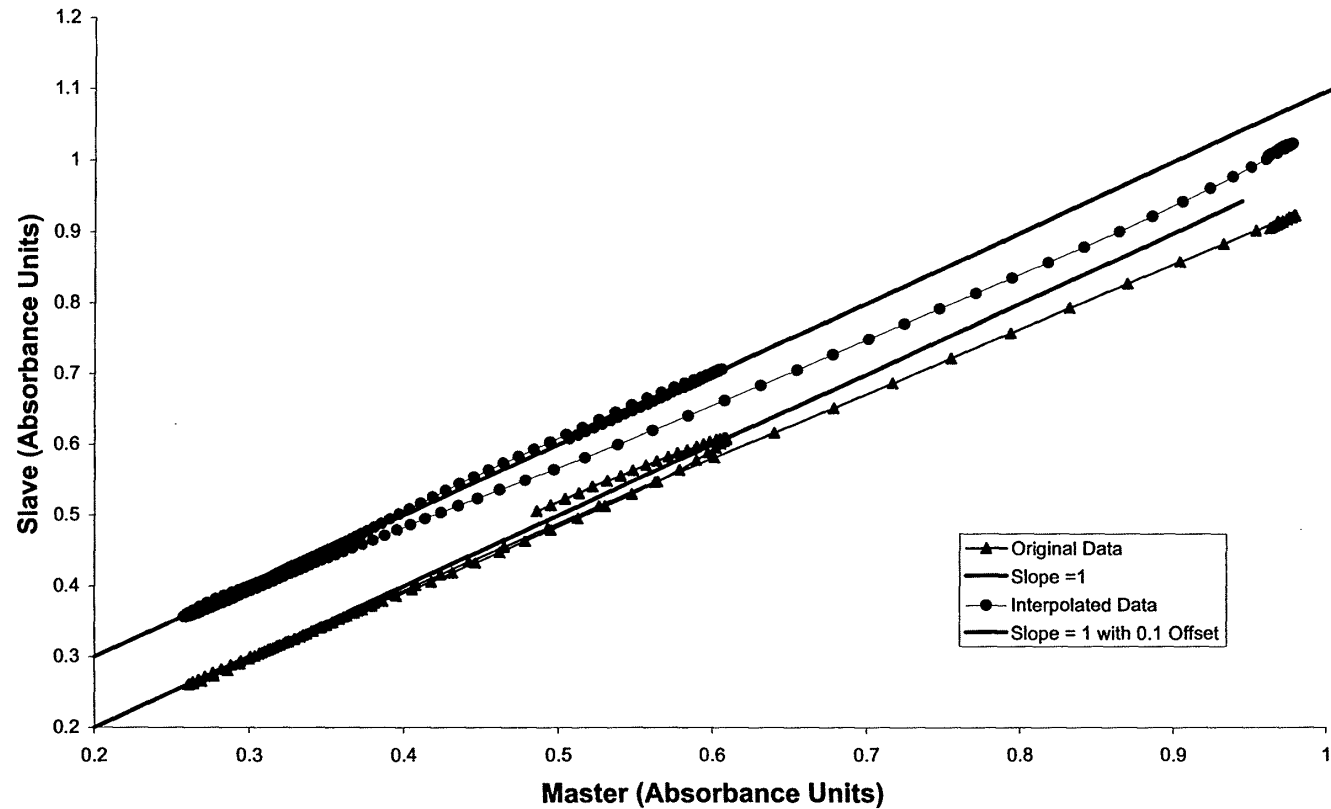


Figure 8.2. A plot of the means of data set A (absorbance units in the range 628 to 1042 nm) highlights differences existing between two typical spectrometers (#726 - Master and #738 - Slave). A second plot of the same data set, interpolated to a common scale and shifted 0.1 absorbance units on the Y axis for clarity, shows that wavelength shift has been significantly reduced but the difference in photometric response remains.

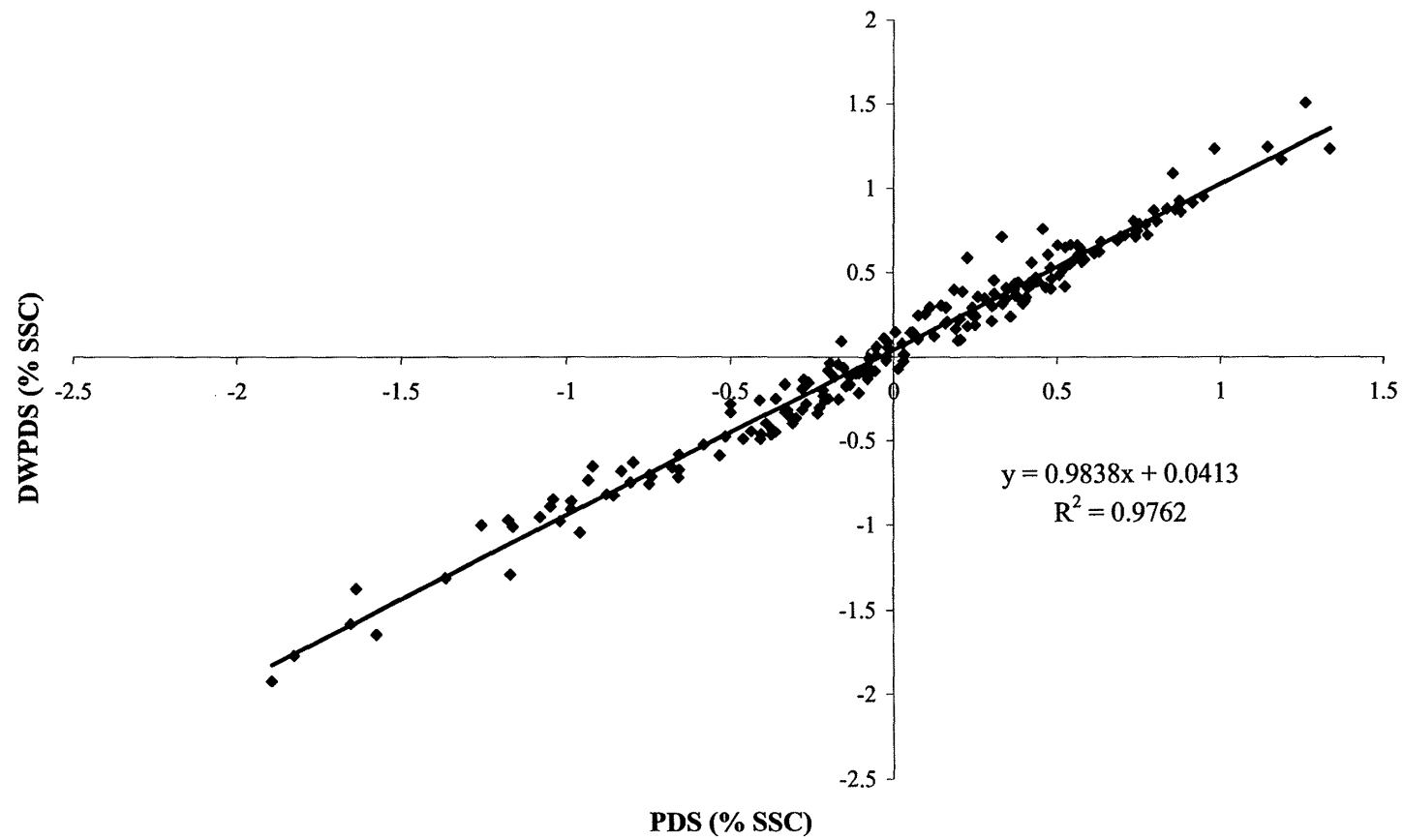


Figure 8.3. PDS residual plotted against DWPDS residuals.

Calibration transfer between NIR spectrometers.

A simple ranking procedure (Table 8.2) indicated that the relative performance of the techniques to be (best to worst): MU, WT, DWPDS, DS, PDS, OSC, Int and Mod. and FIR. Statistical data describing the predictive model performance (RMSEP) was tested for significance using Fearn's criteria. This assessment was achieved by firstly regressing the predicted analyte's residuals of one method against another method, to determine the coefficient of determination (R^2) which was input to the calculation of the significance limits of the RMSEPs (Table 8.4).

Since this assessment is always made in pairs, the standardisation technique achieving the best result in the respective data set was assessed against its five nearest neighbours (closest RMSEPs) (Table 8.3.). RMSEPs achieved by MU and other techniques were not significantly different in 6 of 7 cases. Ignoring MU, when the minimum RMSEP was achieved under WT, the result was significantly better than other treatments. However, when the minimum RMSEP was achieved by another method, this difference was not significantly better than that achieved by WT.

When raw absorbance data of melon population 'B' (standard deviation 1.18 SSC, Table 8.3) was predicted using a calibration developed on spectra, collected using spectrometer 726, of population 'A' an RMSEP of 3.80 and 2.86 was achieved using spectrometers 726 and 738, respectively. When 738 data, from populations A and B were transformed using the WT procedure, an RMSEP of 0.67 and 1.26 was achieved for melon populations 'A' and 'B' respectively.

Table 8.1. Performance of calibration transfer process reported in terms of RMSEP for the prediction of melon SSC using spectra collected on a slave spectrometer and a calibration generated on spectra of the same fruit, collected on a master instrument. Bolded results highlight the standardisation technique with the lowest RMSEP. Spectra from the slave (second listed) instrument were transformed to appear as though originating from the master (first listed) instrument spectra. A and B designate two populations of rockmelons ($\overline{SSC} = 10.68$ and 10.02 , $n = 201$ and 198 and $SD = 1.181$ and 0.873 , respectively) and 155, 726, 730, 738 are spectrometer descriptors. Model parameters in terms of RMSEC are 0.606, 0.485, 0.544 and 0.494 and RMSECV are 0.71, 0.701, 0.695 and 0.635 for spectrometers 726 (Set A), 155, 726, 730 (Set B), respectively.

Melon Population	A	B	B	B	B	B	B
Master	726	155	155	155	726	726	730
Slave	738	726	730	738	730	738	738
RMSEP without standardisation	1.134	2.166	5.990	1.282	1.706	1.034	1.593
RMSEPs of Standardisation Method							
SBC	0.823	30.903	8.169	3.126	0.867	0.878	0.86
DS	0.683	0.768	0.722	0.684	0.632	0.664	0.639
PDS	0.877	0.77	0.826	0.733	0.609	0.668	0.63
DWPDS	0.742	0.773	0.84	0.764	0.608	0.621	0.623
OSC	0.662	2.468	3.349	0.845	1.078	0.617	0.605
FIR	1.177	0.87	0.87	0.87	0.817	0.871	0.87
WT	0.677	0.746	0.629	0.633	0.629	0.657	0.636
Interpolation	1.179	2.250	3.290	3.796	1.342	0.793	0.687
Interp. + Mod.	0.671	1.301	1.153	1.130	0.633	0.627	0.635
Model Updating	0.636	0.660	0.586	0.587	0.583	0.632	0.582

Calibration transfer between NIR spectrometers.

Table 8.2. Ranking on RMSEP values achieved by each standardisation techniques based on 1 = lowest value, 2 = second lowest value etc. (Refer to Table 8.1)

Melon Population	A	B	B	B	B	B	B	Total
Master	726	155	155	155	726	726	730	
Slave	738	726	730	738	730	738	738	
DS	5	3	3	3	5	6	7	32
PDS	7	4	4	4	3	7	4	33
DWPDS	6	5	5	5	2	2	3	28
OSC	2	8	7	6	8	1	2	34
FIR	8	6	6	7	7	8	8	50
WT	4	2	2	2	4	5	6	25
Interp. + Mod	3	7	8	8	6	3	5	40
MU	1	1	1	1	1	4	1	10

Conversely, when raw absorbance data of melon population 'B' (standard deviation 0.87 SSC) was predicted using a calibration developed on spectra, collected using spectrometer 726, of population 'B' an SEP of 6.32 and 6.87 was achieved using spectrometers 726 and 738, respectively. When 738 data, from populations A and B, were transformed using the WT procedure, an SEP of 0.66 and 1.64 was achieved for melon populations 'A' and 'B' respectively.

Table 8.3. Significance testing of the results a comparison of the technique with the lowset RMSEP against five nearest neighbours using Fearn's criteria to determine upper and lower significance limits of the RMSEP value. (Refer to Table 8.2)

Data Set	Method	RMSEP	R ²	High Limit	Low Limit	Significant
Set A (726-738)	OSC	0.662				
	DS	0.683	0.708	0.723	0.606	N
	PDS	0.877	0.361	0.754	0.582	Y
	DWPDS	0.742	0.819	0.71	0.618	Y
	WT	0.678	0.645	0.73	0.601	N
	MU	0.636	0.932	0.691	0.635	N
Set B (155-726)	WT	0.746				
	DS	0.768	0.844	0.795	0.7	N
	PDS	0.77	0.383	0.847	0.657	N
	DWPDS	0.773	0.379	0.847	0.657	N
	OSC	2.468	0.469	0.839	0.663	Y
	MU	0.66	0.638	0.822	0.677	Y
Set B (155-730)	WT	0.629				
	DS	0.722	0.595	0.697	0.567	Y
	PDS	0.826	0.324	0.817	0.551	Y
	DWPDS	0.84	0.312	0.719	0.55	Y
	OSC	3.349	0.501	0.705	0.561	Y
	MU	0.586	0.624	0.695	0.57	N
Set B (155-738)	WT	0.633				
	DS	0.684	0.803	0.68	0.589	Y
	PDS	0.733	0.436	0.714	0.561	Y
	DWPDS	0.764	0.393	0.718	0.558	Y
	OSC	0.845	0.443	0.714	0.561	Y
	MU	0.587	0.628	0.698	0.573	N
Set B (726-730)	DWPDS	0.608				
	DS	0.632	0.703	0.664	0.557	N
	PDS	0.609	0.976	0.623	0.593	N
	WT	0.629	0.711	0.663	0.558	N
	OSC	1.078	0.835	0.649	0.59	Y
	MU	0.583	0.869	0.645	0.574	N
Set B (726-738)	OSC	0.617				
	DS	0.664	0.626	0.681	0.559	N
	PDS	0.668	0.81	0.662	0.575	Y
	DWPDS	0.621	0.885	0.652	0.584	N
	WT	0.657	0.62	0.682	0.558	N
	MU	0.632	0.909	0.648	0.588	N
Set B (730-738)	OSC	0.605				
	DS	0.639	0.64	0.667	0.549	N
	PDS	0.63	0.825	0.648	0.566	N
	DWPDS	0.623	0.835	0.646	0.567	N
	WT	0.636	0.63	0.668	0.549	N
	MU	0.582	0.93	0.632	0.58	N

8.4. Conclusion:

Of the established standardisation methods, direct standardisation of the wavelet coefficients of the first level decomposition (WT) was demonstrated to be the most efficient for the standardisation of a calibration for the non-invasive assessment of SSC in fresh fruit samples (rockmelons) when used to standardise between MMS1 spectrometers. However, predictive model updating, incorporating 'Kennard-Stone' selected representative spectra of the slave spectrometer has also been shown to be capable of achieving equally good or better results (in terms of lowest RMSEP) with significantly better results in one case. Model updating has an added advantage over most standardisation techniques of not requiring the measurement of standardisation samples on both spectrometers and allowing the predictive model to evolve to one containing only slave spectra over time. The disadvantage of this method is that a separate model is required for each instrument.

The SSC of fruit of a separate population was predicted very poorly by a calibration developed on another population, irrespective of whether the same spectrometer was employed to collect spectra across the two populations. This observation suggests that significant spectral variation exists between such groups, limiting the robustness of the calibration¹⁶³. A common response to this issue is to include representatives of the second population into the calibration set, a form of model updating. Interestingly, the performance of prediction using WT transformed spectra of the second population was greatly improved (SEP improved from 2.86 to 1.26 against a population STDev of 1.18, and 6.87 to 1.64 against a STDev of 0.87), although not acceptable in terms of calibration

Calibration transfer between NIR spectrometers.

performance (poor STDev to RMSEP ratio). This improvement indicates that the WT procedure does more than make spectra of one instrument look like originating from another. It probably emphasises spectral regions related to analyte, similar to wavelength selection, thereby more assisting robust predictive model development.

9. Conclusion

In this thesis, criteria important to the design of an NIR system for non-invasive assessment of internal attributes (e.g. SSC) of fruit (predominantly, melons) in an in-line setting have been established, and applied in the development of a prototype system with the aim of grading fruit into sweetness categories. To this end, development of equipment capable of rapidly (< 50 ms) acquiring spectral data of a suitable quality was necessary. Spectral quality was assessed in terms of the performance of predictive models.

The determination of design parameters for NIR spectrometers to be applied to an in-line fruit sorting system required knowledge of required wavelength resolution and signal to noise ratio, detection system and the design of the optical system to 'sample' appropriate volume of fruit. In-line application, with fruit moving on a belt at up to 0.7 m s^{-1} , allows for a ca. 50 ms analysis time which necessitated the design of an optimised illumination/detection system.

Despite the existence of a few miniature spectrometers, the initial aim of this thesis was to design a high quality, low cost spectrometer specific to this application. An assessment of wavelength dispersion elements revealed that prisms were capable of delivering resolutions better than 1 nm and had a linear output across a broad spectral range (e.g. 405 - 2000 nm). In comparison, flat gold coated diffraction gratings could achieve better resolution (0.3 nm) but their output was shared over a number of orders thus reducing efficiency. Although toroidal, holographic concave diffractions had a much flatter efficiency curve

Conclusion

and a throughput and resolution similar to that of prisms they had a higher cost (comparative costing is difficult since a generic cost for these diffraction gratings is not available because they are specially designed and produced for an application whereas prisms are mass produced and readily available through a number of outlets). A conclusion was made that for a low cost instrument to be used in an in-line fruit sorting setting, prisms could be used successfully.

A wavelength resolution better than 16 nm (FWHM) was empirically determined not to significantly improve predictive model (sucrose in a cellulose matrix) performance. PDAs and CCDs were assessed, in terms of SNR, to determine the effect of signal precision on predictive model performance. For models developed to assess sucrose in a cellulose matrix, an SNR of 5000:1 was the lower limit. It was concluded that either PDAs or CCDs could be used in this application since both had similar capabilities, however it was recognised that PDAs have better SNR in high-light situations, whereas CCDs may provide the best SNR in low-light applications and have a slight sensitivity and speed advantage. Also, from these results, a protocol was established (in terms of minimum acceptable performance) to ensure good quality spectral data for good quality predictive model generation. The lower inherent sensitivity of PDAs could be enhanced to a level similar to that of CCDs, by increasing the amount of light collected by increasing physical pixel size. Lower inherent SNR of CCDs could be increased to a level similar to that of PDAs by binning pixels.

A bench-top prototype spectrometer, based on a dual-prism dispersion element and large pixel size PDA, was constructed and preliminary testing commenced.

Conclusion

While early results of this in-house instrument demonstrated that it was technically superior, in terms of higher precision and throughput, economics dictated the use of one of the commercial instruments chosen on criteria identified to be important to performance for this application. The MMS1 instrument (Carl Zeiss, Jena, Germany) was adopted due to its high signal to noise ratio characteristics, temperature stability, wavelength range, sensitivity and robustness. For the MMS1 platform, SNR was achieved at ca. half saturation count level (i.e. > 16000 counts) with a 100 Watt QTH light source and the designed illumination/detector configuration (single spectra acquired at this SNR in 50 ms).

SSC distribution within melon fruit was investigated to determine a protocol for wet chemistry sampling methods and to determine regions to be spectrally sampled for use in predictive model generation. SSC varied in some fruit by > 2.8 % (from inner mesocarp at the equator to outer mesocarp at stem end). Variation of inner mesocarp in a region ~ 30 mm wide at the equator was ~ 0.5% SSC. We recommend that attention be given to the variation in SSC across a sample in the development of calibrations. For example, the attribute of exocarp thickness may vary in fruit grown under different agronomic conditions. As optical data will be derived principally from the outer layers of the fruit, the performance of a calibration may be degraded if exocarp thickness is changed. It is also important that a consistent thickness of skin is removed from the cored sample, with the lower soluble solids content of the outer mesocarp averaged with the higher content of the inner mesocarp.

Conclusion

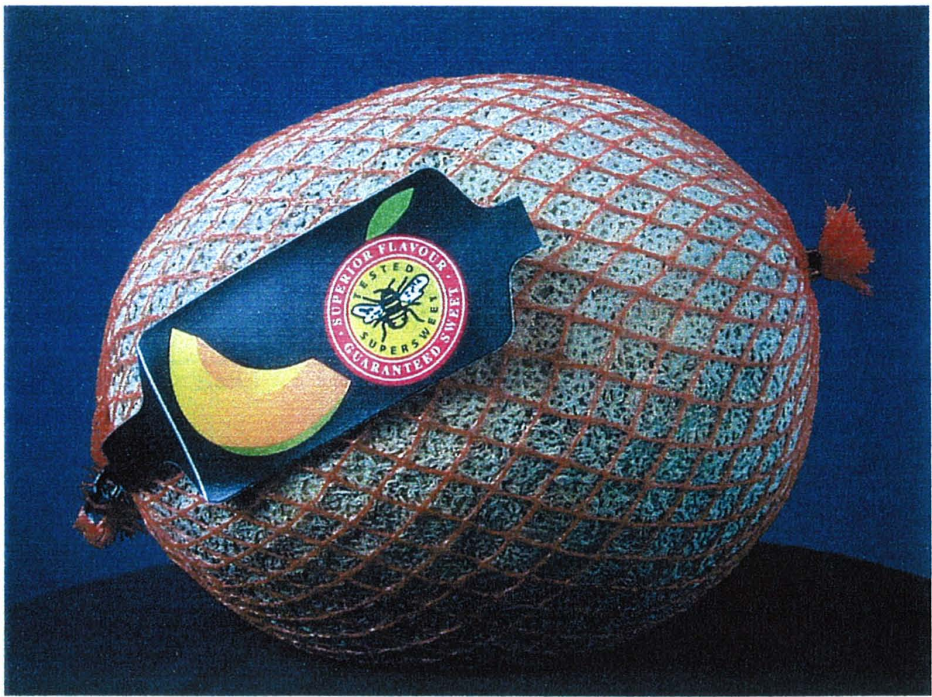
Light distribution from a novel non-contacting illumination/detecting system was assessed to ensure that spectrally sampled and wet chemistry sampled regions aligned and that both were from consumer important areas of the fruit. It was found that spectral information from depths of 5 to 25 mm in the fruit made up > 80% of the total signal.

Ten standardisation techniques were assessed for performance with respect to the transfer of predictive models across fruit grading systems using the described design. Model updating proved at least as effective as any of the specific techniques and has the advantage of not requiring samples to be measured on both systems. This advantage can become important in the advent of a total failure of the master instrument. Of the devoted techniques, a modified wavelet transform incorporating Kennard-Stone sample selection and direct standardisation of the first level decomposition coefficients proved the most successful.

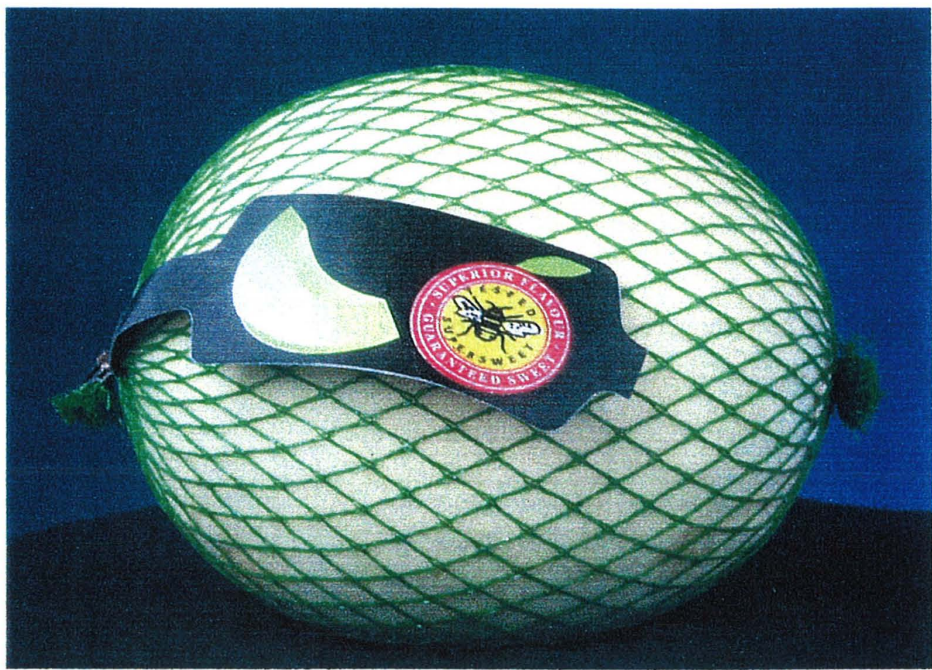
A summary of the criteria identified as important to a rapid fruit sorting system based on NIR spectroscopic technology incorporating Si based detectors is given in Table 9.1. The industrial partner (Colour Vision Systems Pty Ltd, Victoria, Australia) adopted these criteria as the basis of a fruit conveyor-based sorting system in early 2000. Backed by a strong wet chemistry validation of NIR spectroscopy results, fruit identified as sweet were marketed as premium products (Fig. 9.1) through Australia's largest fruit and vegetable retailer in mid 2000.

Figure 9.1. Western Australian (a) rockmelon fruit and honeydew (b) sorted by the prototype system packaged to differentiate this product as a 'premium' article.

(a)



(b)



Conclusion

Table 9.1. Recommended Design Criteria for a Rockmelon Fruit Sorting System Employing Silicon-based NIR Spectroscopy.

Dispersive Element	Prism (2 x SF18 equilateral) or Holographic Concave Diffraction Grating (750 – 800 nm blazed)
Detector	Si PDA (large pixel size to increase sensitivity) or Si CCD (binned to increase SNR)
Wavelength Range	600 to 1100 nm
Wavelength Resolution	< 16 nm
Signal to Noise Ratio (lower limit)	> 5000:1 (> 16000 counts on MMS1, half dynamic range at 15 bits A/D)
Integration Time	Typically < 50 ms for ~15 fruit per second (dependent on desired process rate and SNR).
Electronic Interface	> 15 bit (analogue to digital resolution)
Optical Interface	Optical fibre coupling (low OH)
Optical Path Redirection	Front surface, high NIR reflective coatings (e.g. gold, rhodium).
Spectral Data Acquisition Mode	Body transmittance.
Light Source	Quartz tungsten halogen lamp (> 100 W lamp in parabolic reflector).
White Reference	Teflon (> 6 mm thickness, location during measurement strictly reproducible, monitored for quality control).
Dark Reference	All ambient light excluded (monitored for quality control).
Power Supply	Stabilised, noise free (e.g. Uninterruptable Power Supply (UPS)).
Hardware Environment (Temperature Stability)	All optics enclosed in dust free enclosure. $\pm < 0.5^{\circ}$ C for spectrometer and light source.
Sample Data Acquisition	Optically triggered, non-contact measurement.
Fruit Orientation	Stem peduncle axis in direction of movement, sample to detector distance variation minimised.

Conclusion

Predictive model generation	Partial least squares regression using spectral window 630 to 1040 nm and autoscaled absorbance data. Other data pretreatment may be required dependent on commodity.
Standardisation Across Systems	Model updating or regression of wavelet transform coefficients.
Primary Reference Method	Wet chemistry should be performed on flesh (no skin) excised from a region directly correlated to optically sampling.
Cost	< AU\$10000.

10. References

1. W. F. McClure, et al., (1994), "Chemometrics Sunny-Side Up.", *Anal. Chem.*, **66**, (10), 584A-585A.
2. D. A. Burns and M. Margoshes, in Book "Historical Development.", E. G. Brame, Ed. (Marcel Dekker, New York, 1992), vol. 13, pp. 1-6.
3. F. L. Pedrotti and L. S. Pedrotti, "Introduction to Optics.", (Prentice-Hall, ed. 2nd, 1993).
4. C. L. Putzig, et al., (1994), "Infrared Spectroscopy.", *Anal. Chem.*, **66**, (12), 26R-66R.
5. J. J. J. Workman, (1996), "Interpretive Spectroscopy For Near Infrared.", *App. Spect. Rev.*, **31**, (3), 251-320.
6. J. J. Workman, (1999), "Review of process and non-invasive near-infrared and infrared spectroscopy: 1993-1999.", *App. Spect. Rev.*, **34**, (12), 1-89.
7. J. W. Hall and A. Pollard, "Near infrared spectroscopy brought to life.", G. D. Batten, et al., Eds., 6th International Conference on Near Infrared Spectroscopy NIR-94, Lorne, Australia. (NIR Spectroscopy Group, 1994).
8. K. Matsumoto, et al., "Development of a new near infrared spectrophotometer (NIRF-200).", International Conference on Tropical Fruits, Kuala Lumpur, Malaysia (1996).
9. S. Kawano, et al., (1993), "Nondestructive Determination of Sugar Content in Satsuma Mandarin using by Near Infrared (NIR) Transmittance", *J. Jap. Soc. Hort. Sci.*, **62**, (2), 465-470.

References

10. J. Guthrie and K. Walsh, (1997), "Non-invasive assessment of pineapple and mango fruit quality using near infra-red spectroscopy.", *Aust. J. Exp. Agric.*, **37**, 253-63.
11. M. Ventura, et al., (1998), "Non-destructive determination of soluble solids in apple fruit by near infrared spectroscopy (NIRS).", *Postharvest Biol. Technol.*, **14**, 21-7.
12. V. Bellon, et al., (1993), "Feasibility and performances of a new, multiplexed, fast and low- cost fibre-optic NIR spectrometer for the on-line measurement of sugar in fruits.", *Appl. Spectrosc.*, **47**, (7), 1079-93.
13. W. Herschel, (1800), "Experiments on the Refrangibility of the invisible rays of the sun.", *J. Near Infrared Spectrosc.*, **8**, 75-86.
14. D. A. Burns, "NIR without overtone/combination bands?", G. D. Batten, et al., Eds., 6th International Conference on Near Infrared Spectroscopy NIR-94, Lorne, Australia. (NIR Spectroscopy Group, 1994).
15. L. Bokobza, "Near infrared spectroscopy.", A. Davies, Ed., NIRS 97, Essen, Germany (*J. Near Infrared Spectrosc.*, 1997).
16. R. Eisberg and R. Resnick, "Quantum Physics of Atoms, Molecules, Solids, Nuclei and Particles.", (John Wiley & Sons, New York, ed. 2nd, 1985).
17. R. A. Serway, et al., "Modern Physics.", S. G. S. Series, Ed., Complete Package for Teaching Physics (Harcourt Brace Jovanovich College Publishers, New York, 1989).
18. P. Williams and K. Norris, "Near infrared technology in the agricultural and food industries.", P. Williams and K. Norris, Eds. (Americal Association of Cereal Chemists, Inc. St Paul, Minnesota, USA, 1987).

References

19. E. W. Ciurczak, in Book "Principles of Near-Infrared.", D. A. Burns and E. W. Ciurczak, Eds. (Marcel Dekker, New York, 1992), vol. 13, pp. 7-12.
20. G. S. Birth and C. J. Washam, "Optical Properties of Dairy Products.", Summer Meeting of ASAE (1978).
21. P. Kubelka, (1948), "New Contributions to the Optics of Intensity Light-Scattering Materials. Part 1.", J. Opt. Soc. of Amer., **38**, (5), 448-57.
22. J. M. Olinger and P. R. Griffiths, in Book "Theory of Diffuse Reflectance in the NIR Region.", D. A. Burns and E. W. Ciurczak, Eds. (Marcel Dekker, New York, 1992), vol. 13, pp. 13-36.
23. O. Berntsson, et al., (1999), "Effective Sample Size in Diffuse Reflectance Near-IR Spectrometry.", Anal. Chem., **71**, (3), 617-23.
24. G. S. Birth, (1978), "The Light Scattering of Foods.", J. Food Sci., **43**, 916-25.
25. M. Gerken and G. W. Faris, (1999), "Frequency-domain immersion technique for accurate optical property measurements of turbid media.", Opt. Letters, **24**, (23), 1726-8.
26. J. S. Maier, et al., (1994), "Possible correlation between blood glucose contraction and the reduced scattering coefficient of tissues in the near infrared.", Opt. Letters, **19**, (24), 2062-4.
27. J. S. Reynolds, Doctor of Philosophy, Purdue University (1996).
28. C.-L. Tsai, et al., (1998), "The Near-Infrared Reflectance Spectrum of Skin: A Monte Carlo Simulation.", Biomed. Eng. - Applic. Basis & Communic., **10**, (3), 47-52.

References

29. S. Tsuchikawa and S. Tsutsumi, (1999), "Directional Characteristics Model and Light-Path Model for Biological Material Having Cellular Structure.", *Appl. Spectrosc.*, **53**, (2), 233-40.
30. C.-S. Chen, et al., (1997), "Calibration Transfer from Sample Cell to Fibre-optic Probe.", *Appl. Spectrosc.*, **51**, (5), 744-8.
31. J. K. Holland, et al., (1997), "Transfer of Spectral Data between Fourier-Transform Infrared Spectrometers for use in Discriminant Analysis of Fruit Purées.", *J. Sci. Food Agric.*, **75**, 391-400.
32. T. Iwata and J. Koshoubu, (1998), "Proposal for High-resolution, Wide bandwidth, High-optical-throughput Spectroscopic System Using a Fabry-Perot Interferometer.", *Appl. Spectrosc.*, **52**, (7), 1008-13.
33. J. Lin, et al., (1997), "Calibration transfer from a scanning near-IR spectrophotometer to an FT-near-IR spectrophotometer.", *Analytica Chimica Acta*, **349**, 263-9.
34. M. J. Mattu and G. W. Small, (1995), "Quantitative Analysis of Bandpass-Filtered Fourier Transform Infrared Interferograms.", *Anal. Chem.*, **67**, (13), 2269-78.
35. I. Noda, (1993), "Generalised Two-dimensional correlation method applicable to infrared, Raman, and other types of spectroscopy.", *Appl. Spectrosc.*, **47**, (9), 139-36.
36. C. J. Petty, Doctor of Philosophy, University of Southampton (1991).
37. R. Reshadat and S. T. Balke, (1999), "Correlation In-line NIR and OFF-line MIR Spectra Using Partial Least-Squares: Further Assessment.", *Appl. Spectrosc.*, **53**, (10), 1309-11.

References

38. B. C. Smith, "Fundamentals of Fourier Transform Infrared Spectroscopy.", (CRC Press, Boca Raton, 1996).
39. W. B. Wang, et al., (1998), "Visibility enhancement of fluorescent objects hidden in animal tissues using spectral fluorescence difference method.", *Opt. Communic.*, **147**, 11-5.
40. M. Stelzle, et al., (1996), "An all-fibre-optic fourier transform spectrometer.", *Meas. Sci. Technol.*, **7**, 1619-30.
41. M. Misono, et al., (1996), "High-speed Wavelength Switching and Stabilization of an Acoustooptic Tunable Filter for WDM Network in Broadcasting Stations.", *IEEE Phon. Technol. Let.*, **8**, (4), 572-4.
42. A. R. Korb, et al., (1996), "Portable Fourier Transform infrared Spectroradiometer for Field Measurements of Radiance and Emissivity.", *Appl. Opt.*, **35**, (10), 1679-92.
43. P. Zhao, et al., (1995), "Performance analyses of an infrared single-mode all-fibre-optic Fourier-transform spectrometer.", *Appl. Opt.*, **34**, (21), 4200-8.
44. M. S. Baptista, et al., (1996), "Near-infrared Detection of Flow Injection Analysis by Acoustooptic Tunable Filter-Based Spectrophotometry.", *Anal. Chem.*, **68**, (6), 791-6.
45. G. S. Hayat, et al., (1978), "Holographic Grating Update.", *Electro-Optical Sys. Des.*, **April**, 50-4.
46. M. Hühne, et al., (1995), "Performance and Selected Applications of an Acousto-Optic Tunable Filter Near-Infrared Spectrometer.", *Appl. Spectrosc.*, **49**, (2), 177-80.

References

47. C. D. Tran and G. C. Huang, (1999), "Characterization of the collinear beam acousto-tunable filter and its comparison with the noncollinear and the integrated acousto-optic tunable filter.", *Opt. Eng.*, **38**, (7), 1143-8.
48. J. Wilson and J. F. B. Hawkes, "Optoelectronics: An Introduction.", , Prentice Hall International Series in Optoelectronics (Prentice Hall, New York, ed. 2nd, 1989).
49. R. L. Musselman, (1987), "High-efficiency infrared lamp housing.", *J. Phys. Sci. Instrum.*, **20**, 928-9.
50. P. Martinsen and P. Schaare, "A Near-Infrared Imaging Spectrometer.", D. Pairman, Ed., *Image and Vision Computing New Zealand* (1996).
51. J. F. Senior, "Optical Fibre Communications: Principles and Practice.", P. J. Dean, Ed., Prentice-Hall International Series in Optoelectronics (Prentice-Hall International, London, 1985).
52. Oriel, "Oriel Catalogue.", E. G. Arthurs and D. Zbigniew, Eds. (Oriel, Stratford, Connecticut, 1994), vol. II and III.
53. R. K. Reich, et al., (1997), "High performance charge-coupled-device imager technology for plasma diagnostics.", *Rev. Sci. Instr.*, **68**, (1), 922-5.
54. T. Fujiwara and H. Sakakura, (1999), "The difference of Brix value to distinguish sweetness of melon [Japanese].", *Journal of the Japanese Society for Food Science & Technology-Nippon Shokuhin Kagaku Kogaku Kaishi.*, **46**, (9), 609-12.
55. S. Kawamura, et al., (1997), "Visual and Near-Infrared Reflectance Spectroscopy for Rice Taste Evaluation.", *Am. Soc. Agric. Eng.*, **40**, (6), 1755-9.

References

56. G. G. Dull, et al., (1989), "Near infrared Analysis of Soluble Solids in Intact Cantaloupe.", *J. Food Sci.*, **54**, (2), 393-5.
57. G. S. Birth, et al., "Nondestructive determination of the solids content of horticultural products.", *SPIE: Optics in Agriculture* (1990).
58. G. G. Dull, et al., "Nondestructive measurement of soluble solids in fruits having a rind or skin" . (Secretary of Agriculture, USA, USA, 1992).
59. H. Aoki, et al., "Nondestructive determination of sugar content in melon and watermelon using near infrared (NIR) transmittance.", *International Conference on Tropical Fruits*, Kuala Lumpur, Malaysia (1996).
60. N. Berding and G. A. Brotherton, "Analysis of high-moisture material-fibrated sugarcane.", *7 th International Conference on Near-Infrared Spectroscopy*, Montréal, Canada (1995).
61. W. G. Hansen, et al., (2000), "Tolerance of near infrared calibrations to temperature variations; a practical evaluation.", *J. Near Infrared Spectrosc.*, **8**, 125-31.
62. I. J. Warrington and G. G. Weston, "Kiwifruit Science and Management.", I. J. Warrington and G. G. Weston, Eds. (Ray Richards Publisher, Auckland, NZ, 1990).
63. P. K. Aldridge, Doctor of Philosophy, University of Washington (1991).
64. H. Schulz, et al., (1999), "Application of near-infrared reflectance spectroscopy to the simultaneous prediction of alkaloids and phenolic substances in green tea leaves.", *J. Agric. Food Chem.*, **47**, (12), 5064-7.
65. J. Lammertyn, et al., (1998), "Non-destructive measurement of acidity, soluble solids, and firmness of Jonagold apples using NIR-spectroscopy.", *J. Amer. Soc. Agric. Eng.*, **41**, (4), 1089-94.

References

66. B. G. Osborne, et al., "Practical NIR Spectroscopy with Applications in Food and Beverage Analysis.", (Longman Group UK Limited, ed. 2nd, 1993).
67. V. Bellon, et al., in Book "Interaction between light and biological material: modelisation and application.", K. I. Hildrum, et al., Eds. (Ellis Horwood, New York, 1992) pp. 41-6.
68. S. Kawano, et al., (1993), "Nondestructive Determination of Sugar Content in Satsuma Mandarin using Near Infrared (NIR) Transmittance.", J. Jap. Soc. Hort. Sci., **62**, (2), 465-470.
69. H. Maeda, "The present status of non-destructive measurement technique for analysing the contents of fruit on-line through near infrared spectroscopic analysis." (Fantec Research Institute, 1998).
70. B. A. Rock, (1997), "An Introduction to Chemometrics.", 1998, (18/8/98),
71. M. J. Adams, et al., "Practical Guide to Chemometrics.", S. J. Haswell, Ed. (Marcel Dekker, Inc., New York, 1992).
72. W. F. McClure and D. Moody, "Design of Hand-Held NIR Spectroemter for Measuring in vivo Moisture and Chlorophyll in Plants.", A. Davies, Ed., 8th International Conference on Near-Infrared Spectroscopy, Essen, Germany (J. of Near Infrared Spectrosc., 1997).
73. A. Savitsky and M. J. E. Golay, (1964), "Smoothing and Differentiation of Data by Simplified Least Squares Procedures.", Anal. Chem., **36**, (8), 1627-39.

References

74. A. Candolfi, et al., (1999), "The influence of data pre-processing in the pattern recognition of excipients near infrared spectra.", *J. Pharm. Biomed. Anal.*, **21**, 115-32.
75. J. D. Hoffman, "Numerical Methods for Engineers and Scientists.", B. J. Clark and J. M. Morriss, Eds. (McGraw-Hill, Inc., New York, ed. International, 1993).
76. J. Steinier, et al., (1972), "Comments on Smoothing and Differentiation of Data by Simplified Least Squares Procedure.", *Anal. Chem.*, **44**, (11), 1906-9.
77. V. M. F. Cabanás and A. G. Varo,(1999), "The use of "standard normal variate" and "detrending" as signal improvement tools for the interpretation of near infrared spectra of agro-food products.", *Quimica Analitica*, **18**, (1), 113-8.
78. H. Martens and P. Dardenne, (1998), "Validation and verification of regression in small data sets.", *Chemom. Intell. Lab. Syst.*, **44**, 99-121.
79. T. Isaksson and B. Kowalski, (1993), "Piece-wise Multiplicative Scatter Correction Applied to Near-infrared Diffuse Transmittance Data from Meat Products.", *Appl. Spectrosc.*, **47**, (6), 702-9.
80. T. Fearn, (2000), "On orthogonal signal correction.", *Chemom. Intell. Lab. Syst.*, **50**, 47-52.
81. G. W. Small, et al., (1988), "Detection of Atmospheric Pollutants by Direct Analysis of Passive Fourier Transform Infrared Interferograms.", *Anal. Chem.*, **60**, 264-9.
82. G. W. Small, et al., (1993), "Strategies for Coupling Digital Filtering with Partial Least-Squares Regression: Application to the Determination of

References

- Glucose in Plasma by Fourier Transform Near-Infrared Spectroscopy.", *Anal. Chem.*, **65**, 3279-89.
83. O. E. de Noord, (1994), "The influence of data preprocessing on the robustness and parsimony of multivariate calibration models.", *Chemom. Intell. Lab. Syst.*, **23**, 65-70.
84. C. L. Erickson, et al., (1992), "Relationship between Digital Filtering and Multivariate Regression in Quantitative Analysis.", *Anal. Chem.*, **64**, (24), 1155A-1163A.
85. S. de Jong, (1993), "SIMPLS: and alternative approach to partial least squares regression.", *Chem. Intell. Lab. Syst.*, **18**, 251-63.
86. S. Wold, et al., (1998), "Orthogonal signal correction of near-infrared spectra.", *Chemom. Intell. Lab. Syst.*, **44**, 175-85.
87. P. Geladi and B. R. Kowalski, (1986), "An Example of 2-block Predictive Partial Least Squares Regression with Simulated Data.", *Analytica Chimica Acta*, **185**, 19-32.
88. K.-U. Jagemann, et al., (1995), "Application of Near-Infrared Spectroscopy for Non-invasive Determination of Blood/Tissue Glucose Using Neural Networks.", *Zeitschrift fur Physikansche Chemie*, **191**, (2), 179-90.
89. P. Geladi and H. Martens, (1996), "A calibration tutorial for spectral data. Part 2. Partial least squares regression using Matlab and some neural network results.", *J. Near Infrared Spectrosc.*, **4**, 243-55.
90. C. Mello, et al., (1999), "Pruning neural network for architecture optimisation applied to near infrared reflectance spectroscopic

References

- measurements. Determination of the nitrogen content in wheat leaves.", *The Analyst*, **124**, 1669-74.
91. R. De Maesschalck, et al., (2000), "The Mahalanobis Distance.", *Chemom. Intell. Lab. Syst.*, **50**, 1-18.
92. A. Candolfi, et al., (1998), "Comparison of classification approaches applied to NIR-spectra of clinical study lots.", *J. Pharm. Biomed. Anal.*, **16**, 1329-47.
93. U. G. Indahl, et al., (1999), "Multivariate strategies for classification based on NIR-spectra - with application to mayonnaise.", *Chemom. Intell. Lab. Syst.*, **49**, (1), 19-31.
94. A. Candolfi, et al., (1999), "Identification of pharmaceutical excipients using NIR spectroscopy and SIMCA.", *J. Pharm. Biomed. Anal.*, **19**, .
95. P. Berzaghi, et al., (2000), "LOCAL prediction with near infrared multi-product databases.", *J. Near Infrared Spectrosc.*, **8**, (1), 1-9.
96. E. Bouveresse, et al., (1996), "Standardisation of Near-Infrared Spectrometric Instruments.", *Anal. Chem.*, **68**, (6), 982-90.
97. E. Bouveresse, et al., (1997), "Detection, interpretation and correction of changes in the instrumental response of near-infrared monochromator instruments over time.", *Analytica Chimica Acta*, **348**, 283-301.
98. E. Bouveresse, et al., (1998), "Assessing the validity of near-infrared monochromator calibrations over time.", *Appl. Spectrosc.*, **52**, (4), 604-12.
99. E. Bouveresse, et al., (1998), "Application of standardisation methods to the correct the spectral differences induced by a fibre optic probe used for

References

- the near-infrared analysis of pharmaceutical tablets.", *J. Pharm. Biomed. Anal.*, **18**, 35-42.
100. B. G. Osborne and T. Fearn, (1983), "Collaborative evaluation of universal calibrations for the measurement of protein and moisture in flour by near infrared reflectance.", *J. Food Technol.*, **18**, 453-60.
101. J. A. Jones, et al., (1993), "Development and transferability of near-infrared methods for determination of moisture in freeze-dried injection product.", *J. Pharm. Biomed. Anal.*, **11**, (11-12), 1227-31.
102. J. S. Shenk and M. O. Westerhaus, "Optical instrument calibration system" (USA, 1989).
103. Y. Wang, et al., (1991), "Multivariate Instrument Standardisation.", *Anal. Chem.*, **63**, 2750-6.
104. B. M. Wise and N. B. Gallagher, "PLS_Toolbox Version 2.0 for use with MATLAB.", (Eigenvector Research, Inc., Manson, WA, 1998).
105. J. Sjöblom, et al., (1998), "An evaluation of orthogonal signal correction applied to calibration transfer of near infrared spectra.", *Chemom. Intell. Lab. Syst.*, **44**, 229-44.
106. B. Walczak, et al., (1997), "Standardisation of near-infrared spectra in the wavelet domain.", *Chemom. Intell. Lab. Syst.*, **36**, 41-51.
107. J. Trygg and S. Wold, (1998), "PLS regression on wavelet compressed NIR spectra.", *Chemom. Intell. Lab. Syst.*, **42**, 209-20.
108. P. Geladi, et al., (1999), "Calibration transfer for predicting lake-water pH from near infrared spectra of lake sediments.", *J. Near Infrared Spectrosc.*, **7**, 251-64.

References

109. T. B. Blank, et al., (1996), "Transfer of Near-infrared Multivariate Calibrations without Standards.", *Anal. Chem.*, **68**, (17), 2987-95.
110. H. Swierenga, et al., (1998), "Improvement of PLS model transferability by robust wavelength selection.", *Chemom. Intell. Lab. Syst.*, **41**, 237-48.
111. J. M. Brechley, et al., (1997), "Wavelength Selection Characterisation for NIR Spectra.", *Appl. Spectrosc.*, **51**, (5), 689-700.
112. M. J. McShane, et al., (1999), "Improving Complex Near-IR Calibrations using a new Wavelength Selection Algorithm.", *Appl. Spectrosc.*, **53**, (12), 1575-81.
113. E. Bouveresse, et al., (1994), "Calibration transfer across near-infrared spectrometric instruments using Shenk's algorithm: effects of different standardisation samples.", *Analytica Chimica Acta*, **297**, 405-16.
114. E. Bouveresse and D. L. Massart, (1995), "Modified Algorithm for Standardisation of Near-Infrared Spectrometric Instruments.", *Anal. Chem.*, **67**, 1381-9.
115. O. E. de Noord, (1994), "Multivariate calibration standardisation.", *Chemom. Intell. Lab. Syst.*, **25**, 85-97.
116. R. W. Kennard and L. A. Stone, (1969), "Computer Aided Design of Experiments.", *Technometrics*, **11**, (1), 137-48.
117. W. W. Coblenz, "Investigations of Infrared Spectra: Part I, Infrared Absorption Spectra: Part II, Infrared Emission Spectra.", (Carnegie Institute of Publication No. 35, Republished by Coblenz Society and Perkin-Elmer Corp. (1962), 1905).

References

118. I. Murray and P. C. Williams, "Near-infrared technology in the agricultural and food industries.", P. Williams and K. Norris, Eds. (American Association of Cereal Chemists, Inc., St. Paul, Minnesota, USA., 1987).
119. S. Kawano, et al., "Measurement of sugar contents in intact peaches by NIRS.", 2nd International NIRS Conference, Tsukuba, Japan (1989).
120. D. D. Dull, (1978), "Nondestructive Quality Evaluation of Agricultural Products: A Definition and practical Approach.", *J. Food Protect.*, **41**, (1), 50-3.
121. G. G. Dull, et al., (1989), "Exiting Energy Distribution in Honeydew Melon Irradiated with a Near Infrared Beam.", *J. Food Qual.*, **12**, 377-81.
122. G. G. Dull, et al., (1992), "Instrument for Nondestructive Measurement of Soluble Solids in Honeydew Melons.", *Trans. ASAE*, **35**, (2), 735-7.
123. M. Ito, et al., "Non-destructive sugar content measuring apparatus" (Sumitomo Metal Mining Co., Ltd., USA, 1998).
124. Q. Ding and G. W. Small, (1998), "Genetic algorithm-based wavelength selection for the near-infrared determination of glucose in biological matrices: Initialisation strategies and effects of spectral resolution.", *Anal. Chem.*, **70**, 4472-9.
125. Q. Wang, et al., "Advantages of increases resolution in NIR analysis." (Brüker, 1997).
126. A. J. Berger and M. S. Feld, (1997), "Analytical Method of Estimating Chemometric Prediction Error.", *Appl. Spectrosc.*, **51**, (5), 725--31.

References

127. J. Lu and W. F. McClure, (1998), "Effect of Random Noise on the performance of NIR calibrations.", *J. Near Infrared Spectrosc.*, **6**, 97-104.
128. K. H. Norris, (1998), "Interactions among instrument bandpass, instrument, sample-absorber bandwidth and calibration error.", *NIR News*.
129. I. Ben-Gera and K. H. Norris, (1968), "Direct spectrophotometric determination of fat and moisture in meat products.", *J. Food Sci.*, **33**, 64-67.
130. G. K. Brown and L. J. Segerlind, "Method for detecting bruises in fruit" (Secretary of Agriculturae, USA, USA, 1973).
131. G. K. Brown and L. J. Segerlind, "Method for detecting bruises in fruit" (Secretary of Agriculturae, USA, USA, 1975).
132. T. D. Conway, "Method and Means for Internal Inspection of produce" (Sunkist Growers, Inc., Stockton, California., USA, 1976).
133. J. Burford and H. T. Henry, "Produce grading system using two visible and two invisible colors" (Sortex North America, Inc., Lowell, MI, USA, 1978).
134. J. Burford and H. T. Henry, "Produce grading system using two visible and two invisible colors" (Sortex North America, Inc., Lowell, MI, USA, 1980).
135. Norinsho, "Fruit and vegetable quality measurement by production of spectrum by irradiating fruit with NIR rays non-destructively" (Japan, 1988).

References

136. K. Mikio, et al., "Method and device for measuring quality of vegetable and fruit" (Mitsui Mining and Smelting co. Ltd., Japan, 1988).
137. G. S. Birth, et al., "Nondestructive measurement of soluble solids in fruit by detection and measurement of NIR radiation scattered by internal structure of juice" (USA, 1990).
138. G. S. Birth, et al., "Nondestructive measurement of soluble solids in fruits having a rind or skin" (USA, 1992).
139. T. D. Conway, "Method and Apparatus for Grading Fruit" (Sunkist Growers, Inc., Stockton, California., USA, 1992).
140. M. Iwamoto and S. Kawano, "Method of nondestructively measuring sugar content of fruit by using NIR transmittance spectrum" (National Food Research Institute, Japan, 1994).
141. M. Iwamoto and S. Kawano, "Nondestructive Measurement Method for Fruits Sugar Degree with Near-Infrared Transmission Spectrum" (National Food Re Institute, Japan, 1994).
142. Iwamoto, et al., "Method of nondestructively measuring sugar content of fruit by using NIR transmittance spectrum." (National Food Research Institute, Japan, 1994).
143. I. Toru and T. Hideki, "Apparatus for measuring ripeness of fruit or vegetable on branch" (Techno Ishii KK, Japan, 1995).
144. P. Blanc, "Analysis device for automatically sorting products, especially fruit or vegetables" (Material pour L'Aboriculture Fruitiere (M.A.F.) S.A., Belgium, Switzerland, Germany, Spain, France, Great Britain, Italy, Lithuania, Netherlands, 1996).

References

145. C. H. Salmond and C. V. Greensill, "An Optical Device (Aust)" (Australia, 1998).
146. C. H. Salmond and C. V. Greensill, "An Optical Device" (Japan, 1998).
147. G. S. Birth and K. H. Norris, (1965), "The Difference Meter for Measuring Interior Quality of Foods and Pigments in Biological Tissues.", Agric. Res. Serv., US Dept. Agric., **1341**, 1-17.
148. J. N. Yeatman and K. H. Norris, (1965), "Evaluating Internal Quality of Apples with New Automatic Fruit Sorter.", J. Food Technol., **123**, 123-5.
149. W. E. Ballinger, et al., (1978), "Nondestructive Quality Evaluation from a Horticulturalist's Point of View.", J. Food Protect., **41**, (1), 63-6.
150. H. M. Jaenisch, et al., (1990), "Instrumentation to measure the near-IR spectrum of small fruits.", Opt. Agric., **1379**, 162-167.
151. T. Shiina, et al., "Determination of Brix Value and Acidity in Pineapple Fruits by Near Infrared Spectroscopy.", First International Pineapple Symposium (1993).
152. V. Bellon-Maurel and J. L. Vigneau, in Book "NIR fast spectrometer for fruit internal quality assessment: Reproducibility study.", (1995) pp. 471-6.
153. R. K. Cho, et al., "Application of near infrared spectroscopy for quality evaluation of an intact apple.", A. M. C. Davies and P. Williams, Eds., 7th International Conference on Near Infrared Spectroscopy, Montréal, Canada (NIR Pub., 1995).
154. S. D. Osborne, et al., "Using Near-Infrared (NIR) Light to Estimate the Soluble Solids And Dry Matter Content of Kiwifruit.", PH'96

References

- International PostHarvest Science Conference, Taupo, New Zealand (1996).
155. D. C. Slaughter and C. H. Crisosto, "Nondestructive Internal Quality Assessment of Kiwifruit using Near Infrared Spectroscopy.", 8th International Diffuse Reflectance Conference, Chambersburg, PA (1996).
156. T. Tanabe, et al., "Determination of Total Soluble Solids in Mango Fruit Produced on Okinawa by NIR Spectroscopy.", International Conference on Tropical Fruits, Kuala Lumpur, Malaysia (1996).
157. C. V. Greensill and D. S. Newman, "A Comparison of Simple NIR Spectrometer Configurations for the Determination of Total Soluble Solids in Fruit.", 8th International Conference on Near Infrared Spectroscopy, Essen, Germany (NIRS Publications, 1997).
158. J. Guthrie and K. Walsh, "NIR analysis of soluble solids in pineapple and dry matter in mango.", Proceedings from the Sensors for nondestructive Testing International Conference and Tour Holiday Inn International Drive Resort, Orlando, Florida (1997).
159. S. D. Osborne, Doctor of Philosophy in Physics, The University of Waikato (1997).
160. K. H. S. Peiris, et al., "Non-destructive determination of soluble solids content of peach by near infrared spectroscopy.", Sensors for Non-destructive Testing, Orlando, Florida, USA. (Northeast Regional Agricultural Engineering Service, 1997).
161. K. Akimoto, (1998), "Present State in Quality Evaluations of Horticultural Products.", J. Jap. Soc. Hort. Sci., **67**, (6), 1171-5.

References

162. W. H. Chang, et al., (1998), "Development of a Universal Algorithm for Use of NIR in Estimation of Solubles Solids in Fruit Juices.", *Am. Soc. Agric. Eng.*, **41**, (6), 1739-45.
163. J. Guthrie, et al., (1998), "Robustness in NIR calibrations for soluble solids in intact melon and pineapple.", *J. Near Infrared Spectrosc.*, **6**, 1-7.
164. S. Kawano, (1998), "New Application of Nondestructive Methods for Quality Evaluation of Fruits and Vegetables in Japan.", *J. Jap. Soc. Hort. Sci.*, **67**, (6), 1176-9.
165. J. Lammertyn, et al., (1998), "Non-destructive Testing of Acidity, Soluble Solids and Firmness of Jonagold Apples using NIR-Spectroscopy.", *Am. Soc. Agric. Eng.*, **41**, (4), 1089-94.
166. P. Martinsen and P. Schaare, (1998), "Measuring solubles distribution in kiwifruit using near-infrared imaging spectroscopy.", *Postharvest Biol. Technol.*, **14**, 271-81.
167. V. A. McGlone and S. Kawano, (1998), "Firmness, dry-matter and soluble-solids assessment of postharvest kiwifruit by NIR spectroscopy.", *Postharvest Biol. Technol.*, **13**, (2), 131-41.
168. A. D. Mowat and P. R. Poole, (1998), "Use of visible-near infrared spectral properties as a maturity indicator in non-astringent persimmon (*Diospyros kaki* L.).", *J. Hort. Sci. Biotechnol.*, report.
169. K. H. S. Peiris, et al., (1998), "Near-infrared spectrometric method for nondestructive determination of soluble solids content of peaches.", *J. Amer. Soc. Hort. Sci.*, **123**, (5), 898-905.

References

170. K. H. S. Peiris, et al., (1998), "Near-infrared (NIR) spectrometric technique for nondestructive determination of soluble solids content in processing tomatoes.", J. Amer. Soc. Hort. Sci., **123**, (6), 1089-93.
171. C. V. Greensill and D. S. Newman, (1999), "An Investigation into the Determination of the Maturity of Pawpaws (*Carica papaya*) from NIR Transmission Spectra.", J. Near Infrared Spectrosc., **7**, (2), 109-116.
172. J. Guthrie and K. Walsh, (1999), "Influence of environmental and instrument variables on the non-invasive prediction of Brix in pineapple using near infra-red spectroscopy.", Aust. J. Exp. Agric., **39**, 73-80.
173. S. D. Osborne, et al., (1999), "A low-cost system for the grading of kiwifruit.", J. Near Infrared Spectrosc., **7**, 9-15.
174. K. H. S. Peiris, et al., (1999), "Spatial Variability of Soluble Solids or Dry-matter Content within Individual Fruits, Bulbs or Tubers: Implications for the determination and Use of NIR Spectrometric Techniques.", Postharvest Biol. Technol., **34**, (1), 114-8.
175. J. Sugiyama, (1999), "Visualization of sugar content in the flesh of a melon by near-infrared imaging.", J Agric. & Food Chem., **47**, (7), 2715-8.
176. C. V. Greensill and D. S. Newman, (2000), "An Experimental Comparison of Simple NIR Spectrometers for Fruit Grading Applications.", Applied Engineering in Agriculture, **Revised 21 July 1999**, .
177. C. V. Greensill and K. B. Walsh, (2000), "A Remote Acceptance Probe and Illumination Configuration for Spectral Assessment of Internal

References

- Attributes of Intact Fruit.", *Journal of Measurement Science and Technology*, **in press**.
178. C. V. Greensill and K. B. Walsh, (2000), "Optimisation of instrumentation precision and wavelength resolution for the performance of NIR calibrations of sucrose in a water-cellulose matrix.", *Appl. Spectrosc.*, **54**, (3), 426-30.
 179. J. Lammertyn, et al., (2000), "Light penetration properties of NIR radiation in fruit with respect to non-destructive quality assessment.", *Postharvest Biol. Technol.*, **18**, (2), 121-32.
 180. Z. Schmilovitch, et al., (2000), "Determination of mango physical indices by near-infrared spectrometry.", *Postharvest Biol. Technol.*, **19**, 245-52.
 181. V. H. Segtnan and T. Isaksson, (2000), "Evaluating near infrared techniques for quantitative analysis of carbohydrates in fruit juice model systems.", *J. Near Infrared Spectrosc.*, **8**, 109-16.
 182. K. B. Walsh, et al., "A hardware platform for NIRS based, packline sorting of melons for soluble solids.", 9th Australian Near Infrared Spectroscopy Conference, Horsham, Victoria (2000).
 183. Z. Wen and Y. Tao, (2000), "Dual-camera NIR/MIR imaging for stem-end/calyx identification in apple defect sorting.", *Transactions ASAE*, **43**, (2), 449-52.
 184. J. Malinen, et al., (1998), "LED-based NIR spectrometer module for handheld and process analyser applications.", *Sensors and Actuators*, **51**, 220-6.

References

185. J. G. Schnable, et al., (1998), "Portable LED-Array VIS-NIR spectrophotometer/nephelometer.", *Field Anal. Chem. Technol.*, **2**, (1), 21-8.
186. O. Nakamura, et al., (1999), "Nondestructive inspection of *Phaseolus coccineus* L. soya beans by use of near infrared lasers.", *Appl. Opt.*, **38**, (2), 2724-7.
187. M. Meurens and E. Moons, "Spectral Amplification in NIR spectroscopy and sorting of whole apples.", *From Sensors to Decision Support System in Agriculture, Food Industry and Environment*, Montpellier-Narbonne, France (CEMAGREF, Agro, INRA, 1998).
188. L. Godfrey, (1998), "Choosing the Detector for your Unique Light Sensing Application.", **1998**, (11/8/98),
189. S. Prunet, et al., (1999), "Exact calculation of the optical path difference and description of a new birefringent interferometer.", *Opt. Eng.*, **38**, (6), 983-90.
190. P. Dardenne, et al., in Book "Calibration transferability across NIR instruments.", K. I. Hildrum, et al., Eds. (Ellis Horwood, U.K., 1992) pp. 453-458.
191. F. Despagne, et al., (1998), "Transfer of calibrations of near-infrared spectra using neural networks.", *Appl. Spectrosc.*, **52**, (5), 732-45.
192. F. Despagne, et al., (2000), "Intersite transfer of industrial calibration models.", *Analytica Chimica Acta*, **406**, 233-45.
193. E. Dreassi, et al., (1998), "Transfer of calibration in near-infrared reflectance spectrometry.", *The Analyst*, **123**, 1259-64.

References

194. L. Duponchel, et al., (1999), "Standardisation of near-IR spectrometers using artificial neural networks.", *J. Near Infrared Spectrosc.*, **7**, 156-66.
195. J. S. Shenk and M. O. Westerhaus, "Comparison of standardisation techniques.", A. M. C. Davies and P. Williams, Eds., 7th International Conference on Near Infrared Spectroscopy, Montréal, Canada (NIR Publications, 1995).
196. M. Blanco, et al., (1999), "Wavelength Calibration Transfer between Diode Array UV-Visible Spectrometers.", *Appl. Spectrosc.*, **49**, (5), 593-7.
197. S. Kawano and M. Iwamoto, "Advances in R & D on Near Infrared Spectroscopy in Japan.", SPIE: Optics in Agriculture (1990).
198. M. Millikan, (1996), "NIR applications in the food packaging industries.", *Journal of Chemistry in Australia*, **Dec.**, 554-6.
199. G. S. Birth, et al., (1984), "An Optical Method for Estimating Papaya Maturity.", *J. Amer. Soc. Hort. Sci.*, **109**, (1), 62-6.
200. T. Temma, et al., "Measurement of Sugar contents in apples by near infrared spectroscopy and development of a compact near infrared sugar-measuring instrument.", A. M. C. Davies and P. Williams, Eds., 7th International Conference on Near Infrared Spectroscopy, Montréal, Canada (NIR Pub., 1995).
201. D. C. Slaughter and C.H. Crisosto, (1996), "Non-destructive internal quality assessment of kiwifruit using near infrared spectroscopy.", 8th International Diffuse Reflectance Conference, (1996).
202. W. Demtröder, "Laser Spectroscopy.", Springer's Series in Chemical Physics Number 5 (Springer Verlag, Berlin, 1982).

References

203. E. A. Baldwin and R. E. Paull, in Book "Biochemistry of Fruit Ripening.", G. B. Seymour, et al., Eds. (Chapman & Hall, London, 1993) pp. 107-49, 291-323.
204. W. R. Forbus, et al., (1987), "Measurement of papaya maturity by delayed light emission.", J. Food Sci., **52**, (2), 356-60.
205. W. R. Forbus and H. T. Chan, (1989), "Delayed light emission as a means of predicting papaya susceptibility to fruit fly infestation.", J. Amer. Soc. Hort. Sci., **114**, (3), 521-5.
206. S. T. Seo, et al., (1982), "Oriental Fruit Fly: Ripening of fruit and its effect on the index of infestation of Hawaiian papayas.", J. Econ. Entomol., **75**, 173-8.
207. H. M. Couey, et al., (1984), "Quarantine procedure for Hawaiian papayas using heat and cold treatments.", J. Econ. Entomol., **77**, (4), 984-8.
208. M. Känkäkoski, et al., (1998), "The performance of near infrared analysers can be improved by digital filtering techniques.", J. Near Infrared Spectrosc., **6**, 97-104.
209. K. B. Walsh, et al., (2000), "Application of commercially available, low-cost, miniaturised NIR spectrometers to the assessment of the sugar content of intact fruit.", Aust. J. Plant Physiol., , in press.
210. K. B. Walsh, et al., "Development and use of an 'at-line' NIR instrument to evaluate robustness of melon Brix calibrations.", 9th International Conference on Near-Infrared Spectroscopy, Verona, Italy (NIR Publications, 1999).
211. G. S. Birth, (1975), "How Light Interacts with Foods.", J. Food Eng., **73**, 6509-14.

References

- 212. T. Fearn, (1996), "Comparing Standard Deviations.", *JNIRS News*, **7**, (5), 5-6.
- 213. G. W. Snedecor and W. G. Cochran, "Statistical Methods.", (Iowa State University Press, ed. 6th, 1967).
- 214. Y. Wang, et al., (1992), "Improvement of Multivariate Calibration through Instrument Standardisation.", *Anal. Chem.*, **64**, 562-4.
- 215. R. S. Park, et al., (1999), "The development and transfer of undried grass silage calibrations between near infrared reflectance spectroscopy instruments.", *Anim. Feed Sci. Technol.*, **78**, 325-40.
- 216. B. G. Osborne, et al., (1999), "Optical matching of near infrared reflectance monochromator instruments for the analysis of ground and whole wheat.", *J. Near Infrared Spectrosc.*, **7**, 167-78.
- 217. P. Tillmann, (2000), "Networking of near infrared spectroscopy instruments for rapeseed analysis: a comparison of different procedures.", *J. Near Infrared Spectrosc.*, **8**, 101-7.
- 218. J. Lin, (1998), "Near-IR Calibration Transfer between Different Temperatures.", *Appl. Spectrosc.*, **52**, (12), 1591-6.

11. Appendices

11.1. Appendix A

Band Assigned Wavelengths

Band assignments of experimentally observed peaks by Osborne *et al.*⁶⁶ and Murray¹¹⁸ in the NIR region. In the SW-NIR region precise band assignment is difficult due to the broad nature of the features¹⁴ (~ 40 nm) and their dependence on temperature and other matrix contributions^{61, 218}.

Note: Bolded bands indicate SSC identifying wavelengths.

Italicised bolded bands indicate water identifying bands.

‘**’ indicates overlapping SSC and water bands.

Wavelength (nm)	Bond vibration	Structure
713	C-H str. fourth overtone	benzene
738	O-H str. third overtone	ROH
740	C-H str. fourth overtone	CH ₃
746	C-H str. fourth overtone	CH ₂
747	O-H str. third overtone	ArOH
760	O-H str. third overtone	H ₂ O
762	C-H str. fourth overtone	CH ₂
779	N-H str. third overtone	RNH ₂
790	N-H str. third overtone	ArNH ₂
806	N-H str. third overtone	RNH ₂

Appendices

808	2 x N-H str. + 2 x N-H def. + 2 x C-N str.	RNHR'
815	N-H str. third overtone	RNHR'
832	2 x N-H str. + 2 x N-H def. + 2 x C-N str.	RNHR'
840	3 x C-H str. + 2 x C-C str.	benzene
874	C-H str. third overtone	benzene
880	C-H str. third overtone	CHCl ₃
900	C-H str. third overtone	CH ₃
910	C-H str. third overtone	protein
913	C-H str. third overtone	CH ₂
928	C-H str. third overtone	oil
938	C-H str. third overtone	CH ₂
970*	O-H str. second overtone	ROH, H ₂ O
990	O-H str. second overtone	starch
1000	O-H str. second overtone	ArOH
1015	2 x C-H str. + 3 x C-H def.	CH ₃
1020	2 x N-H str. + 2 x amide I	protein
1020	N-H str. second overtone	ArNH ₂
1030	N-H str. second overtone	RNH ₂
1037	2 x C-H str. + 2 x C-C def. + (CH ₂) _n	oil
1053	2 x C-H str. + 2 x C-C def. + (CH ₂) _n	CH ₂
1060	N-H str. second overtone	RNH ₂
1080	2 x C-H str. + 2 x C-C str.	benzene
1097	2 x C-H str. + 2 x C-C str.	cyclopropane
1143	C-H str. second overtone	aromatic
1152	C-H str. second overtone	CH ₃

Appendices

1170	C-H str. second overtone	HC=CH
1195	C-H str. second overtone	CH ₃
1215	C-H str. second overtone	CH ₂
1225	C-H str. second overtone	CH
1360	2 x C-H str. + C-H def.	CH ₃
1395	2 x C-H str. + C-H def.	CH ₂
1410	O-H str. first overtone	ROH
1415	2 x C-H str. + C-H def.	CH ₂
1417	2 x C-H str. + C-H def.	aromatic
1420	O-H str. first overtone	ArOH
1430	N-H str. first overtone	CONH ₂
1440	O-H str. first overtone	sucrose, starch
1440	2 x C-H str. + C-H def.	CH
1446	2 x C-H str. + C-H def.	aromatic
1450*	O-H str. first overtone	starch, H ₂ O
1460	N-H str. first overtone	CONH ₂
1471	N-H str. first overtone	CONHR
1480	O-H str. first overtone (intramol. H-bond)	glucose
1483	N-H str. first overtone	CONH ₂
1490	N-H str. first overtone	CONHR
1490	N-H str. first overtone (intramol. H-bond)	CONH ₂
1490	O-H str. first overtone (intramol. H-bond)	cellulose
1492	N-H str. first overtone	ArNH ₂
1500	N-H str. first overtone	NH
1510	N-H str. first overtone	protein

Appendices

1520	O-H str. first overtone	CONH ₂
1520	N-H str. first overtone (intramol. H-bond)	ROH
1528	O-H str. first overtone (intramol. H-bond)	starch
1530	N-H str. first overtone	RNH ₂
1533	C-H str. first overtone	C=H
1540	O-H str. first overtone (intramol. H-bond)	starch
1570	N-H str. first overtone	-CONH-
1580	O-H str. first overtone (intermol. H-bond)	starch, glucose
1620	C-H str. first overtone	=CH ₂
1645	C-H str. first overtone	$\begin{array}{c} \text{R} - \text{CH} - \text{CH} \\ \quad \backslash \quad / \\ \quad \quad \text{O} \end{array}$
1660	C-H str. first overtone	<i>cis</i> -RCH=CHR ¹
1685	C-H str. first overtone	aromatic
1695	C-H str. first overtone	CH ₃
1705	C-H str. first overtone	CH ₃
1725	C-H str. first overtone	CH ₂
1740	S-H str. first overtone	-SH
1765	C-H str. first overtone	CH ₂
1780	C-H str. first overtone	cellulose
1820	O-H str. + 2 x C-O str.	cellulose
1900	O-H str. + 2 x C-O str.	starch
1900	C=O str. second overtone	-CO ₂ H
1908	O-H str. first overtone	POH
1920	C=O str. second overtone	CONH

Appendices

1940	O-H str. + O_H def.	H ₂ O
1950	C=O str. second overtone	-CO ₂ R
1960	N-H asym. str. + amide II	CONH ₂
1980	N-H asym. str. + amide II	protein
2000	2 x O_H def. + C-O def.	starch
2000	N-H asym. str. + amide II	CONH ₂ , CONHR
2030	C=O str. second overtone	CONH ₂
2050	N-H asym. str. + amide II	protein
2050	N-H asym. str. + amide III	CONH ₂
2080	OH str. + O-H def.	ROH, sucrose, starch
2100	2 x O-H def. + 2 x C-O str.	starch
2110	N-H asym. str. + amide III	CONH ₂ , CONHR
2132	N-H str. + C=O str.	amino acid
2140	=C=H str. + C=C str.	HC=CH
2150	2 x amide I + amide III	CONH ₂
2160	2 x amide I + amide III	CONHR
2180	2 x amide I + amide III	protein
2190	CH ₂ asym. str. + C= str.	HC=CH
2200	C-H str. + C=O str.	-CHO
2242	N-H str. + NH ₃ ⁺ def.	amino acid
2252	O-H str. + O-H def.	starch
2276	O-H str. + C-C str.	starch
2280	C-H str. + C-H def.	CH ₃
2294	N-H str. + C=O str.	amino acid
2310	C-H str. + C-H def.	CH ₂

Appendices

2323	C-H str. + C-H def.	CH ₂
2336	C-H str. + C-H def.	cellulose
2347	CH ₂ sym. str. + =CH ₂ def.	HC=CHCH ₂
2352	C-H def. second overtone	cellulose
2380	O-H def. second overtone	ROH
2461	C-H str. + C-C str.	starch
2488	C-H str. + C-C str..	starch
2500	C-H str. + C-C str.	starch

11.2. Appendix B

Representative list of spectrometer manufacturers detailing type of wavelength selection method used, resolution, SNR and range.

(Specifications from manufacturer's data sheets.)

Manufacturer	Configuration	Resolution FWHM (nm)	Maximum SNR	Detector Type	Range (nm)
Acton Research Corp. (SpectruMM)	Diffraction Grating (stationary)	0.4	2560:1(binned)	CCD (Si)	400-1100
Agricultural Innovations (OM 200)	Diffraction Grating (stationary)	9	-	PIN (Si)	800-1050
Analytical Spectral Devices	Diffraction Grating (stationary)	4.2	-	PDA (Si)	350-1050
Bran & Leubbe	Filter	-	-	-	1445-2348
Bran & Leubbe	AOTF	-	-	-	900-1700
Brimrose (Free-Space Luminar 2030)	AOTF	2-10	10000:1	PIN (InGaAs)	850-1700
Bruker (Vector 22-NIR)	FT-NIR	0.3	30000:1	PIN (Ge, InGaAs)	600-3030
NIRSystems, Inc. (6500)	Diffraction Grating (moving)	8.5	4000:1(Si), 16000:1 (PbS)	PIN (Si, PbS)	400-2500

Nicolet Instrument	FTIR	0.09	>60000:1	PIN (Si,InGaAs)	400-2500
Ocean Optics (S2000)	Diffraction Grating (stationary)	0.3 – 10	250:1	CCD (Si)	400-1100
Ocean Optics (S1024DW)	Diffraction Grating (stationary)	(dependent	2500:1	PDA (Si)	400-1100
Ocean Optics (S1024DWX)	Diffraction Grating (stationary)	on slit width)	8000:1	PDA (Si)	400-1100
Opti-Sciences, Inc (OS5-SP).	Grating (stationary)	10	10000:1	PDA (Si)	300-900
Oriel (MS127i)	Grating (stationary)	0.4	1000:1	CCD(Si)	180-1100
Pixel Vision, Inc. (ImSpec)	Grating/Prism	5	-	CCD (Si)	700-1000
Perten (DA7000)	Diffraction Grating (stationary)	-	-	PDA (Si,InGaAs)	500-1700
Sentronics (CDNIR 1.7)	Diffraction Grating (stationary)	8	2000:1	PDA (InGaAs)	900-1700
Shimadzu (UV-1601PC)	Grating (moving)	2	1395:1	PIN (Si)	190-1100
Zeltex (ZX-50)	Filter	20	8000:1	PIN (Si)	890-1045
Zeiss	Grating (stationary)	10	10000:1	PDA (Si)	400-1100

Appendices

11.3. Appendix C

Calculation of Euclidean Distance and (ED) Mahalanobis Distance (MD):

Replicate sample measurements are expected to be very similar. Differences result from spectrometer drift, differences in sample handling, changing environmental conditions such as humidity, as well as batch to batch variations in the sample material. However, when the spectra are all of the same material, the relative intensities at all the wavelengths should remain approximately the same. A plot of absorbance at two wavelengths of a series of samples might be expected to give a circular cluster however, frequently an elliptical cluster shape, typical of spectra from the same material, is formed by the group around the mean. The formation of an elliptical cluster is indicative of the subtle differences between the spectra (both in terms of baseline shift, pathlength and concentration). The mean position of the cluster is unique to the particular material of interest, since the intensities at these two wavelengths would be different for a different material. Two well-known mathematical techniques which can mathematically determine similarity of groups of spectra are the Euclidean distance and the other is the Mahalanobis distance.

Euclidean distance (ED):

The Euclidean distance does not give any statistical measurement of how well the unknown data matches the training set. In addition, the Euclidean distance only measures a relative distance from the mean point in the group. It does not take into account the distribution of the points in the group. The Euclidean distance describes a circular boundary around the mean point and does not take into account the variability of the values in all dimensions.

Appendices

The Euclidean distance (ED) is the geometric distance in multi-dimensional space. For two variables it is computed as:

$$ED = \sqrt{(x_{i1} - \bar{x}_1)^2 + (x_{i2} - \bar{x}_2)^2} \text{ for } i = 1 \text{ to } n.$$

where x_{i1} and x_{i2} are the values of the object i for x_1 and x_2 , respectively and \bar{x}_1 and \bar{x}_2 are the means of n values at x_1 and x_2 , respectively. Note that Euclidean (and squared Euclidean) distances are computed from raw data, and not from standardised data.

Mahalanobis distance (MD):

The Mahalanobis distance, however, does take the sample variability into account. Instead of treating all values equally when calculating the distance from the mean point, it weights the differences by the range of variability in the direction of the sample point. The Mahalanobis distance constructs a space that weights the variation in the sample along the axis of elongation less than in the shorter axis of the group ellipse. Further, Mahalanobis distances look at not only variations (variance) between the responses at the same wavelengths, but also at the inter-wavelength variations (covariance). The Mahalanobis group defines a multi-dimensional space whose boundaries determine the range of variation that are acceptable for unknown samples to be classified as members. The Mahalanobis model tends to overfit very quickly if a high number of variables is used. Consequently variable number is frequently reduced by using scores from model space.

Appendices

Independent variables (in a multivariate regression equation) define a multi-dimensional space in which each observation can be plotted. A plot of points representing the means for all independent variables in the multi-dimensional space is called the centroid. The Mahalanobis distance is the distance of a case from the centroid in the multi-dimensional space, defined by the correlated independent variables. If the independent variables are uncorrelated, MD is the same as the simple Euclidean distance. Thus, the measure of MD provides an indication of whether or not an observation is an outlier with respect to the independent variable values. However, the scale of this measure is ill-defined, difficult to interpret and dependent on the independent variable used. For example, PC scores are frequently used in place of raw absorbance data to reduce dimensionality¹⁹⁵. The first step in calculating MD requires the calculation of the variance-covariance matrix C_x^{-1} .

$$C_x = \frac{1}{n-1}(\mathbf{X}_c)^T(\mathbf{X}_c) \quad \text{Eqn 11.1}$$

where \mathbf{X} is the data matrix of $n \times p$ (objects \times variables) and \mathbf{X}_c is the column centred matrix $(\mathbf{X} - \bar{\mathbf{X}})$. When two variables (x_1 and x_2) are used \mathbf{C} becomes

$$C_x = \begin{bmatrix} \sigma_1^2 & \rho_{12}\sigma_1\sigma_2 \\ \rho_{12}\sigma_1\sigma_2 & \sigma_2^2 \end{bmatrix} \quad \text{Eqn 11.2}$$

where σ_1^2 and σ_2^2 are the variances of the first and second variables, respectively and $\rho_{12}\sigma_1\sigma_2$ is the covariance between the two variables.

To determine the Mahalanobis distance for the object x_i :

Appendices

$$MD_i = \sqrt{(\mathbf{x}_i - \bar{\mathbf{x}}) \mathbf{C}_x^{-1} (\mathbf{x}_i - \bar{\mathbf{x}})}^T \quad \text{Eqn 11.3}$$

by substitution this leads to

$$MD_i = \sqrt{\left(\frac{x_i - \bar{x}}{\sigma_1} \right) + \left[\left\{ \frac{(x_{i2} - \bar{x}_2)}{\sigma_2} - \rho_{12} \frac{(x_{i1} - \bar{x}_1)}{\sigma_1} \right\} \frac{1}{\sqrt{1 - \rho_{12}^2}} \right]^2} \quad \text{Eqn 11.4}$$

Appendices

11.4. Appendix D

Statistical terms used in this thesis:

Nomenclature used:

Symbol	Description
a, A	Principal Component (PC) and Number of PCs.
b_0, \mathbf{b}_0	y -offset
$b, \mathbf{b}, \mathbf{B}$	B-coefficients (estimated)
d	Degrees of freedom.
E_a	X-residual for a model using (a) PCs.
f, F_a	Y-residual for a model using (a) PCs.
i, I	Sample number and number of samples.
j, J	Y-variable number and number of Y-variable.
k, K	X-variable number and number of X-variables.
N	Number of elements.
p, \mathbf{P}	X-loadings
β	B-coefficients (exact)
t, \mathbf{T}	Scores
w, \mathbf{W}	Loading weights
\bar{x}, \bar{X}	Mean values in x or X
$x, \mathbf{x}, \mathbf{X}$	x -value (single, vector, matrix)(independent variable)
\bar{y}, \bar{Y}	Mean values in y or Y
$y, \mathbf{y}, \mathbf{Y}$	y -value (single, vector, matrix)(dependent variable)
\hat{y}	Predicted y value.
df	Degrees of freedom

Appendices

R	Correlation coefficient
R^2	Coefficient of determination
σ	Standard deviation

General linear regression model equation:

$$y = \beta_0 + \beta_1 x_1 + \beta_2 x_2 + \dots + \beta_K x_K + f \quad \text{Eqn 11.5}$$

(in matrix notation $y = \mathbf{B}x + f$.)

B Coefficients:

A line in a two dimensional or two-variable space is defined by the equation $Y=a+bX$; the Y variable can be expressed in terms of a constant (a) and a slope (b) times the X variable. The constant is also referred to as the intercept, and the slope as the regression coefficient or B coefficient. The regression coefficients (or B coefficients) represent the independent contributions of each independent variable to the prediction of the dependent variable.

$$b_1 = \frac{n \left(\sum_{k=1}^K x_k y_k \right) - \left(\sum_{k=1}^K x_k \right) \left(\sum_{k=1}^K y_k \right)}{n \left(\sum_{k=1}^K x_k^2 \right) - \left(\sum_{k=1}^K x_k \right)^2} \quad \text{Eqn 11.6}$$

$$b_0 = \frac{1}{n} \left(\sum_{i=1}^I y_i - b_1 \sum_{i=1}^I x_{ik} \right) \quad \text{Eqn 11.7}$$

Standard Deviation:

Appendices

The standard deviation is one of several indices of variability used to characterise the dispersion among the measures in a given population.

Standard deviation:

$$S_x(k) = \sqrt{\frac{1}{I_k - 1} \sum_{i=1}^I (x_{ik} - \bar{x}_k)^2} \quad \text{for } k=1 \dots K. \quad \text{Eqn 11.8}$$

Correlation Coefficient:

Given a pair of related measures (X and Y) on each of a set of samples, the correlation coefficient (R) provides an index of the degree to which the paired measures co-vary in a linear fashion. In general, R will be positive when items with large values of X also tend to have large values of Y whereas items with small values of X tend to have small values of Y. Correspondingly, R will be negative when items with large values of X tend to have small values of Y whereas items with small values of X tend to have large values of Y. Numerically, r can assume any value between -1 and +1 depending upon the degree of the relationship. The coefficient of correlation (R) between two variables k_1 and k_2 is calculated by:

Uncorrected:

$$R = \sqrt{1 - \frac{\sum_{i=1}^I (y_i - \hat{y}_i)^2}{\sum_{i=1}^I (y_i - \bar{y}_i)^2}} \quad \text{Eqn 11.9}$$

Corrected for degrees of freedom:

Appendices

$$R = \sqrt{1 - \frac{\sum_{i=1}^I (y_i - \hat{y}_i)^2 / (N - K - 1)}{\sum_{i=1}^I (y_i - \bar{y}_i)^2 / (N - 1)}} \quad \text{Eqn 11.10}$$

Coefficient of determination (R^2) of predictive model = *correlation coefficient*².

Root mean squared error of prediction:

Root mean squared error of prediction (RMSEP) is a true measure (within 1 σ , i.e. $\sim 67\%$) of the accuracy of the predicted value in an analytical application.

$$\text{RMSEP} = \sqrt{\frac{1}{I-1} \sum_{i=1}^I (\hat{y}_i - y_i)^2} \quad \text{Eqn 11.11}$$

Root mean squared error of cross validation:

Root mean squared error of cross validation is calculated using the same equation (Eqn 14.7) as for RMSEP with the predicted being determined on the sample/s left out of the calibration set during that iteration.

Standard error of prediction:

Standard error of prediction (SEP) is an estimate of the accuracy of the predicted values which compensates for bias, if present. To achieve this, all reference values must be made for the population before a prediction is made.

$$\text{SEP} = \sqrt{\frac{1}{I-1} \sum_{i=1}^I (\hat{y}_i - y_i - \text{Bias})^2} \quad \text{Eqn 11.12}$$

Appendices

Bias:

Bias is the average value of the residuals of the predictive model:

$$Bias = \frac{1}{I} \sum_{i=1}^I (\hat{y}_i - y_i) \quad \text{Eqn 11.13}$$

Standard Deviation Ratio:

Standard Deviation Ratio (SDR) is calculated by:

$$SDR = \frac{\sigma}{RMSECV} \quad \text{Eqn 11.14}$$

where σ is the standard deviation of the concentration of the population.

Degrees of freedom:

Degrees of freedom (*df*) is a term used in statistics to characterise the number of independent pieces of information contained in a statistic. For example, if we begin with a random sample of n observations and estimate the mean by the sample average, we are left with only $(n-1)$ independent measurements from which to estimate the variance or deviations around the mean. In a simple regression, where we estimate both an intercept and a slope, only $(n-2)$ degrees of freedom remain to measure variability around the fitted line.

Coefficient of variation:

Coefficient of variation (CV) is the ratio of the standard deviation divided by the mean, multiplied by 100, so that it is expressed as a percent. It is sometimes called the relative standard deviation. This summary statistic is often employed in the natural sciences, where the standard deviation of measurement error is

Appendices

often proportional to the magnitude of the values being measured. Since the CV provides a measure of relative variation and is unitless, it is particularly useful in making comparisons between different samples.

Cross-validation:

Cross-validation refers to the process of assessing the predictive accuracy of a model using a test sample (sometimes also called a cross-validation sample). Ideally, with an adequately large sample population, a portion of the population can be designated as belonging to the calibration set and the remainder to the test set. For assessment of a model within a given population, cross-validation (in which calibrations are developed with some samples from the population left out, cycling through samples until all samples have been left out at some time and used for prediction) is superior to the use of a single separate test set. Cross validation allows the use of larger data sets in the calibration set.

Outliers:

An outlier is an observation which does not correspond to the phenomenon being studied, but instead has its origin in background or in a gross measurement (or assignment) error. Nearly all experimental data samples are subject to contamination from outliers. This reduces the real efficiency of theoretically optimal statistical methods. Methods which perform well even in the presence of outliers are called robust methods. Outliers may reflect genuine properties of the underlying phenomenon (variable), or be due to measurement errors or other anomalies which should not be modelled. Because of the way in which the regression line is determined in Multiple Regression (that is, based on

Appendices

minimising the sum of squares of distances of data points from the line), outliers have a significant influence on the slope of the regression line and consequently on the value of the correlation coefficient.

Overfitting:

When attempting to fit a curve to a set of data points, producing a curve with high curvature which fits the data points well, but does not model the underlying function well (its shape being distorted by the noise inherent in the data) is called overfitting.